Quantitative mapping of stress in soft materials by mechanochemistry

Yinjun Chen

THÈSE DE DOCTORAT

de l'Université de recherche Paris Sciences et Lettres
PSL Research University

Préparée à Ecole Supérieure de Physique et de Chimie Industrielles de la Ville de Paris

Quantitative mapping of stress in soft materials by mechanochemistry

Ecole doctorale n°397

Physique et Chimie des Matériaux

Spécialité Physico-chimie

COMPOSITION DU JURY :

M. NICOLAY Renaud
ESPCI Paris, le président du jury

M. CIPELLETTI Luca
Université de Montpellier, Rapporteur

M. SIJBESMA Rint
Eindhoven University of Technology, Rapporteur

M. BICO José
ESPCI Paris, examinateur

M. FAYOLLE Bruno
Arts et Métiers Paris Tech-ENSAM, examinateur

M. CRETON Costantino
ESPCI Paris, Directeur de thèse

Soutenue par Yinjun **CHEN**
le 19 Septembre 2018

Dirigée par **Costantino CRETON**

ESPCI PARIS
EDUCATION SCIENCE INNOVATION

PSL
RESEARCH UNIVERSITY PARIS

THÈSE DE DOCTORAT

de l'Université de recherche Paris Sciences et Lettres
PSL Research University

Préparée à Ecole Supérieure de Physique et de Chimie Industrielles de la Ville de Paris

Quantitative mapping of stress in soft materials by mechanochemistry

Ecole doctorale n°397

Physique et Chimie des Matériaux

Spécialité Physico-chimie

COMPOSITION DU JURY :

M. NICOLAY Renaud
ESPCI Paris, le président du jury

M. CIPELLETTI Luca
Université de Montpellier, Rapporteur

M. SIJBESMA Rint
Eindhoven University of Technology, Rapporteur

M. BICO José
ESPCI Paris, examinateur

M. FAYOLLE Bruno
Arts et Métiers Paris Tech-ENSAM, examinateur

M. CRETON Costantino
ESPCI Paris, Directeur de thèse

Soutenue par Yinjun **CHEN**
le 19 Septembre 2018

Dirigée par **Costantino CRETON**

ESPCI PARIS
EDUCATION SCIENCE INNOVATION

PSL
RESEARCH UNIVERSITY PARIS

Acknowledgement

Upon the completion of this thesis, I would like to express my gratitude to those who have offered me encouragement and support during the course of my study.

First, I would like to thank the Chinese Scholarship Council (CSC) and Centre National de la Recherche Scientifique (CNRS) for their financial support, which allowed me to realize my dream of studying in France.

A profound gratitude goes to my supervisor, Costantino Creton whose conscientious manner and modest, open-minded personality inspire me both in my academic study and daily life. Thank you for your support, encouragement and offering me the opportunity to pursue my research interests. You always helped me overcome countless difficulties with your patience and profound knowledge in the field of polymer mechanics. You will always be my role model as a supervisor, which I aim to be in the future.

Also, I sincerely express my thanks to my collaborators: Professor Rong Long and his PhD student Yuan Qi who visited from the University of Colorado. Thank you for your advice and help on the construction of the strain fields.

My thanks also go to Christian Fretigny, the director of the lab SIMM of ESPCI, for his help on my application and registration to be a PhD student.

I would like to express hearfelt thanks to all the members in my jury: Professor Rint Sijbesma, Professor Luca Cipelletti, Professor Renaud Nicolay, Professor Bruno Fayolle, and Professor José Bico. I appreciate their evaluations and suggestions on my thesis.

I am glad to work with all the members of SIMM; thanks for all your help. Thank you for organizing various amusing activities, including lab weekend, board games, parties, etc. These three years will be an unforgettable time in my life

I also want to express my appreciation to all the permanent staff members for your kind help. Especially Bruno, who gave me a lot of help on the confocal microscope and the Deben micro-tensile stage tests, and Alba, who gave me great suggestions on the Instron tensile tests.

I would like to also thank all the students in the lab for their discussion, help, encouragement, and support. Especially, I wish to thank
Robert, Pierre, Hui, Menghua, Jingwen, Thitima, Ekkchai, Juillet, Ludovic, Gabriel, Francisco, Mehdi, Cécile, Alice, Valentine, Ménani, Paul, etc.
I would like to give my sincere gratitude to Josh and Artem, who worked with me

during the last year of my PhD study. With your help, I was able to perform the tough experiments and analysis.

Meanwhile, I would like to show my gratitude to my Chinese friends in ESPCI. Thank you for enriching my life in France.

I would like to extend my deep gratefulness to my family and friends, especially my parents and sister. It would have been impossible to finish my PhD journey without your support and encouragement. Thank you for your selfless love.

Finally, I am deeply indebted to my wife, Xiaoli. Thank you for your support, encouragement and patience in the past three years. Although we could not be together in France, you still supported me to finish my PhD. Thank you so much for your patience. Your love is always the source of my strength during the period of my PhD. And I love you, my sweet heart.

List of abbreviations

BA	Butyl Acrylate
BDA	1,4- Butandiol diacrylate
DMSO	Dimethylsulfoxyde
DN	Double Network
Ea	Ethyl Acetate
EA	Ethyl Acrylate
HMA	Hexyl Methacrylate
HMP	2-Hydroxyethyl-2-methylpriopiophenone
IPN	Interpenetrated Polymer Network
MC	Merocyanine
NMR	Nuclear Magnetic Resonance
QN	Quadruple Network
TMI	2,3,3-Trimethylindolenine
SN	Simple Network
SP	Spiropyran
THF	Tetrahydrofuran
TN	Triple Network
UV	Ultra Violet
RGB	Chromatic value in Red, Green and Blue channels
ΔRGB	Chromatic change

List of symbols

C_∞	Characteristic ratio for an infinite number of monomers
C_N	Characteristic ratio for N monomers
Mx	Average molecular weight between crosslinks
N_A	Avogadro's number
k_B	Boltzmann constant
E_e	Contribution of the entanglements to the Young's modulus
Ex	Contribution of the crosslinks to the Young's modulus
G	Energy release rate
$M0$	Molecular weight of a monomer
Me	Average molecular weight between entanglements
U_{C-C}	Energy of a carbon bond
Γ	Fracture energy
$\dot{\lambda}$	Strain rate
$\lambda_{correct}$	Corrected elongation
λ_0	Prestretching of the first network
λ	Stretch ratio
$W(\lambda_C)$	Strain energy density at critical strain
λ_C	Critical strain
σ_N	Nominal Stress
σ_{act}	The threshold of stress to activate SP
χ	Mixing parameter
ϕ_{SN} or ϕ	Fraction of first network in multiple network elastomers
E	Young's modulus
R	Gas constant
T	Temperature
ν	Number of elastic polymer chains per unit volume
ρ	Polymer network density
a	Length of notch
h	Thickness of sample
h_{SN}	Thickness of single network
h_{DN}	Thickness of double network
L	The distance between two black marks
L_0	Initial distance between two black marks
d	Width of sample
r_{RC}	Ratio of red channel

r_{GC}	Ratio of green channel
r_{BC}	Ratio of blue channel
Δr_{RC}	Chromatic change in red channel
Δr_{GC}	Chromatic change in green channel
Δr_{BC}	Chromatic change in blue channel
Σ_{FN}	Areal density of chains of the first network in multiple networks
Σ_{SN} or Σ_{FN0}	Areal density of chains of the first network single networks
$U_{hyst}(n)$	Hysteresis in the n^{th} each cycle
I_0	The incident light intensity
I	Transmitted light intensity
ε	Molar extinction coefficient

Table of Contents

General Introduction

Elastomers, a category of polymer materials, are widely used in engineering applications. Elastomers are appreciated due to their large range of reversible deformation even up to several hundred percent strain. Generally, elastomers are made of flexible crosslinked and highly entangled polymer chains. Simple elastomers, however, usually suffer from a trade-off between fracture toughness and stiffness. A pure highly cross-linked polymer network has a high initial modulus but is generally rather brittle. In contrast, a loosely crosslinked polymer network is extensible and possess a large range of reversible elasticity but has a lower Young's modulus.

In industry, a common approach to toughen polymer materials is to use inorganic nanofillers, including carbon black, silica, carbon nanotubes, graphene etc.. Indeed, this strategy improves both toughness and stiffness by introducing new dissipative mechanisms, which involve attachment and detachment of adsorbed chains, cavitation and breakup of the interactions between fillers. However, this approach reinforces elastomers by sacrificing the transparency and increases the density of polymer materials, which limits their application in some fields where high purity, transparency or low density may be desirable. Additionally, the approach increases the difficulty of processing for product.

To circumvent the limitations derived from using nanofiller, lots of strategies have been tried to reinforce elastomer by using pure polymer networks. The main idea is to incorporate some molecular mechanisms that dissipate energy in large deformations and delocalize the damage ahead of cracks delaying their propagation. The sacrificial mechanism, so far, includes the irreversible scission of covalent bond and the reversible break-up of supramolecular interactions. Supramolecular interactions consist of hydrogen bonding, metal-ligand, pi-pi stacking, hydrophobic interactions and electrostatic interactions. These interactions act as physical cross-links and dissociate early when a force is applied and avoid sharp stress concentrations to protect the covalent bonds in the polymer network during deformation. In addition, this process of reversible dissociation/association may extend the lifetime of polymer materials by providing self-recovery capabilities. However due to the stretching rate dependence of these dissociation processes, they greatly increase the viscoelasticity of the material. Furthermore, physical interaction are generally sensitive to the external environment (temperature, UV, nature of the main polymer…), for example, hydrogen bonding dissociates at high temperature and is less effective in more polar matrix materials, causing the material to soften. That limits the generalization of the incorporation of supramolecular interaction.

Another class of dissipative mechanisms involving the scission of overstressed covalent bonds has attracted a great deal of interest due to the lack of viscoelastic behavior and high energy dissipation per bond. An example are multimodal networks, utilizing the heterogeneity of molecular weight of polymer chains between crosslinks (short chains and long chains) to selectively cleave the carbon-carbon bonds in the short chains to dissipate energy. But the efficiency of that strategy to toughen the elastomer is not impressive.

Over the past fifteen years, a successful solution to simultaneously improve fracture toughness and modulus of pure polymer materials emerged from the field of hydrogels. Generally, hydrogels are soft and extensible or brittle and stiff. But double network hydrogels proposed by Gong's group are tough and extensible. They managed to reinforce hydrogels by interpenetrating a highly swollen and highly cross-linked polymer network (filler network) into a soft and extensible hydrogel. The improvement of the toughness derives from the breakage of covalent bonds in the filler network.

Inspired from the double network hydrogels, recently our group designed innovative multiple interpenetrated network elastomers. The objective was to extend the principle of double network hydrogels to the field of elastomers. By interpenetrating a highly pre-stretched and cross-linked network (which we will call filler network) into extensible multiple networks reinforced the elastomers. Etienne Ducrot in his PhD work has successfully proposed this strategy and applied it to increase the fracture toughness and elongation of multiple poly(methyl/ethyl acrylate) networks by at least 40 and 10 times, respectively. This strategy was then extended during the PhD of Pierre Millereau and he completely answered some additional questions, including the influence of cross-link density and degree of pre-stretch in the filler network on the mechanical properties, the failure of the filler network in extension. However, due to the absence of molecular models, the details of the macroscopic fracture mechanism at the molecular scale are still an open topic:

How is the stress or deformation distributed around the crack tip?
How many bond scissions in the filler network do occur around the crack tip before the crack propagates?
What is the length scale at which the filler network breaks and dissipates energy?
How is the stress transferred between the different networks in extension, especially,

during the necking, where large amounts of the filler network are being damaged?

To answer these questions based on experiments, the best strategy is to gain insight in the fracture mechanisms of multiple network elastomers at a molecular scale. To do so, mechanochemistry is a very good novel tool. Mechanochemistry, a new approach to initiate chemical reactions by external mechanical stimuli, was developed in the last ten years. In mechanochemistry applied to soft polymer networks, mechanically responsive groups, namely, mechanophores, are incorporated into the backbone of polymer chains. When a sufficient force is applied to the polymer chain, mechanophores can be activated and induce various signals, including color change, luminescence, fluorescence etc.. These mechanophores in general are sensitive to the force and are able to sense the force field distribution in the materials. In this manuscript, spiropyran, a mechanochromic mechanophore, is used to detect the stress distribution in multiple network elastomers by its color change during activation. The manuscript is organized as follows:

In the first chapter, diverse strategies to reinforce elastomers and different mechanophores are introduced. In addition, various macro-models or hypothesis to describe and model the fracture mechanism of multiple polymer networks are also presented and will be used as reference for our results.

The second chapter introduces the synthesis of a spiropyran mechanophore cross-linker and of mechanically responsive multiple network elastomers and describes different characterization methods for multiple network elastomers.

In the third chapter, at first, the mechanical properties of the multiple networks are examined in detail. Then the relationship between the color change of spiropyran and the stress is constructed by color analysis. A calibration curve of the chromatic change as a function of stress was obtained to map the stress distribution in the elastomers. Finally, the stress maps of different materials display the evolution of the stress field around the crack tip prior to propagation.

In chapter four, the reversible color change of spiropyran once it has been converted to Merocyanine is being discussed. We show that two different isomers of Merocyanine, with slightly different absorption spectra, can be present in the materials depending on whether the bond is loaded or unloaded. These results are then used to map the unloaded areas behind the crack tip during propagation.

In chapter five, spiropyran was incorporated into the second/third network to detect the onset of high tensile stresses in this network, which occur after the filler network is highly damaged but before the sample macroscopically breaks. Furthermore, the role of the second/third network in the resistance to crack propagation was also studied by detecting the fluorescent signal of active spiropyran.

Then in the sixth chapter, a new approach to map the strain field around the crack tip by tracking fluorescent beads was carried out and its potential to obtain accurate data was assessed.

In the seventh chapter, we discuss the results we have obtained throughout this manuscript and the perspectives which we can open up in the future to deepen the understanding of the fracture mechanism.

In the last part, a general conclusion is proposed to summarize the main achievements obtained in this manuscript and the contribution to the understanding of the fracture mechanism in multiple network elastomers.

Chapter 1- The design of robust elastomers and mechanochemistry

Introduction

A great number of approaches have been proposed by material scientists to design tough elastomers, including of course introducing nanofillers, but also introducing dynamic cross-links or interpenetrated multiple network structures. For interpenetrated multiple networks, despite numerous macroscopic theories which have been proposed to explain the mechanism of reinforcement[1-5], and which work well, a molecular model to understand the increase in toughness and the fracture is still missing. Due to the heterogeneous network[6-10], some side reactions during polymerization (including chain transfer reaction[11,12]) and polymer entanglements[11,13,14] etc., the stress and deformation in the polymer network is inhomogeneous. Thus the understanding of mechanical strength and fracture propagation in elastomers is still a challenge.

The main purpose of this work is to develop a new method to measure the stress and strain distribution near the crack tip in multiple network elastomers by using a molecular force probe.

In this chapter we first review the state of the art concerning the various strategies to improve the mechanical properties of elastomers. We present the strategies of nanofillers, supramolecular interactions and interpenetrated multiple networks to toughen elastomers.

In the second part we introduce the models of fracture propagation in elastomers, including the special case of interpenetrated double networks. We list some existent and reliable models to explain and predict the reinforcement mechanism for the interpenetrated double networks.

In the third part, we review the chemistry of diverse mechanophores, which are able to emit luminescence and to modify their absorption spectrum under mechanical activation. Being introduced in the elastomer network, these mechanophores can be used as molecular force probes.

Finally, we formulate the motivation of this thesis and the approach applied to detect the fracture in multiple network elastomers.

1. Traditional tough elastomers and multiple network elastomers

Commercial elastomers are polymer materials that possess a high range of reversible elasticity and generally a high fracture toughness. Most of elastomers consist of polymer chains and cross-linkers. They can be imaged as a flexible and extensible “fishing net” structure and their elasticity derives from their structure. The polymer chains are able to reconfigure themselves to distribute an applied stress and the covalent cross-linkers ensure that the elastomers can return to their original configuration. Due to their low density and outstanding mechanical properties at high deformations, elastomers usually are used as seals, tires, adhesives, shoe soles, etc. different applications from those of metals, ceramics or polymer glasses. The excellent mechanical properties of elastomers are due to their unique molecular and microstructure. During the deformation of the elastomer network, not only reversible deformations occur but also various dissipative processes can take place, including the scission of physical and/or chemical interactions. These dissipative processes have been shown to be essential in delaying crack nucleation and propagation and result in the improvement in stress at break and fracture toughness[4,15]. Due to the tremendous demands of application for tough elastomers, intensive researches have been carried out to reinforce them and the material structure has been shown to be the key factor of reinforcement. These structures can be mainly separated into three groups: nano-composite elastomers, supramolecular interaction elastomers and multiple network elastomers, which are shown in Figure 1.1.

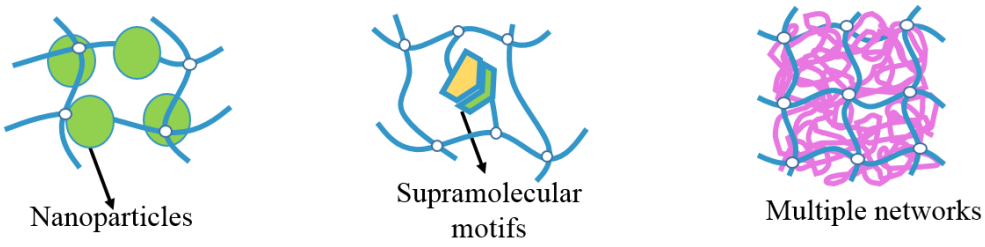

Figure 1.1: Schematic of various tough elastomers

1.1 Nano-composite elastomers

In this toughening strategy, a wide variety of nano scale fillers can be covalently or physically incorporated into elastomers. The nanofillers may have strong or weak interactions with the polymer network and they act as additional multifunctional permanent or transient cross-links. Different from chemical cross-links, the transient cross-links are mobile, and allow some chain rearrangement during loading at high strain. This leads to strong energy dissipation which will delay the nucleation of micro-cracks.

In general, diverse nanofillers have been applied to prepare tough elastomers[16], such as nanoparticles[17-20], carbon nanotubes[21], graphene[22-24] and fibres[25]. For instance, silica and carbon black nanoparticles, are widely applied in the industry for reinforcement. It has been proven that the degree of improvement of toughness by introducing nanofillers depends on the surface properties, size and volume fraction of fillers[26]. A classic example is given in Figure 1.2, where carbon black is used to reinforce the mechanical properties of natural rubber for the fabrication of tires. The reinforcement depends on the degree of aggregation of carbon black individual particles and on the interaction between carbon black and polymer chains. The aggregates of carbon black form a second network[26], as it has been originally proposed by Payne and Whittaker[27] and the filler network is weakly held together by Van der Waals' interactions. The interaction between filler and polymer chains is mainly by physical absorption. Upon deformation, the network of fillers reorganizes, which leads to high dissipation of energy. The introduction of a filler greatly increases the stress at break and fracture toughness without reducing the strain at break.

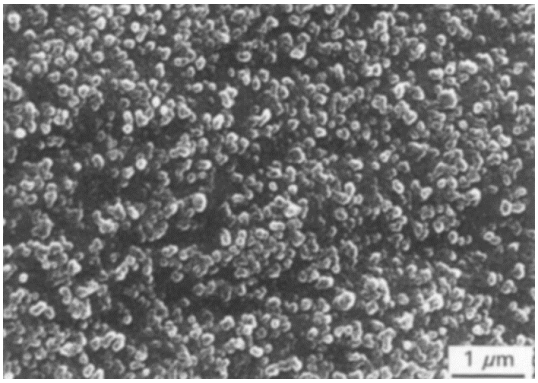

Figure 1.2: SEM photograph of carbon black in natural rubbers[28]

However, although nanofillers improve the mechanical properties of elastomers, the transparency of the materials is often lost and imposes constraints on the processing parameters and increases the density. That limits the application of polymer materials in some fields, where transparency is important. Therefore, other approaches were proposed without fillers.

1.2 Supramolecular interaction elastomers

Thermoplastic polyurethanes, a category of polyureas, are commercial and tough elastomers without nanofiller additives and have found widespread engineering application. However, their reversible elasticity is less than for conventional elastomers and when they are deformed in large strain they typically retain some residual deformation after unloading. The advantage of these thermoplastic elastomers is on the other hand their reprocessability due to the absence of permanent crosslinks.

To tune the balance or properties, one of the effective approaches has been to incorporate various supramolecular interactions into the polymer network. These segments are able to associate due to supramolecular (non-covalent) bonds, acting as transient cross-linkers. These transient ("physical") cross-linkers may coexists with permanent ("chemical") ones formed by covalent bonds. The strength of supramolecular interaction ranges between that of covalent bond and Van der Waals' interactions. For example, the dissociation energy of hydrogen bonds is about 8-35 kJ/mol and the dissociation energy for Carbon-Carbon (C-C) is 347 kJ/mol. This suggests that the physical cross-linker is non-permanent and easier to dissociate with respect to the chemical one. This leads to the increased mobility of the polymer chains linked by the physical cross-linker. Unlike the pure chemically cross-linked polymer network, the elastomers with hybrid cross-links (physical and chemical) are tough due to the transient associations and have improved resistance to crack propagation. At the same time, the presence of permanent cross-links in the same network, gives them shape memory property. Since the degree of association of the physical cross-linkers can be controlled by the external environmental conditions (temperature, light, etc.), it opens the way to synthesize stimuli responsive elastomers.

According to the literature published in last two decades, supramolecular interactions commonly used in polymer materials can be separated into four categories (Table 1.1): hydrogen bonding, metal-ligand interactions, host-guest interactions and π-π interactions etc. The following sections show examples of materials based on each type of interaction.

Table 1.1. Types of supramolecular interactions used for the elaboration of tough elastomers

Supramolecular type	Examples	Interaction	References
Hydrogen bonding	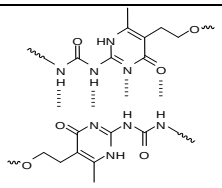	Multiple hydrogen bonding	30-33
Metal-ligand	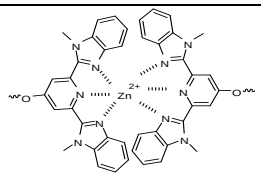	Coordination bonds	34-36
Host-guest	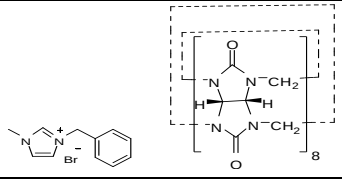	Electrostatic interaction Or Hydrophobic interaction	38
Other kinds	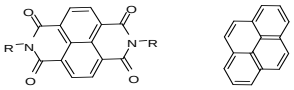	π-π stacking interaction	41,42

1.2.1 Hydrogen bonding

Hydrogen bonding is an electrostatic attraction between a hydrogen atom and electronegative atoms, such as nitrogen, oxygen or fluorine. Nitrogen and hydrogen elements are present in proteins, DNA, glycogen etc. natural products, where they induce strong hydrogen bonding interactions and are responsible for the formation of multilevel structures and double helixes. In order to imitate biological processes, various hydrogen-bonding moieties can be introduced in the polymer chains. For instance, Meijer et al.[29-31] designed and synthesized the ureidopyrimidinone (UPy) group, which is a quadruple hydrogen bonding unit. Two UPy groups are able to assemble to form dimers. When UPy groups were incorporated into the polymer chains as endgroups, each two UPy units coming from different polymer chains were able to aggregate into UPy dimers, which was called supramolecular polymerization. In addition, the polymer chains can self-assemble into fiber structures by forming dimers stacks as shown in Figure 1.3b. Similar to nanocomposites, the fibers remarkably improve the mechanical properties, which leads to solid-like behavior of materials with UPy while non-modified polymers behave as a liquid (Figure 1.3a).

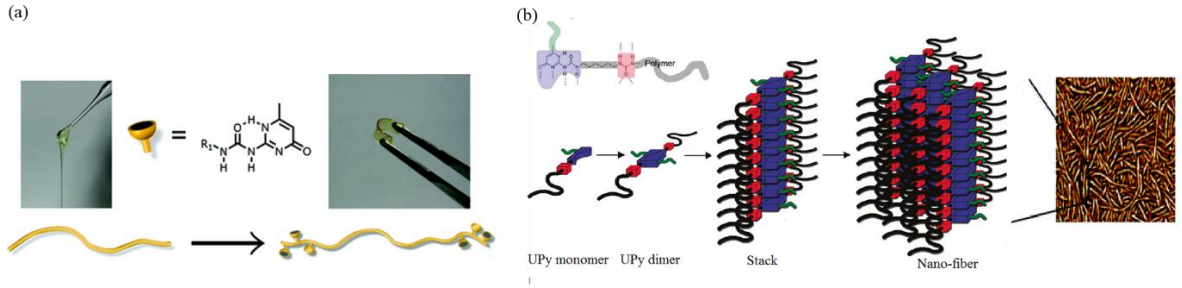

Figure 1.3: (a) Behavior of polymer materials before and after modification by UPy moieties. (b) AFM image of polymer materials with UPy moieties[31,32]

Utilizing the same hydrogen bonding moieties, Guan et al.[33] synthesized a cyclic UPy core and converted it to a terminal diolefin monomer, which was further used to prepare polymer materials (Figure 1.4). Compared to the brittle control sample without hydrogen bonding motifs in the main chains, the polymer exhibits a rare combination of high modulus and high toughness resulting in the dissipation of the dissociation of hydrogen bonding. Additionally, it also shows other properties, including self-healing and shape memory. They demonstrated the first biomimetic modular polymer materials displaying a great combination of high toughness and modulus. Moreover, the polymer exhibits self-healing and shape memory behavior.

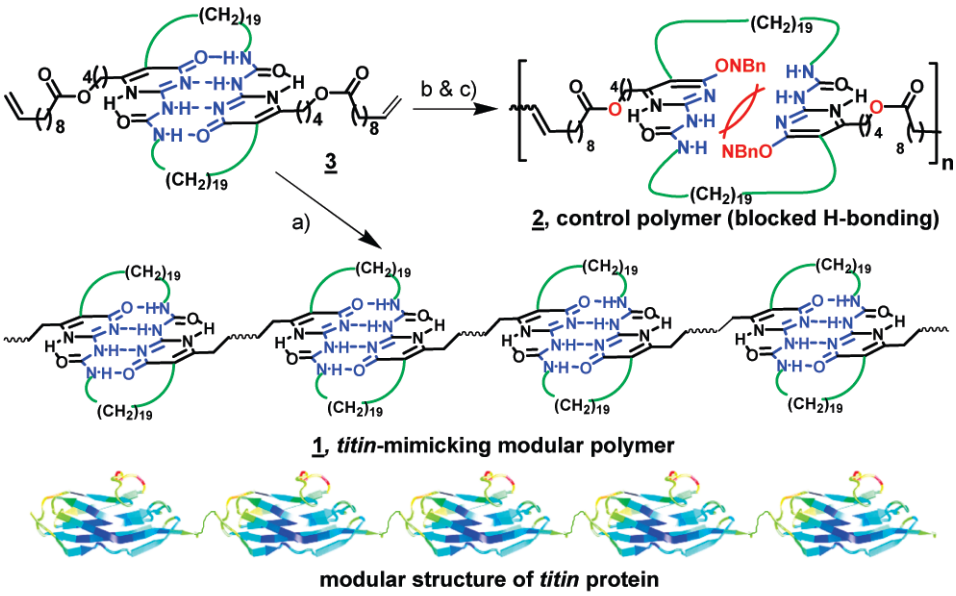

Figure 1.4: Aggregation of UPy dimer in the polymer chains and imitation of titin protein[33]

1.2.2 Metal-ligand interaction

Generally， a metal-ligand interaction describes the coordination complexes between a transition metal and π-donor ligands. The ligand acts as a donor of an ion pair to the metal *d* orbitals and the metal center can form multiple coordination bonds. The coordination bond can be very stable but still responsive to light, solvent or heat. These stimuli will cause temporary dissociation of the metal-ligand motifs. When the ligand is covalently coupled into the end group of the polymer backbone, the polymer undergoes supramolecular polymerization through metal-ligand interaction. On the other way, if the ligand is located in the middle of the polymer chains, metal-ligand association will act as physical cross-linkers by forming intermolecular cross-links or intramolecular loops.

Rowan et al.[34,35] modified 2,6-bis(1'-methylbenzimidazolyl) pyridine (Mebip) ligands at the end of poly (ethylene-co-butylene) chains. These end-functionalized materials showed good mechanical properties and also showed efficient defect healing under ultraviolet light. Figure1.5 illustrates how low molecular weight polymers with ligand end groups are cross-linked through metal-ion binding and form a polymer network. Under a transmission electron microscope (TEM), the materials show a pronounced microphase separation.

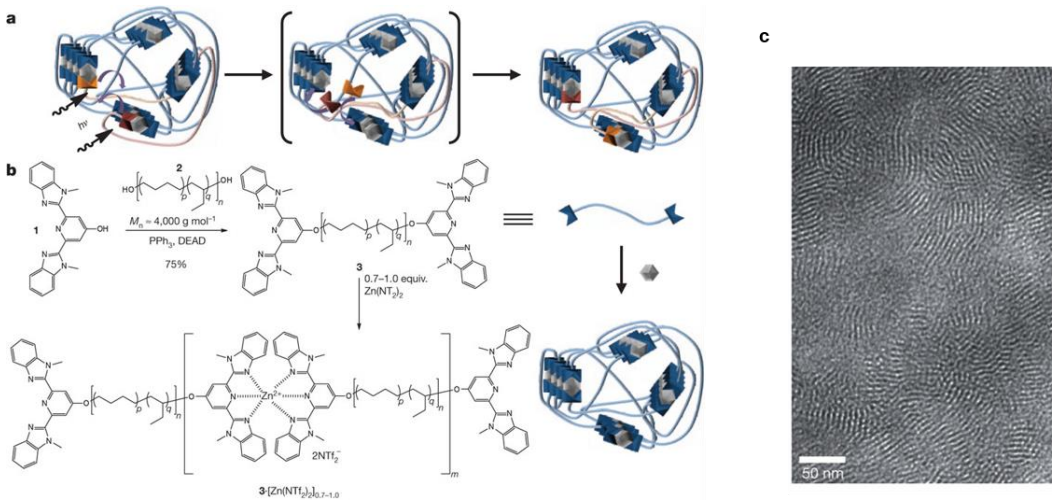

Figure 1.5: The association of Tridentate ligand 2,6-bis(1,2,3-triazol-4-yl)pyridine modified on the terminal of polymer chains and TEM image of resulting phase separation[35].

Extensive studies of metal-ligand super-molecular interactions have been carried out on poly(urethane) by Weng et al[36]. The tridentate ligand 2,6-bis(1,2,3-triazol-4-yl)pyridine was incorporated into the polymer backbone to prepare ligand macromolecules. Upon coordinating with transition metal ions (Zn^{2+} and Eu^{3+}), the materials show a rare combination of high modulus, good toughness and high deformability and self-healing capability in the presence of solvent (Figure 1.6).

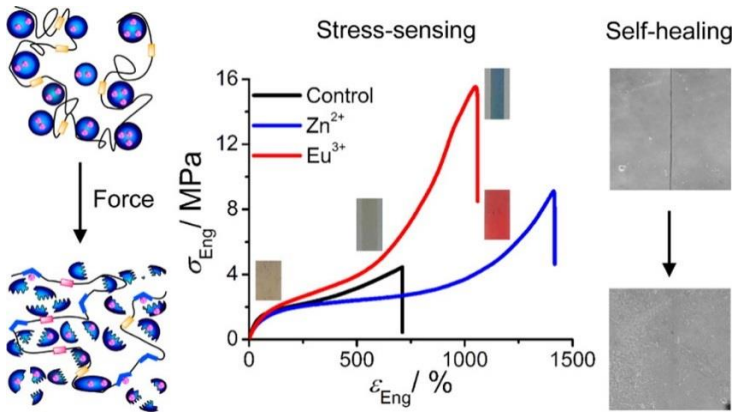

Figure 1.6: Reinforcement and self-healing of polyurethane by metal-ligand interactions[36]

1.2.3 Host-guest interaction

Host-guest interaction is another class of supramolecular associations, where one component are host molecules and the other component are guest molecules. Typical host molecules are cyclodextrins, crown ethers, pillararenes and cucurbiturils etc. cyclic molecules forming a large cavity and guest molecules mainly including some ammonium salt frequently possess a

cationic group[37]. This two categories associate to form complexes. They are often utilized to form a supramolecular binding motif and serve as a tool for the fabrication of various self-assembled structures, such as micelles, nanotubes nanorods, nanosheets and vesicles[37]. If the functional groups are introduced in the polymer chains, they can act as non-covalent supramolecular cross-linkers upon complexation. Moreover, the association is controlled by experiment conditions (temperature, pH, ionic strength). This dynamic and reversible properties of host-guest interactions brings excellent stimuli-responsive features to the resultant elastomers.

Due to their advantages described above, Scherman et al[38]. covalently grafted cucurbit[8]uril on the side chains of a loosely cross-linked polymer network. In this system, the host-guest interaction was used to form sacrificial bonds which improved the fracture resistance, fatigue resistance and energy dissipation, which was achieved by the dynamic disassociation/re-association of the cucurbit[8]uril complexes (Figure 1.7).

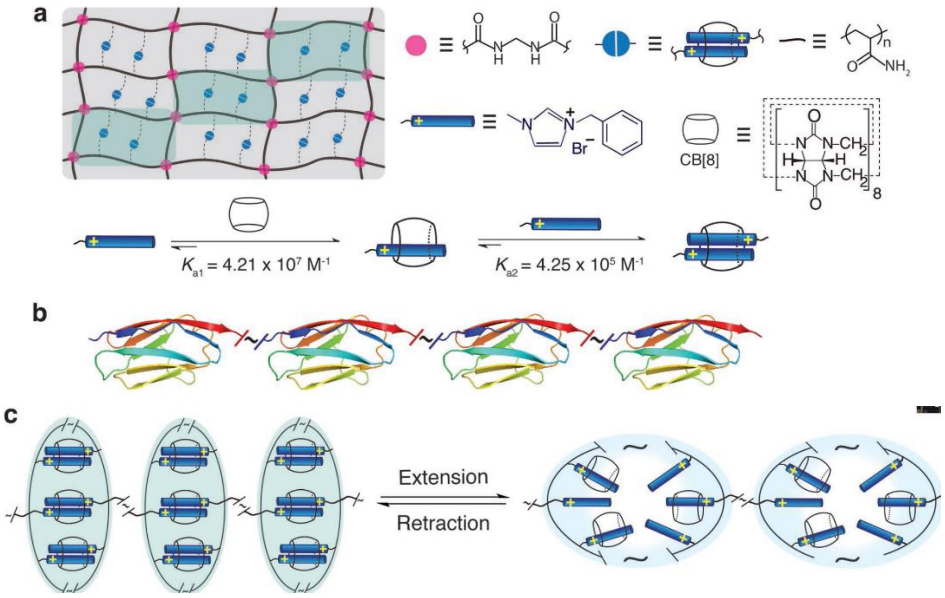

Figure 1.7: (a) Schematic of a modular dual network composed of host-guest interactions and chemical cross-linkers; (b) a typical modular section of titin structure; (c) schematic of mechanical induced dissociation of CB[8] host-guest complexes[38].

1.2.4 Other kinds of super-molecular interaction

Phase separation interaction and π-π stacking interactions are another two types of supramolecular interactions which have been used in polymer materials in the past few decades. These interactions trigger supramolecular assembly. They produce a variety of well-aligned anisotropic structures[39], such as fibers, spheres, cylinders and lamellae etc. which form ordered micro-phase structures at longer range. These secondary structures enhanced

toughness of elastomers. Weng and his coworker[40] fabricated different PnBA-PS-PnBA triblock copolymers and adjusted the length of PS to tailor the mechanical properties of elastomers. Suitable length of polymer chains allows them to assemble into a spherical structure, which improves the toughness of these thermoplastic elastomers.

Using on the π-π stacking interaction of pyrene derivatives, elaborated polymers have been synthesized by Colquhoun, Rowan and their coworkers[41]. The polymer chain-segment is composed of two naphthalene-diimide unites, as shown in Figure 1.8a. When they increased the concentration of naphthalene-diimide units, it resulted in a progressive increase in binding constant of 2 orders of magnitude. Furthermore, an unexpected enhancement of toughness and self-healing ability was observed when the naphthalene-diimide units were separately incorporated into two polymer chains as illustrated in Figure 1.8b.

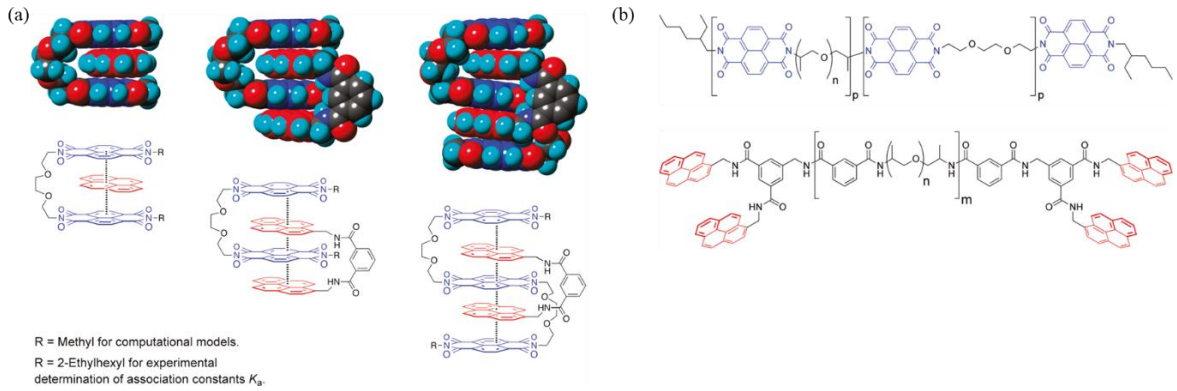

Figure 1.8: (a) Scheme representation of π-π stacking supramolecular interaction; (b) polymer containing naphthalene-diimide units on the backbone [41]

Many additional studies about π-π stacking interaction, hydrogen bonding, metal-ligand etc. supramolecular chemistry have been carried out more recently and the last several decades have witnessed great progress in the utilization of supramolecular interactions to control self-assembly and architecture of tough elastomers[42]. However, these supramolecular elastomers are generally strongly viscoelastic due to the dynamic association of supramolecular interaction making it difficult to obtain fully reversible elasticity and fatigue toughness.

1.3 Multiple networks

In the previous section, we described some approaches to develop tough elastomers through the incorporation of nanoparticles to form nanocomposites and the use of supramolecular or coordination chemistry to obtain self-healing properties. In this section we present an alternative approach to make unfilled elastomers with minimal viscoelasticity but a higher

toughness through network design. In this type of approach covalent bonds are used as 'sacrificial bonds'. Here, the term of sacrificial bond means that during the extension of the polymer network a fraction of the covalent bonds in the polymer network are overloaded (through network design) and can rupture and dissipate energy before the macroscopic failure of the material occurs. Compared to supramolecular interactions, the rupture of embedded covalent bonds can dissipate more energy per bond due to their higher bond association energy but typically cannot be easily reformed.

In this section, we present several approaches to design the networks in order to introduce such sacrificial bonds (Table 1.2). First, we will introduce the concept of bimodal networks which is known from the end of last century. Next, we present a general reinforcement strategy using the double network structure which was first invented for hydrogels. Finally, we focus on the extension of this method to multiple network elastomers developed by our group to synthesize soft but tough materials.

Table 1.2. Different kinds of polymer networks

Types	Bimodal networks	Double networks	Multiple networks
Scheme	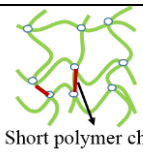	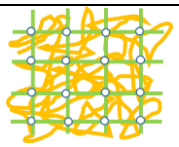	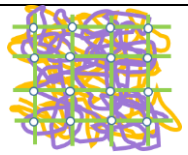
Examples	Mark's group[43]	Gong's group[44]	Creton's group[15]
Mechanical property	Brittle	tough	Robust

1.3.1 Bimodal networks

Monomers, oligomers, and cross-linkers are used to synthesize polymer networks by various polymerization reactions. In non-controlled types of polymerizations of networks, the molecular weight of the polymer chains between two neighboring cross-links varies significantly due to side reactions or to the random activation and termination of the polymerization reaction. When only one kind of monomer and cross-linker are used in polymerization (or when they possess similarly reactivity), the distribution of the length of polymer chains between two cross-links is unimodal. When the polymer network is submitted to an external stress, the shortest chains and more extended chains in the polymer network break first. These chains are considered to be the 'culprits' in causing fracture of elastomer materials by nucleating macroscopic defects.

The term bimodal network means an elastomer with two populations of polymer chain length between the cross-links. For the population of short chains, it is easy to reach their maximum elongation and their rupture dissipates efficiently the energy. In principle if both populations were bicontinuous, the bimodal polymer network should perform as a tough material. For example, a PDMS bimodal network was synthesized by Mark et al[43]. They polymerized two

kinds of PDMS precursor polymers with different chain lengths with alkoxy and hydroxyl (or vinyl) end-groups, respectively. The bimodal polymer networks were prepared through the chemical reaction between alkoxy and hydroxyl end groups. Adjusting the ratio of short /long polymer chains, they compared a series of bimodal network elastomers (Figure 1.9). However the desired significant reinforcement of the ultimate properties and of the fracture toughness was not very large compared with the unimodal network. This was presumably due to the fact that the short and long chains phase separate and form distinct regions.

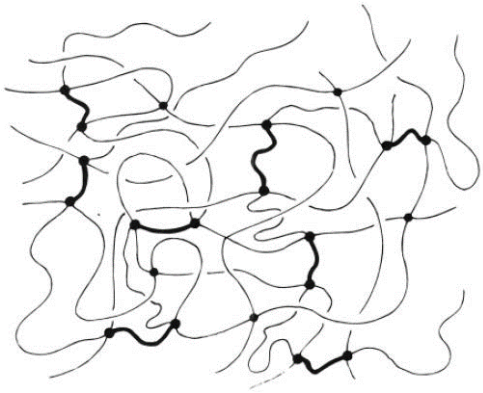

Figure 1.9: Schematic of bimodal network in which the short chain are drawn in heavier[43]

More recently, Cohen et al[45,46]. utilized vinyl-terminated precursor chains with average molecular weights of 800-8500-91000 g/mol and a tetrakis(dimethylsiloxy)silane cross-linker to synthesize trimodal networks. Compared with the unimodal networks with a similar modulus, the trimodal networks achieved a higher toughness and elongation at break (Figure 1.10), but these networks are still too brittle for industrial applications. Therefore, other strategies to design covalent networks are desired to achieve significant improvement of the fracture toughness of "unfilled" elastomers.

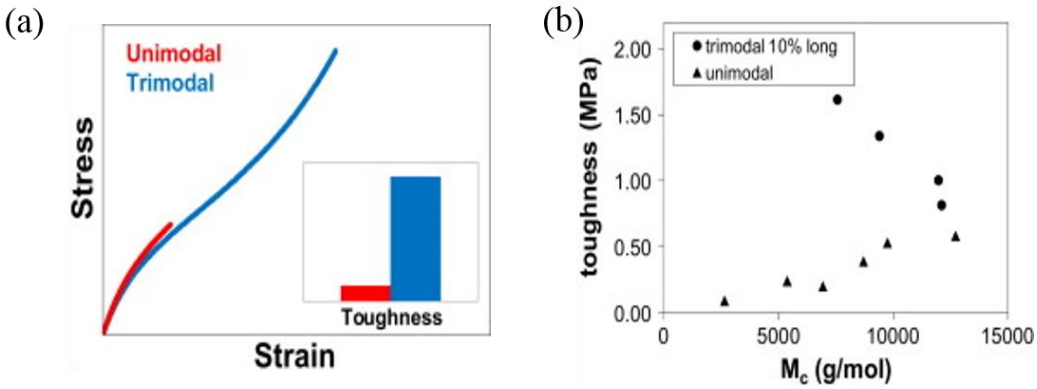

Figure 1.10: (a) The schematic view of stress-strain curves of unimodal and trimodal networks; (b) the toughness of trimodal and unimodal networks as a function of molar mass between effective cross-linker[45]

1.3.2 Double network hydrogels

Hydrogels, have attracted a great interest in the past few years due to their potential use for artificial soft tissues. Conventional hydrogels are composed of a single network of hydrophilic polymer swollen in water and are usually very brittle, like fragile jellies, which may seriously restrict the application. This is particularly true in applications in which the mechanical properties are essential, such as articular cartilage, semilunar cartilage, tendons and ligaments and other connective tissues.

During the last decade, a great breakthrough has been achieved by Gong's group[44] in the design and synthesis of a particular class of tough hydrogels defined as double networks (DN) hydrogels. A double network hydrogel is a heterogeneous network (IPN) consisting of interpenetrated polymer networks synthesized sequentially (Figure 1.11), which is different from a conventional hydrogel. A DN hydrogel typically contains 80-90 weight percent of water, yet its toughness is comparable to that of conventional unfilled elastomers. The tough DN hydrogels were synthesized for the first time in 2003 by Gong and her coworkers using two sequential steps of photo-polymerization[44]. At first, a densely cross-linked polyelectrolyte (poly(2-acrylamido-2-methylpropanesulfinic acid (PAMPS)) network was synthesized by a UV-initiated polymerization carried out at a very slow polymerization rate in the glove box, and then this single network was swollen by a neutral monomer (acrylamide) solution containing a very low concentration of cross-linker and initiator. When the single network was swollen to equilibrium, a double network was obtained by performing a second UV-polymerization on the swollen PAMPS single network. The swelling in the second step caused the densely cross-linked first network to become isotropically stretched and to almost reach the maximum extensibility of the polymer chains between two cross-linkers. Therefore, the first network is stiff and the second network is soft and extensible because of its low chemical cross-link density. According to Gong's research, the essential features of tough DN hydrogels are due to the structure and the mechanical properties of first and second network[6], which can be summarized into three points as follows:

(1) The mechanical behavior of the first network is stiff and brittle, such as that of a highly stretched polyelectrolyte. On the contrary, the second network is soft and ductile such as an unstretched neutral polymer.
(2) The second network forms the majority of the DN hydrogel (about 90%).
(3) The DN possesses a highly stretched first network and a loosely cross-linked second network.

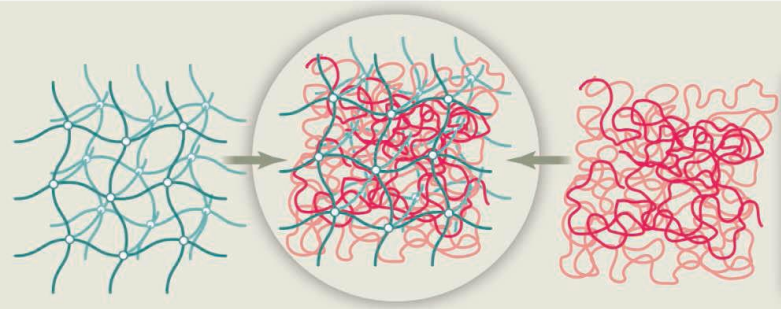

Figure 1.11: The schematic view of the interpenetrated double network hydrogels[47]

Following these principles, a series of tough DN hydrogels with various compositions were prepared by Gong's group. For instance, the DN hydrogel of PAMPS/PAAm shown in Figure 1.12. Here, PAMPS, PAAm and PAMPS/PAAm stand for poly (2-acrylamido-2-methylpropanesulfonic acid), polyacrylamide and double network, respectively. The materials were tested in uniaxial compressive and tensile tests. PAMPS/PAAm DN showed much higher stress and strain at break compared to PAMPS and PAAm gels. Compression data illustrates that highly cross-linked PAMPS is brittle as expected. On the other hand, loosely cross-linked PAAm is soft and can be highly deformed. Whereas DN of PAMPS/PAAm remains quite extensible but shows obvious strain hardening leading to high stress at break. Figure 1.12b illustrates that the PAMPS gel is brittle and breaks during the compression process, while the DN gel is tough and is able to sustain a stress of 17.2 MPa under compression despite the presence of 90 wt% of water.

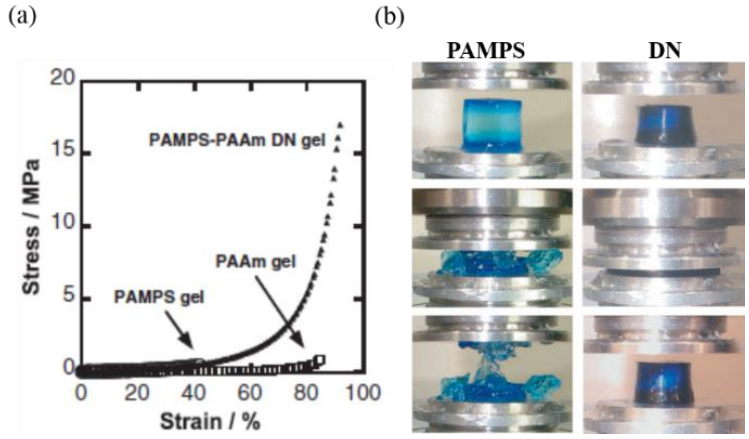

Figure 1.12: (a) The compression stress-strain curves of hydrogels including PAMPS, PAAm and DN of PAMPS-PAAm; (b) The images of PAMPS and DN of PAMPS-PAAm under compression[44]: PAMPS, SN gel, breaks easily and PAMPS-PAAm DN gel can sustain up to λ=75%.

Figure 1.13 shows the uniaxial extension test performed on a of PAMPS/PAAm DN hydrogel.[6,44] For this sample, one observes a necking process which leads to two strain

hardening regimes. The presence of a necking extends the maximum strain of the DN before rupture. In cyclic loading, when comparing the first and second cycle, the DN shows a large hysteresis and after the first cycle the sample becomes fairly soft, because of an internal fracture of the first network embedded in the DN. Based on the results obtained by small angle neutron scattering (SANS), the neutron scattering pattern from the DN hydrogels in the deformed state is anisotropic. Thus it is assumed that in the necking area the first network ruptures into numerous clusters which play the role of physical cross-linkers for the second network. The details of the fracture mechanism of the DN will be discussed in the next section.

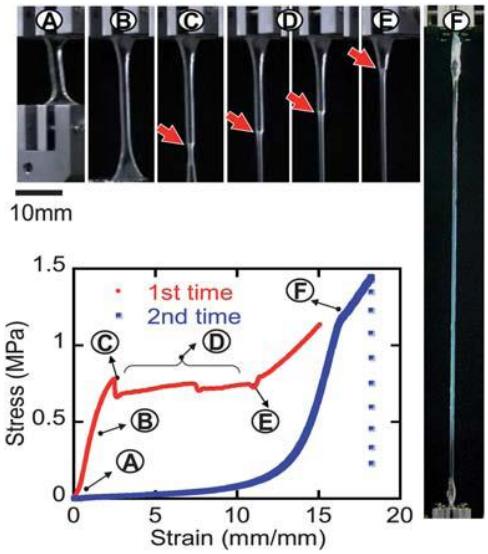

Figure 1.13: The necking process of DN hydrogels during the stretching process[6]

The fracture of polymer networks usually starts by the breakage of the shortest chains. In order to avoid this effect, Sakai and Gong et al.[7] prepared a well-defined "homogeneous" first network using an end-group reaction (Figure 1.14a), similar to the synthesis of bimodal elastomers by Mark[43]. To ensure the swelling ratio of the first network made from a neutral polymer, a "molecular stent" method was proposed for the synthesis of tough DN[48]. The molecular stent method is a technique to synthesize tough DN hydrogels based on a neutral first network. In this technique, linear, strong polyelectrolyte chains or ionic micelles are introduced in the neutral first network[48]. Comparing the nominal tough DN hydrogels made from a heterogeneous first network, with this DN hydrogel made from a more homogeneous first network, both possess almost the same toughness, but a different initial modulus and hysteresis ahead of the necking region as shown in Figure 1.14b. The difference in the hysteresis is due to the better homogeneity of first network. Before yielding, the DN with a homogeneous first network shows much less evidence of fracture of polymer chains. This also leads to a lower reduction of the Young's modulus after yielding in cyclic loading tests.

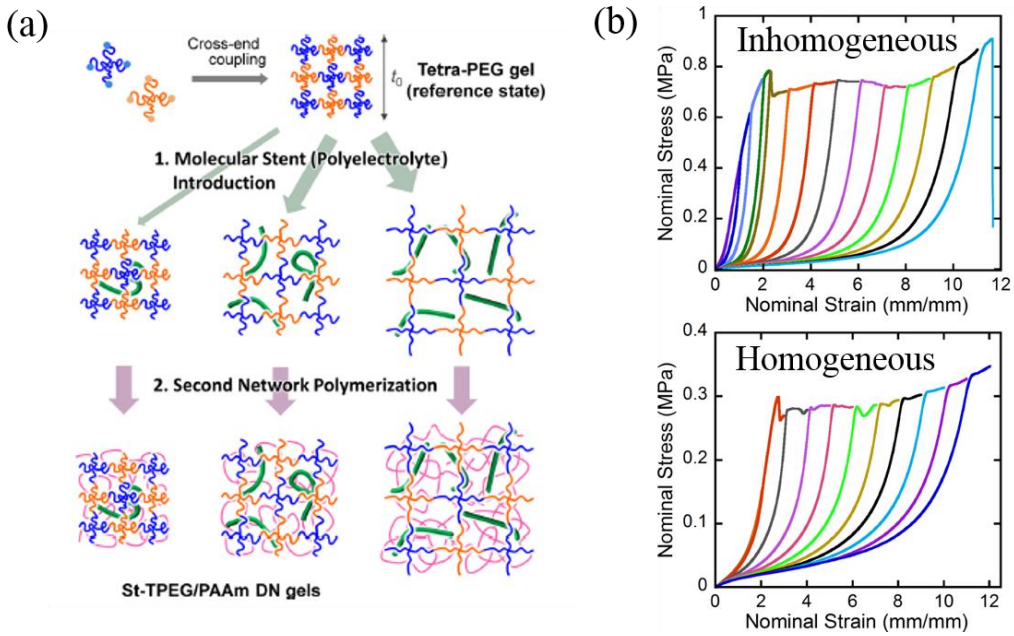

Figure 1.14: (a) The schematic of the synthesis of DN hydrogel with homogeneous first network; (b) the stress-strain curves of homogeneous and inhomogeneous DN hydrogels[7]

The interpenetrating DN concept is a powerful approach to toughen hydrogels and is promising for other materials. In the next section we present the interpenetrated multiple network elastomers proposed by Ducrot and Creton[15] in our group.

1.3.3 Multiple network elastomers

Inspired by the interpenetrated network of DN hydrogels, our group developed a new approach to prepare tough elastomers by using interpenetrating multiple networks without solvent. Different from previous double network elastomers made by Mark[49], Yoo[50], Baysal et al.[51], multiple network elastomers possess a highly pre-stretched first network, which is usually constituted of short, stretched polymer chains with a high cross-link density. Etienne Ducrot[52] and Pierre Millereau[11], two doctors who graduated from our group, studied the effect of the first network on the mechanical properties of elastomers. In Figure 1.15a, a significant improvement in Young's modulus, the stress at break and toughness is observed for the multiple networks elastomers. The results indicate that this approach is promising to make tough elastomers. Furthermore, the elastomers toughness increases with the number of interpenetrated polymer networks. Figure 1.15b shows the mechanical performance of DN elastomers with different cross-link densities of the first network, and the results further indicate the critical relationship between the mechanical properties of elastomers and cross-linker density of the first network. The more densely cross-linked is the first network and the higher is the Young's modulus.

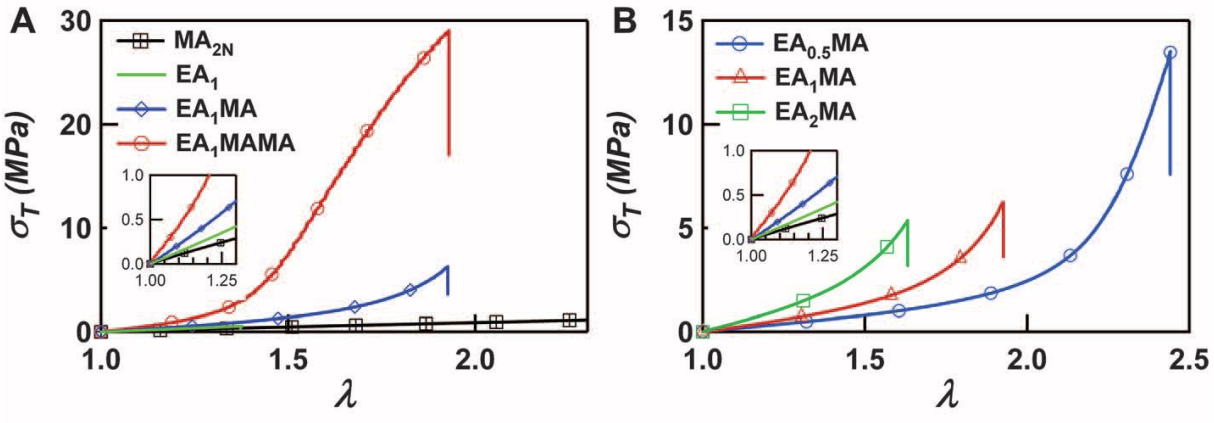

Figure 1.15: (a) The stress-strain curves of interpenetrated multiple network elastomers; (b) the stress-strain curves of DN elastomers with various cross-linker density in the first network[15]

Pierre tailored the level of pre-stretch in the first network by using some solvent during the preparation of the second or additional networks. The results of the extension tests illustrate that elastomers become more and more robust (Figure. 1.16) with a high modulus and fracture toughness. Moreover, although the same monomer composition is used between the first network and the other networks (second, third network), all the elastomers have outstanding mechanical properties. The comparison of the results suggests that the reinforcement of multiple network elastomers originates mostly from the pre-stretched polymer chains in the first network which can fail without a macroscopic breakage of the whole material.

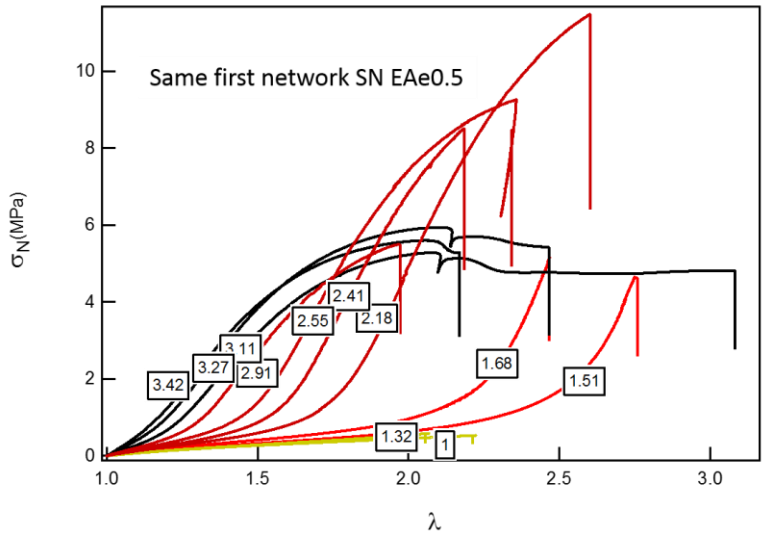

Figure 1.16: The stress-strain curves of multiple network elastomers with different pre-stretch in the first network[11].

In this section, we described how the concept of DN hydrogels can be extended to the reinforcement of elastomers. A difference with hydrogels is that we developed multiple steps of swelling and polymerization (as opposed to only two) and showed that even if the same or

similar monomer was used to prepare the first and second networks, the enhancement in the mechanical properties for multiple network elastomers is still particularly significant.

2. Theory of crack propagation

The fracture of elastomers is difficult to model and the fracture energy is currently very hard or impossible to predict from the knowledge of its molecular structure alone due to the presence of entanglements and the heterogeneity of the polymer network. There are a large proportion of theories that are proposed based on an ideal polymer network structure as the Lake-Thomas model. Recently, several models were constructed to explain and predict the reinforcement of DN hydrogel, as listed in Table 1.3. Thus in this part we introduce several theories about the calculation of the dissipated energy during crack propagation.

Table 1.3. Introduction of various model applied in DN gels

Names	Lake-Thomas model	Brown's model	Tanaka's model
schematic	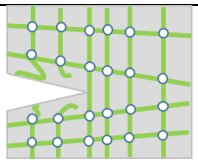	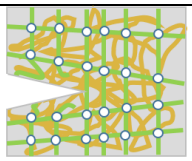	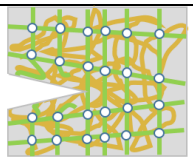
Equations	$\Gamma = 2 * \Sigma N U_{C-C}$	$\Gamma_{global} = \frac{4 * \Gamma_1 \Gamma_2}{(\lambda_m - 1) E_2 \Delta b}$	$\Gamma_{global} = \Gamma_2 + \sigma_c \varepsilon_c h$
Application conditions	ideal polymer network	double networks	double networks
Dissipation energy(J/m^2)	10	400	100

(Γ: fracture energy; Γ_1, Γ_2: toughness of the first and second network in DN; N: number of monomer between two neighbor cross-linkers; $\sum$: areal chain density of chains crossing the fracture plane; $U_{c\text{-}c}$: the energy of C-C bond; E_2: Young's modulus of the second network; λ_m: the maximum strain of the second network; Δb:the width of micro-crack; σ_c: the critical stress of yield; ε_c: the critical strain of yield.)

2.1 Lake-Thomas model

The classical Lake-Thomas model[2] predicts the threshold fracture energy in an ideal homogeneous single polymer network. Figure 1.17 shows schematically a polymer chain composed of N monomers between two cross-linkers located at the crack tip. During the crack propagation along the dotted plane, all the polymer chains crossing the plane are being cut. The minimum energy to break a bond is the bond energy. However, the key idea in the Lake and Thomas model is that all the C-C bonds in the polymer strand between two cross-linkers irreversibly lose their energy as the strand breaks and contribute to the dissipation of energy.

Assuming that these bonds are stretched to the same level as the broken one, the fracture energy Γ_c of one polymer strand equals to $2NU_{c\text{-}c}$, where 2N is the number of C-C bond between two cross-linkers and $U_{c\text{-}c}$ is the energy of C-C bond. The factor of 2 means every monomer contributes two C-C bonds for the strand. In addition, the areal chain density $\sum$ which is the bulk density of polymer strands ν times the average distance between strands d divided by two, can be calculated by Eq. (1), where E, C_∞, a, k_B and T are the Young's modulus, the structure factor of the polymer chain relating end-to-end distance with number of monomers, the length of C-C bond, the Boltzmann constant and temperature, respectively.. Therefore, the total fracture energy can be calculated by Eq. (2).

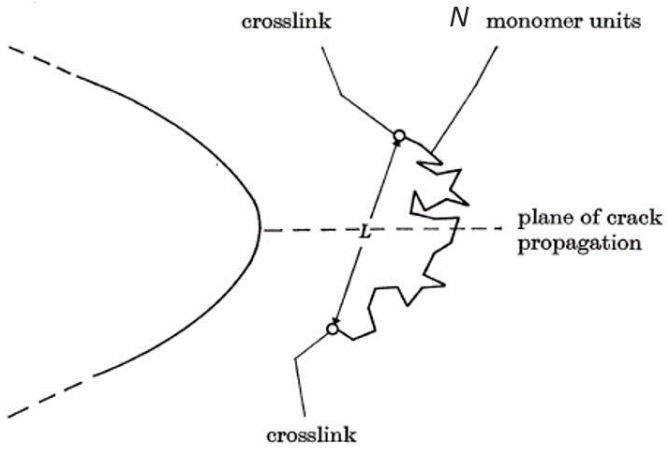

Figure 1.17: Schematic of a polymer chain across the plane of crack propagation

$$\Sigma = \frac{aE\sqrt{C_\infty N}}{6k_BT} \qquad \text{Eq. (1)}$$

$$\Gamma = 2 * \Sigma N U_{C-C} \qquad \text{Eq.(2)}$$

In this model, it is assumed that the fracture energy is only dissipated by the breakage of covalent bonds in the fracture plane and that before crack propagation the polymer material is elastic. However, in the DN or in real networks there are mechanisms of energy dissipation in the bulk, which may lead to a distinct hysteresis in a cyclic loading[6]. For instance, DN gels described above show significant hysteresis in the first cycle loading. Recently, Creton et al.[9] discussed the deviations observed for DN elastomers from the Lake-Thomas model. Figure 1.18 shows a sketch of the heterogeneous structure of the real single network. It is likely that the shortest polymer strands near the crack tip break first in the cross-linked regions. Therefore, when a crack propagates through this structure the flaw probably follows the shortest strands distribution in densely cross-linked regions instead of a straight and defined plane. In this process, more bonds are likely to break and a larger energy can potentially be dissipated.

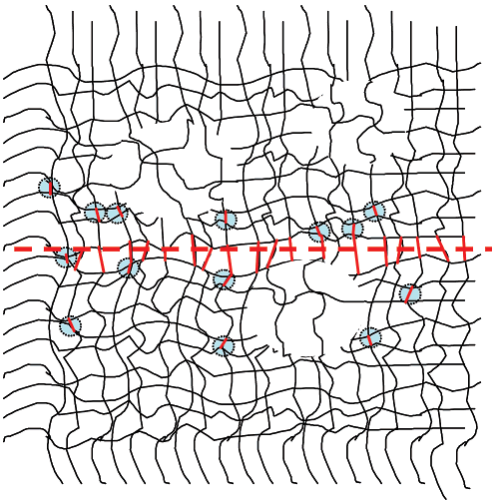

Figure 1.18: Schematic of a heterogeneous network with a plane (dashed line) of fracture and circles showing the preferential fracture of short strands

Although the Lake-Thomas model is inapplicable by itself for DN gels, it defines the process of crack propagation and provides an estimate of the minimum tear energy for a polymer material.

2.2 Brown's model

To quantify the reinforcement in the fracture energy due to the DN special structure, several attempts have been carried out[1,3,4,53]. Such as the molecularly based model proposed by Hugh R. Brown (called Brown's model) targeted at explaining the necking in DN hydrogels. This model[1] is based on the Lake-Thomas theory but includes the number of strands caused by the enhancement of the distinctly unusual DN microstructure. In this model crack propagation occurs in two stages. First, the stiff and brittle first network breaks under the external stress due to its high degree of stretching and dense cross-linking density. This happens before necking and leads to the formation of internal micro-cracks. The Brown microcrack is imagined with a defined length "a" and width "Δb", as shown in Figure 1.19 and the space inside it, is bridged by the second network strands to retain the continuous structure of the sample. If we assume the second network to be linearly elastic, the strain energy release rate G can be calculated from the far field average stress "σ" by Eq. (3)

$$G = \Delta b\sigma/2 \qquad \text{Eq. (3)}$$

The maximum width of the micro-crack should be of the order the contour length of the strand in the second network. This means a contour length of 3 μm typically contain about 10000 repeating chain units for a PAAm second network. For a first network with the toughness Γ of 0.5 J/m^2, Eq. (3) gives a critical stress value of 0.3 MPa to nucleate a micro-crack, which is very close to the experimental value of 0.2 MPa for the necking stress.

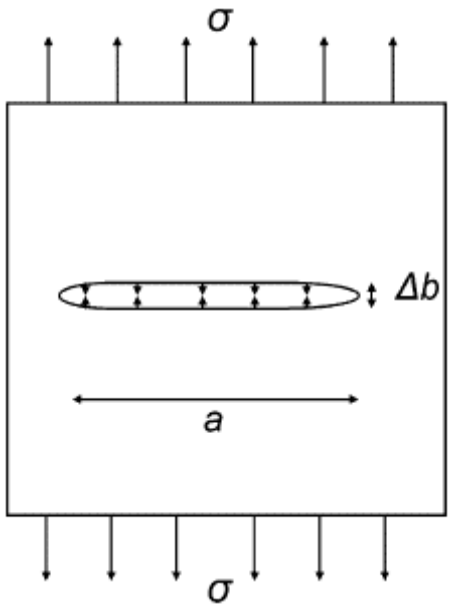

Figure 1.19: Schematic representation of a micro-crack in the first network of a DN[1]

The second step is a crack propagation in the second network which leads to the failure of sample. When the external stress increases above σ, more micro-cracks are formed in the region around the crack tip, as shown in Figure 1.20a. In this region, the elastic properties of the material is similar to those of the second network because of the strong damage of the first network in this zone. This zone has a much lower modulus E_2, when compared with the zone far away from the crack tip, where the modulus E_1 is mainly controlled by the undamaged first network. As a consequence, when the crack propagates within the second network, it can be modeled as a pure shear fracture. During this second step the critical strain energy release rate Γ' can be given by Eq. (4).

$$\Gamma' = \mathrm{h}(\lambda_m - 1)^2 E_2/2 \qquad \text{Eq. (4)}$$

Where "h" is the unloaded width of the damage zone, $\boldsymbol{\lambda}_m$ is the maximum deformation of the second network. In this assumption, Brown deduced the total toughness of DN using the Eq (5), where Γ_1 and Γ_2 are the toughness of first and second network, respectively. Brown also estimated the reinforcement of the DN compared to a single network to be a factor of about 40, which agrees with experimental results obtained by Gong et al.[54] Moreover, a similarly damaged region around the crack tip was also observed in the experiment by Gong's group [55]shown in Figure1.20b.

$$\Gamma_{global} = \frac{4*\Gamma_1\Gamma_2}{(\lambda_m - 1)E_2\Delta b} \qquad \text{Eq. (5)}$$

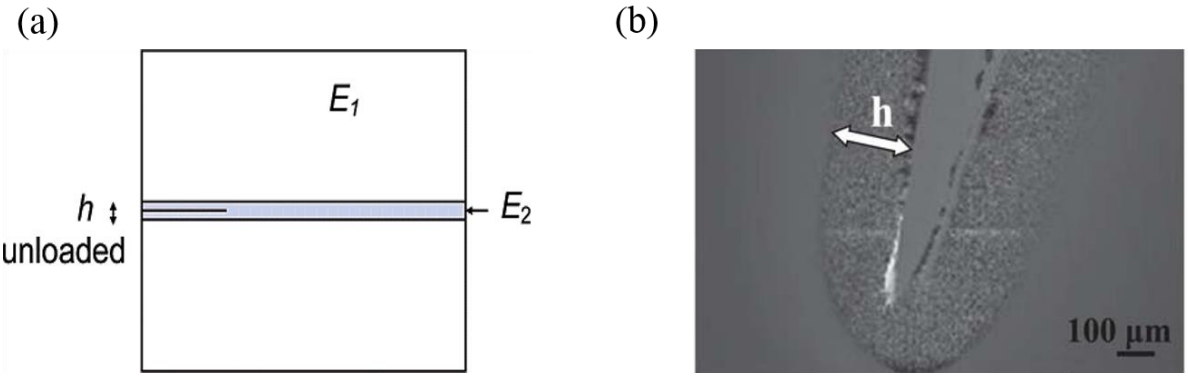

Figure 1.20: (a) Geometry of the damaged region around the crack tip[1]; (b) the image of the damaged region near the crack tip captured on DN hydrogel using a laser scanning microscope[55]

2.3 Tanaka's model

Brown's model considered the crack propagation at the molecular level. In the same year, Tanaka[3] proposed another analogous but macroscopic model aiming to explain the reinforcement due to the necking phenomenon observed in extension. The model assumes a damage zone over a thickness h formed around the crack tip and is located on both sides of the fracture surfaces after propagation (in Figure 1.21a). There is a sharp boundary between the damaged and undamaged regions. The damaged boundary is defined by the principal tensile stress corresponding to the necking in extension. Assuming that the intrinsic fracture energy of the damaged zone is Γ_0, the size of damaged zone can be defined as $h = \Gamma_0/U(\sigma_c)$, where $U(\sigma_c)$ is the elastic energy density of the uniform stretching at the critical stress σ_c. Due to the fracture of the first network, Γ_0 is approximately equal to the intrinsic fracture energy of the second network. To estimate the fracture energy, the cyclic uniaxial tensile test curve is simplified as shown in Figure 1.21b. The segment OA corresponds to the elastic region before necking and the segment AC represents the softening process of materials due to the damaging of the first network. Upon unloading the damaged material, the stress follows the curve OBC. The area surrounded by the curves OACB is the irreversible work dissipated by the breakage of the covalent bonds in the first network and can be estimated to be $\sigma_c*\varepsilon_c$, where ε_c is the strain at the point C. Considering the dimension of damaged zone, the total irreversible work is $\sigma_c \times \varepsilon_c \times h$. The global fracture energy consists of two parts: the intrinsic fracture energy of the second network and the irreversible work. It is given by Eq. (6).

$$\Gamma = \Gamma_0 + \sigma_c \varepsilon_c h = \Gamma_0 \times (1 + \frac{\sigma_c \varepsilon_c}{U(\sigma_c)}) \qquad \text{Eq. (6)}$$

It should be noted that the fracture energy can be given by the intrinsic fracture Γ_0 and a dimensionless enhancement factor. In the calculation, the softened zone is regarded as the second network and the intrinsic fracture energy Γ_0 can be calculated by the Lake-Thomas

theory. In addition, the elastic energy density U(σ_c) can be deduced from the modulus of the stiffened region after damage as $U(\sigma_c) \cong \sigma_c^2/E_{st}$, where E_{st} is the stiffened modulus from the BC curve (Figure 1.21b).

Tanaka's estimate of the fracture energy is about 100 J/m^2, which is consistent with Gong's results (400 J/m^2). Because of the heterogeneity of the first network, additional damage produces a pronounced necking. That gives rise to a larger irreversible work compared to $\sigma_c \times \varepsilon_c \times h$. As a consequence, this model is appropriate to estimate the order of the effective fracture energy of the DN gels.

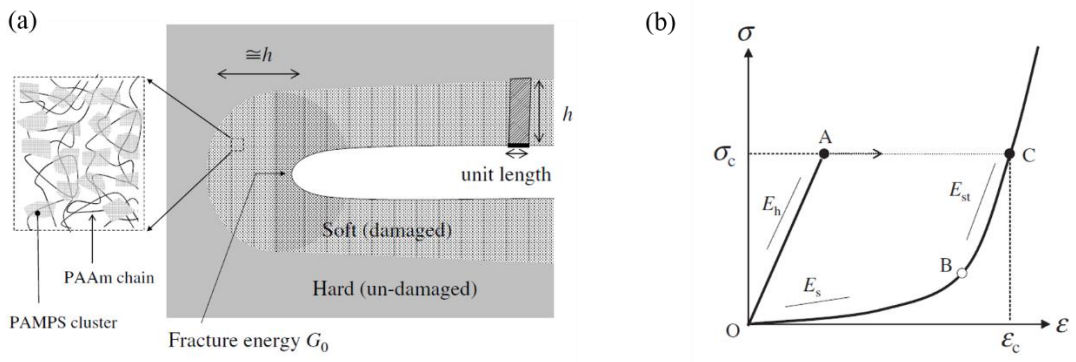

Figure 1.21: (a) Schematic representation of the locally damaged zone at the crack tip of DN hydrogels; (b) Assumed stress-strain curve for the undamaged (OAC) and damaged zones (OBC) of DN hydrogels[3]

2.4 The fracture mechanism of multiple network elastomers

A great amount of experimental work has been carried out to explore the mechanism of reinforcement of multiple network hydrogels and elastomers including the investigation of the effect of the monomer composition, cross-linker concentration, degree of heterogeneity of the first network, pre-stretch and entanglement density of the first network, cross-linker density in the second network, etc. In the following we summarize the main experimental results and the main conclusions we can draw so far:

Multiple network hydrogels (Gong's and Creton's groups):

(1). Gong group[14] summarized that the entanglement in the second network was essential for tough DN hydrogel with a second network of linear chains. In addition, they found that the lower the cross-linker density in the second network, the tougher DN hydrogel (in 2005).
(2). Creton Brown and Gong et al.[9] demonstrated that the hysteresis was due to internal breakage (in 2007).

(3). Gong et al.[9,13,14,47] speculated that at the yield point, the first network fractured into clusters which subsequently acted as physical cross-linkers of the second network (Figure 1.22), the polymer strands of the second network sustaining then most of loading (in 2010).
(4). Gong et al.[7] considered that before the macroscopic yield some bonds will rupture which makes the first network more homogeneous, and assumed that the yielding process was due to a large numbers of covalent bonds breakage in the first network and created heterogeneities in swelling ratio inside the damaged gel (based on the result of small angle neutron scattering) (in 2013).
(5). Gong et al.[6,7,54,56] proved that heterogeneity in the first network is not the origin of reinforcement but is important for mechanical strength (in 2013).

Multiple network elastomers (Creton's group):

(1). Ducrot et al.[15] confirmed by incorporating mechanoluminescent molecules that during uniaxial elongation tests the first network of multiple network elastomers, fractures first, (in 2014).
(2). Ducrot et al.[52,57] observed the fracture of the first network around the crack tip before propagation and verified that the fracture of the first network reinforced the toughness of multiple network elastomers (in 2014).
(3). Young's modulus of multiple network elastomers is controlled by the cross-link density of the first network[57] (in 2016).
(4). Millereau et al.[11] demonstrated that the pre-stretch in the first network is an essential factor for tough multiple network elastomers[11] (in 2017).

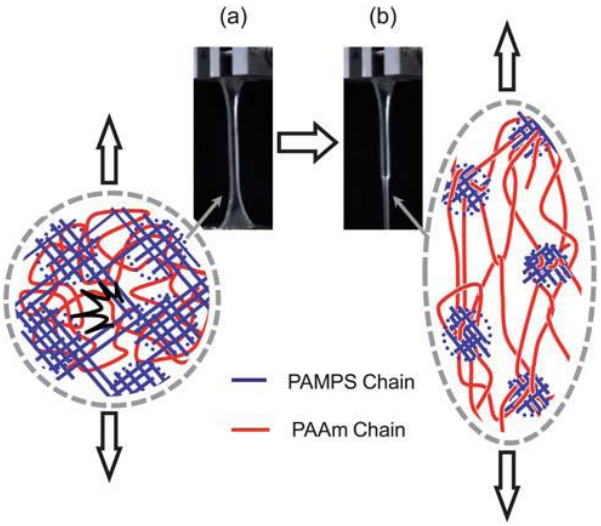

Figure 1.22: The schematic of the fracture mechanism in the necking regions of the DN hydrogel

In summary, comparing to the previous elastomers studied by Yoo[50] and Baysal et al[51]. , interpenetrated multiple networks provide a significant improvement in the Young's modulus,

stress at break and fracture toughness. The reinforcement derives from the stretched first network and the scission of polymer chains in the first network dissipates a great amount of energy. Assuming that the first network fragments into small clusters, these clusters may play a role of physical cross-links for the second network. Thus the physical cross-linkers could slide in the second network in response to deformation and adjust the polymer chain length between cross-linkers in the second network. This homogenization process delays in turn the nucleation of cracks.

2.5 Finite element model

Recently, Zhao et al[4]. proposed a finite element model based on the experimental data in cyclic uniaxial tension to predict the fracture energy for tough DN gels. Similar to the two models above, they also separated the contribution of the overall fracture toughness Γ into two parts. The first part is called the intrinsic fracture energy Γ_0 and should in principle characterize the scission of polymer chains localized at the crack tip. The second part arises from the integral of the damage of each material point of the entire specimen called dissipative fracture toughness Γ_D. Figure 1.23a shows the deformation history of a material element in a process zone around the crack as the crack propagates (the zone is called damaged region in other models). In this process, as the crack propagates, it changes the deformation distribution of the system and leads to a loading and unloading hysteresis of each material point which results in energy dissipation Γ_D (Figure 1.23b). Consequently, the total fracture energy is expressed as Eq.(7).

$$\Gamma = \Gamma_0 + \Gamma_D \qquad \text{Eq. (7)}$$

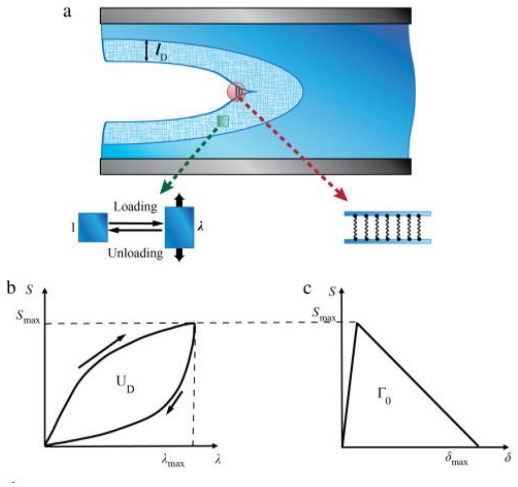

Figure 1.23: Schematics of theory and model for crack propagation in soft tough materials. (a) crack propagation under a pure-shear test; (b) the mechanical dissipation in the cyclic loading is characterized by a macroscopic damage called Mullins effect; (c) the intrinsic fracture energy of the soft material (at the interface) is characterized by the area under the triangular traction separation law

In order to calculate the fracture energy, Zhao combined a triangle cohesive-zone for Γ_0 (Fig. 1.23c) and a damage model[58] to predict the intrinsic fracture energy Γ_0 by subtracting the dissipative energy Γ_D done on the materials, from the total fracture energy. After fitting the uniaxial data to an Ogden model, they used an empirical equation to estimate Γ_D, and were able to quantitatively predict the experiments by adjusting the value of Γ_0. This model verifies that the fracture toughness of a soft material can be enhanced greatly by incorporating stiff sacrificial bonds and long stretchy polymer network, which consistent with the principles of the fabrication of tough DN hydrogels.

So far, there has been lots of attention on modeling the mechanical performance of tough multiple network gels. Several insightful theories for the origin of the high fracture energy have been proposed. Among them, Brown's and Tanaka's models are regarded as the most promising ones even if they are quite simplified. Yet the real damaged regions and fracture energy are still larger than the predictions and the models are not able to explain or predict the onset of crack propagation quantitatively. Development of better molecular models will clearly require experiments providing molecular information on the fracture process.

3. Mechanochemistry

3.1 Introduction

In recent years, mechanochemistry has attracted a great deal of interest, since it connects the comprehensive investigations spanning molecular and macroscopic scales[59-62]. Mechanophores, i.e. mechanically sensitive chemical groups, contain some weak covalent bonds which are able to selectively break under external mechanical stimuli and exhibit a change in chemical structure in response. Of particular interest for us are those that combine this change in chemical structure with an optically detectable response (color change, luminescence and fluorescence etc.) as shown in Scheme1.1.

When mechanophores are covalently fixed in the polymer backbones, the force loading the polymer materials can transmit to mechanophores through the polymer chains. Mechanophores can then be activated by an adequate force which is usually lower than the threshold scission force of C-C bonds. If the bond scission or activation gives an optical signal, these mechanophores can act as labelled molecules to detect the variation of stress and deformation in materials. Activation of optically active mechanophores induces a change in optical properties such as color, fluorescence or mechanically induced luminescence. These distinctive signals can be used for in situ quantitative evaluation of polymer chain scission and detection of stress, especially around the crack tip. Such molecular information may then be used to develop molecular models of fracture.

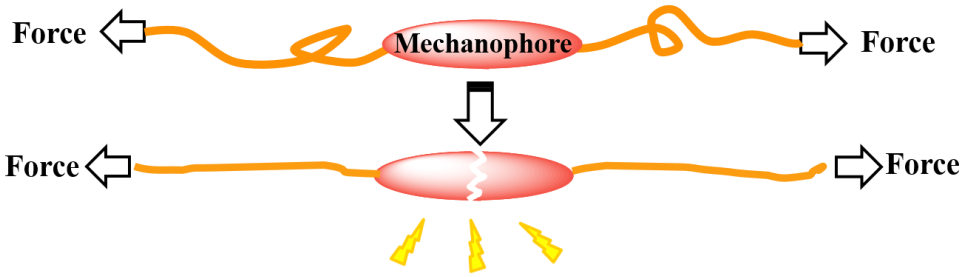

Scheme 1.1: The activation of mechanophore under an external mechanical stimuli

3.2 Optically inactive mechanophores

Before we focus on optically responsive mechanophores let's briefly discuss mechanophores in more general terms.

According to the type of chemical reaction produced by mechanical activation. mechanophores, can be classified into two types: scission type (homolytic cleavage[63], dative bond scission[64] and cycloreversion[65]) and nonscission type (electrocyclic ring opening etc.). Figure 1.24 shows various mechanophores used in the field.[66] For instance, Sheiko et al.[67] reported the activation of disulfide bond located in the centre of brush-like macromolecules which were deposited on a substrate. The adsorption of brushlike macromolecules onto the substrate generates the intramolecular tension due to steric repulsion between densely grafted side chains. The authors tuned the force in the main chain by varying the substrate surface or brush structure and observed the mechanical activation of the disulfide bonds through the length distribution of brush molecules. Xu and his co-workers[68] developed another polymer composite in which a platinum-acetylide complex mechanophore was incorporated into the polymer backbone. The mechanophore in the polymer chains could be activated by sonication in solution and released catalytically active platinum species to catalyze the olefin hydrosilylation process. The mechanical response of platinum-acetylide was investigated by detecting the conversion of olefin hydrosilylation of 1-octene with ^{1}H-NMR. This work shows an example of the use of mechanical activation to initiate the catalysis of the chemical reaction. Recently, Xia and Martinez et al.[69] reported the transformation of insulating polyladderene to semiconducting polyacetylene by a mechanochemical stimuli. This confirms that mechanochemistry is a promising tool to convert mechanical stimuli into a diverse array of chemical functions. However, the mechanical response of the mechanophores described above is not easy to directly observe since the signals of the mechanical response do not have any optical signature. In general, this type of mechanical response needs other setups for the characterization. This strongly limits the application of these mechanophores in the study of the fracture of polymer materials.

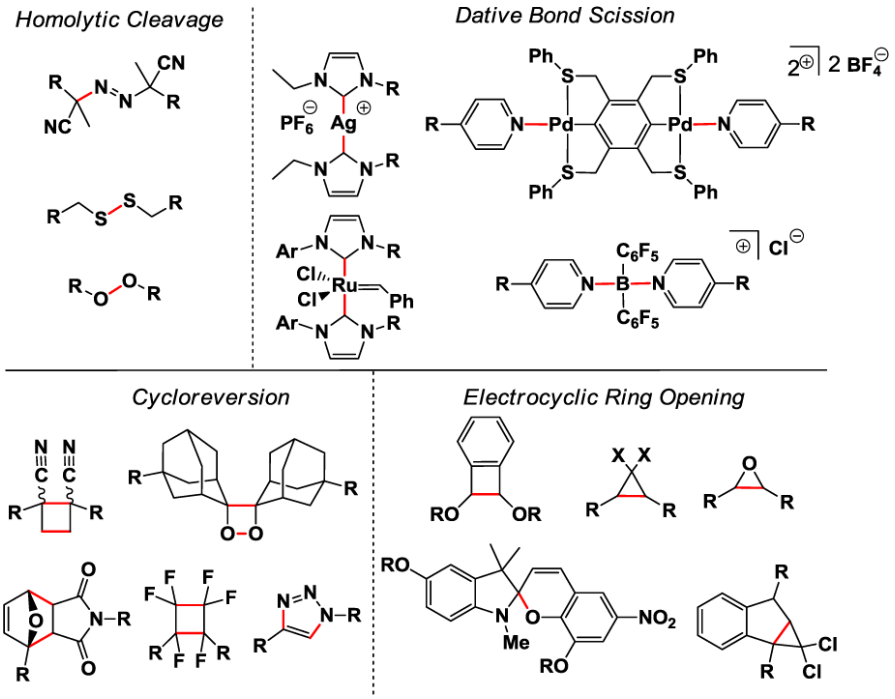

Figure 1.24: Various types of mechanically induced reaction in mechanophores[66](the red bonds in these molecules are the weak bonds and easy to break under the mechanical stimulation)

3.3 Optically active mechanophores

In this part, we will introduce mechanophores that provide visual and optical signals after activation, when they are covalently coupled into the polymer backbone or network. These polymer materials can be separated into two groups depending on the signals they display[70]. One group is constituted of mechanochromic polymers, which present a change in light absorption in the visible range resulting in a color change before and after mechanical stimuli. Another class are mechanoluminescent polymers. All the mechanophores are shown in Table 1.4.

Table 1.4. Different kinds of mechanophores present in this manuscript

Species	Examples	Mechanical response
Mechanofluorescent polymers	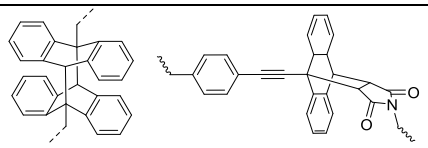	Dimer of anthracene: red fluorescence π-extend anthracene: blue fluorescence
Mechanoluminescent polymers	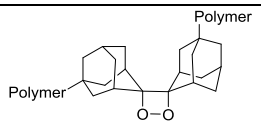	1,2-Dioxetane: bright blue light
Mechanochromic polymers	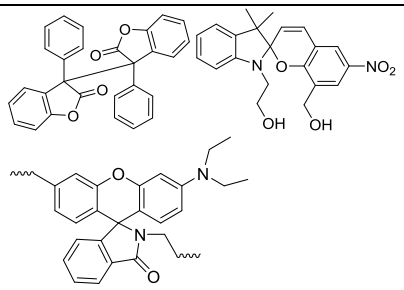	Diarylbibenzofuranone: yellow to blue Spiropyran：colorless to purple Rhodamine:dark red

3.3 Mechanoluminescent polymers

Mechanoluminescent polymers include mechanofluorescent polymers and mechanochemiluminescent polymers. The difference between them is that mechanofluorescent polymers need optical excitation to emit fluorescence after activation.

3.3.1 Mechanofluorescent polymers

Bare anthracene is frequently used as a fluorescent probe in biology. When its conjugated electronic system is extended (π-extended anthracene (Figure 1.26)), it possesses a higher quantum yield of fluorescence. If the anthracene participates in a Diels-Alder reaction, the Diels-Alder adduct loses the ability to fluoresce. Using this feature, Chung et al.[71,72] incorporated a dimer of anthracene into the polymer backbone. In the tear experiment, the materials emitted a fluorescent signal around the crack (Figure 1.25). Similar approach was employed by Sijbesma and Heut et al.[73]. They synthesized an amphipathic block copolymer by the Diels-Alder reaction of anthracene and maleimide (Figure 1.26). The amphipathic block copolymer self-assembled into micelles and promoted the mechanochemical reaction of the Diel-Alder adduct.

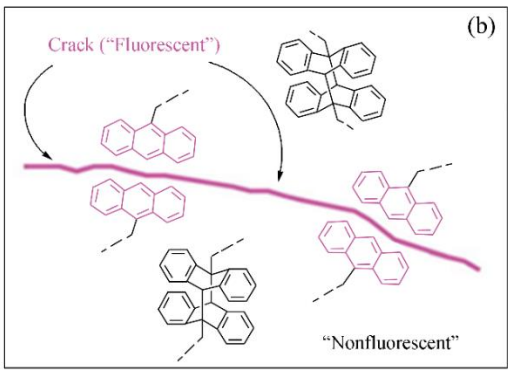

Figure 1.25: Scheme of mechanical cleavage of the dimer of anthracene leading to fluorescence near the crack[72]

Furthermore, in order to increase the fluorescence quantum yield, Sijbesma and coworkers designed a π-extended anthracene shown in Figure 1.26a and then incorporated it into the centre of the polymer backbone[74]. Under compression, the materials emitted intense fluorescence. So far this is the first report to be devoted to the reinforcement of the intensity of the mechanical response by extending a conjugated electronic system.

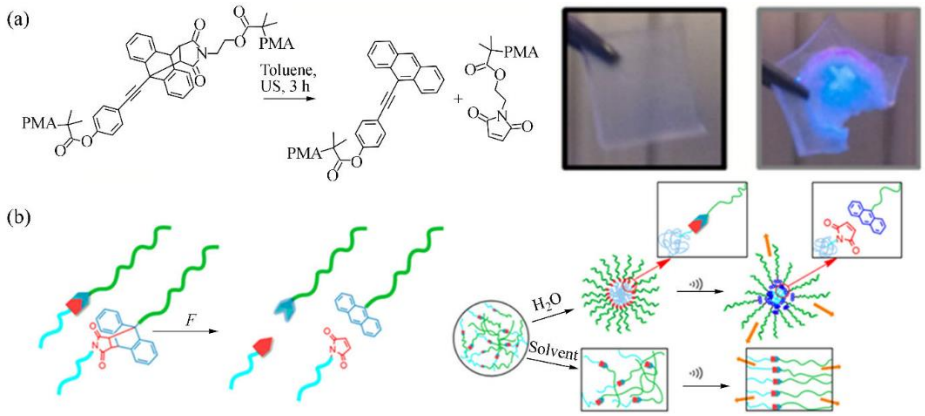

Figure 1.26: (a) Scission of anthracene adduct and fluorescent signal before and after compression; (b) Scheme of the activation of the anthracene adduct and the self-assembling process by hydrophobic interaction

3.3.2 Mechanochemiluminescent polymers

Mechanochemiluminescent polymers emit luminescence responding to external mechanical stimuli. Comparing with mechanofluorescent polymers, the advantage of chemiluminescent polymers is their autoluminescent nature, so that no excitation light source is required. The field of chemiluminescent mechanophores is very limited and the recent progress of this field is mostly due to Sijbesma and his co-workers[65]. In 2012 they reported a 1,2-dioxetane mechanophore, which is a highly-energetic and thermally labile molecule. When it is

activated in polymer chains by mechanical force, the square cycle with the O-O bonds breaks and generates two ketones, one of which is in the excited state and emits bright blue luminescence when it relaxes to the ground state (Figure 1.27a). The emission wavelength of the luminescence is located at 420 nm, hence it is possible to directly see the fracture regions of polymer materials in the tensile test by the naked eyes. Moreover, the mechanophore can transfer the energy to other fluorescent accepters by Forster resonance energy transfer (FRET). This can be used to further enhance its efficiency and to tune the emission color. These excellent properties promote the application of 1.2-dioxetane mechanophore to the study of polymer fracture behavior and the thermoplastic elastomers failure[18,75].

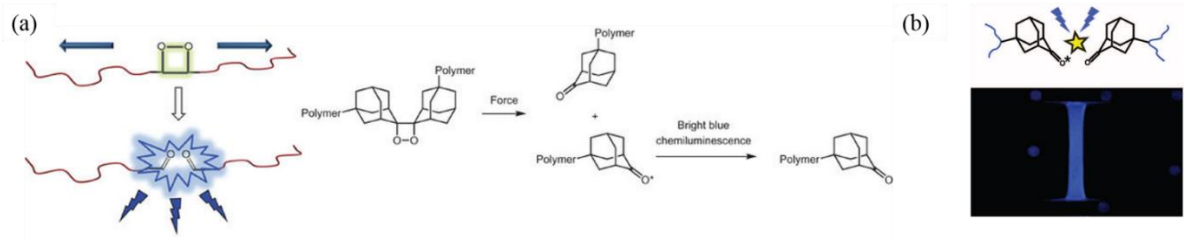

Figure 1.27: (a) The schematic representation of the activated process of 1, 2-dioxetane mechanophore[65]; (b) the image of a sample containing activated 1,2-dioxetane[15]

Recently, the 1,2-dioxetane mechanophore was used as a molecular probe to study the damage and failure mechanism in soft polymer materials as reported by Creton and Sijbesma[15] in 2014. 1,2-Dioxetane was incorporated as a cross-linker into the first network of tough multiple network elastomers. In extension, the stress transmits along the polymer chains to the 1,2-dioxetane and activates the mechanophore in the highly pre-stretched first network. As shown on Figure 1.27b, the triple network elastomers show a strong luminescence under loading. Comparing the single, double and triple network elastomers, the difference of the intensities of the luminescent signal can be used to interpret, at least qualitatively the reinforcement mechanism of multiple network elastomers. First, multiple network elastomers emit luminescence during uniaxial tensile test. That proves that the first network used as a filler undergoes bond scission to dissipate energy. In addition, in Figure 1.28 the luminescence illustrates that a great fraction of the scission of polymer chains takes place in the first network around the crack tip. Moreover, the region of luminescence region in triple network elastomers (damaged region) is larger than for the double networks. This demonstrates that the fracture of the first network reduces the stress concentration and delays the crack propagation and the final failure of elastomers. A more exciting thing is that it is the first time that the spatial distribution of broken bonds ahead of crack tip is mapped by mechanochemistry.

An important point is the lifetime of the luminescence. It is only 20 nS after the scission of 1,2-dioxetane mechanophore and the activation is irreversible. In addition, the weak blue luminescence demands a relatively dark environment. All of these demand rigorous

requirements for the sensor. Furthermore, the polymer chains connecting with 1,2-dioxetane relax after the activation due to the scission type mechanophore of 1,2-dioxetane, which is a disadvantage for the construction of a model by simulation. The 1,2-dioxetane has however a good potential as a molecular probe for the time-resolved damage in polymer materials. However, the immediate character of the luminescence and the relatively low emission intensity makes it unsuitable for static observations such as confocal microscopy or for fatigue experiments where a small damage as a function of time needs to be monitored.

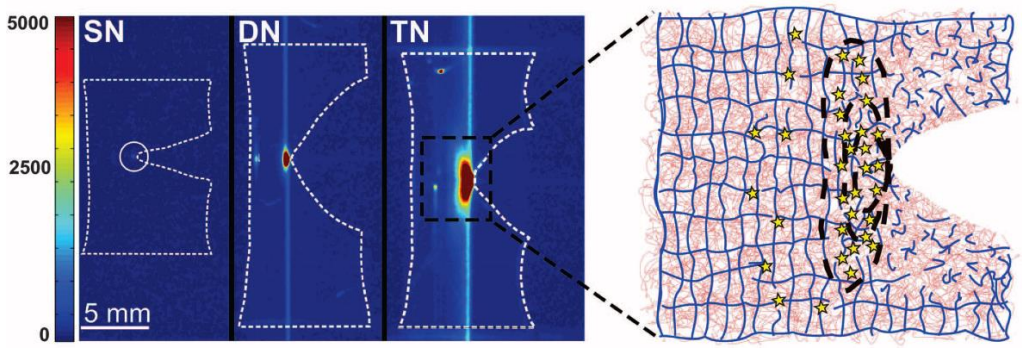

Figure 1.28: The distribution of luminescence intensity due to bond breakage around the crack in the multiple network elastomers[15]

3.4 Mechanochromic polymers

Distinctly different from mechanoluminescent polymers, mechanochromic polymers display a more stable (and reversible) response to mechanical activation by changing their color. Owing to the visible signal of color change, it is more convenient and feasible for mechanochromic polymers to sense and map molecular forces and from these the stress distribution in polymers.

The first mechanophore used in polymer research is spiropyran (SP). In 2009, Moore's group[76] was the first scientist to covalently incorporate SP into the polymer backbone of poly(methyl acrylate) and to demonstrate its color change upon mechanical stress as shown in Figure 1.29a. SP can transform into merocyanine (MC) by applying a force or UV light. This reaction was accompanied by a color change from colorless to purple. Furthermore, if the molecule is not broken but simply unloaded, the MC is able to return to its original configuration SP and the color will disappear again. Moore et al. used a SP derivative as the initiator to prepare poly(methyl acrylate) by controlled free radical polymerization or as a cross-linker to synthesize poly (methyl methacrylate) networks. In elongation tests, the color of these materials turned from colorless to red as shown in Figure 1.29b. Since then the SP was widely applied in the study of mechanical properties of polymer materials. Weng et al

used SP as a tool to study the effect of supramolecular interactions on the mechanical behavior of polyurethane[36,77-79]; Craig and Zhao et al[80]. , utilizing the reversible activation of SP imitated the color change of cephalopods and analyzed the stress distribution of soft robots; etc[81-83].

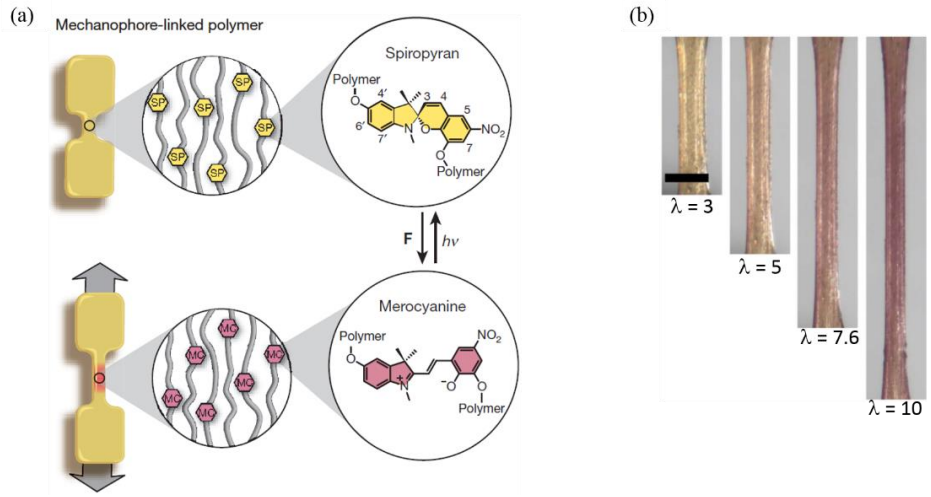

Figure 1.29: (a) Schematic representation of the active process of spiropyran; (b) the images of the specimen in the tensile test[76]

Another example was reported recently by Weng's group[84]. They used spirothiopyran (STP), which possesses a similar structure to SP. STP shows multiple functionalities including mechanochromism and the capability to undergo an addition reaction after activation. In STP, the S-C bond is easy to rupture under stress with formation of green thiomerocyanine (TMC). The thiolate moiety in the TMC is released after the activation of STP and may undergo a rapid thiol-ene click reaction, which provides an approach to crosslink polymer materials in the damaged regions. Weng et al. combined STP with polyester or polyurethane and demonstrated the mechanical responsivity of STP in solution and in a bulk polymer as shown in Figure 1.30a. Both the solution and the polymer sample turned from yellow to green after stimulation using ultrasound or stretch, respectively. Meanwhile, they also proposed the occurrence of a local reinforcement of polymer materials in the damaged zone by the cross-linking reaction of TMC with N-ethylmaleimide.

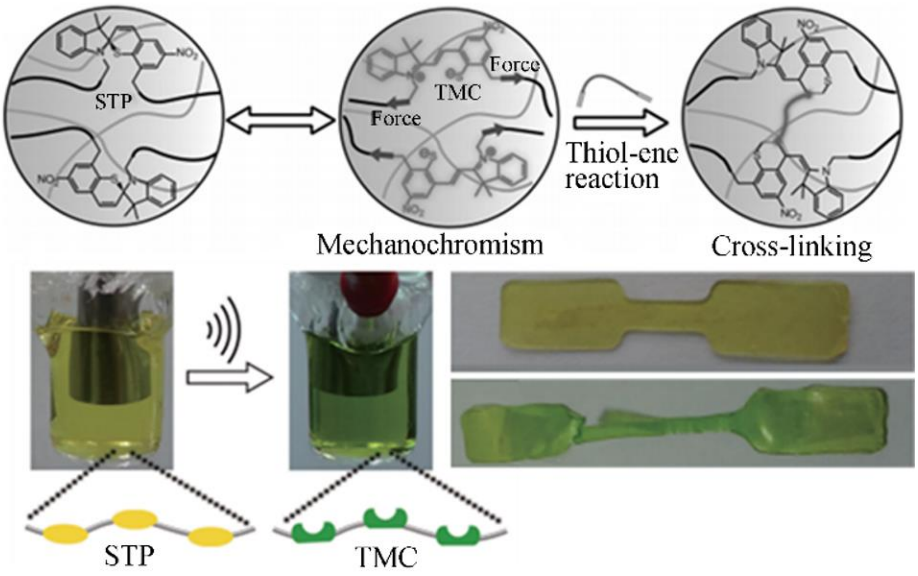

Figure 1.30: Mechanical activation of STP mechanophore

Another example of mechanochromic molecules are diarylbibenzofuranone (DABBF) derivatives, which form a new group of mechanochromic agents, synthesized by Otsuka et al.[85,86] in 2015. DABBF has a yellow color and undergoes a mechanically induced hemolytic cleavage of the central C-C bond with the formation of a blue radical compound (Figure 1.31)[85]. As a result, when DABBF was covalently coupled into the chain of polystyrene with various structures and different lengths, the observation of the color change confirmed that long polymer chains and star polymers structure had a higher sensitivity to mechanical stimuli. This work suggests which polymer architectures can improve the sensitivity of mechanochromic polymers.[86] Because of the reversible dynamic covalent bonding in DABBF the elastomers show a self-healing property and can be used for the initiation of concurrent reactions. For instance, Sijbesma et al. applied it for the secondary radical polymerization of non-volatile acrylate, which is triggered by mechanical forces. The strategy is useful for self-healing.

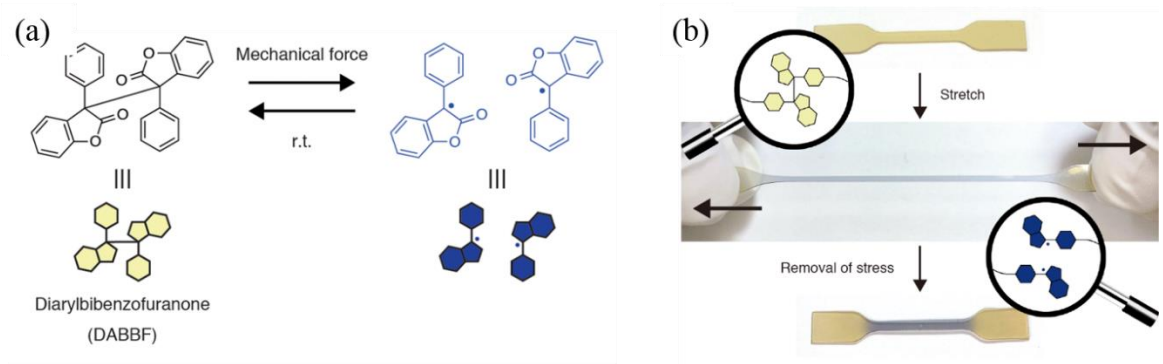

Figure 1.31: (a) Scheme of the activation of DABBF mechanophore; (b) the image of sample with activated DABBF

Recently, rhodamine (Rh-OH), a biocompatible molecule, was chosen as mechanophore by Jia and his co-workers[87]. Due to its high energy barrier of activation and multiple synthesis steps of modification of the active terminal group, its use as mechanophore was very limited until 2015 besides its widespread application in the biological field. In this report, Rh-OH was cross-linked into a polyurethane network and showed a distinct color and fluorescence change under compression (in Figure 1.32a). In order to enhance the mechanical response of Rh-OH, Bai and co-workers[88] designed and synthesized a new Rh-OH modified with two electron-donating tertiary amino groups (Figure 1.32b). In this work, the elastomer coupled with Rh-OH showed a color transformation from colorless to dark red in tensile tests. In the cyclic loading tests, elastomers showed three-primary-color fluorescent emission bands when they were exposed to UV light (in Figure 1.32c). The three primary fluorescence color (light blue-red-yellow) are attributed to the conformation transition of Rh-OH in the activation process. Once the C-N bond in the spirolactam was broken, the zwitterion planarized instantaneously which extended the conjugated system resulting in red-shifts in both the absorption and fluorescence spectra. In unloading, the zwitterions immediately returned to the bent geometry leading to a blue-shift in fluorescent spectrum (Figure 1.32b). These characteristic above make Rh-OH a potential molecular force probe too.

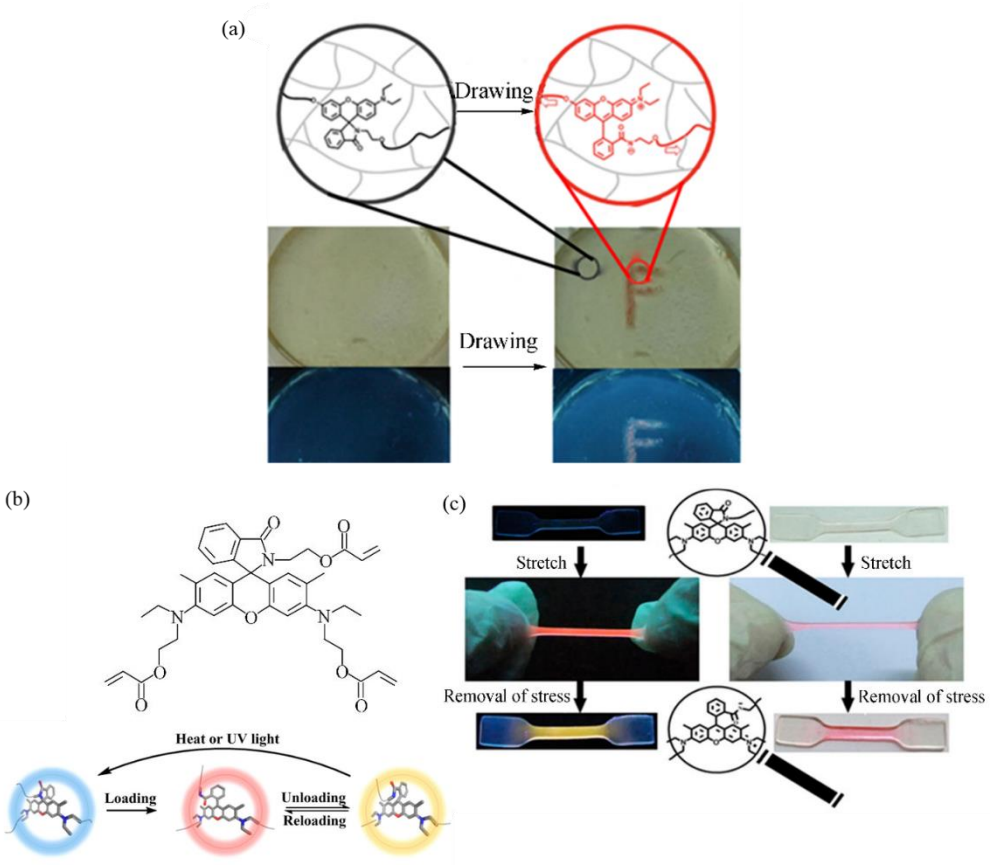

Figure 1.32: (a) The activation of rhodamine with compression[84]; (b) The structure of the rhodamine cross-linker; (c) the fluorescent (left) and optical (right) images of TN elastomers with rhodamine in the loaded and unloaded states[88]

Comparing all the mechanophores described above, SP is the most promising molecular force probe and we plan to use SP to map the stress, deformation and damage distribution in multiple network elastomers. The main reasons are the following:

(1). SP is provided with a simple and well developed synthesis scheme, which leads to high productivity. In addition, SP is stable.

(2). SP activation has a low energy barrier which makes it more sensitive to mechanical force. The single molecular force spectrum of SP measured by the Craig's group[89] demonstrated that 240 pN only are needed to activate one molecule of SP (in Figure 1.33a).

(3). After activation, MC is sufficiently stable to be compatible with better spatially resolved "post-mortem" imaging.

(4). SP can be incorporated into the first and second network, respectively. We then can study the fracture mechanism of multiple network elastomers.

(5). SP can be activated by UV light. Dividing by this saturated SP fluorescence or color intensity (activated by UV), we are able to quantify the activated SP percent and map the stress and strain.

(6). Finally one of the most important points is that the SP molecular probe can be used to map the stress during the unloading process. The reason is attributed to the different isomers of MC that lead to slight changes in color between the loaded and the unloaded state as observed by Craig et al.[82] and Weng et al.[79]. As shown in Figure 1.34b, after activation of SP into MC, the color of the elastomers changes from blue to purple when the materials are submitted to cycles of loading and unloading. According to the results of Craig[89], it is due to the diverse conformations of MC. When MC is in its stretched tensile state, it manifests a meta-stability, where the main composition is the CTC or TCC isomer shown in Figure 1.33b. During relaxation, it transform into the more stable TTC or TTT ground-state isomer through internal conversion between different isomers[90-92]. The transformation of SP into MC is reversible under visible light and it is possible to reuse the polymer materials for further investigations. It is also interesting for potential applications in industry.

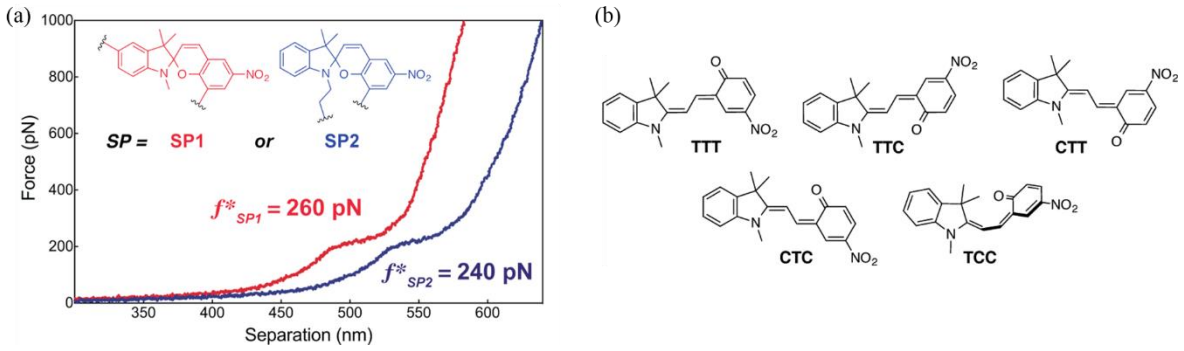

Figure 1.33: (a) The single molecular force spectrum of SP measured by AFM; (b) the different isomers of MC[89]

In Chen's and Weng's previous research about SP[79], they incorporated SP into the backbone of polyurethane networks and observed that the elastomers show two colors around the crack tip in fracture tests (in Figure 1.34c). The result demonstrates the potential of the SP as an insightful molecular probe for mapping the stress distribution in polymer materials. It was not only used to measure the stress, but also to identify the relaxed regions. The reports of Zhu et al[93,94] are also consistent with this conclusion. However, due to the limitations of the viscoelasticity of polyurethane containing hydrogen bonding interactions, the quantitative analysis of the stress or of the deformation was difficult to carry out for the zone around the crack tip.

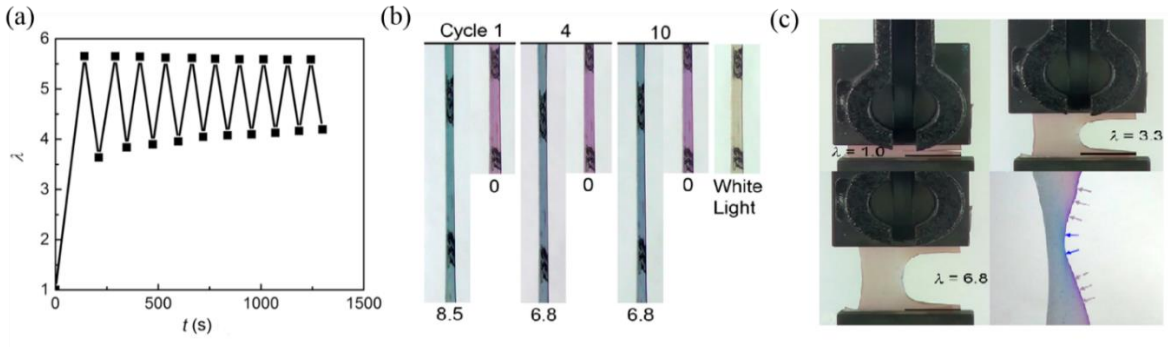

Figure 1.34: (a) the strain-time curve of polymer material under cyclic loading test; (b) the images of sample in the cycle loading; (c) the images of sample in the fracture test

Conclusion and motivation of the manuscript

We have described different strategies to synthesize tough elastomers. The use of a nanofiller is a cheap industrial strategy, however, it leads in most cases to the loss of optical transparency and increases the density of the elastomer. The reinforcement by the supramolecular interactions leads to significant viscoelasticity and viscoplasticity (residual deformation). Compared to these systems, the interpenetrated multiple network present an effective strategy to toughen elastomers and to control the mechanical strength by the properties of the first network without becoming viscoelastic or losing the transparency. However, the reinforcement and fracture mechanism of multiple network elastomers at the molecular level is still an open question, especially in case of the crack propagation as it involves great energy dissipation. A comprehensive study requires an approach allowing to map the stress, deformation and damaged region in the materials, in particular, around the crack tip. the objective here is to develop a physically based model of the mechanism of reinforcement, which can then guide the design and synthesis of robust elastomers in the future.

In mechanochemistry, mechanophores can be incorporated in the polymer chains to exhibit various mechanical response after activation under mechanical stimuli. Spiropyran (SP) is one of the photochromic mechanophores that is used as molecular force probe for real-time stress sensing. This is due to its high sensitivity to stretching force, and strong optical response by the color change.

In order to construct a molecular model to understand the fracture mechanism of interpenetrated multiple network elastomers, SP as a molecular force probe can be incorporate into the different networks of multiple network elastomers. The color change of SP is able to monitor the distribution of the real-time stress and strain state of polymer networks during extension. We hypothesize that there will be a close correlation between color change and stress, and will attempt to quantify the stress according to the color distribution. Furthermore, the fascinating feature of MC that shows different colors in loading and unloading is critical to detect the tensile history in fracture test and during crack propagation. Additionally, few people focused on the transfer of stress from the stiff first network to the extensible second network after large damage occur in the first network. However, it is a critical factor that needs to be understood for the molecular model or the simulation of fracture. We are hopeful that the color change coming from SP incorporated in different networks separately will provide crucial new information. The work in this manuscript presents the mapping of stress at the molecular level by mechanochemistry and will lead to a better understanding of the reinforcement mechanisms.

Reference：

1. Brown, H. R.; *Macromolecules* **2007**, *40*, 3815.
2. Lake, G. J.; Thomas, A. G.; *Proceedings of the Royal Society of London Series a-Mathematical and Physical Sciences* **1967**, *300*, 108.
3. Tanaka, Y.; *Europhysics Letters (EPL)* **2007**, *78*, 56005.
4. Zhang, T.; Lin, S. T.; Yuk, H.; Zhao, X. H.; *Extreme Mechanics Letters* **2015**, *4*, 1.
5. Tirumala, V. R.; Tominaga, T.; Lee, S.; Butler, P. D.; Lin, E. K.; Gong, J. P.; Wu, W. L.; *Journal of Physical Chemistry B* **2008**, *112*, 8024.
6. Gong, J. P.; *Soft Matter* **2010**, *6*, 2583.
7. Nakajima, T.; Fukuda, Y.; Kurokawa, T.; Sakai, T.; Chung, U.-i.; Gong, J. P.; *ACS Macro Letters* **2013**, *2*, 518.
8. Nakajima, T.; Furukawa, H.; Tanaka, Y.; Kurokawa, T.; Osada, Y.; Gong, J. P.; *Macromolecules* **2009**, *42*, 2184.
9. Rebecca, E. W.; Costantino, C.; Hugh, R. B.; Jian, P. G.; *Macromolecules* **2007**, *40*, 9.
10. Chassé, W.; Schlögl, S.; Riess, G.; Saalwächter, K.; *Soft Matter* **2013**, *9*, 6943.
11. Millereau, P.; *Université Pierre et Maire Curie: Paris* **2017**.
12. Mayo, F. R.; *Journal of the American Chemical Society* **1943**, *65*, 2324.
13. Huang, M.; Furukawa, H.; Tanaka, Y.; Nakajima, T.; Osada, Y.; Gong, J. P.; *Macromolecules* **2007**, *40*, 6658.
14. Tsukeshiba, H.; Huang, M.; Na, Y. H.; Kurokawa, T.; Kuwabara, R.; Tanaka, Y.; Furukawa, H.; Osada, Y.; Gong, J. P.; *Journal of Physical Chemistry B* **2005**, *109*, 16304.
15. Ducrot, E.; Chen, Y.; Bulters, M.; Sijbesma, P. R.; Creton, C.; *Science* **2014**, *344*, 4.
16. Wan, S.; Cheng, Q.; *Advanced Functional Materials* **2017**, *27*, 1703459.
17. Yatsuyanagi, F.; Suzuki, N.; Ito, M.; Kaidou, H.; *Polymer* **2001**, *42*, 9523.
18. Clough, J. M.; Creton, C.; Craig, S. L.; Sijbesma, R. P.; *Advanced Functional Materials* **2016**, *26*, 9063.
19. Persson, B. N. J.; Albohr, O.; Heinrich, G.; Ueba, H.; *Journal of Physics: Condensed Matter* **2005**, *17*, R1071.
20. Gent, A. N.; *Hanser: Munich, Germany* **2001**, *1*, 365.
21. Moniruzzaman, M.; Winey, K. I.; *Macromolecules* **2006**, *39*, 5194.
22. Ha, H.; Ha, K.; Ellison, C. J.; *Journal of Polymer Science Part B: Polymer Physics* **2017**, *55*, 1406.
23. Li, H.; Yang, L.; Weng, G.; Xing, W.; Wu, J.; Huang, G.; *Journal of Materials Chemistry A* **2015**, *3*, 22385.
24. Wang, X.; Liu, X.; Yuan, H.; Liu, H.; Liu, C.; Li, T.; Yan, C.; Yan, X.; Shen, C.; Guo, Z.; *Materials & Design* **2018**, *139*, 372.
25. Pei, A.; Malho, J.-M.; Ruokolainen, J.; Zhou, Q.; Berglund, L. A.; *Macromolecules* **2011**, *44*, 4422.
26. Fröhlich, J.; Niedermeier, W.; Luginsland, H. D.; *Composites Part A: Applied Science and Manufacturing* **2005**, *36*, 449.
27. Payne, A. R.; Wheittaker, R. e.; *Rubber Chemistry and Technology* **1971**, *44*, 440.
28. KARASEK, L.; SUMITA, M.; *Journal of materials Science* **1996**, *31*, 281.
29. Feldman, K. E.; Kade, M. J.; Meijer, E. W.; Hawker, C. J.; Kramer, E. J.; *Macromolecules* **2009**, *42*, 9072.
30. Guo, M.; Pitet, L. M.; Wyss, H. M.; Vos, M.; Dankers, P. Y.; Meijer, E. W.; *Journal of the American Chemical Society* **2014**, *136*, 6969.
31. Koevoets, R. A.; Versteegen, R. M.; Kooijman, H.; Spek, A. L.; Sijbesma, R. P.; Meijer, E. W.; *Journal of the American Chemical Society* **2005**, *127*, 2999.
32. Appel, W. P. J.; Portale, G.; Wisse, E.; Dankers, P. Y. W.; Meijer, E. W.; *Macromolecules* **2011**, *44*, 6776.

33. Kushner, A. M.; Vossler, J. D.; Williams, G. A.; Guan, Z. B.; *Journal of the American Chemical Society* **2009**, *131*, 8766.
34. Burnworth, M.; Rowan, S. J.; Weder, C.; *Macromolecules* **2011**, *45*, 126.
35. Burnworth, M.; Tang, L.; Kumpfer, J. R.; Duncan, A. J.; Beyer, F. L.; Fiore, G. L.; Rowan, S. J.; Weder, C.; *Nature* **2011**, *472*, 334.
36. Hong, G.; Zhang, H.; Lin, Y.; Chen, Y.; Xu, Y.; Weng, W.; Xia, H.; *Macromolecules* **2013**, *46*, 8649.
37. Yu, G.; Jie, K.; Huang, F.; *Chemical reviews* **2015**, *115*, 7240.
38. Liu, J.; Tan, C. S.; Yu, Z.; Lan, Y.; Abell, C.; Scherman, O. A.; *Advanced materials* **2017**, *29*.
39. Widin, J. M.; Schmitt, A. K.; Schmitt, A. L.; Im, K.; Mahanthappa, M. K.; *Journal of the American Chemical Society* **2012**, *134*, 3834.
40. Jiang, S.; Zhang, L.; Xie, T.; Lin, Y.; Zhang, H.; Xu, Y.; Weng, W.; Dai, L.; *ACS Macro Letters* **2013**, *2*, 705.
41. Burattini, S.; Greenland, B. W.; Hayes, W.; Mackay, M. E.; Rowan, S. J.; Colquhoun, H. M.; *Chemistry of Materials* **2011**, *23*, 6.
42. Higaki, Y.; Kiyoshima, Y.; Suzuki, K.; Kabayama, H.; Ohta, N.; Seo, Y.; Takahara, A.; *RSC Adv.* **2017**, *7*, 46195.
43. Mark, J. E.; *Acc. Chem. Res.* **1994**, *27*, 8.
44. Gong, J. P.; Katsuyama, Y.; Kurokawa, T.; Osada, Y.; *Advanced materials* **2003**, *15*, 1155.
45. Genesky, G. D.; Cohen, C.; *Polymer* **2010**, *51*, 4152.
46. Urayama, K.; Kawamura, T.; Kohjiya, S.; *Polymer* **2009**, *50*, 347.
47. Gong, J. P.; *Science* **2014**, *344*, 161.
48. Nakajima, T.; Sato, H.; Zhao, Y.; Kawahara, S.; Kurokawa, T.; Sugahara, K.; Gong, J. P.; *Advanced Functional Materials* **2012**, *22*, 4426.
49. Mark, J. E.; Ning, Y.-P.; *Poly. Eng. Sci.* **1985**, *25*, 824.
50. Yoo, S. H.; Cohen, C.; Hui, C.-Y.; *Polymer* **2006**, *47*, 6226.
51. E. Elif, H.; Bahattin, M. B.; *Macromol. Chem. Phys.* **1995**, *196*, 6.
52. Ducrot, E.; *Université Pierre et Maire Curie: Paris* **2013**.
53. Long, R.; Hui, C. Y.; *Soft Matter* **2016**, *12*, 8069.
54. Na, Y. H.; Tanaka, Y.; Kawauchi, Y.; Furukawa, H.; Sumiyoshi, T.; Gong, J. P.; Osada, Y.; *Macromolecules* **2006**, *39*, 4641.
55. Yu, Q. M.; Tanaka, Y.; Furukawa, H.; Kurokawa, T.; Gong, J. P.; *Macromolecules* **2009**, *42*, 3852.
56. Matsuda, T.; Nakajima, T.; Fukuda, Y.; Hong, W.; Sakai, T.; Kurokawa, T.; Chung, U.; Gong, J. P.; *Macromolecules* **2016**, *49*, 1865.
57. Ducrot, E.; Creton, C.; *Advanced Functional Materials* **2016**, *26*, 2482.
58. Ogden, R. W.; Roxburgh, D. G.; *Proc. R. Soc. A-Math. Phys. Eng. Sci.* **1999**, *455*, 2861.
59. Karthikeyan, S.; Sijbesma, R. P.; *Nature chemistry* **2010**, *2*, 436.
60. Black, A. L.; Lenhardt, J. M.; Craig, S. L.; *J Mater Chem* **2011**, *21*, 1655.
61. Caruso, M. M.; Davis, D. A.; Shen, Q.; Odom, S. A.; Sottos, N. R.; White, S. R.; Moore, J. S.; *Chemical reviews* **2009**, *109*, 5755.
62. Wiggins, K. M.; Brantley, J. N.; Bielawski, C. W.; *Chemical Society reviews* **2013**, *42*, 7130.
63. Berkowski, K. L.; Potisek, S. L.; Hickenboth, C. R.; Moore, J. S.; *macromolecules* **2005**, *38*, 8975.
64. Paulusse, J. M.; Sijbesma, R. P.; *Chemical communications* **2008**, 4416.
65. Chen, Y.; Spiering, A. J.; Karthikeyan, S.; Peters, G. W.; Meijer, E. W.; Sijbesma, R. P.; *Nature chemistry* **2012**, *4*, 559.
66. Larsen, M. B.; Boydston, A. J.; *Journal of the American Chemical Society* **2013**, *135*, 8189.
67. Park, I.; Sheiko, S. S.; *Macromolecules* **2009**, *42*, 1805.
68. Wei, K.; Gao, Z.; Liu, H.; Wu, X.; Wang, F.; Xu, H.; *ACS Macro Letters* **2017**, *6*, 1146.
69. Chen, Z.; Mercer, J. A. M.; Zhu, X.; Romaniuk, J. A. H.; Pfattner, R.; Cegelski, L.; Martinez, T. J.; Burns, N. Z.; Xia, Y.; *science* **2017**, *357*, 475.
70. Yuan, Y.; Chen, Y.-l.; *Chinese Journal of Polymer Science* **2017**, *35*, 1315.
71. Cho, S.-Y.; Kim, J.-G.; Chung, C.-M.; *Sensors and Actuators B: Chemical* **2008**, *134*, 822.

72. Song, Y.-K.; Lee, K.-H.; Hong, W.-S.; Cho, S.-Y.; Yu, H.-C.; Chung, C.-M.; *J. Mater. Chem.* **2012**, *22*, 1380.
73. Li, H.; Göstl, R.; Delgove, M.; Sweeck, J.; Zhang, Q.; Sijbesma, R. P.; Heuts, J. P. A.; *ACS Macro Letters* **2016**, *5*, 995.
74. Gostl, R.; Sijbesma, R. P.; *Chemical science* **2016**, *7*, 370.
75. Chen, Y.; Sijbesma, R. P.; *Macromolecules* **2014**, *47*, 3797.
76. Davis, D. A.; Hamilton, A.; Yang, J.; Cremar, L. D.; Van Gough, D.; Potisek, S. L.; Ong, M. T.; Braun, P. V.; Martinez, T. J.; White, S. R.; Moore, J. S.; Sottos, N. R.; *Nature* **2009**, *459*, 68.
77. Chen, Y.; Zhang, H.; Fang, X.; Lin, Y.; Xu, Y.; Weng, W.; *ACS Macro Letters* **2014**, *3*, 141.
78. Fang, X.; Zhang, H.; Chen, Y.; Lin, Y.; Xu, Y.; Weng, W.; *Macromolecules* **2013**, *46*, 6566.
79. Zhang, H.; Chen, Y.; Lin, Y.; Fang, X.; Xu, Y.; Ruan, Y.; Weng, W.; *Macromolecules* **2014**, *47*, 6783.
80. Wang, Q.; Gossweiler, G. R.; Craig, S. L.; Zhao, X.; *Nature communications* **2014**, *5*, 4899.
81. Gossweiler, G. R.; Brown, C. L.; Hewage, G. B.; Sapiro-Gheiler, E.; Trautman, W. J.; Welshofer, G. W.; Craig, S. L.; *ACS applied materials & interfaces* **2015**, *7*, 22431.
82. Gossweiler, G. R.; Hewage, G. B.; Soriano, G.; Wang, Q.; Welshofer, G. W.; Zhao, X.; Craig, S. L.; *ACS Macro Letters* **2014**, *3*, 216.
83. Wang, Q.; Gossweiler, G. R.; Craig, S. L.; Zhao, X.; *J. Mech. Phys. Solids* **2015**, *82*, 320.
84. Zhang, H.; Gao, F.; Cao, X.; Li, Y.; Xu, Y.; Weng, W.; Boulatov, R.; *Angewandte Chemie* **2016**, *55*, 3040.
85. Imato, K.; Kanehara, T.; Ohishi, T.; Nishihara, M.; Yajima, H.; Ito, M.; Takahara, A.; Otsuka, H.; *ACS Macro Letters* **2015**, *4*, 1307.
86. Oka, H.; Imato, K.; Sato, T.; Ohishi, T.; Goseki, R.; Otsuka, H.; *ACS Macro Letters* **2016**, *5*, 1124.
87. Wang, Z.; Ma, Z.; Wang, Y.; Xu, Z.; Luo, Y.; Wei, Y.; Jia, X.; *Advanced materials* **2015**, *27*, 6469.
88. Wang, T.; Zhang, N.; Dai, J.; Li, Z.; Bai, W.; Bai, R.; *ACS applied materials & interfaces* **2017**, *9*, 11874.
89. Gossweiler, G. R.; Kouznetsova, T. B.; Craig, S. L.; *Journal of the American Chemical Society* **2015**, *137*, 6148.
90. Cremar, L. D.; *Doctoral thesis, University of Illinois at Urbana-Champaign, Champaign, IL* **2012**.
91. Hirano, M.; Osakada, K.; Nohira, H.; Miyashita, A.; *J. Org. Chem.* **2002**, *67*, 533.
92. Wohl, C. J.; Kuciauskas, D.; *J. Phys. Chem. B* **2005**, *109*, 22186.
93. Li, M.; Liu, W.; Zhu, S.; *Polymer* **2017**, *112*, 219.
94. Li, M.; Zhang, Q.; Zhu, S.; *Polymer* **2016**, *99*, 521.

Chapter 2. Synthesis and characterization of mechanically responsive multiple network elastomers

Introduction

This chapter focuses on the synthesis of multiple interpenetrated network elastomers, including the synthesis of the mechano-responsive spiropyran (SP) cross-linker. This thesis will be focused on this class of materials.

Also, details on the synthesis of different elastomers based on varying the cross-link densities and the SP concentration in the first network will be discussed. Multiple networks were prepared based on the same first network made from mainly ethyl acrylate. To examine mechanical behavior and responsiveness of the elastomers, several general methods have been developed and used and will be described, including uniaxial tensile tests and most importantly the analysis of the color change during traction with the use of a color camera providing an RGB signal.

1. Standard synthesis of multiple networks

The preparation of multiple network elastomers consists in a sequence of free radical photo polymerizations following the methodology developed by Ducrot[1-3] and Millereau[4]. In our case, and in contrast with the methods previously used, no solvent was used for the synthesis of the first network avoiding therefore the rinsing step and shortening the synthesis time. The first network was prepared by mixing monomers, two types of cross-linkers, and an UV initiator. From that basic classical elastomeric network that we will often refer to as single network (SN) or filler network, multiple iterations of swelling, photo polymerization and drying were carried out to synthesize a standard family of multiple networks elastomers.

1.1 Chemical reagents

Table 2.1: Chemical reagents used for synthesizing multiple network elastomers.

Notation	Chemical name	Molar mass	Purity	origin	CAS
EA	Ethyl acrylate	100.12	99%	Aldrich	140-88-5
HMA	Hexyl methacrylate	170.25	98%	Aldrich	142-09-6
BDA	1.4-Butanediol diacrylate	198.22	90%	Aldrich	1070-70-8
HMP	2-hydroxy-2-methyl propiophenone	164.20	97%	Aldrich	7473-98-5
Ea	Ethyl acetate	88.11	Technical	Aldrich	141-78-6
THF	tetrahydrofuran	72.11	99.9%	Aldrich	109-99-9
Ethanol	ethanol	46.07	Technical	Aldrich	64-17-5
MAC	Methacryloyl chloride	104.53	97%	Aldrich	920-46-7
	3-Chloromethyl-5-nitrosalicylaldehyde	215.59	97%	abc	16644-30-7
	2-Iodoethanol	171.97	99%	Aldrich	624-76-0
	Chloroform	119.38	99%	Aldrich	67-66-3
TMI	2,3,3-Trimethylindolenine	159.23	98%	Aldrich	1640-39-7
KOH	Potassium hydroxide	56.11	80%	Aldrich	1310-58-3

Ethyl acrylate (EA) or hexyl methacrylate (HMA), 1.4-butanediol diacrylate (BDA), 2-hydroxy-2-methylpropiophenone (HMP) were used as monomers, crosslinker and UV initiator, respectively. An aluminum oxide column was used to purify and remove additives contained in as-received EA, HMA and BDA. Other reagents were used without further purification. Ethyl acetate (Ea) was used in some of the polymerizations to tune the level of pre-stretch in the first network. Other reagents were used to synthesize the spiropyran (SP) mechanophore and to add reactive functionality to SP, resulting in an SP-diene crosslinker. A list of the chemical reagents is provided in Table 2.*1*.

1.2 Polymerization conditions of the networks

Free radical photo polymerization is chosen for the synthesis of multiple network elastomers. In the photo polymerization, HMP is used as ultraviolet initiator and its reactive mechanism is shown in the Scheme 2.*1*. HMP decomposes into two radicals under the stimulation of UV. The radicals react with the double bonds on the monomers or crosslinkers and then the polymer chains grow rapidly and form the polymer network.

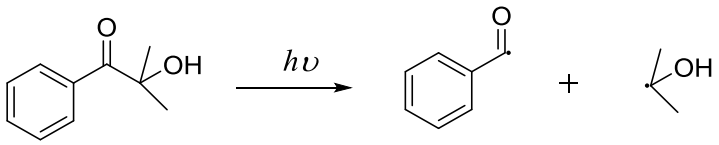

Scheme 2.1: The activated mechanism of HMP UV initiator

During such free radical polymerization, the acrylate monomer is susceptible to chain transfer reactions since the H in alpha position of the acrylate function is labile, as shown in Figure 2.*1*. The side reaction can lead to unwanted network connectivity between networks. Inspired from Gong's synthesis of DN hydrogel[5], and in order to avoid chain transfer reactions and the number of termination reactions during polymerization, the UV intensity and initiator concentration was set to be < 10 μW/cm^2 and < 1 mol/% relative to the monomer. At the same time, the low UV intensity and initiator concentration decrease the number of chains growing simultaneously and then increases the gelation time. Another approach to decreasing the transfer reactions is to use methacrylate monomer instead of acrylate monomer (Figure 2.*1*): the methyl group on the methacrylate monomer is unreactive towards radicals.

It should be noted that the polymerization should be conducted under a low initiator concentration. When the concentration of initiator was set to 10 mol/%, under UV irradiation large amounts of chains growed simultaneously resulting in a large increase of the termination

reactions. Additionally the polymerization produced many short polymer chains. When the single networks prepared with a high initiator concentrations were washed into ethyl acetate, 10 wt% of the single network were extracted, and it is likely that the architecture of the remaining network was also more heterogeneous affecting its mechanical properties. However, if the initiator is set at 1 mol/%, the percent of short polymer chains is below 1%. This was attributed to the reduction of termination reactions between two radicals, resulting in a less distribution of linear polymer chains in the single network. In addition, to ensure radical stability and to prevent oxygen inhibition, all the polymerization steps were carried out in a glove box in a nitrogen atmosphere, in which the concentrations of oxygen and water are both below 0.1 ppm.

Figure 2.1: The difference between acrylate and methacrylate monomers

1.3 Synthesis of the spiropyran (SP) cross-linker

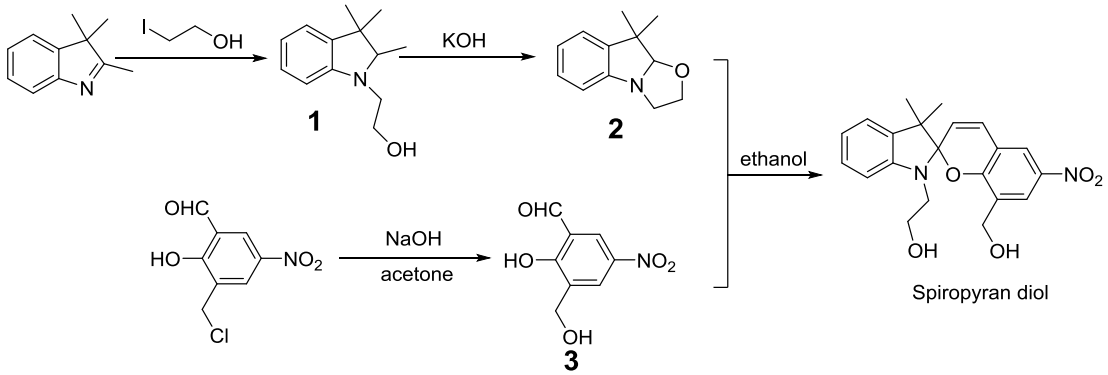

Scheme 2.2: Synthesis of the synthesis of SP diol

The mechanophore SP diol is readily prepared by a procedure adapted from Greg O'Bryan's reported method[6-8]. The synthesis is represented in Scheme 2.*2*. 2,3,3-trimethylindolenine was dissolved into chloroform and the solution was poured into a sealed reflux unit and degassed by sequential freezing, pumping and filling with nitrogen gas for three times. Then 110 mol% 2-iodoethanol, with respect to indole, was injected into the device. This chemical reaction was conducted for about 48 hours under a nitrogen atmosphere at 68 ℃. The raw product **1** was

obtained by removing the solvent under vacuum after the reaction and was washed with petroleum ether. The raw product was then dried overnight in vacuum. Indolium iodide **1** was converted to indole **2** by grinding in a mortar and pestling with potassium hydroxide until a yellow paste was obtained. The indole **2** was extracted from the yellow paste with petroleum ether. Methylhydroxy substituted salicylaldehyde **3** was obtained by hydrolysis of 3-chloromethyl-5-nitrosalicylaldehyde in a 50% acetone aqueous solution (volume fraction). Finally, SP diol was synthesized by the condensation reaction of compound **2** and **3** in a 50 % ethanol aqueous solution[6,7,9].

For SP to participate in the crosslinking reaction, the diol functionality was replaced with diacrylate terminal groups as shown in Scheme 2.*3*. 0.25 g spiropyran-diol and 455.5 µL trimethylamine were mixed and dissolved in 30 mL of tetrahydrofuran in a 100 mL round bottom flask and the solution was subsequently cooled to 0 ℃ with ice. Then 319.3 µL methacryloyl chloride (MAC) was added dropwise over 5 min using a syringe. After 24 h, the solution color changed from yellow to pink. Subsequently, the solvent was removed under vacuum. The solid raw product was purified with a chromatographic column eluting with dichloromethane resulting in a purple paste. The purple product was purified again by hexane recrystallization yielding a yellow powder. The NMR spectrum is shown in Figure 2.*2* and the detailed analysis of the spectrum is as follows: ^{1}H NMR (400 MHz, $CDCl_3$) d 8.09 (s, 1H), 7.98 (s, 1H), [7.19-6.66] (m, 5H), 6.05 (s, 2H), [5.91&5.88] (d, 1H), 5.57 (m, 2H), 4.97 (s, 2H), [4.31-4.27] (t, 2H), [3.57-3.37] (m, 2H), 1.91 (m, 3H), 1.27(s, 6H),

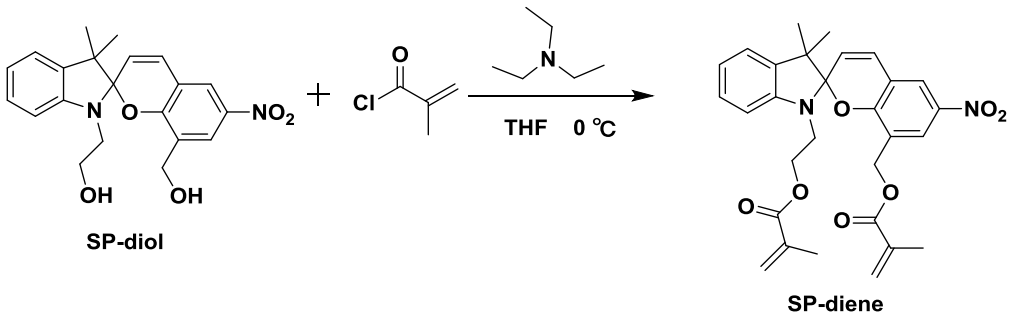

Scheme 2.3: Synthesis of SP-diene from SP-diol

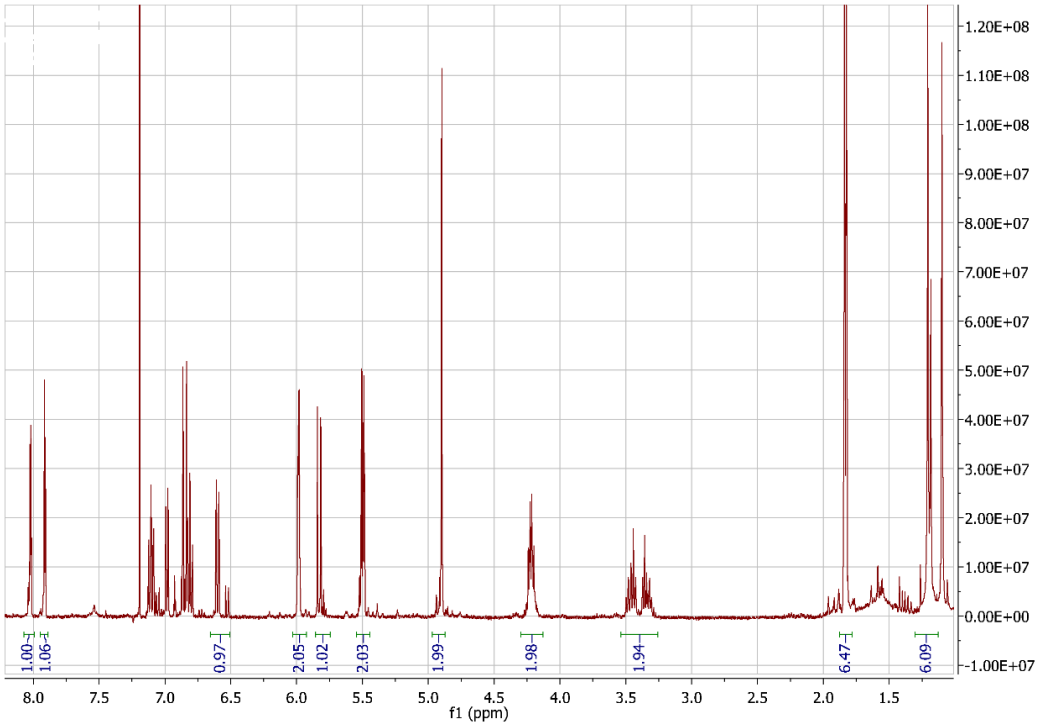

Figure 2.2: NMR spectrum of SP-diene

1.4 Synthesis of the first (or filler) network

Single networks were prepared without solvent. Therefore, crosslinked samples did not need to be washed with mixed solvent baths to extract unreacted species before carrying out the second polymerization and it effectively reduced the time needed for the synthesis. The detailed synthesis protocol of multiple networks was similar to what was reported in a previous publication by Ducrot[3]. SP was covalently incorporated into the first network along with BDA. To accomplish this, 1 mol% 2-hydroxy-2-methylpropiophenone (HMP) UV initiator, 0.5 mol% cross-linker (0.05 mol%SP and 0.45 mol% BDA) were dissolved into ethyl acrylate (EA) and a purple pre-gel solution was prepared. Note that molar percentages are respective to moles of EA. The solution was poured into a mold (Figure 2.*3*) composed of two glass plates with a silicone spacer to control the film thickness. The whole device was tightened by two metal frames to seal the mold. Polymerization was initiated by UV light (by a Vilbert Lourmat lamp: model VL-215.L). After polymerization, a uniform purple rubbery single network formed and was subsequently dried in a vacuum desiccator for one day, to remove unreacted monomers. After drying, the single network exhibited a reddish color and was stored at room temperature in a dark environment for later use. This polymerization is shown in Scheme 2.*4*.

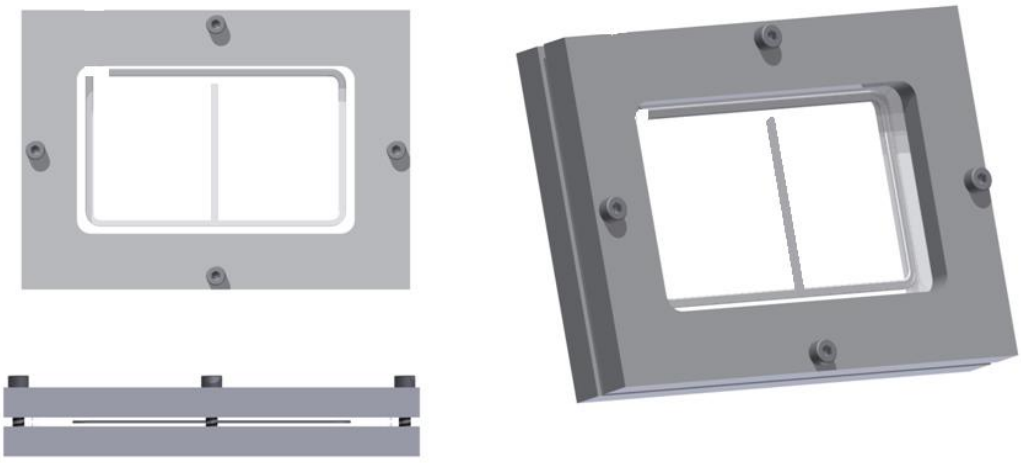

Figure 2.3: Custom made mold for the polymerization of a single network.

During the polymerization, the solution reached the gel point in approximately 15 mins under UV light exposure. After the gel point, the viscosity significantly increased and the solution converted into a film. At the same time, undesired and heterogeneous shrinkage of the polymer sheet was observed resulting in the detachment of the sample from the glass plates and a formation of irregular fingering patterns on the surface of film. This detachment process was attributed to the variation of density during the transformation from monomer to polymerized polymer film. During the polymerization the volume of film decreased and the film debonded from the glass surface. But the detachment did not occur simultaneously.

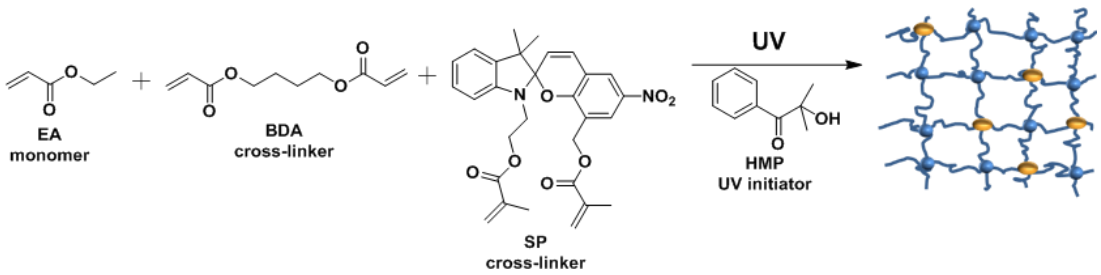

Scheme 2.4: Synthesis of standard single network

To make smooth surfaces, compatible with optical observations, several approaches were explored. One of the approaches was increasing the space between the two glass plates in the mold and leaving an empty space between the top glass plate and the solution, which avoided the debonding process during polymerization. However, due to the exothermic reaction of polymerization, monomers evaporated quickly and condensed on the top glass. In turn these condensed droplets varied the uniformity of the UV intensity on both sides of polymer films.

This approach provided smooth surfaces but a gradient in properties through the thickness of the film, and after polymerization the polymer film curled.

Another strategy was adopted, two pieces of transparent PET films with a hydrophobic surface were placed as liners on the internal glass surfaces of the mold. Due to the strong interaction between the PET and the samples, the detachment between the PET films and samples did not occur and provided a smooth surface. After polymerization, the elastomeric network was peeled from the PET film. To avoid fracture during peeling, a little acetone was smeared on the reverse side of the PET film. Acetone diffused into the PET film. The surface of polymerized network attaching to the PET film was swollen and was easy to detach from the PET film. Silicone spacers with different thicknesses were used to control the thickness of polymerized networks. In addition, this setup resulted in reproducible samples with smooth surfaces.

1.5 Preparation of a family of multiple networks elastomers

The multiple networks were prepared by sequentially swelling and polymerizing as shown in Scheme 2.5. Due to the high swelling ratio (about 4) of the single network in the monomer bath, only a small piece (about 3 cm length and 2 cm width) of the single network with mass (m_{SN}), was cut out from the first network film and soaked in a solution containing dilute BDA cross-linker (0.01 mol/% respective to EA), 0.01 mol/% HMP, and EA. When the equilibrium swelling was reached double networks (DN) were synthesized by polymerizing the swollen single network. After drying in a vacuum desiccator, the sample appeared colorless and its mass (m_{DN}) was measured. During swelling, polymer chains in the filler network were isotropically stretched to a level given by the inverse of the third power of the equilibrium swelling (Equation 3) and this stretching level was then fixed by the subsequent polymerizations of the swelling monomer EA.

To obtain even higher levels of pre-stretch (λ_0), these two steps were repeated on the DN to prepare triple networks (TN) and quadruple networks (QN). Due to the presence of the second polymerized network, the entropy of mixing between the monomer and the network was available again as a driving force to swell the DN to equilibrium giving the possibility to pre-stretch the first network further. The different samples were categorized under different families of materials based on the properties of the first network. Due to the varying numbers of swelling and polymerization steps within the same family of materials, the different samples possessed different pre-stretch. Especially, in the TN and QN, the first networks were pre-stretched significantly. Indeed, SP in the first network was activated during the swelling

process itself to prepare TN and QN. The swollen materials changed to a blue color. After polymerization and drying the TN returned to colorless indicating reversion of the MC into SP. However the blue color of QN was not easy to fade indicating that some of the chains of the first network are fully stretched and maintain a force > 250 pN. According to the literature[4], the pre-stretch would dramatically affect the mechanical properties of multiple networks and can be calculated by Equation 1, Equation 2 and Equation 3:

$$\phi_{SN} = \frac{m_{SN}}{m_{DN}} \qquad \textit{Equation 1}$$

$$\lambda_0 = \frac{h_{DN}}{h_{SN}} = \left(\frac{V_{DN}}{V_{SN}}\right)^{\frac{1}{3}} = \left(\frac{m_{DN}}{m_{SN}}\right)^{\frac{1}{3}} \qquad \textit{Equation 2}$$

$$\lambda_0 = \left(\frac{1}{\phi_{SN}}\right)^{\frac{1}{3}} \qquad \textit{Equation 3}$$

where h_{SN}, h_{DN}, V_{SN} V_{DN} and ϕ_{SN} are the thickness of SN and DN, the volume of SN, DN and the weight percent of SN, respectively. In addition, the level of pre-stretch of the filler network could be tailored to an arbitrary value by using solvent to replace part of monomers in the swelling process as described in Pierre Millereau's thesis.

Many samples with diverse composition have been synthesized. Hereafter, all the materials will be referred as follows:

Ax-y(z)B

A: Monomer of the first network
B: Monomer of the other networks including second, third or fourth networks
x: Total cross-linker density in the first network
y: SP concentration in the first network
z: Pre-stretch in the first network

For example, EA0.5-0.05(2.23)EA means that the sample possesses a filler network composed of EA monomer, 0.5 mol-% of cross-linker including 0.05 mol-% SP, $\lambda_0 = 2.23$ of pre-stretch and a second network consisting of EA. Table 2.2 shows all the materials where SP is incorporated in the filler network only.

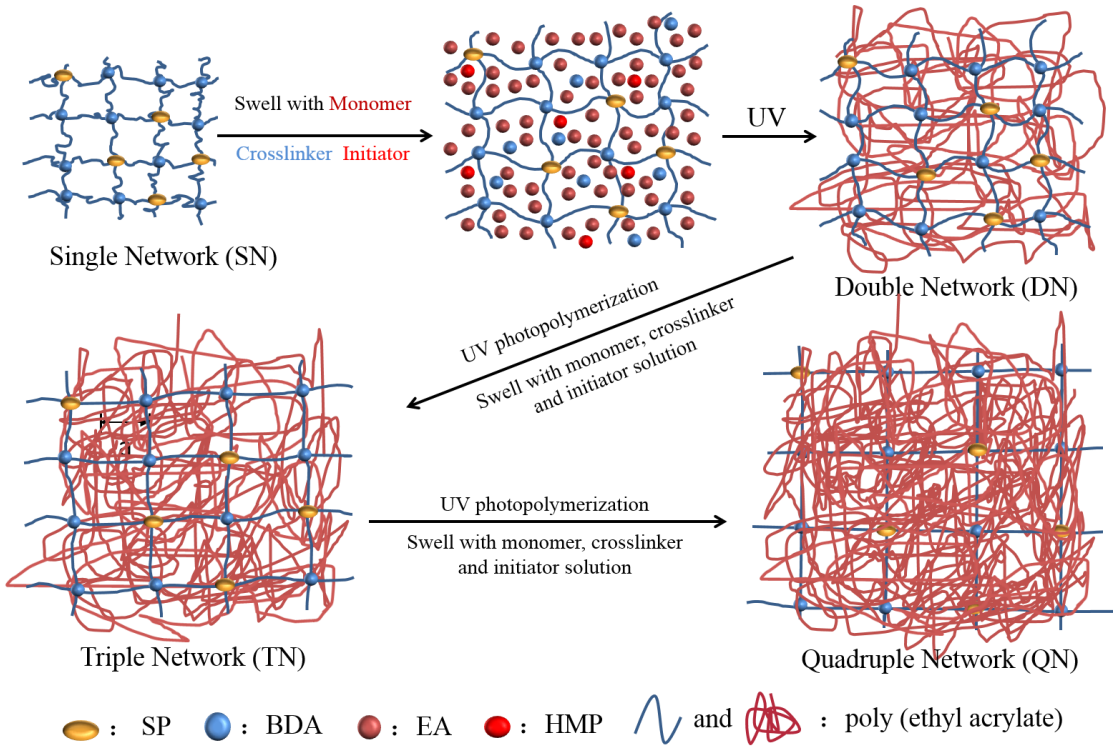

Scheme 2.5: Synthesized procedure of multiple networks elastomers

2. Synthesis of various multiple network elastomers

To explore the effects of cross-linking density and SP concentration on the mechanical response, single networks with various concentrations of SP and cross-linkers were synthesized.

2.1 Effects of cross-linking in the first network

The first network acts as a percolating filler which quantitatively controls the mechanical properties of multiple networks[2] and the mechanical properties of this filler network are significantly affected by the cross-linking density. To study the effect of cross-linking density on the mechanical response, various single networks with different cross-linker densities at a fixed SP concentration were synthesized.

The cross-linking density in the first network was varied from 0.5% to 0.01%, respectively. Based on this SN network, a family of materials were synthesized as shown in the Table 2.2. In order to explore the mechanical properties of multiple network composed of a loosely cross-linked first network, another family of materials was prepared.

Table 2.2: The description of all the materials used in this manuscript.

Polymer name	First network	SN wt%	N_{poly}	λ_0
EA0.5-0.05(1)		100	1	1
EA0.5-0.05(1.56)EA	EA0.5-0.05(1)	26.5	2	1.56
EA0.5-0.05(2.23)EA	EA0.5-0.05(1)	9.0	3	2.23
EA0.5-0.05(2.84)EA	EA0.5-0.05(1)	4.4	4	2.84
EA0.2-0.05(1)		100	1	1
EA0.2-0.05(1.70)EA	EA0.2-0.05(1)	20.2	2	1.70
EA0.2-0.05(2.61)EA	EA0.2-0.05(1)	5.6	3	2.61
EA0.2-0.05(3.55)EA	EA0.2-0.05(1)	2.2	4	3.55
EA0.01-0.01(1)		100	1	1
EA0.01-0.01(1.96)EA	EA0.01-0.01(1)	13.2	2	1.96
EA0.01-0.01(3.28)EA	EA0.01-0.01(1)	2.8	3	3.28

(N_{poly} is the number of polymerization steps)

2.2 Various SP concentrations in the first network

Color changes originate from the activation and deactivation of the mechanophore. Therefore, chromaticity correlates with the concentration of MC. In order to study the effects of SP concentration on the color change, it is necessary to prepare elastomers possessing identical (or at least very similar) mechanical properties. Because the mechanical properties are controlled by the first network, the cross-linking density in the first network was kept constant, but the ratio between SP mechanophore crosslinker and BDA crosslinker was varied. A series of single networks were synthesized and the respective double, triple and quadruple networks were also prepared as shown in Table 2.3.

Table 2.3: The information about multiple network elastomers with diverse SP concentration in the first network

Polymer name	First network	SN wt%	N_{poly}	λ_0
EA0.5-0.025(1)EA		100	1	1
EA0.5-0.025(1.60)EA	EA0.5-0.025(1)	24.3	2	1.60
EA0.5-0.025(2.35)EA	EA0.5-0.025(1)	7.8	3	2.35
EA0.5-0.025(3.05)EA	EA0.5-0.025(1)	3.5	4	3.05
EA0.5-0.0125(1)EA		100	1	1
EA0.5-0.0125(1.58)EA	EA0.5-0.0125(1)	25.3	2	1.58
EA0.5-0.0125(2.36)EA	EA0.5-0.0125(1)	7.6	3	2.36
EA0.5-0.0125(3.11)EA	EA0.5-0.0125(1)	3.3	4	3.11

2.3 Different monomers in the first network

Due to the labile hydrogen on the alpha position of ethyl acrylate as shown in Figure 2.*1*, chains transfer reaction occurs during the polymerization. Chain transfer reaction results in the increase of covalent crosslinker density of the filler networks and in the subsequent polymerization it leads the connection between the first network and the networks that are synthesized afterwards. However, methacrylate monomers can avoid this side reaction because of the absence of the labile hydrogen on the alpha position. Takin advantage of this feature of methacrylate monomers and the methodology of mechanochemistry, the stress transmission between different networks and the fracture mechanism of the interpenetrated multiple networks can be further studied. SP as a molecular probe was crosslinked into the second or third network to sense the stress and deformation in extension. Since the crosslinker density is much lower than the first network. To ensure the sensitivity and resolution, SP was the only crosslinker when it was incorporated into the second or third networks. The other synthesized condition and quantity are the same as the standard family (EA0.5-0.05). For the group of materials whose monomer in the first network is HMA, the UV exposure time is increased to 6 hour to ensure the complete polymerization and other condition (crosslinker density, UV intensity, initiator concentration etc.) keeps constant. All the materials used to study the stress transmission are shown in Table 2.*4*. The notation of polymers are a little different from the standard family. A number is added behind the original notation and it represents the position in the multiple networks. For instance, EA0.5-0(2.34)EA2 illustrates the SP concentration in the first network is 0 and the SP is located in the second network. The detailed research that these materials is used will be presented in chapter 5.

Table 2.4: Various multiple network elastomers consist of different first networks and SP is incorporated into the second or third networks.

Polymers	First network	SN wt%	N_{poly}	λ_0
EA0.5-0(1)		100	1	1
EA0.5-0 (1.62)EA	EA0.5-0(1)	23.5	2	1.62
EA0.5-0(2.4)EA	EA0.5-0(1)	7.2	3	2.4
EA0.5-0(3.1)EA	EA0.5-0(1)	3.4	4	3.1
EA0.5-0(1)		100	1	1
EA0.5-0 (1.62)EA2	EA0.5-0(1)	23.5	2	1.62
EA0.5-0(2.34)EA2	EA0.5-0(1)	7.8	3	2.34
EA0.5-0(2.98)EA2	EA0.5-0(1)	3.8	4	2.98
EA0.5-0(1)		100	1	1

EA0.5-0(1.56)EA	EA0.5-0(1)	26.3	2	1.56
EA0.5-0(2.34)EA3	EA0.5-0(1)	7.8	3	2.34
EA0.5-0(2.76)EA3	EA0.5-0(1)	4.8	4	2.76
HMA0.5-0(1)		100	1	1
HMA0.5-0(1.71)EA2	HMA0.5-0(1)	20	2	1.71
HMA0.5-0(2.85)EA2	HMA0.5-0(1)	4.3	3	2.85
HMA0.5-0(3.84)EA2	HMA0.5-0(1)	1.8	4	3.84

3. Characterization of multiple network elastomers

3.1 Tensile tests

Uniaxial extension experiments were performed on a standard tensile Instron machine, model 5565, fitted with a 100 N load cell and custom made pneumatic clamps (Figure 2.*4*(a)). The clamps reduced slippage and damage to the samples by allowing precise control over clamp pressure. To measure the strain during the uniaxial deformation, two black marks were made on the homogeneously deformed zone of the specimens. An RGB camera (SENTECH: STC-MCS241U3V, image sensor: SONY IMX174, cell size: 5.86 μm×5.86 μm) with a frame rate of 25 fps was used to record the relative displacement of the two black markers (Figure 2.*4*(b)). MATLAB scripts were used to analyze the position of the marks from the recorded videos, which allowed for accurate determination of the applied uniaxial stretch. The nominal strain was defined as Equation 4:

$$\lambda = \frac{L}{L_0} \qquad \textit{Equation 4}$$

where L_0 and L are the distances between the two centroid of the marks before and after stretching, respectively. The engineering stress was obtained from the Instron machine. Before performing tensile tests, all specimens were exposed to white light for 5 mins to ensure that all of the mechanophores were in its unactivated SP form.

3.1.1 Uniaxial extension

For uniaxial tensile tests, samples with a dog-bone shape were made by using a pre-made punch as shown in Figure 2.*4b*. The gauge length of the central part is about 20 mm and the thickness of samples varied from 0.6 to 2 mm. Tests were performed with nominal stretch rate $\dot{\lambda}$ ranging from 0.01 to 1 s^{-1}.

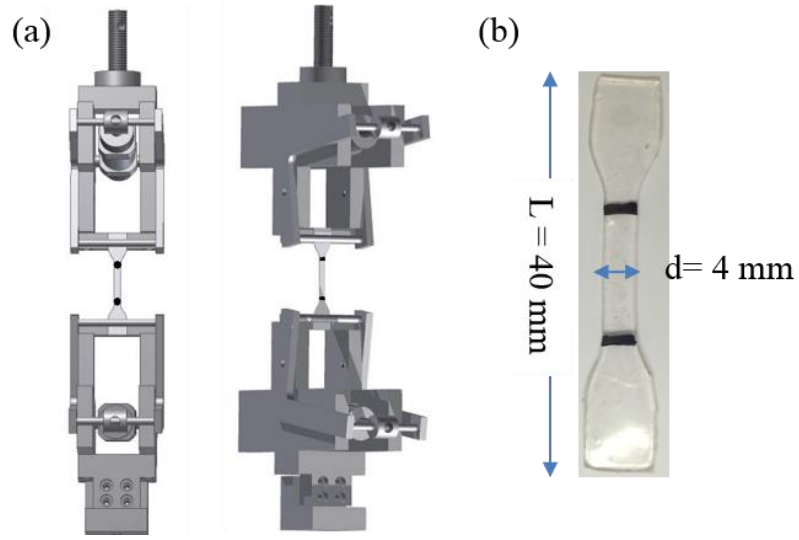

Figure 2.4: (a) The pneumatic clamps and (b) the specimens for extension tests

The nominal stress was determined by normalizing the measured force, *F*, by the initial sample cross-sectional area as defined in Equation 5:

$$\boldsymbol{\sigma_N = \frac{F}{dh}} \qquad \textit{Equation 5}$$

where *d* and *h* represent the sample width and thickness, respectively. The Young's modulus was calculated from data obtained at low strains.

3.1.2 Cyclic loading tests

To explore the reversibility of the activation of SP, cyclic loading tests were performed with EA0.5-0.05(2.23)EA sample. A dog-bone sample was used in the test and the stretch rate was set at $\frac{d\lambda}{dt} = \dot{\lambda}$ = 0.05 s^{-1}. To ensure that the fracture of sample did not occur during the test, the maximum stretch was set to $\lambda = 2.3$, below the critical value of failure of the samples. Figure 2.5 shows four cycles of tensile loading.

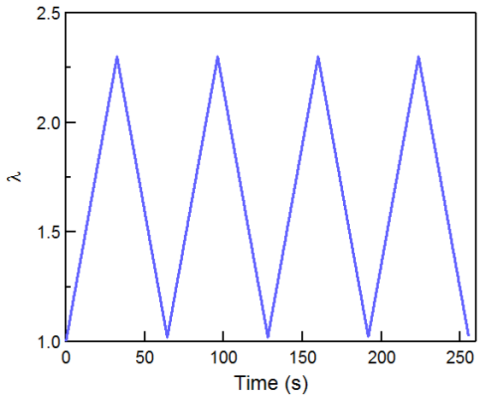

Figure 2.5: Cycle stress-strain curves of EA0.5-0.05(2.23)EA

3.1.3 Step cycle elongation tests

To study the energy dissipation in tensile tests, various TNs elastomers with different cross-linking densities and SP concentrations in the first network were used to perform step cycle loading tests. The stretch rate was set to 0.05 s-1 in the loading and unloading and the maximum strain started from $\lambda = 1.5$ with a 0.1 interval until samples failed as shown in Figure 2.6. Due to the different mechanical properties, varying categories of samples exhibited various stretches to failure and different numbers of cycle.

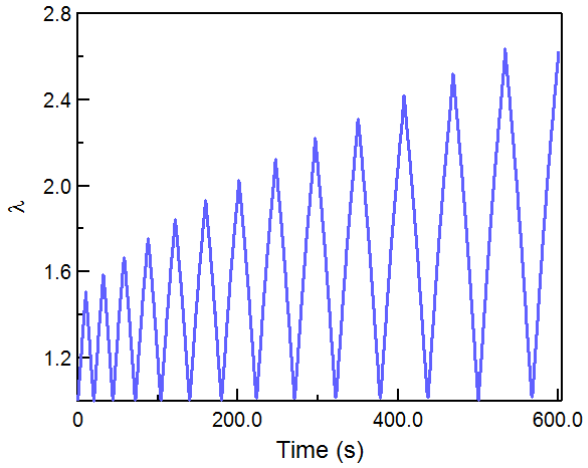

Figure 2.6: Strain as a function of time of EA0.5-0.05(2.23)EA in step cycle elongation test

3.1.4 Relaxation test

To explore the stability of MC in the tensile tests, relaxation tests were performed with EA0.5-0.05(2.23)EA sample. A dog-bone sample was stretched to $\lambda = 2.3$ and maintained 7 mins at that fixed stretch as shown in Figure 2.7. The whole procedure was recorded by the RGB camera and the video was used to do color analysis to examine the behavior of SP after activation. The methodology for the color analysis will be introduced in the next section.

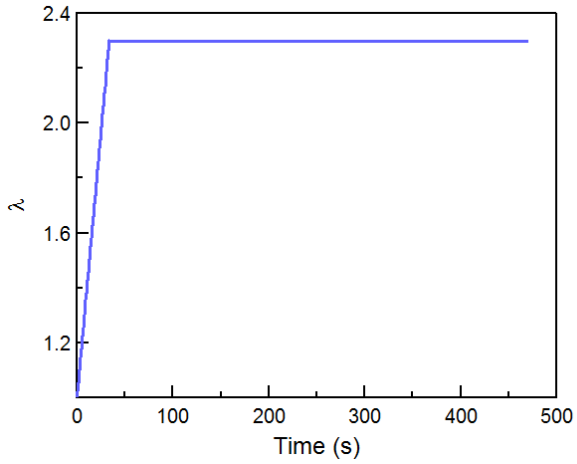

Figure 2.7 : Relaxation curve of EA0.5-0.05(2.23)EA sample

3.1.5 Fracture tests

To study the fracture toughness and mechanical response of the multiple networks around the crack tip, fracture tests were performed with the standard family of materials and part of some other groups of materials. Furthermore, due to the tedious procedure of synthesis for multiple networks, it took a long time to prepare a family of elastomers. Unfortunately, those elastomers can not be reused after tests. In order to save the elastomers, a uniform rectangular sample was made by a strip punch with a size of 20 mm (length), 10 mm (width). A 1 mm long notch was made with a razor blade on one side of sample as shown in Figure 2.*8*. The sample was fixed on the pneumatic clamps and the original length of sample between clamps was controlled at around 10 mm. A camera was also set to record the mechanical response during the crack propagation and the stretch rate was set at $\dot{\lambda}$ = 0.05 s^{-1}. After the tests the videos made by this camera was used to calculate the precise strain. Tracking two dots (two marks or two defect points) located on the both sides of the crack by MATLAB, the distance of the two dots was detected until the crack propagated. Then the precise critical strain λ_c of crack propagation could be measured. The strain energy density $W(\lambda_c)$ was calculated by integrating the stress-strain curves of un-notched samples up to the critical strain. The fracture energy Γ of materials finally was calculated by:

$$\Gamma = 2\,C \times W(\lambda_C) \times a \qquad \text{Equation 6}$$

$$C = \frac{3}{\sqrt{\lambda_C}} \qquad \text{Equation 7}$$

Where C is a strain dependent empirical correction associated to the lateral contraction of the sample in extension and 'a' is the length of notch.

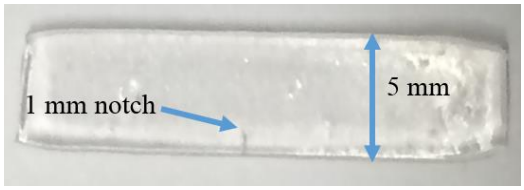

Figure 2.8: The image of sample for the fracture tests

3.2Color analysis: basic principles[10]

To map the stress and strain distribution in the materials, the relationship between the optical response (color change) and stress or strain needs to be examined. Color change can be quantified precisely using a spectrometer of course but if the goal is to map the color change pixel by pixel an RGB color camera presents distinct advantages. RGB stands for the three base color composition, namely, red, green and blue. A white background was placed behind the samples and a video recording of the entire experiment was made. A subset of snapshots (5 frames per second) were extracted from the video. The series of snapshots were processed and analyzed using a MATLAB script. Specifically, the frames were color corrected based on a white reference area. The color channel in the reference area was rescaled to the same mean intensity. The scaling factor was used to rescale the RGB values in the entire frame. An example of the color correction is shown in Figure 2.9 (a). The chromaticity for each pixel in the frame was determined as:

$$r_{RC} = \frac{R}{R+G+B} \qquad \textit{Equation 8}$$

$$r_{GC} = \frac{G}{R+G+B} \qquad \textit{Equation 9}$$

$$r_{BC} = \frac{B}{R+G+B} \qquad \textit{Equation 10}$$

where r_{RC}, r_{GC} and r_{BC} represent the red, green and blue chromaticity, respectively. R, G and B are the intensities of the red, green and blue channels for each pixel. The chromatic change (ΔRGB ratio) was calculated as:

$$\Delta r_{RC} = \frac{R}{R+G+B} - 0.333 \qquad \textit{Equation 11}$$

$$\Delta r_{GC} = \frac{G}{R+G+B} - 0.333 \qquad \textit{Equation 12}$$

$$\Delta r_{BC} = \frac{B}{R+G+B} - 0.333 \qquad \textit{Equation 13}$$

where chromatic change is relative to the sample chromaticity at the start of the experiment and 0.333 represents the chromaticity of the rescaled white background. The chromaticity of the background forms the base line before the chromatic change of the white samples occurs and factors out little differences between samples in terms of thickness and planarity (causing unwanted reflection) in particular. But the difference did not affect the chromatic change. The whole process described above is called color analysis.

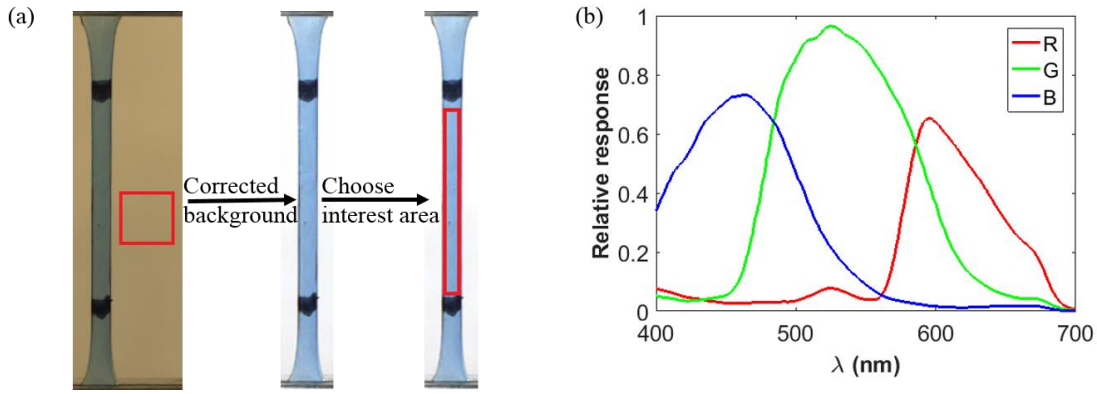

Figure 2.9: (a) The procedure of the RGB analysis; (b) the relative response of the camera sensor for various visible light

An important factor in the color analysis is the sensor of the RGB camera which affects the sensitivity of color change. Figure 2.9(b) shows the relative response of the sensor to various wavelengths of visible light. Since the color change (colorless to blue) is located at 450-475 nm, the blue and green channels will be more sensitive than the red channel. During the unloading process, since samples change from blue to purple, the blue channel will have the most sensitive response.

Conclusion

An SP cross-linker has been synthesized and was covalently incorporated into rubbery single networks. In addition, the mold was modified to synthesize single networks with smooth surfaces. Starting from diverse single networks, various categories of multiple network elastomers have been synthesized. They were categorized into four families with different cross-link densities and SP concentrations in the first network.

Tensile tests were performed to detect the mechanical properties of the four groups of materials, including uniaxial extension tests, cyclic loading tests, relaxation and fracture tests. To quantify the chromatic change of samples, color analysis was used.

The synthesized protocol of SP mechanophore crosslinker and the multiple networks have been described. This approach was able to synthesize categories of multiple networks by tailoring the cross-linking density and SP concentration in the filler network. The rapid synthesis of the multiple network with smooth surfaces was proposed by altering the standard synthesis method and modifying the mold used by Ducrot[1-3] and Millereau[4].

After the synthesis, various tests to detect the mechanical properties of multiple networks were introduced. Additionally, the strategy to quantify the mechanical response of multiple networks by color analysis was present in this chapter.

Finishing the synthesis and tests, the mechanical properties and mechanical response will be introduced in the following chapter.

Reference:

1. Ducrot, E.; *Université Pierre et Maire Curie: Paris* **2013**.
2. Ducrot, E.; Creton, C.; *Advanced Functional Materials* **2016**, *26*, 2482.
3. Ducrot, E.; Chen, Y.; Bulters, M.; Sijbesma, P. R.; Creton, C.; *Science* **2014**, *344*, 4.
4. Millereau, P.; *Université Pierre et Maire Curie: Paris* **2017**.
5. Gong, J. P.; Katsuyama, Y.; Kurokawa, T.; Osada, Y.; *Advanced materials* **2003**, *15*, 1155.
6. Chen, Y.; Zhang, H.; Fang, X.; Lin, Y.; Xu, Y.; Weng, W.; *ACS Macro Letters* **2014**, *3*, 141.
7. Fang, X.; Zhang, H.; Chen, Y.; Lin, Y.; Xu, Y.; Weng, W.; *Macromolecules* **2013**, *46*, 6566.
8. O'Bryan, G.; Wong, B. M.; McElhanon, J. R.; *ACS applied materials & interfaces* **2010**, *2*, 1594.
9. Jiang, S.; Zhang, L.; Xie, T.; Lin, Y.; Zhang, H.; Xu, Y.; Weng, W.; Dai, L.; *ACS Macro Letters* **2013**, *2*, 705.
10. Gossweiler, G. R.; Hewage, G. B.; Soriano, G.; Wang, Q.; Welshofer, G. W.; Zhao, X.; Craig, S. L.; *ACS Macro Letters* **2014**, *3*, 216.

Appendix

1. The detailed protocol of SP synthesis

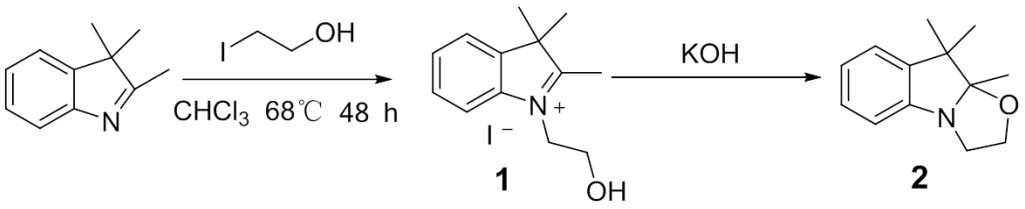

Scheme 2.6: Synthesis of 2-hydroxyethyl-2,3,3-trimethyl-3H-indolium iodide

2,3,3-Trimethylindolenine (1.5 mL, 9.3 mmol, 1.0 eq.) and 30 mL chloroform was poured into a sealed reflux setup composed of a Schlenk flask (nitrogen flask) and a condenser. Sequential freezing with liquid nitrogen, pumping, filling with nitrogen gas were carried out to pump out most of the oxygen in the setup. 2-iodoethanol (0.8 mL, 10.2 mmol, 1.2 eq.) was injected into the setup and the chemical reaction as shown in Scheme 5 was conducted under a nitrogen atmosphere at 68 ℃. After 48 hours, the red suspension was cooled to room temperature and the solvent was removed under vacuum. The solid was collected and washed with petroleum ether and ether, respectively. A deep red powder (3.0 g, 9.1 mmol, 96%) was obtained by drying under vacuum overnight.

^{1}H-NMR (400 MHz, $CDCl_3$): δ (ppm)=7.80-7.76 (m, 1 H, Ar-H), 7.61-7.55 (m, 3 H, Ar-H), 4.88 (t, 2 H, -NC*H*$_2$CH$_2$O-), 4.20 (t, 2 H, -NCH$_2$C*H*$_2$O-), 3.10 (s, 3 H, CH_3), 1.65 (s, 6 H, CH_3).

KOH (0.31g, 5.5 mmol) and the indolium iodine **1** (0.97 g, 2.9 mmol) was placed in a mortar and grinded with a pestle until a yellow paste was obtained. The indole **2** (0.55 g, 2.7 mmol, 93%) (orang liquid) was collected by extracting the yellow paste with petroleum ether, evaporating under vacuum, drying in vacuum overnight.

1H-NMR (400 MHz, CDCl3): δ (ppm)=7.07 (m, 2 H, Ar-H m-NR2), 6.84 (m, 1 H, Ar-H p-NR2), 6.76 (m, 1 H, Ar-H o-NR2), 3.86 (m, 2 H, -NCH2CH2O-), 3.73 (m, 1 H, -NCH2CH2O-), 3.57 (m, 2 H, -NCH2CH2O-), 1.37 (s, 3 H, C(N)(O)CH3), 1.31 (s, 3 H, CH3), 1.23 (s, 3 H, CH3).

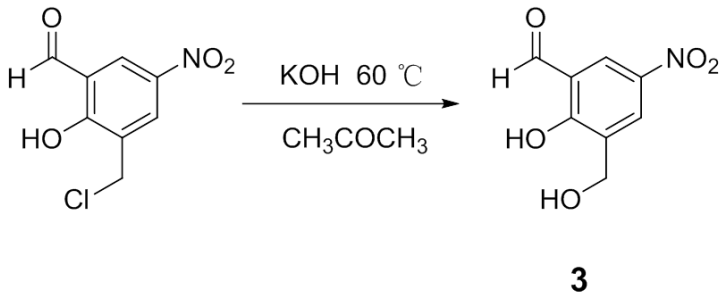

3

Scheme 2.7: Synthesis of nitrosalicylaldehyde

3-chloromethyl-5-nitrosalicylaldehyde (0.2 g, 0.93 mmol) was dissolved into 1 mL acetone and the solution was diluted by 0.35 mL H_2O. After 20 min reflux, 0.15 mL 6 mol/L NaOH aqueous solution was instilled into the acetone solution above. After 3 hours of hydrolysis, acetone and water were removed under vacuum. The raw product was wash with bits of H_2O twice and a light yellow powder (0.15 g, 0.76 mmol, 82%) was obtained.

1H-NMR (400 MHz, CDCl3): δ (ppm)=11.93 (br s, 1 H, phenol), 10.24 (s, 1 H, -C(O)H), 8.72 (d, 1 H, J=3 Hz, Ar-H ortho CH2OH), 8.62 (m, 1 H, Ar-H para CH2OH), 4.82 (s, 2 H, -CH2OH), 4.64 (br s, 1 H, CH2OH).

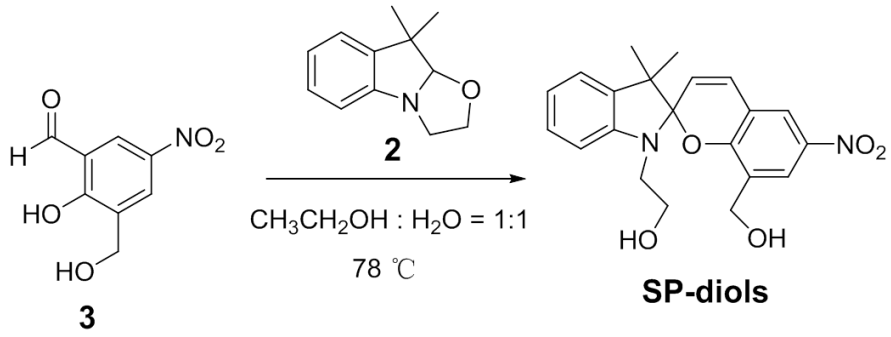

Scheme 2.8: Synthesis of SP-diols

Indole **2** (1.0 g, 4.9 mmol, 1.1 eq.) and nitrosalicylaldehyde **3** (0.81 g, 4.1 mmol, 1 eq.) were dissolved into mixed solvent of 15 mL H_2O and 15 mL ethanol. The solution refluxed overnight under 78 ℃. Ethanol was removed under vacuum and the deep purple raw product was washed with H_2O by ultrasound. The raw product was recrystallized in another mixed solvent of acetonitrile and H_2O (volume fraction= 7:3). SP with a bolarious powder (1.5 g, 3.9 mmol, 80%) was obtained.

^{1}H-NMR (400 MHz, $CDCl_3$): δ (ppm)=[8.12 & 7.97] (d, 2 H, *J* =3 Hz, Ar-H *o*-NO_2), 7.17 (d, 1 H, *J* =10.5 Hz, Ar-C*H*=CH-), 7.12 (m, 2 H, Ar-H *m*-NR_2), 6.81 (t, 1 H, *J* =7 Hz, Ar-H *p*-NR_2), 6.64 (d, 1 H, *J* =7.5 Hz, Ar *o*-NR_2), 5.89 (d, 1 H, *J* =10.5 Hz, -C*H*=CH-Ar), [4.57, 4.42] (m, 2 H, ArC*H*$_2$OH), 3.74(m, 2 H, NCH_2CH_2OH), [3.48 & 3.31] (m, 2 H, NCH_2CH_2OH), [1.29 & 1.21] (s, 3 H, $C(CH_3)_2$).

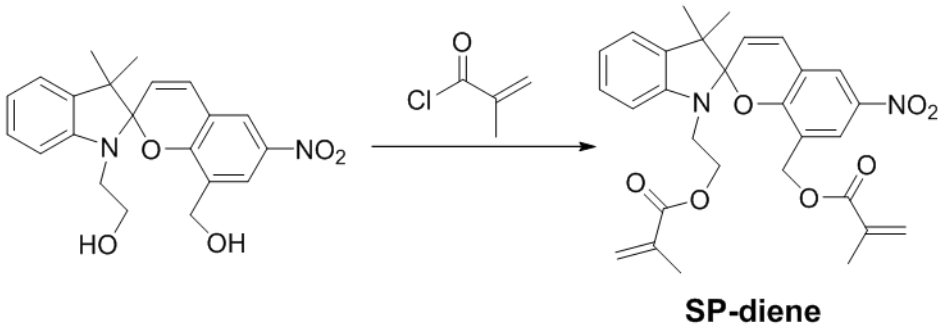

Scheme 2.9: Synthesis of SP mechanophore crosslinker

SP-diols (250 mg, 0.65 mmol, 1.0 eq.) and triethylamine (907 µL, 6.5 mmol, 10 eq.) was dissolved in 30 mL tetrahydrofuran. The color of the solution was deep blue and when tetrahydrofuran was mixed, it changed to deep purple. The solution was mixed in ice bath for 15 min, and then methacryloyl chloride was instilled into the solution. The color of solution changed from purple to yellow. The temperature of this chemical reaction could be increased to the room temperature in 3 hours. After 24 hours, some pink precipitate generated at the bottom of flask and the color of solution turned to pink. The solvent was evaporated under vacuum after filtration. The raw product was dissolved into 50 mL dichloromethane and the solution was washed with saturated K_2CO_3 aqueous solution for three time. The dichloromethane was removed and purple paste was obtained. To purify the SP-diene, a column chromatography of silica was used and dichloromethane was used as the eluent. There are three composition flowing out from the column and SP-diene is the middle one. The SP-diene solution was collected and the solvent was removed under vacuum. The recrystallize of n-hexane can be used for the further purify of the SP-diene. Finally, the pure product of yellow powders (223 mg, 0.43 mmol, 66%) can be obtained.

Chapter 3: Mechanical properties and optical response of multiple network elastomers

Introduction

Four families of multiple network elastomers containing SP mechanophores have been prepared. As discussed in the introduction, according to previous work, SP in the polymer chains can be activated by force. But a sufficient force in the polymer chain is necessary to activate SP. To obtain an optical response (color change in this manuscript), materials possessing tough mechanical properties, characterized by a high stress at break and high fracture toughness, is required. Before characterizing the mechanical response of samples containing SP, examining the mechanical properties of elastomers without SP is necessary. The EA0.5-0.05 standard family materials was used as a reference and its mechanical properties were compared to other groups of materials.

To explore the correlation between the mechanical and optical responses, color analysis was used to quantify the chromatic change. Color analysis of the optical response to a mechanical stimulus provides information on the relationship between the variation of chromaticity and stress (or strain). The development of the color analysis is important for constructing a quantitative stress mapping. In this chapter we will introduce the approach of mapping stress around a crack by analyzing the color change with increasing loading.

1. Mechanical properties

1.1 Standard family multiple network elastomers

According to Ducrot and Millereau[1], the first network controls the mechanical properties of multiple network elastomers. To examine the effects of incorporating SP as a crosslinker instead of BDA on the mechanical properties of the SN, diverse single networks with 0.5 mol% cross-linker density were synthesized, and uniaxial extension tests were carried out. Figure 3.1 shows stress-strain curves of networks with varying SP concentrations at the same total crosslinker concentration. No significant differences in the stress-strain response were observed in the single networks. Thus, SP does not affect the mechanical properties of SNs, indicating that SP can be used as a molecular probe for the measurement of stress and strain in elastomers. Due to the similar mechanical properties of first network, the DN, TN and QNs containing SP did not show obvious difference compared with a blank sample (without SP in the first network).

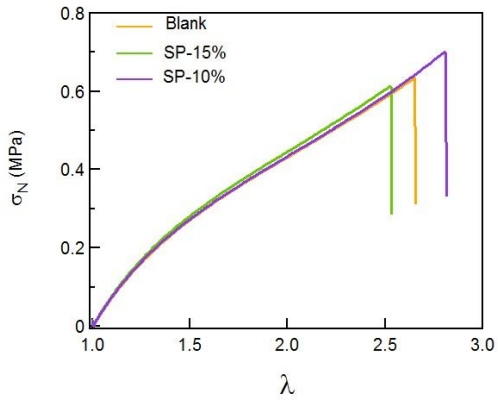

Figure 3.1: The stress-strain curves of various single networks containing different SP concentrations. This concentration refers to mol% of SP relative to the total crosslinker.

To study the mechanical properties of interpenetrated multiple network elastomers, tensile tests with various polymer networks were carried out. The data presented are based on the EA0.5-0.05 family of materials, which contain the same SN concentration. To ensure reliability, triplicate measurements were performed for each specimen type. The main results of the mechanical tests are shown in Table 3.1. The increase in Young's modulus and maximum stress shows the typical reinforcement effect observed for multiple networks.

Table 3.1: The mechanical properties of EA0.5-0.05 family of multiple network elastomers.

Sample name	λ_0	SN wt%	Type of Polymers	E/ MPa	Stress at break /MPa
EA0.5-0.05(1)	1	100	SN	0.85	1.1
EA0.5-0.05(1.56)EA	1.56	26.5	DN	1.16	4.6
EA0.5-0.05(2.23)EA	2.23	9.0	TN	1.88	15.7
EA0.5-0.05(2.81)EA	2.81	4.5	QN	3.96	10.6

The SNs shows a typical neo-Hookean behavior until fracture at around 200% extension, DNs display initial strain hardening before fracture, and TNs possess a strain hardening and strain softening behavior leading to a high stress at break, as shown in Figure 3.2 (a). QNs behaved qualitatively similarly with stiffening followed by softening. However, EA0.5-0.05(2.81)EA (QNs) exhibited a softer stress at break and toughness (Table 3.1) than EA0.5-0.05(2.23)EA despite its higher Young's modulus due to the softening.

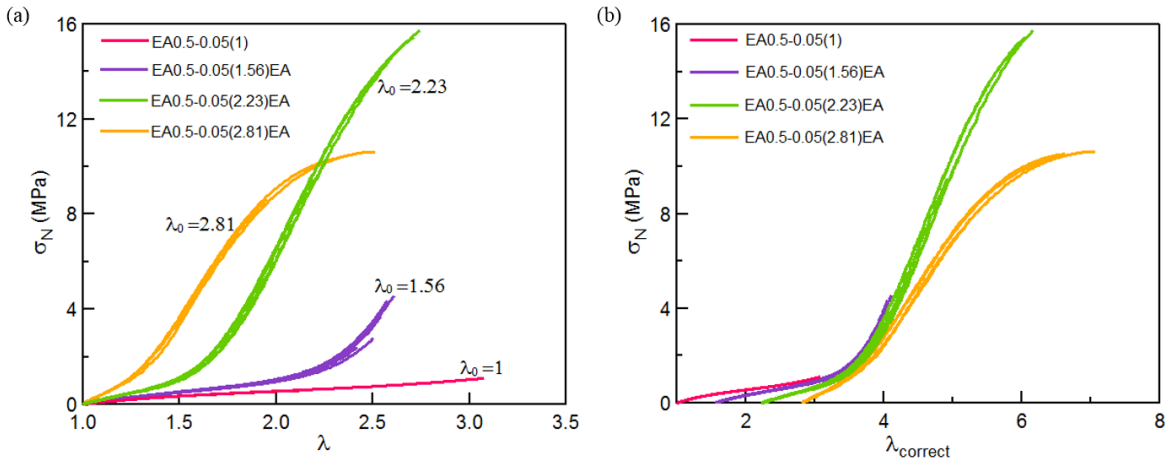

Figure 3.2: The stress-strain curves of the EA0.5-0.05 family of elastomers (a) before and (b) after correction due to the pre-stretch.

Due to the different swelling steps during the synthesis, DNs, TNs and QNs possess different degrees of pre-extension as shown in Table 3.1. Although the multiple networks have a lower strain at failure compared to the SNs, the actual strain at failure of the first network embedded in the multiple networks was enhanced. This increase in strain at failure of the SN can be observed by applying a renormalization, to the nominal extension ratio as defined by Equation 1:

$$\lambda_{correct} = \lambda \times \lambda_0 \qquad \text{Equation 1}$$

In Figure 3.2(b), all the curves except SNs show the onset of hardening behavior at $\lambda_{correct}$ ~

3.5. This suggests a high stress in the polymer chains of the first network. A difference between this work and the work of Ducrot et al[2]. or Millereau et al[1]. is that no solvent was used in the synthesis of the SN, which may have resulted in an increase in chain transfer reactions between networks during polymerization and in the presence of more entanglements in the SN. Chains transfer reactions and entanglements induced an increase of the coupling between networks. This results in a less clear overlap of the renormalized stress-strain curves (after strain and stress correction) than what is reported in the literature[1].

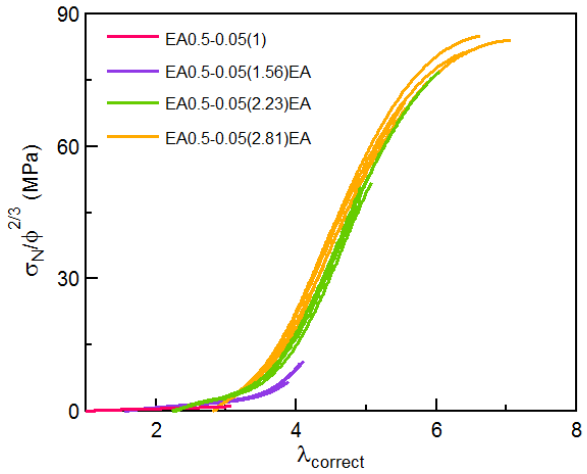

Figure 3.3: Corrected nominal stress as a function of corrected strain with EA0.5-0.05 family group materials

As shown by Millereau et al[1,3]. softening is caused by the scission of polymer strands of the first network that are oriented in the tensile direction, since the stress prior to necking is sustained by the first network. Considering the dilution of the SN in multiple networks, the stress can be renormalized by the areal density of the SN chains for each material as shown in Equation 2:

$$\Sigma = \Sigma_{SN}\phi_{SN}^{2/3} \qquad \text{Equation 2}$$

where Σ and Σ_{SN} are the areal density of chains of the first network in multiple and single networks, respectively. Similarly, a correction for the stress is also considered for the stress-strain curves, which is shown in Figure 3.3. The corrected stress-strain curves of this family form a master curve. These results confirm the standpoint that the first network acts as a rigid and continuous filler in multiple networks and bears the stress in tensile tests.

1.2 Various stretching rates

Mechanical performance can depend on the stretch rate when some physical cross-linkers or entanglements exist in polymer networks resulting in viscoelastic properties of the polymer

materials. To examine the viscoelastic properties of the multiple network systems, extension tests were performed over a range of strain rates. Comparing the curves in Figure 3.4, the DNs or TNs samples exhibit the same Young's modulus and strain hardening at low strain rates from 0.001 s^{-1} to 0.1 s^{-1}. However there seems to be an effect of the strain rate on the fracture process since the elastomers fail at a higher stress when they are deformed at a high strain rate. It illustrates that viscoelastic effects due to chain entanglement have a negligible effect on the DN and TN elastomers for the EA0.5 family of elastomers.

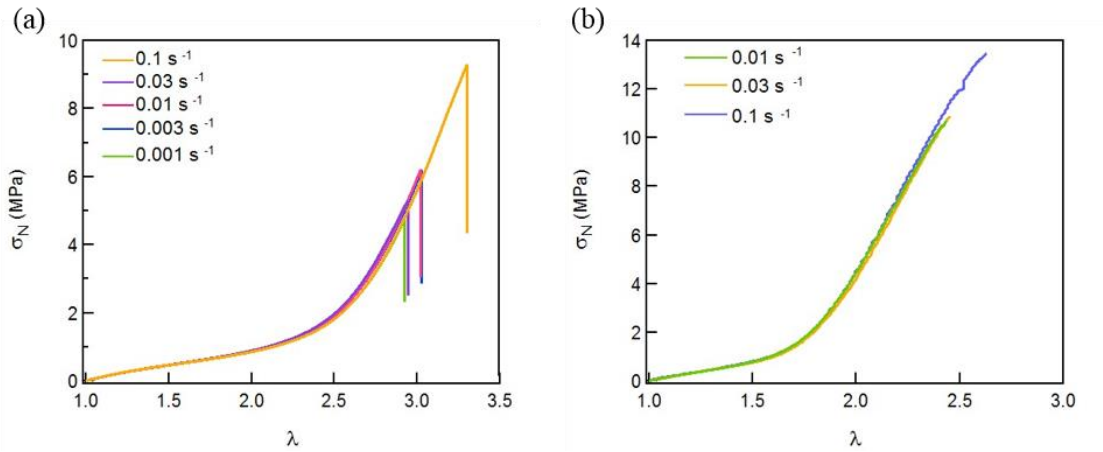

Figure 3.4: The stress-strain curves of (a) EA0.5-0.05(1.56)EA and (b) EA0.5-0.05(2.23)EA materials with various tensile velocities.

1.3 Different cross-link densities

Acting as a filler network, the cross-linking density of the first network heavily impacts the bulk mechanical properties of the multiple network elastomers. The mechanical properties of multiple network elastomers with various crosslinker densities of the filler network was examined. Figure 3.5 shows the stress-strain curves of SNs with various crosslinker densities. EA0.01-0.01(1) has a same cross-linker density as the second/third/fourth network in EA0.5-0.05 family of elastomers and it can also be considered as a single second network or as a matrix network. Theses SNs have clearly different mechanical properties, including varying Young's modulus, extensibility and stress at break. The modulus increases with increasing the cross-linker density but it is the opposite for the elongation. Furthermore, the EA0.01-0.01(1) shows a marked softening, due to the presence of entanglements and strain hardening at the end of extension, which is not observed for the more crosslinked materials that break at a lower extension.

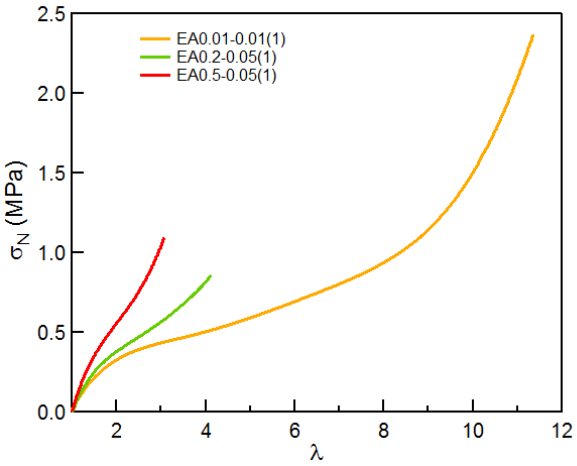

Figure 3.5: Stress-strain curves for various SN with different crosslinker densities

These SNs were used to prepare different families of multiple network elastomers. Subsequently, the three families of materials were tested in uniaxial extension. The results are shown in Figure 3.6. The color code refers to the number of swelling-polymerization steps used to prepare the sample. Red is one, purple is two, green is three and yellow is four.
Comparing the stress-strain curves of the EA0.5-0.05 and EA0.2-0.05 families, the reduction in cross-linker density of the filler network results in a decrease in the modulus with no decrease in the observed nominal stress at break. Also, the EA0.2-0.05 family of materials is more extensible that the EA0.5-0.05 family. Note that after softening, EA0.2-0.05(3.49)EA exhibits a stress plateau as shown in Figure 3.6. This is a yielding phenomenon, which is sometimes observed in the tensile tests of EA0.5-0.05(2.81)EA samples. The EA0.01-0.01 family of materials displays a soft and extensible mechanical behavior. In addition, the EA0.01-0.01(1.96)EA shows a hardening regime above $\lambda = 5$. The similar phenomenon is observed for DNs in other families at varying stretch ratioλ. EA0.01-0.01(3.28)EA exhibited strain hardening, followed by a stress plateau; this was also observed in the QNs of the other two families. Although a decrease in cross-linker density results in a lower modulus in the three groups above, the breakage stress and toughness remain high.

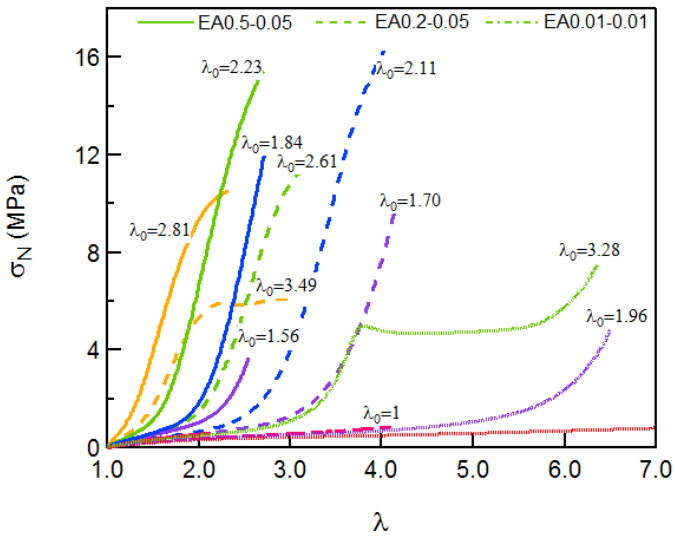

Figure 3.6: Stress-strain curves of EA0.5-0.05, EA0.2-0.05 and EA0.01-0.01 families of multiple network elastomers. The color code refers to the number of swelling-polymerization steps used to prepare the sample. Red, purple, green, and blue correspond to single, double, triple, and quadruple networks.

The results for the three family of materials are summarized in Table 3.1 and Table 3.2, respectively. It is interesting to note that the improvement is most evident for materials with high crosslinker density in the filler network, which illustrates that the first network behaves as the filler network that largely determines their mechanical properties. This is also evident in Figure 3.6, where systems made from SNs with differing cross-linking densities exhibit qualitatively different stress-strain curves consistent with previous reports[4-6]. Due to the pre-stretch of the filler network initiated by the swelling in the synthesis, the strain of multiple network can be rescaled by λ_0 and the stress can be replotted as a function of $\lambda_{correct}$ as shown in *Figure 3.7* (a). This correction leads to the formation of three master curves, as shown in *Figure 3.7* (a). Samples with the higher cross-linking density display an onset of strain hardening at lower corrected stretch due to lower molecular weight between cross-links. The average molecular weight between cross-links can be estimated as Equation 3:

$$E = \frac{3\rho RT}{M_x} \qquad \text{Equation 3}$$

here M_x,ρ, R and E are the molecular weight between cross-linkers, polymer density, the gas constant and Young's modulus. According to Equation 3, Young's modulus increases with the decrease of the molecular weight between cross-links, namely, the increase of cross-link density. This is consistent with the results as shown in Figure 3.6. But the variation in modulus is not proportional to the variation in cross-linker density and does not agree with the relationship in Equation 3. Especially, when the cross-link density decreases 50 times (from 0.5 mol% to 0.01 mol%), the modulus of EA0.01-0.0(1) only reduces to half of EA0.5-0.05(1).

This is attributed to the presence of entanglements and to the occurrence of chain transfer reactions. Chains transfer reactions directly increase the concentration of crosslinks resulting in the increase of modulus. For the entanglements, when the molecular weight between cross-links increases to the threshold (about 8200 g/mol for poly(ethyl acrylate)) of entanglement, the modulus is composed of two contributions:

$$E = \frac{3\rho RT}{M_x} + \frac{3\rho RT}{M_e} \qquad \text{Equation 4}$$

The effect of entanglements on the modulus significantly increases as the molecular weight between cross-links increases. The two factors above alter the structure of the filler network and change its mechanical properties.

Table 3.2:Young's modulus of EA0.2-0.05 and EA0.01-0.01 families of materials

Sample name	λ_0	SN wt%	Type of Polymers	E/ MPa	Stress at break /MPa
EA0.2-0.05(1)	1	100	SN	0.62	0.86
EA0.2-0.05(1.70)EA	1.70	20.2	DN	0.9	10
EA0.2-0.05(2.61)EA	2.61	5.6	TN	1.24	11.3
EA0.2-0.05(3.49)EA	3.49	2.2	QN	2.16	6.0
EA0.01-0.01(1)	1	100	SN	0.46	2.4
EA0.01-0.01(1.96)EA	1.96	13.2	DN	0.58	4.9
EA0.01-0.01(3.28)EA	3.28	2.8	TN	0.83	7.5

For the DNs, TNs and QNs in the two groups of EA0.5-0.05 and EA0.2-0.05, materials show very similar strain hardening slopes after the neo-Hookean behavior suggesting that the mechanical properties and fracture behavior share a similar physical mechanism. For the two highly prestretched materials EA0.2-0.05(3.49)EA and EA0.01-0.01(3.28)EA a stress plateau caused by the necking phenomenon is observed. The necking phenomenon is attributed to the high pre-stretch of the filler network and its high level of dilution. The high value of λ_0 and low value of ϕ_0 causes significant bond scission (about 10%) in the filler network without propagation of a macroscopic crack as described in reference[1]. This necking process is examined in more detail in Chapter 5.

Although the first network in the EA0.01-0.01 family of materials has the same cross-linking density as the second and/or other networks, reinforcement in the multiple networks is also significant, which can be seen in Figure 3.6. Comparing all the Young's moduli of the EA0.2-0.05 and EA0.01-0.01 families of materials in Table 3.2, it is obvious that the improvement of EA0.2-0.05 in the Young's modulus is more marked than for the EA0.01-0.01, which supports the conclusion that the interpenetrated multiple networks provide a general strategy for effective reinforcement of elastomers.

If the stretch and stress of the three groups of materials are renormalized by the pre-stretch λ_0 and by the areal density of the first network Σ, respectively one obtains Figure 3.7 (b). Interestingly, the renormalization of the stress works only when there is a large contrast in crosslinking between the filler network and the matrix networks, such as the EA0.5-0.05 family. For the less crosslinked first networks, entanglements and chain transfer reactions increase the coupling between networks, which cannot be treated as independent even in the elastic region. Thus, the stress-strain curves of the EA0.01-0.01 family cannot completely overlap.

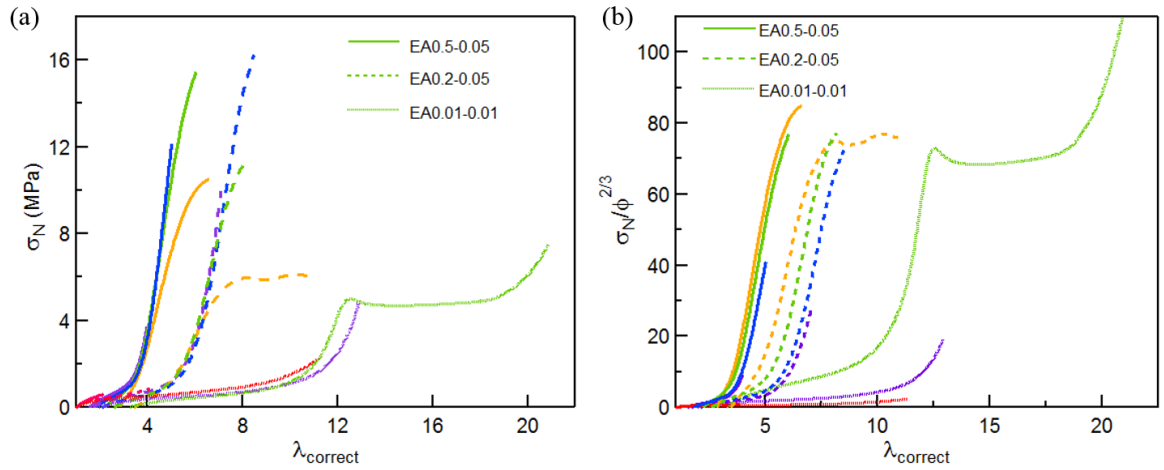

Figure 3.7: Renormalized tensile for the three families of materials with 0.01, 0.2 and 0.5 mol/% of cross-linker density in the first network. Nominal stress as a function of (a) corrected strain; (b) stress is corrected by the dilution of the areal density of the first network and is plotted as a function of the corrected strain.

1.4 Behavior of samples under cyclic loading tests

When irreversible damage occurs in the materials upon loading, it cannot be observed by simple uniaxial tensile tests to failure. However, the cyclic loading test shows the damage in the first cycle with a hysteresis. In addition, if part of the damages is recoverable, another smaller hysteresis would be seen in subsequent cycles compared to the first cycle with the same deformation. Recoverable hysteresis is generally caused by viscoelasticity due to some physical interactions in unfilled elastomers, including hydrogen bonding[7-10], hydrophobic interactions[11-13], electrostatic interactions[14], etc. Four cyclic loading tests were carried out on the EA0.5-0.05(2.23)EA sample as shown in Figure 3.8. A large hysteresis occurs during the first cycle, while subsequent cycles show no hysteresis. This behavior suggests that the damage occurring in the first cycle is irreversible due to bond breakage. Damage occurs during the first cycle, dissipating energy, but the damage does not cause failure of the materials. In particular, there is an insignificant decrease of modulus upon reloading.

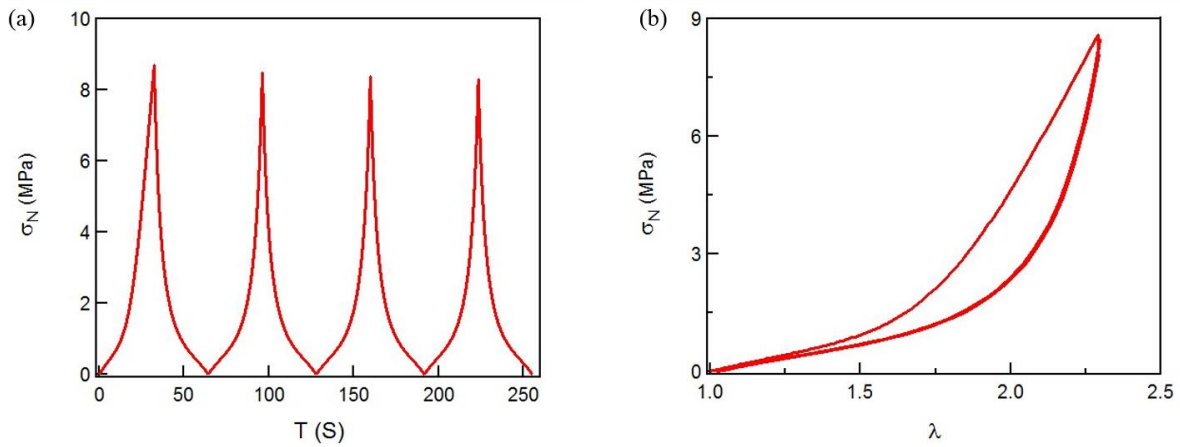

Figure 3.8: Four cyclic loading test with the EA0.5-0.05(2.23)EA samples

To detect damage in uniaxial extension, a step cyclic loading was performed on a EA0.5-0.05(2.23)EA sample. From the curves of *Figure 3.9* (b), significant hysteresis is not apparent in the beginning of the step cyclic loading (for $\lambda_{max} < 1.75$). As shown in *Figure 3.9* (c), the hysteresis increases with maximum deformation. The hysteresis ($U_{hyst}(n)$) and the total hysteresis ($total\ \mathrm{U_{hyst}}(n)$) in the step cycle loading was calculated with Equation 5 and Equation 6, respectively.

$$U_{hyst}(n) = \int_{1}^{\lambda(n)} \sigma_N d\lambda \qquad \text{Equation 5:}$$

$$total\ U_{hyst}(n) = \sum_{i=1}^{n} U_{hyst}(n) \qquad \text{Equation 6:}$$

where $\lambda(n)$ and n are the maximum stretch ratio in each cycle and the number of cycles, respectively. *Figure 3.9* (c) and (d) show that the hysteresis (and hence the damage and bond scission) starts at $\lambda \sim 1.75$ and $\sigma_N = 2.9\ MPa$. According to the pre-stretch of EA0.5-0.05(2.23)EA, the initial damage of the filler network occurs at $\lambda_d = 2.23 \times 1.75 = 3.90$. Larger hysteresis is associated with higher energy dissipation, since more and more scission of bonds occurs in the first network. Furthermore, a progressive reduction in the Young's modulus is observed due to the damage of the first network acting as the percolating filler of multiple networks[1]. In addition, when two consecutive cycles are compared (after the first damaging cycle), the unloading and reloading curves overlap, which demonstrates minimal viscoelastic dissipation between cycles.

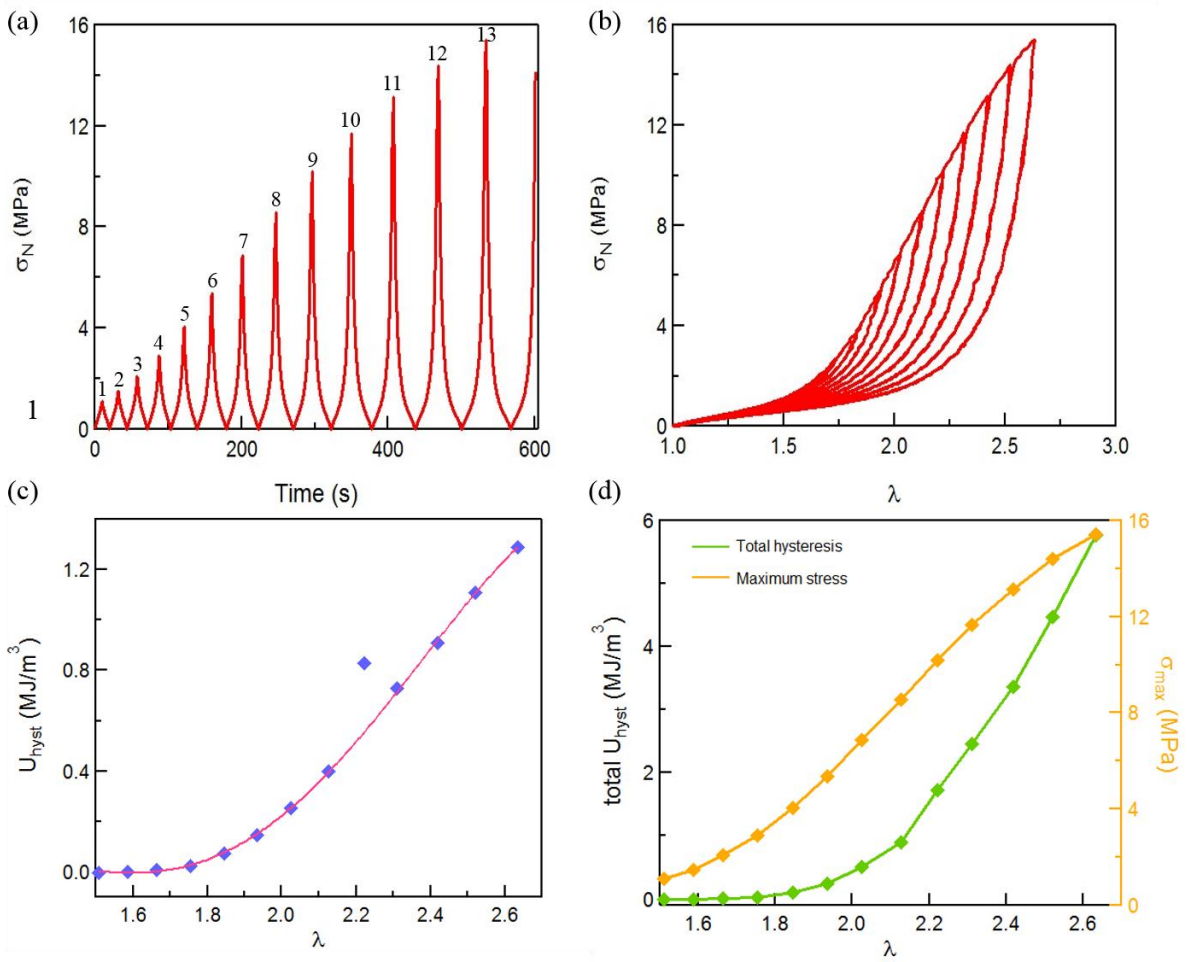

Figure 3.9: Nominal stress as a function of (a) time and (b) strain in step cycle elongation tests with EA0.5-0.05(2.23)EA materials; (c) hysteresis ($U_{hyst}(n)$) and (d) total hysteresis ($total\ U_{hyst}(n)$) as as function of λ in step cycle loading test of EA0.5-0.05(2.23)EA

1.5 Fracture energy

A high fracture energy is important to avoid the propagation of an existing crack. The fracture energy (Γ) is the necessary energy for a crack to propagate and create two new fracture surfaces. In order to investigate the stress field around the crack prior to propagation using SP, a sufficient volume around the crack should be able to sustain stresses above the detection limit in the color change caused by the activation of the mechanophore. In other words, materials exhibiting high fracture toughness are needed to probe the stress distribution, which makes the EA0.5-0.05 and EA0.2-0.05 families of materials an ideal system to use.

Based on the value of λ where the crack propagates, λ_c, the fracture energy can be calculated according to the approach first proposed by Rivlin and Thomas[15] and modified for a single edge notch geometry, as described by Greensmith[15]:

$$\Gamma = 2C \times W(\lambda_C) \times a \qquad \text{Equation 7}$$

$$C = \frac{3}{\sqrt{\lambda_C}} \qquad \text{Equation 8}$$

Where a, λ_C and W(λ_C) are the length of notch, critical strain for crack propagation and strain energy in the unnotched sample at $\lambda = \lambda_C$. C in Equation 7 is a strain dependent empirical correction and that can be calculated from Equation 8. To obtain the fracture energy, fracture tests were carried out with EA0.5-0.05 and EA0.2-0.05 families of materials.

As described in chapter 1, a uniaxial tensile test was performed along the length direction of a rectangular sample with a notch that had been previously cut with a razor blade. The critical strain (λ_C) was defined as the maximum value of nominal stress and was directly obtained from the stress-strain curves of notched samples as shown in Figure 3.10 (a). Then the strain energy densities (W(λ_C)) were calculated by integrating the stress-strain curves of identical but unnotched samples up to λ_C as shown in Figure 3.10 (b). The results of the measured fracture energies are listed in Table 3.3. Compared to the samples without notches, Figure 3.10 (a) shows a clear reduction of stretch and stress at break due to the presence of a crack.

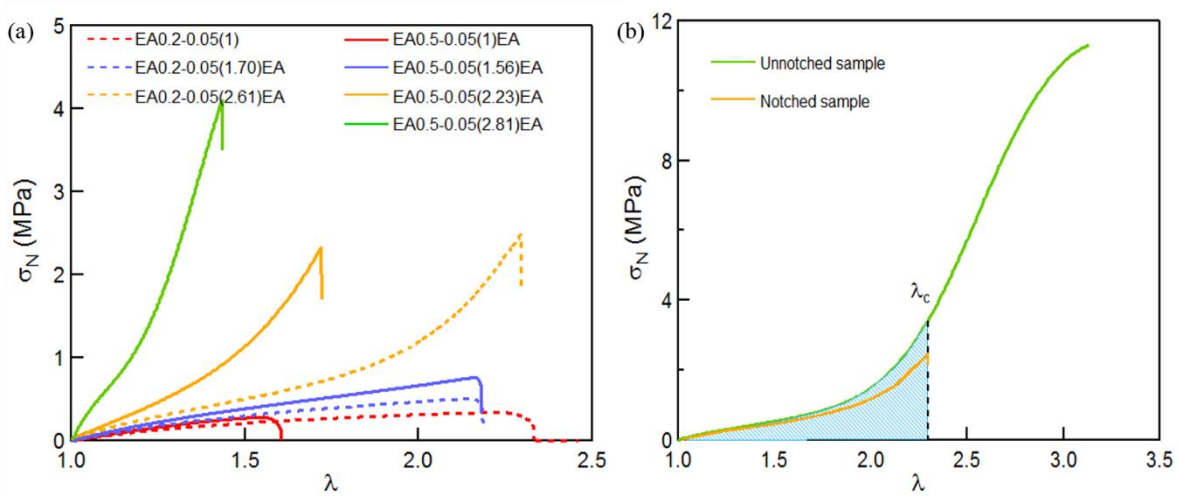

Figure 3.10: (a) Stress-strain curves of EA0.5-0.05 and EA0.2-0.05 families materials with notches; (b) Stress-strain curves of EA0.2-0.05(2.61)EA samples with and without a notch: the gray area represents the energy density W(λ_C).

From the values of the fracture energy in Table 3.3, a significant increase in Γ is observed for both families of materials, which is consistent with the observation of mechanical reinforcement in multiple network elastomers. When comparing the fracture energy of EA0.5-0.05(2.23) and EA0.5-0.05(2.81)EA, the fracture energies are almost the same, despite a higher pre-stretch level in the EA0.5-0.05(2.81)EA sample. The same phenomenon was also observed in reference [1] and [2]. According to their conclusion, for λ_0>2.5, the fracture energy increases more slowly and tends to saturate. But this result is still difficult to explain.

When the cross-linker density in the first network was decreased, the effect of pre-stretch on the fracture energy is more obvious, and can be observed by comparing the EA0.2-0.05(1.70)EA and EA0.2-0.05(2.61)EA samples. It may be because materials containing a lower cross-link density filler network can reach a higher pre-stretch, which leads to a higher amount of damage in the first network or some damage in the second (maybe third) network that contributes to the fracture energy.

Table 3.3: Energy density and fracture energy of EA0.5-0.05 and EA0.2-0.05 families

Polymer	Cross-linking density	W(λ_c) (MJ/m^3)	Fracture energy / Γ (KJ/m^2)
EA0.5-0.05(1)	0.5	0.06	0.3
EA0.5-0.05(1.56)EA	0.5	0.34±0.07	1.44±0.19
EA0.5-0.05(2.23)EA	0.5	0.82±0.26	3.48±0.48
EA0.5-0.05(2.81)EA	0.5	0.66±0.13	3.27±0.5
EA0.2-0.05(1)	0.2	0.15±0.02	0.68±0.08
EA0.2-0.05(1.70)EA	0.2	0.53±0.2	1.54±0.15
EA0.2-0.05(2.61)EA	0.2	1.44±0.33	5.1±0.64

2. Optical response to mechanical stress

2.1 Color analysis for the EA0.5-0.05 standard family of materials

From the results of the extension tests above, multiple network elastomers containing spiropyran as a crosslinker are tough, soft elastic materials. Figure 3.11(a) shows the color change of a EA0.5-0.05(2.23)EA sample during a uniaxial elongation test. The observed color changes progressively from colorless to blue. The blue color then rapidly changes to purple when the sample fails. The color change from colorless to blue is due to the transformation of SP into MC. MC possesses a larger intramolecular conjugated area than SP, which results in a red shift of the absorption spectrum. According to the Beer-Lambert law as shown in Equation 9, the absorbance is proportional to the concentration of the absorbing species (*c*) and to the length of the light path (*l*) in dilute solution:

$$A = lg\frac{I_0}{I} = \varepsilon lc \qquad \text{Equation 9}$$

In this equation, I_0, I, and ε are the incident light intensity, transmitted light intensity and molar extinction coefficient. In our system, *c* and *l* are dependent on the concentration of MC and on the thickness of the sample, respectively. Therefore, the blue chromaticity increases with MC concentration as shown in Figure 3.11 (b). As the stress increases during the

elongation tests, SP converts to MC and the color changes from light to deep blue.

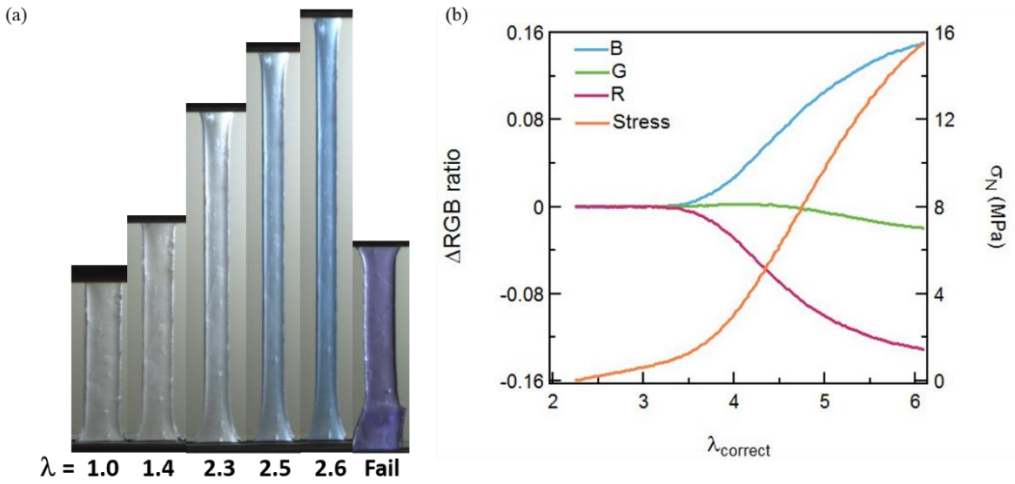

Figure 3.11: (a) The optical response of a EA0.5-0.05(2.23)EA sample during a tensile test; (b) Nominal stress σ_N and chromatic change ΔRGB ratio as a function of corrected stretch for the same sample

Another factor that impacts color change is the variation of the thickness of samples in extension. In extension tests, the thickness of the samples decreases with increasing extension. Assuming that the materials are incompressible and do not damage by cavitation in uniaxial extension, the deformation in the thickness direction (λ_z) and thickness (d) during extension can be deduced from the stretch ratio λ (x direction) as shown in Equation 10, Equation 11, Equation 12, and Equation 13.

$$\lambda_x \lambda_y \lambda_z = 1 \quad \text{Equation 10}$$

$$\lambda_x = \lambda = 1 + \varepsilon \quad \text{Equation 11}$$

$$\lambda_z = \lambda_y = \frac{1}{\sqrt{\lambda}} \quad \text{Equation 12}$$

$$d = d_0 \times \frac{1}{\sqrt{\lambda}} \quad \text{Equation 13}$$

($\lambda_x, \lambda_y, \lambda_z$ are the stretch ratios in the direction of the stretch, width and thickness. ε is the deformation of sample starting from 0 and d_0 is the initial thickness of sample)

To verify the impact of thickness on chromaticity, a control sample was synthesized (the synthesis procedure is in Chapter 5), where SP was incorporated into the third network to minimize the mechanical chemical reaction of SP in extension. Before the uniaxial test, the sample was exposed to UV light for 5 mins to convert all the SP in the material into MC. Then, the sample was tested in uniaxial tension, while the camera recorded the color change.

Since SP in the third network only sustained a low force during this process, the chromatic change is an estimate of how thickness independently affects color change. The color change was quantified by color analysis as described in the introduction of Chapter 2. *Figure 3.12* (a) shows the chromatic change with stretch ratio. According to Equation 13, the thickness in real time is proportional to $\lambda^{-1/2}$. Thus, the influence of the thickness can be determined for the case of complete conversion from spiropyran to merocyanine with an absorption spectrum induced by UV radiation, as shown in Figure 3.12. However, the results from Figure 3.11 cannot be used to simply correct the measured chromaticity for a uniaxial test. As the sample is stretched, the absorptivity spectrum, merocyanine concentration, and thickness are dynamically changing, affecting the color response recorded by the camera. If samples have the same (or very similar) thicknesses, the results of the color analysis can be compared between the samples. This is justified by the weak slope for low strains as shown in Figure 3.12.

The variation of ΔRGB ratio with increasing λ is small, especially, at $\lambda > 1.5$. The influence of the thickness on red and green channels is weaker than in the blue channel. *Figure 3.12* (b), shows the corrected and uncorrected ΔRGB ratio and in both cases the onset of color change due to stress occurs at around $\lambda = 1.5$ and most of SP was activated around $\lambda = 2$. In addition, the same mold was used in the synthesis for all the samples so they all have a similar thickness. In conclusion we will consider that the effect of thickness on the chromatic change is weak and in the range of experimental error.

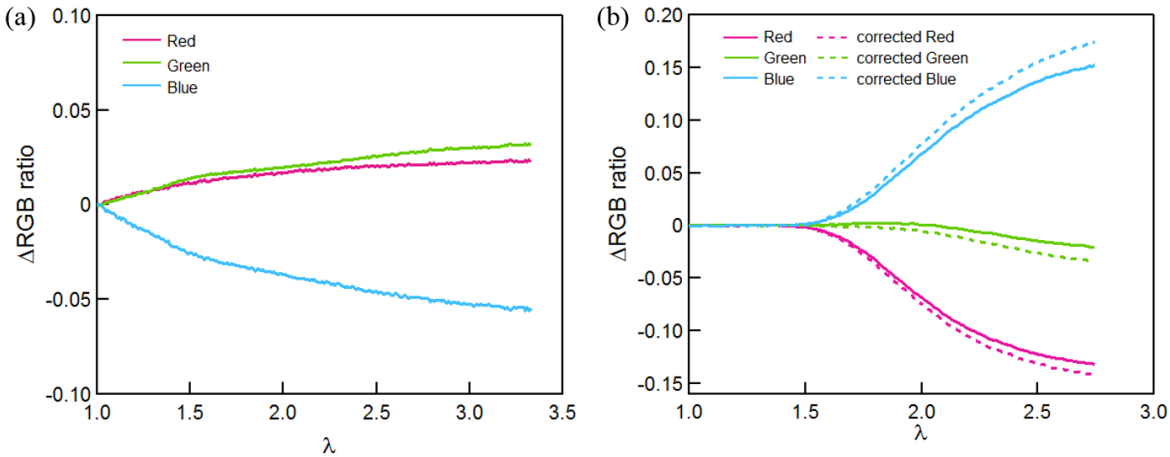

Figure 3.12: Chromatic changes as a function of thickness.

In these experiments, the SP was incorporated into the filler network. Thus, the color change reflects the application of the stress to the filler network. The isotropic deformation of the chains of the filler network due to swelling can be calculated with Equation (3) in Chapter 2. The chromatic change is plotted as a function of the total strain of the filler network $\lambda_{correct}$ in *Figure* 3.12 and of the nominal stress in *Figure 3.12* (b). In both cases, there is a sharp increase in the blue channel and a decrease in the red channel for $\lambda_{correct} > 3.3$ and for $\sigma_N >$

1.5 MPa respectively, while the green channel remained relatively constant. Thus, the red and blue channel will be used to correlate stress and strain with chromatic change for uniaxial loading.

To validate the quality of our results, three specimens punched from different EA0.5-0.05(2.23)EA sheets were used to perform elongation tests to observe the reproducibility in the color change. *Figure 3.13* shows a high reproducibility in the color change, indicating that SP can be used reliably as a molecular probe.

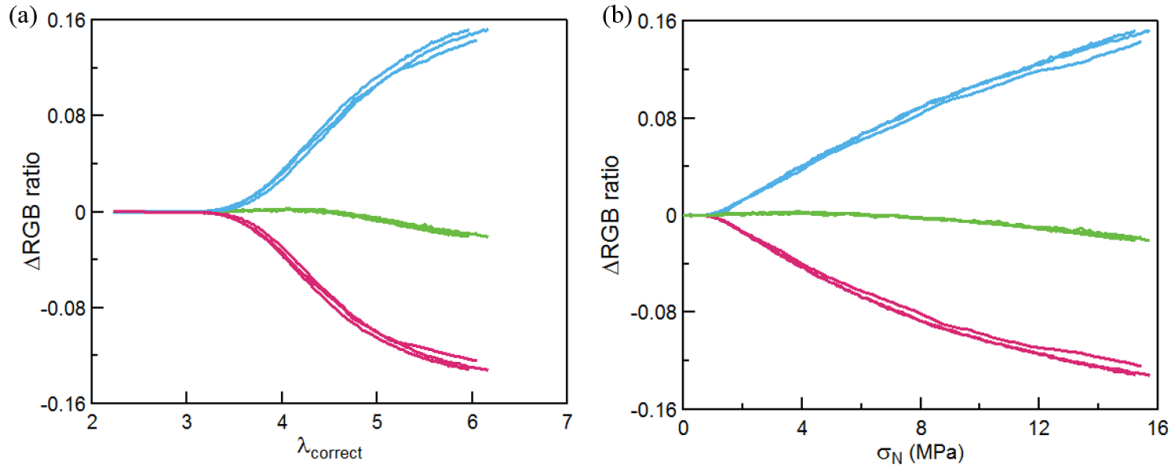

Figure 3.13 The reproducibility of the color change for EA0.5-0.05(2.23)EA: chromatic change as a function of (a) total strain and (b) stress

To examine the correlation between the chromatic change and stress or strain, the EA0.5-0.05 family was tested in uniaxial extension. Color analysis was performed for each video to quantify the color change in the extension test. The chromatic change plotted against the stress and corrected stretch responses for the family of networks is shown in Figure 3.14. Comparing Figure 3.14 (a) and (b), the onset of the chromatic change is detected at $\lambda_{correct} =$ 3.2 or σ_N~1.5MPa). Blue and red channels of the EA0.5-0.05(1)EA samples remain at the base line, which means no color change was detected before fracture for the single crosslinked network. This is quite remarkable in that simple elastomers break (by localized crack propagation) well before any of the chains of the network are really loaded.

Note that EA0.5-0.05(1.56)EA and EA0.5-0.05(2.23)EA contain filler networks with different degrees of pre-stretch, their chromatic curves overlap when plotted as a function of $\lambda_{correct}$. However, EA0.5-0.05(2.81)EA displays a lower chromatic variation at the same stress or $\lambda_{correct}$ relative to EA0.5-0.05(1.56)EA and EA0.5-0.05(2.23)EA after the onset point, which is explained by the initial activation of SP prior to testing. This discrepancy is attributed to the high level of pre-stretch of the chains in that sample.

During the synthesis, when the EA0.5-0.05(2.23)EA was swollen to prepare EA0.5-0.05(2.81)EA, a color change (colorless to blue) was observed during the swelling process and the blue color did not fade easily after synthesis despite the exposure of strong white

light. This shows that the synthesis imposes an isotropic level of pre-stretch which is above the level where the SP starts to be activated into MC. To reconvert MC into SP, samples were stored in dark two weeks to wait for the relaxation of polymer chains in the filler network and/or exposed to strong white light. Although lots of strategies were carried out, some of the MC remain. Since the chromatic change that we measure is relative to the initial samples at the same applied stress or strain, the chromatic change of EA0.5-0.05(2.81)EA is still lower. Based on the results shown in Figure 3.14, a correlation between the variation of color and stress (or strain) exists, which allows for the mapping of stress and/or strain fields.

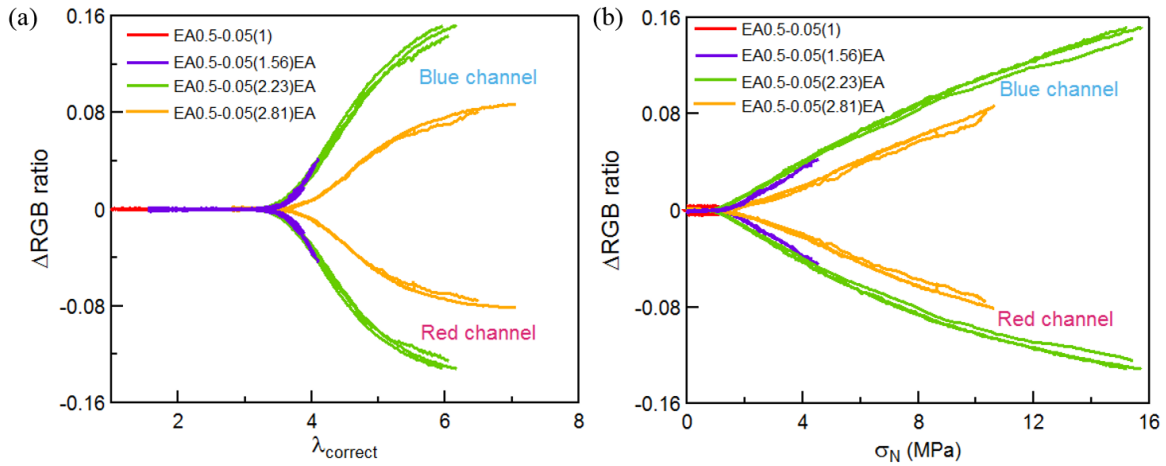

Figure 3.14: ΔRGB ratio of the EA0.5-0.05 family as a function of (a) strain or (b) stress

A calibration curve for the EA0.5-0.05 family was constructed from the color analysis as shown in Figure 3.14. From the curves, the family of materials can be separated into three groups. According to the differences of pre-stretch, they are $\lambda_0 = 1$, $1.5 < \lambda_0 < 2.3$ and $\lambda_0 > 2.8$. Comparing the images before and after the tensile tests in Figure 3.15, different chromatic responses of the three groups were also observed. For $\lambda_0 = 1$, the color change solely occurs near the crack. For $1.6 < \lambda_0 < 2.3$, the color change is observable across the region between the two clamps, where higher values of λ_0 exhibit a higher chromatic change. This is attributed to the higher pre-stretch of the first network, where a high level of mechanophore activation occurs at a low applied strain despite a decrease in SP concentration. However, multiple networks with $\lambda_0 > 2.8$ behave differently from the other networks. Prior to tensile testing, EA0.5-0.05(2.81)EA samples appear light blue after synthesis. The level of pre-stretching in the first network is sufficiently high to activate the SP mechanophore. . To estimate the fraction of activated SP after synthesis, EA0.5-0.05(2.81) was exposed to UV for 5 min to activate all the SP in the material. The chromaticity of the material before and after UV exposure was obtained to calculate the proportion of MC before extension. It is about 64% SP that transferred into MC in EA0.5-0.05(2.81)EA due to swelling. Note that the EA0.5-0.05(2.81)EA after failure exhibits both blue and purple colors. The blue color suggests that some polymer chains covalently attached to MC are in the stretched state and the purple corresponds to areas of relaxation. This illustrates that the SP mechanophore is quite sensitive

to the force.

Assuming that the activation of SP in the networks with λ_0>2.8 after the synthesis is due to the swelling process before the polymerization, we can estimate the osmotic swelling pressure. Based on the equilibrium swelling equation and osmotic pressure theory, the pre-stress in the filler network can be calculated.

Following Flory-Huggins theory the free energy of mixing of a binary mixture of polymers A and B ΔF_{mix} is given by

$$\Delta F_{mix} = RT\left[\frac{\phi_A}{N_A} ln\phi_A + \frac{\phi_B}{N_B} ln\phi_B + \chi\phi_A\phi_B\right] \qquad \text{Equation 14}$$

where ϕ_A, ϕ_B, N_A, N_B are the volume fractions and the degrees of polymerization of A and B, respectively and χ is the interaction parameter between A and B.

For a polymer and a solvent, the free energy of mixing simplifies since N = 1 for the solvent.

$$\Delta F_{mix} = RT\left[\frac{\phi_P}{N} ln\phi_P + (1-\phi_P) ln(1-\phi_P) + \chi\phi_P(1-\phi_P)\right] \qquad \text{Equation 15}$$

The osmotic pressure of a solvent in a gel (or elastomer) is the derivative of the free energy of mixing of the solvent and the polymer, ΔF_{mix}, relative to the volume.

$$\Pi = \frac{\partial \Delta F_{mix}}{\partial V} = -\frac{RT}{V_1}\left(ln(1-\phi_P) + \phi_P + \chi{\phi_P}^2\right) \qquad \text{Equation 16}$$

For the swelling of monomer into the polymer we can assume that χ = 0 and the equation simplifies to:

$$\Pi = -\frac{RT}{V_1}(ln(1-\phi_P) + \phi_P), \qquad \text{Equation 17}$$

where ϕ_P is the polymer volume fraction at equilibrium swelling and V_1 is the molar volume of the monomer. At equilibrium swelling this osmotic pressure is the same as the true stress, σ, applied to the polymer chains during swelling. In our swollen and polymerized samples, the stress is carried essentially by the chains of the filler network oriented in the tensile direction.

However, during the uniaxial deformation of the fully polymerized sample, the nominal stress acting on the filler network is equal to the true stress applied by the swelling process. For example, in the EA0.5-0.05 family, the swelling from EA0.5-0.05(1) to EA0.5-0.05(1.56)EA gives a λ_0=1.56 and ϕ_P=${\lambda_0}^{-3}$= 0.26. Using Equation 17 the osmotic pressure Π is 0.96 MPa,

which is lower than the threshold of activation of SP. Thus, no activation of SP is predicted. For the EA0.5-0.05(2.23)EA the swelling stretch is λ=2.23/1.56 = 1.43 and $\phi_P = \lambda_0^{-3}$= 0.342, then the osmotic pressure increases 1.74 MPa. The osmotic pressure is a little higher than the onset of the damage (1.5 MPa) as shown in Figure 3.14. According to the prediction, some of the SP in the filler network is activated. Indeed, during the swelling to prepare TN, when the swelling reached the equilibrium the swollen DN changes its color to light blue. But after the polymerization and drying, the color fades due to removal of some unreactive monomers in the polymer network, decreasing the swelling ratio and osmotic pressure. Therefore, the color disappeared after drying. From EA0.5-0.05(2.23)EA to EA0.5-0.05(2.81)EA, the swelling stretch is λ= 1.26 and ϕ_P=0.5, which corresponds to an osmotic pressure of 4.38 MPa. The pressure is much higher than the nominal stress of the activation of SP, so that the EA0.5-0.05(2.81)EA is blue after synthesis and this blue color is difficult to fade. The accuracy of these simple predictions show that for these multiple networks the equilibrium swelling is controlled by the highly stretched chains of the first network only and not by the moderate extension of the majority of the chains in the Gaussian regime.

From the prediction of the osmotic pressure at equilibrium in the EA0.5-0.05(2.81)EA, the pre-stress in the first network can be calculated by Equation 18:

$$\bar{F} = \frac{\Pi}{\Sigma_{FN}}, \qquad \text{Equation 18}$$

whereΣ_{FN} is the areal chain density of filler network in EA0.5-0.05(2.81)EA. $\Sigma_{FN} = 1.66 \times 10^{16}$(the calculation is shown in the next paragraph), the predicted average force in the polymer chains of the filler network is about 264 pN that is very close but slightly above the threshold of the activation of SP (240 pN detected by Craig's group with AFM single molecular force spectrum[16]). The simple calculation of the osmotic pressure explains the blue color we observed after the preparation of the EA0.5-0.05(2.81)EA.

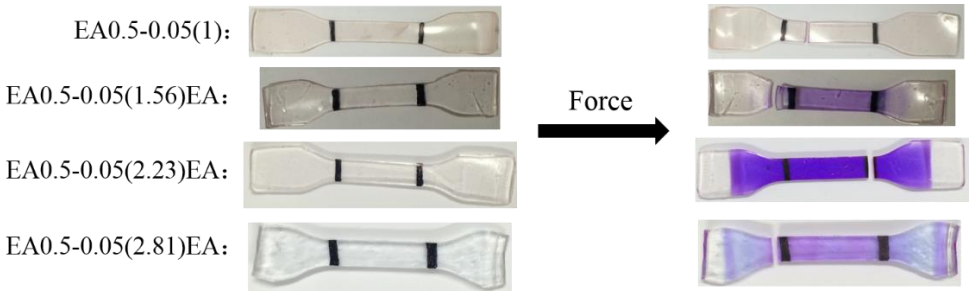

Figure 3.15: The mechanical response of the EA0.5-0.05 family group of elastomers

To estimate the average activation stress of the SP into MC based on the filler network structure, the areal chain density inside the simple network can be calculated by assuming

Gaussian chain statistics as done by Miquelard-Garnier[17,18] and Millereau[1]. If the crosslinking is random and has a functionality of four, the areal chain density of the filler network Σ_{FN0} can be estimated using Equation 19 with ν, the number of crosslinking points per unit volume, and $\langle {R_0}^2 \rangle^{1/2}$, the average distance between crosslinks. From Gaussian statistics, we can then obtain Equation 20 where all parameters are independently known: l_0 is the length of a C-C bond (1.54 Å), E_{FN0} is the tensile modulus of the filler network, C_∞ the polymer characteristic ratio and N_x the number of carbon bonds between crosslink points estimated previously. When the filler network is swollen with monomer during the multiple steps of polymerization, the initial surface chain density Σ_{FN0} is diluted as described in Equation 21, so that the filler network areal chain density Σ_{FN} can be estimated for our entire set of samples.

$$\boldsymbol{\Sigma_{FN0}} = \frac{\boldsymbol{\nu} * \langle \boldsymbol{{R_0}^2} \rangle^{\mathbf{1/2}}}{\mathbf{2}} \qquad \text{Equation 19}$$

$$\boldsymbol{\Sigma_{FN0}} = \frac{\boldsymbol{l_0 E_{FN0}} \sqrt{\boldsymbol{C_\infty N_x}}}{\mathbf{6\, k\, T}} = \boldsymbol{l_0} \left(\frac{\boldsymbol{E_{FN0} \rho N_A C_\infty}}{\mathbf{6 M_0 k T}} \right)^{\mathbf{1/2}} \qquad \text{Equation 20}$$

$$\boldsymbol{\Sigma_{FN}} = \boldsymbol{\Sigma_{FN0}} \boldsymbol{\phi}^{2/3} \qquad \text{Equation 21}$$

Once the surface chain density $\boldsymbol{\Sigma_{FN}}$ is calculated, the prediction of the activation stress $\boldsymbol{\sigma_{act}}$ for the whole family of materials can be made. It is shown in Equation 22:

$$\boldsymbol{\sigma_{act}} = \boldsymbol{F}(SP \rightarrow MC) \boldsymbol{\Sigma_{FN}} \qquad \text{Equation 22}$$

In case of the EA0.5-0.05 family of materials, $\boldsymbol{\rho}$=1120 kg/m^3, $\boldsymbol{M_0}$=100 g/mole, $\boldsymbol{F}(SP \rightarrow MC)$= 240 pN. Combining Equation 20 and Equation 21 into one equation, the activation stress $\boldsymbol{\sigma_{act}}$ depends only on $\boldsymbol{E_{FN0}}$ and on $\boldsymbol{\lambda_0}$ as shown in Equation 23:

$$\boldsymbol{\sigma_{act}} = \mathbf{60000} \frac{\sqrt{\boldsymbol{E_{FN0}}}}{\boldsymbol{\lambda_0^2}} \qquad \text{Equation 23}$$

For the SN of EA0.5-0.05 family of materials the initial modulus is 0.85 MPa, so $\boldsymbol{\sigma_{act}}$ = 55 MPa for the SN and for a multiple network with $\boldsymbol{\lambda_0}$ = 2.8, $\boldsymbol{\sigma_{act}}$ should be of the order of 7 MPa. Our experimental result for onset is 1.5 MPa but for 50% of the chains activated (those in the tensile direction) the experimental stress is close to 7 MPa.

2.2 The effect of strain rate

The influence of stretch rate on the color change is examined despite the low viscoelasticity of the multiple network elastomers. The videos captured during the tensile tests carried out at

various stretch rates were used to do color analysis and the results are shown in Figure 3.16. Although the materials show negligible viscoelasticity, the chromatic change had some strain rate dependence. At the same stress or first network extension, the higher strain rates resulted in a lower chromatic change. This rate dependence is attributed to a characteristic time associated with the mechanophore activation, which is also observed by Craig et al[16]. in the detection of the force to activate SP. Even though it takes certain time to reach the equilibrium of SP activation, the chromatic change does not depend significantly on strain rates.

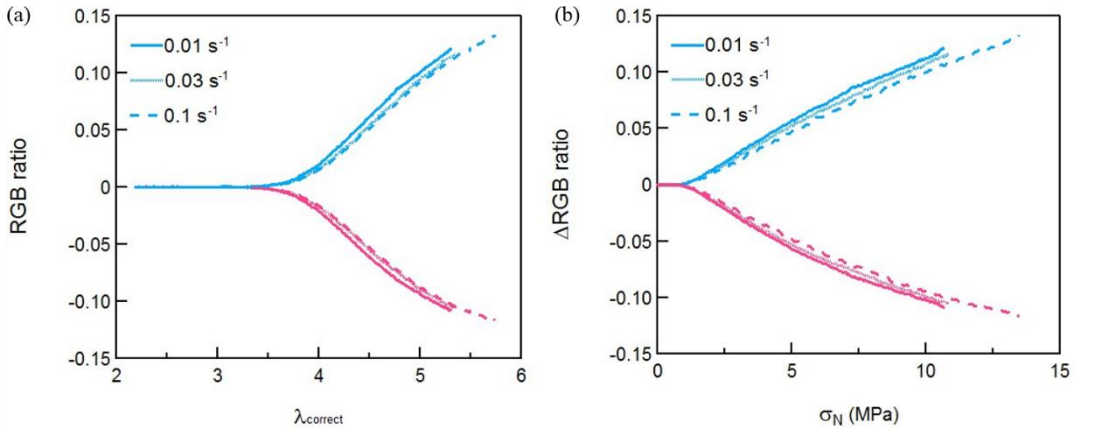

Figure 3.16: ΔRGB ratio of EA0.5-0.05 (2.23)EA as a function of (a) corrected strain and (b) stress with different stretched velocities

2.3 The effect of various cross-link densities in the filler network

The cross-linker density in the filler network directly controls the mechanical properties of multiple network elastomers, including the Young's modulus, stress and strain at break. The color change was detected in materials prepared from SN with different crosslink densities. The motivation of this experiment was to examine the reproducibility of the chromatic calibration curve for different materials. It is critical for mapping the stress and/or strain by the calibration curve. In Figure 3.17 (a), the two groups of materials show two types of renormalized chromatic calibration curves, when the chromatic change is plotted as a function of the total strain of the filler network. In the EA0.2-0.05 group the color change occurs at a value of $\lambda_{correct}$ ~5, which is significantly larger compared to the case of the more crosslinked EA0.5-0.05. This is attributed to the decrease of the crosslinker density in the filler network resulting in the increase of the length of polymer chain between crosslinkers. It is necessary to own a larger deformation to carry the threshold of stress to activate SP. Therefore, the curves of chromatic change as a function of stress overlap for different types of samples (Figure 3.17 (b)). This result confirms that SP is more sensitive to stress than strain. In addition, when the first network in the multiple network elastomers possesses a pre-stretch below that needed for SP activation and the same SP concentration, the chromatic calibration curves can be applied to all the multiple network elastomers despite their different mechanical properties.

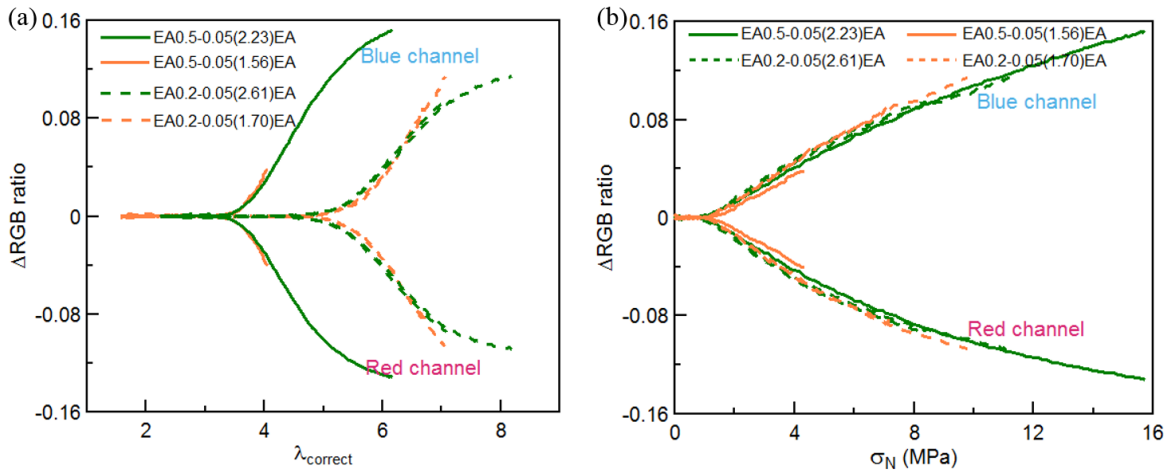

Figure 3.17: Chromatic change of EA0.5-0.05 and EA0.2-0.05 family groups as the function of (a) corrected strain or (b) nominal stress

2.4 The effect of varying the SP concentration

In the previous section, the influence of the concentration of MC on the magnitude of chromatic change was mentioned. Tailoring the initial concentration of SP in the filler network must modify the chromatic change curves. To normalize the effect of SP concentration, tensile tests of materials with different SP concentrations were carried out. Figure 3.18 (a) shows the chromatic change calibration curves of EA0.5-0.05, EA0.5-0.025 and EA0.5-0.0125 groups of materials which all have the same total crosslinker density but different fractions of crosslinker being SP. The onset of color change occurs roughly at the same strain, but the slope of the change in ΔRGB ratio as a function of stress is clearly different showing a strong dependence on SP concentration. However, after normalization of the ΔRGB ratio by the SP concentration, a fascinating result is shown in Figure 3.18 (b). The three different curves form a master curve and overlap into a more universal calibration curve for the different materials showing that the magnitude of the chromatic change is directly proportional to the initial concentration of SP, an intuitive but nevertheless useful result showing that at least in that range of concentrations there are no non-linear effects on the light absorption.

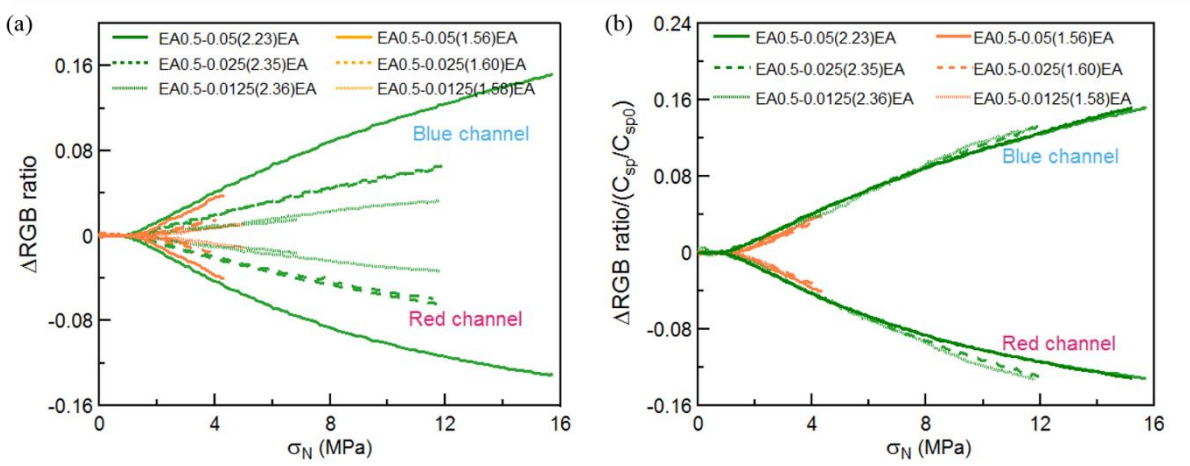

Figure 3.18: Chromatic change as a function of (a) nominal stress and (b) renormalized ΔRGB ratio as a function of nominal stress in the materials containing various SP concentrations (the C_{sp} and C_{sp0} are the initial concentration of SP in the two groups and EA0.5-0.05(1), respectively.

3. Accurate calibration of the Stress: Toward Quantification

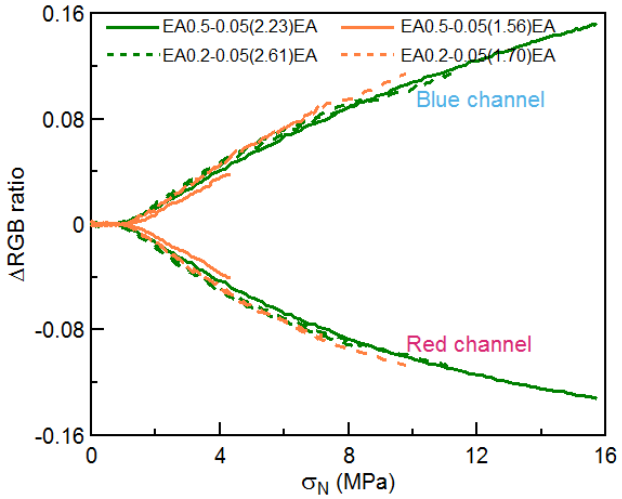

Figure 3.19: ΔRGB ratio as a function of nominal stress for four different multiple network elastomers with two different cross-link densities in the first network

The relationship between the chromatic change and nominal stress needs to be examined in detail to quantitatively map the stresses as shown in Figure 3.19. While the change in blue and red channel appear quite similar there are small differences that can be exploited.

The curves where the nominal stress acts as a function of ΔRed ratio orΔBlue ratio are plotted in Figure 3.20. Based on the calibration curves in Figure 3.20(a) or (b), stresses above 1.5 MPa) can be mapped. The difference for the two master curves of ΔRed ratio and ΔBlue ratio is the minimum stress. During color analysis, the signal to noise ratio is used to decide the

threshold detection of the chromatic change. Only when the ratio increases to 70%, the signal is regarded as a useful information. Thus the red and blue present different minimums due to the various sensitivities for different colors. The threshold stress in uniaxial tension for the ΔRed and ΔBlue ratio are 1.54 MPa and 1.81 MPa, respectively, so that the decrease in the red hue is a bit more sensitive than the increase in the blue hue. Another important point of this approach is that it can only provide a scalar value but not the direction of the stress. The SP can be activated in response to the force coming from different directions in the polymer materials. Here, the measured scalar value is representative of the average force seen by the SP crosslinkers in the particular volume element in the material. In uniaxial tension experiments, the scalar value of the stress is the resultant force in the tensile direction since the force can only activate SP in this direction. The measurement of the directionality of the stress will be introduced in sixth and seventh chapters.

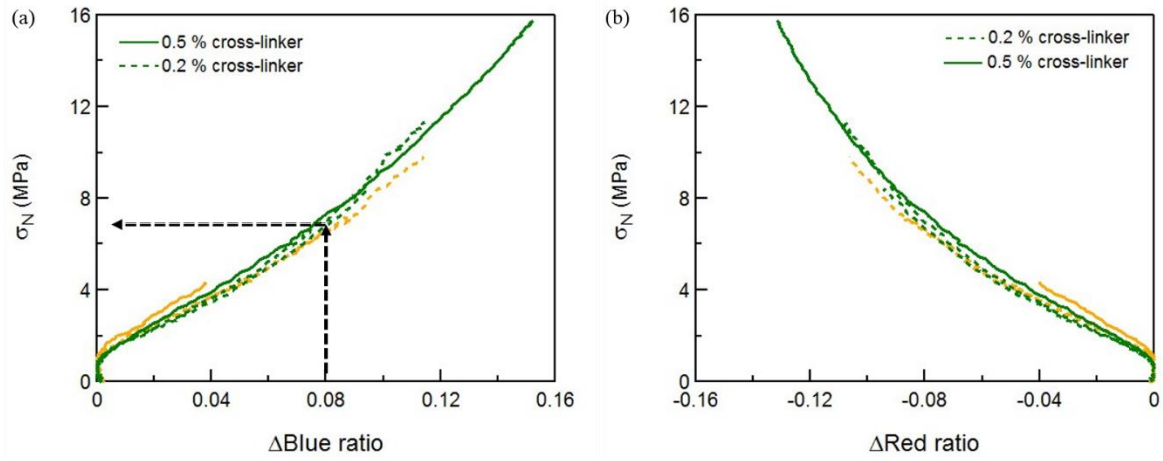

Figure 3.20: The master curve of the nominal stress as a function of (a) ΔBlue and (b) ΔRed ratio

Each master curves of ΔBlue and ΔRed ratio on its own only partially describes the chromatic change. The ΔRed ratio curve possesses a lower threshold stress than the ΔBlue ratio, but the ΔBlue ratio is more sensitive to the color change (a larger variation in ΔBlue ratio for an equivalent increase in stress). Additionally, a color change corresponds to the variation of the three components of the chromaticity. But in uniaxial extension, the green channel does not significantly change. To create a more accurate mapping of the stress distribution, both the red and blue chromatic changes are needed, as shown in Figure 3.21. At low chromatic changes in the red and blue channels, the calibration curve overlaps to the line of $y = -x$, but deviates at higher change in chromaticity. This deviation is attributed to measurable contribution to the chromatic change of the green channel at high stresses. Comparing the ΔRed vs. ΔBlue curves for the two different families of materials in Figure 3.21(a) and (b) or Figure 3.17 (b), one notes that they possess almost the same master curve of chromatic change due to the same SP concentration. However, the master curve for the EA0.5-0.05 family of materials extends to a maximum stress of 12 MPa.

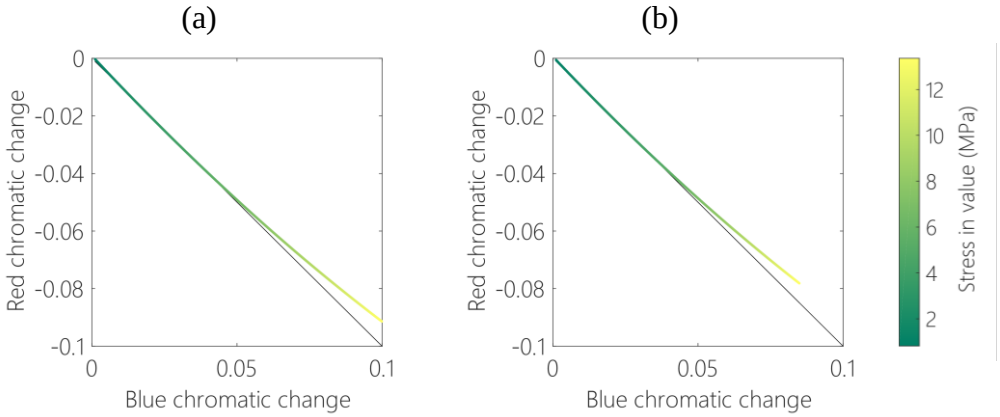

Figure 3.21: Chromatic-stress plots derived from uniaxial tensile tests for EA0.5-0.05 (a) and EA0.2-0.05 (b) family of materials. The color code is the nominal stress measured in uniaxial extension.

4. Optical response in fracture tests

4.1 Optical response around the crack in EA0.5-0.05 family

To be able to measure the stress field around the crack tip by mechanochemistry, the color change of the sample in a fracture test should first be detectable. The fracture tests were filmed with an RGB camera and then used to perform a pixel by pixel color analysis. As shown in Figure 3.22 six frames were taken from different locations on the stress-strain curve during the fracture test of EA0.5-0.05(2.23)EA material. The six representative frames were used to investigate the optical response of EA0.5-0.05(2.23)EA material around the crack tip as shown in Figure 3.233. As the loading is increased, a strong color change is clearly visible around the crack tip before propagation. The blue zone close to the crack tip represents the presence of high stress. The color intensity and size of this zone gradually increases and amplifies to the area where blue color appears even relatively far away (several mm) from the crack tip. At the same time, the chromaticity around the crack tip increases rapidly before crack propagation, especially in the area closest to the crack tip on both sides.

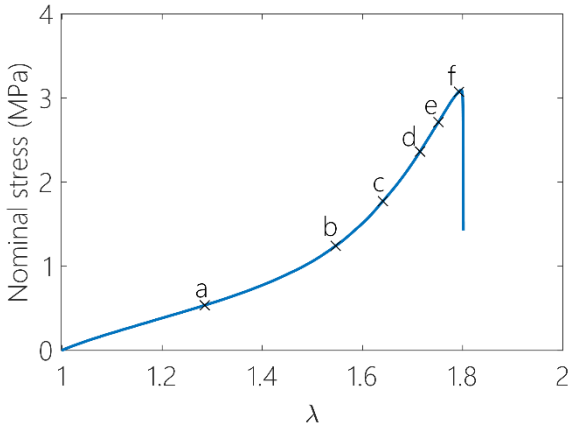

Figure 3.22 Stress-strain curve of EA0.5-0.05(2.23)EA sample with a notch: a, b, c, d, e, f represent the six positions where the frames are extracted to do color analysis and stress mapping.

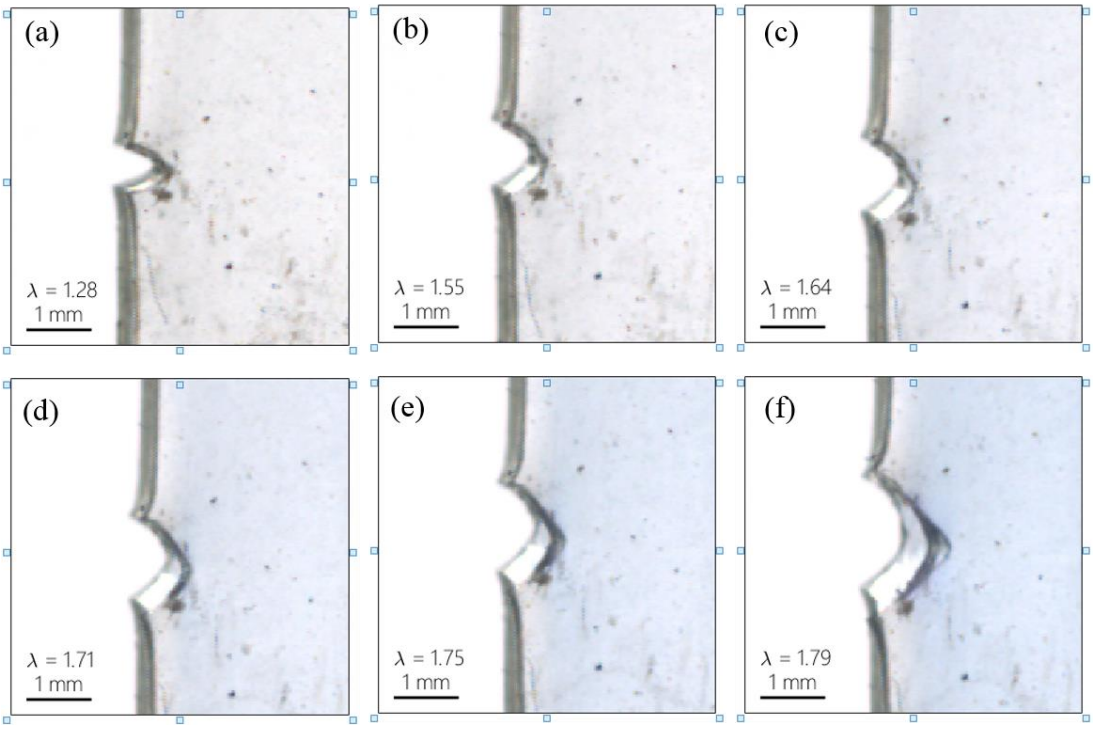

Figure 3.23: The chromatic change around the crack tip in the fracture test of EA0.5-0.05(2.23)EA materials.

When compared to the EA0.5-0.05(2.23)EA, the less prestretched EA0.5-0.05(1.56)EA did not show an obvious blue region around the crack tip as shown in Figure 3.24. But a clear blue region is however visible at the crack tip in the wake of the crack as shown in Figure 3.24 (f). The result[1,19] is consistent with ref. 3 and 4. When the crack propagates (Figure 3.24(f)), small purple areas were also observed near the crack edges. The purple area in EA0.5-0.05(2.23)EA are larger than EA0.5-0.05(1.56)EA suggesting that the high stress area is more delocalized for the EA0.5-0.05(2.23)EA than for the EA0.5-0.05(1.56)EA. Based on Table 3.3, EA0.5-0.05(2.23)EA possesses higher fracture toughness than EA0.5-0.05(1.56)EA.

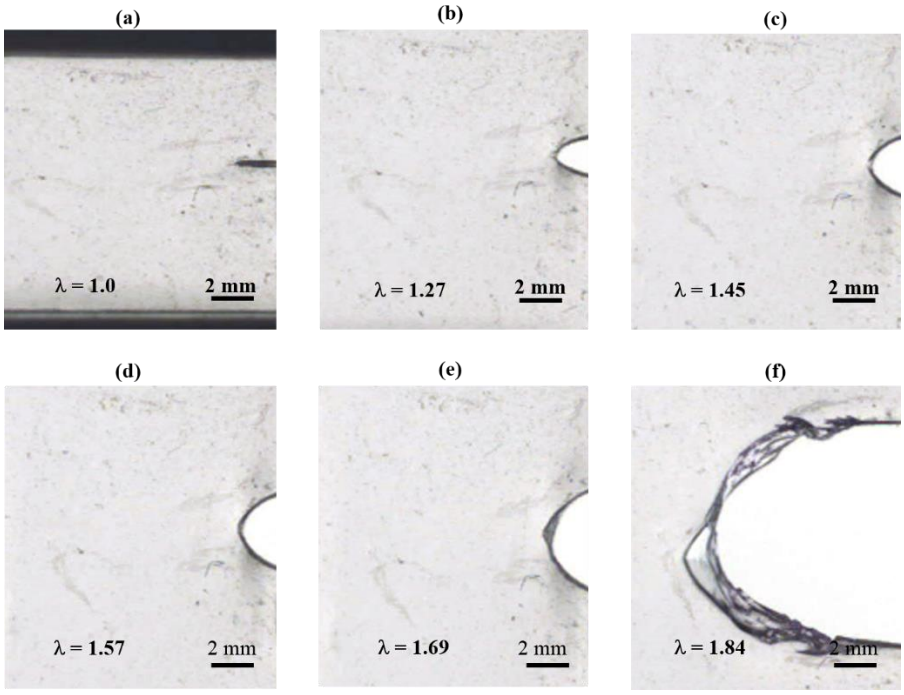

Figure 3.24: The frames of EA0.5-0.05(1.56)EA in the fracture test

4.2 Optical response around the crack for EA0.2-0.05(2.61)EA sample

The EA0.2-0.05 group of materials were also examined to study the effects of varying the cross-link density in the first network on the fracture process and the stress distribution. Figure 3.25 shows the chromatic change of the EA0.2-0.05(2.61)EA material around the crack tip. Comparing EA0.2-0.05 (figure 3.25 (c)) and EA0.5-0.05 (Figure 3.23 (f)), there is a significant difference in the chromaticity near the crack tip. The frame of EA0.5-0.05(2.23)EA prior to the propagation shows a deeper blue than EA0.2-0.05(2.61)EA even if the prestretching is lower. It illustrates that the stress in the filler network of the EA0.2-0.05(2.61)EA material is lower than in the EA0.2-0.05(2.23)EA due to the lower cross-linking density in the first network.

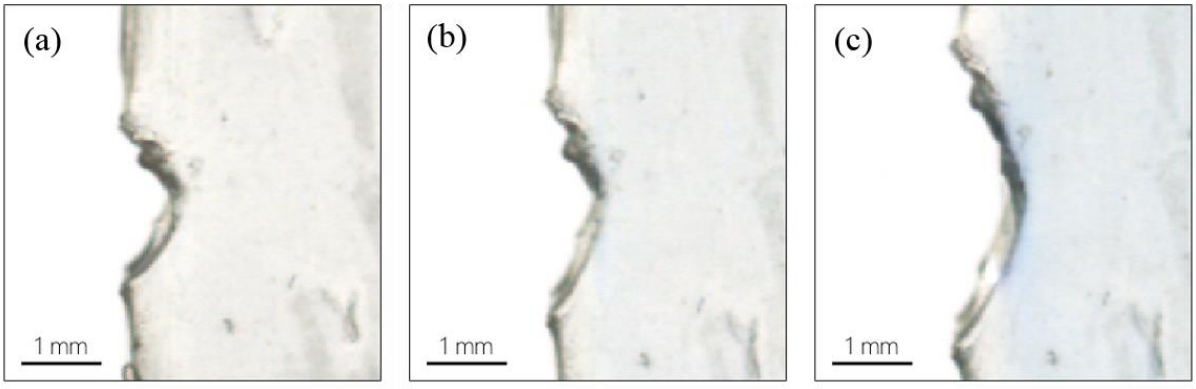

Figure 3.25: Images of EA0.2-0.05(2.61)EA sample in the fracture test

5. Quantitative Stress distribution around the crack tip before propagation

Knowing the stress distribution around the crack tip is helpful for the study of the fracture mechanisms and of the reinforcement of multiple network elastomers. The master curve in *Figure 3.21* can in principle be used to map the nominal stress around the crack tip during the loading process. According to the calibration curves, the stress distribution around the crack tip can be detected for any material containing SP but in particular for the family of multiple network materials described here.

5.1 Stress distribution in standard multiple network elastomers

Representative frame captures of the EA0.5-0.05 and EA0.2-0.05 families of materials were used to perform color analysis. The spatial distribution of chromatic change was then obtained. Based on the chromatic-stress calibration curves in Figure 3.21, the stress map is finally calculated by interpolation as shown in Figure 3.26.

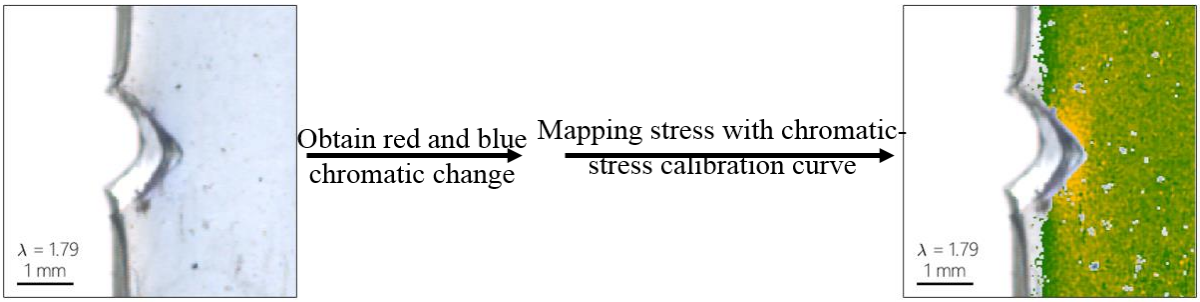

Figure 3.26: The methodology to map the stress distribution around the crack tip based on chromatic change calibration curve

The map of the stress distribution of the EA0.5-0.05(2.23)EA based on the master curve of ΔRed ratio and ΔBlue ratio is shown in the Figure 3.27 for different values of applied λ. The color represents the uniaxial tensile stress obtained from the calibration curve obtained from uniaxial tensile tests. But here we only can map the stresses above the threshold stress (1.54 MPa) since the activation of SP by force needs 240 pN. The gray area means that the stress is below the threshold and cannot be detected by the SP activation. Figure 3.27 shows that the stress around the crack tip increases gradually with increasing loading of the crack. Initially, the stress pattern reveals a high stress distribution located on both sides of the crack tip. The high stress zone subsequently grows with increasing applied strain. When the extension reaches 1.7, the region rapidly extends in size and covers now a large zone in front of the crack tip. At the onset of crack propagation, the stress around the crack tip, within the spatial resolution of the technique, reaches a maximum stress of 4 MPa, while the far-field regions sustain stresses above 2.5 MPa.

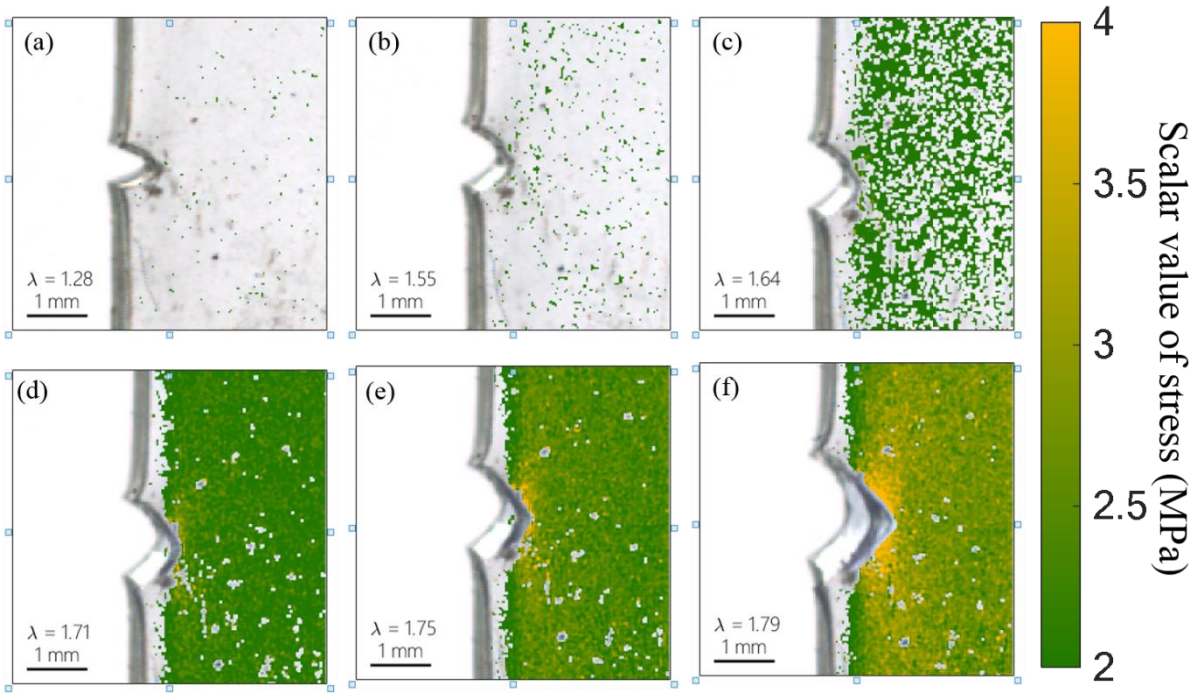

Figure 3.27: The map of stress distribution around the crack tip detected by the calibration curve in EA0.5-0.05(2.23)EA materials

The force to activate SP is around 240 pN[16,20] while about 4 nN[21,22] is needed to break a carbon-carbon bond in a polymer chain, which is about 15 times compared to the threshold force of the SP activation. Therefore the activation of SP should in principle occur at a lower strain than scission of polymer chains, at the stress where damage of the filler network is detected by hysteresis in the step cyclic loading test. However, the activation of SP does not lead to the scission of polymer chain. The region that shows a color change does not represent the damage of materials and it simply exhibits high stress and deformation distribution within the first network. The damage region is actually smaller than the zone that can be detected by color change due to the low threshold of force to activate SP. To estimate the damage area before propagation around the crack, the stress map in Figure 3.27 (f) should be compared with the stress-strain curve in the step cyclic loading in *Figure 3.28* (a). In the step cyclic loading, damage occurs at $\lambda = 1.75$ and its corresponding stress is 2.9 MPa. This means that the region shown in light green toward yellow color in Figure 3.27 (f) is the damaged area. For a clear view of damage zone, a map of stress above 3 MPa is plot in *Figure 3.28* (b). It is visible that the damage zone distributes on both sides close to the crack tip over dimensions of several hundred micrometers (~250 µm), close to the predictions estimated by Brown[23] and Tanaka[24] for DN hydrogels.

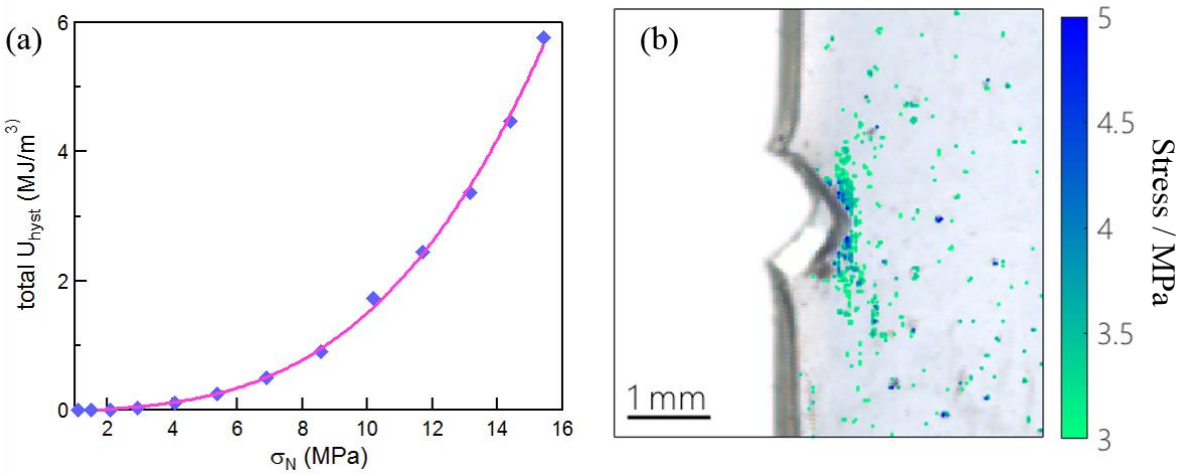

Figure 3.28: (a) Total hysteresis as a function of nominal stress in the step cyclic loading of EA0.5-0.05(2.23)EA. The blue dots are the experimental points and the pink curve is a polynomial fitl; (b) the distribution of stress above 3 MPa was mapped by the master curve.

5.2 Stress distribution in various elastomers at the same energy release rate

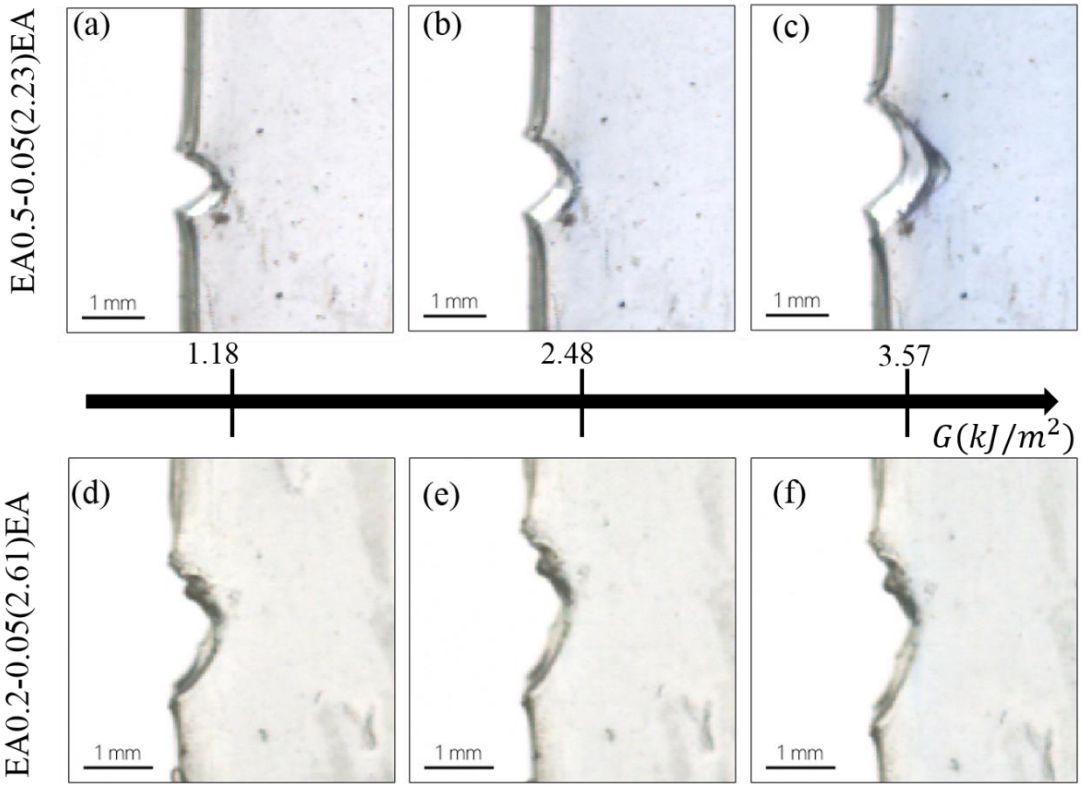

Figure 3.29: Color corrected images at G = 1.18, 2.48, and 3.57 kJ/m^2 for EA0.5-0.05(2.23)EA (a-c) and EA0.2-0.05(2.61)EA (d-e).

Multiple networks made from filler networks with different cross-linking densities have different mechanical properties, including Young's modulus and fracture toughness. To compare the different mechanical behaviors, EA0.5-0.05(2.23)EA and EA0.2-0.05(2.61)EA were used to perform fracture tests. *Figure 3.29* shows the different color-corrected frames of EA0.5-0.05(2.23)EA and EA0.2-0.05(2.61)EA samples taken at the same energy release rate (G), and corresponding therefore to different values of λ as shown in *Figure 3.30* (the black dots). Since cracks propagate when the energy release rate exceeds a critical value, it made sense to make this comparison.

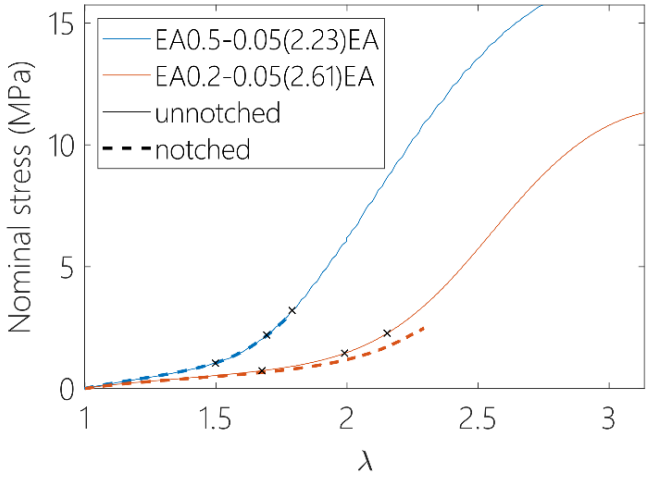

Figure 3.30: Stress-strain curves of the EA0.5-0.05(2.23)EA and EA0.2-0.05)2.61)EA samples with or without notch are compared and the black dots are three pairs of points. At the two points in each pair the both sample have the same energy release rate.

In *Figure 3.29*, these samples show significant differences in color change. EA0.5-0.05(2.23)EA shows clearly a large color change ahead of the crack tip at $G = 2.48\ kJ/m^{-2}$. However, little is any color change is observed for the EA0.2-0.05(2.61)EA sample until $G = 5.1\ kJ/m^{-2}$. A weak color change appears at the area in front of the crack tip as shown in *Figure 3.29* (f).

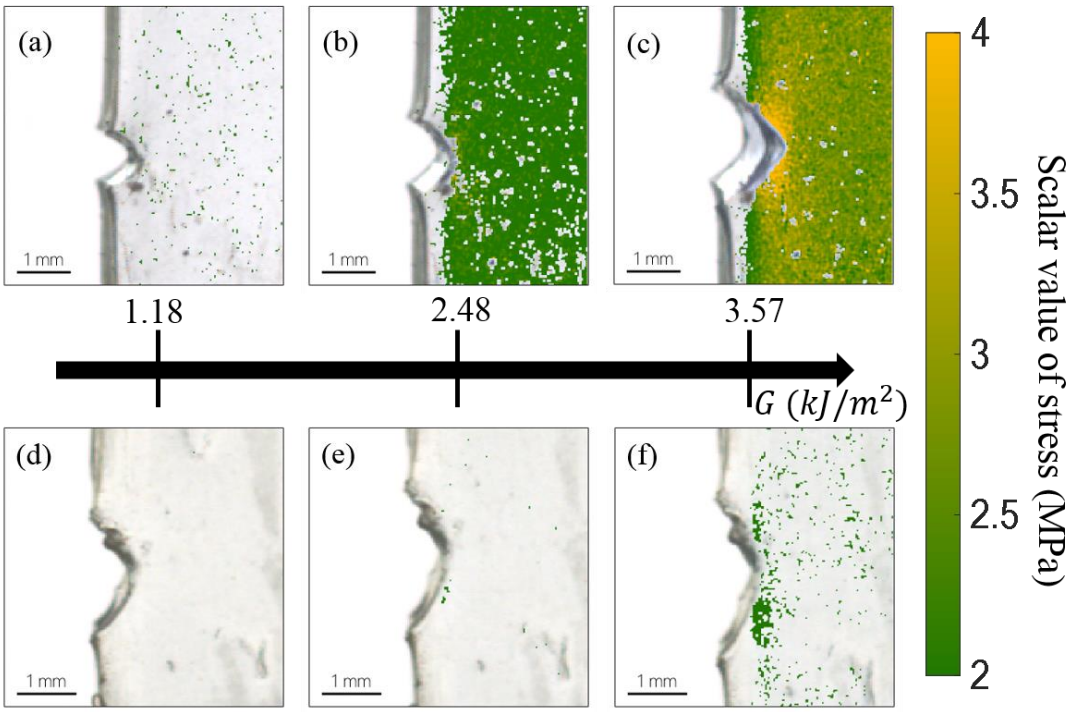

Figure 3.31: Stress maps for EA0.5-0.05(2.23)EA (a-c) and EA0.2-0.05(2.61)EA (d-f) at three levels of energy release rate G: 1.18, 2.48, and 3.57 kJ/m^2.

The master curves combining the ΔRed and ΔBlue chromatic change of Figure 3.21 were used to map the stresses in the EA0.5-0.05(2.23)EA and EA0.2-0.05(2.61)EA samples. From *Figure 3.31*, the stress distribution can be compared in *Figure 3.31* (b), (c) and (f). At relatively low G values, the filler network already sustains a high stress in EA0.5-0.05(2.23)EA and prior to the crack propagation, around the crack tip, even the regions far away from the crack tip, are under a high stress. The stress gradually decreases with increasing distance away from the crack tip as shown in *Figure 3.31* (c).

In contrast to the EA0.5-0.05(2.23)EA sample, only a small area of high stress is observed at the crack tip of EA0.2-0.05(2.61)EA. According to the phenomenon above, the first network with dense cross-linking density sustains a much higher stress resulting in more scission of chemical bonds at the same G and in principle it should then dissipate more energy.

The key difference between these two materials, is the lower cross-linking density of the filler network which delays the critical strain at which the strain hardening is observed and the SP can be activated. Figure 3.6 and Figure 3.16 shows that for the EA0.5-0.05(2.23)EA the SP is activated at λ = 1.5 in uniaxial tension while it is only activated at λ = 2 for the softer EA0.2-0.05(2.61)EA. Yet the comparison of figure 3.31 is done at equivalent G, i.e. at the same value of stored elastic energy. In those conditions the softer material will reach the same value of G with a higher extension but a lower stress, hence activating less the SP. The real question is however why does the softer EA0.2-0.05(2.61)EA fail at a larger G (5.1 kJ/m^2) than the stiffer EA0.5-0.05(2.23)EA? To try to answer that let's look at the stress map of EA0.2-0.05(2.61)EA sample just before crack propagation (at Γ=*5.1 kJ/m^2)* as shown in Figure 3.32.

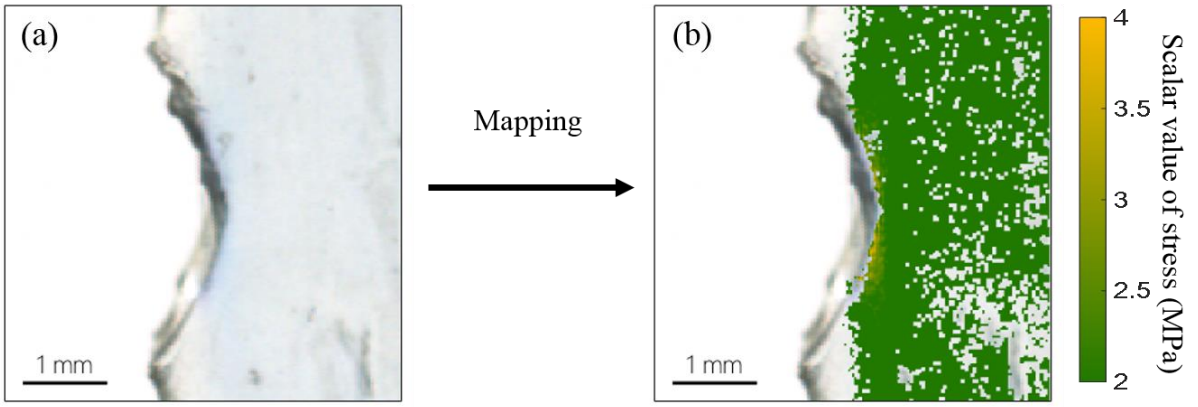

Figure 3.32: The stress invariant map (a) and the color corrected image of the last captured frame prior to crack propagation (Γ=5.1 kJ/m^2) for the EA0.2-0.05(2.61)EA sample.

The comparison of the two materials for G = Γ i.e. at the point of crack propagation, shows that in this case high stresses are detectable also in the EA0.2-0.05(2.61)EA but over a much smaller region. This is really a puzzling result since the threshold stress value for damage is the same (around 3 MPa) for both materials. Hence comparing Figure 3.31 (c) and Figure 3.32 (b) one would have expected a larger damage zone in the tougher but softer EA0.2-0.05(2.61)EA.

The explanation may lie in the role played by the matrix networks, which we have so far ignored. Once the filler network is damaged part of the stress has to be taken over by the second (and maybe third) network.

This important aspect of the transfer of the stress between polymer networks during fracture will be discussed in the fifth chapter.

6. Mapping the Strain Energy Density

Taking advantage of the calibration curve between chromatic change and nominal stress obtained in uniaxial tensile tests, the local stress around the crack tip was detected as described above. However, in uniaxial tension the chromaticity can clearly relate to the stress in the tensile direction, while near a crack tip the stress can be multiaxial. In addition, SP is responsive to force coming from all directions. Therefore, the stress maps in *Figure 3.27*, *Figure 3.31* and *Figure 3.32* are the aggregation of stress from all the direction in the planes of width and length. To display our results more precisely, the map of stress value can be modified into a distribution of the scalar quantity of energy density. The transformation between stress and strain energy density is based on the stress-strain curves in uniaxial tension. According to the stress-color map, the stress in each pixel can be detected and the energy density can be calculated pixel by pixel by integrating the stress-strain curves up to the stress of the pixels.

The map of the energy density for both samples of EA0.5-0.05(2.23)EA and EA0.2-0.05(2.61)EA are shown in Figure 3.33. At low same energy release rate, the stress in the soft material is too low and therefore the strain energy is also not detectable even if it should be identical to that of the stiffer sample far from the tip.

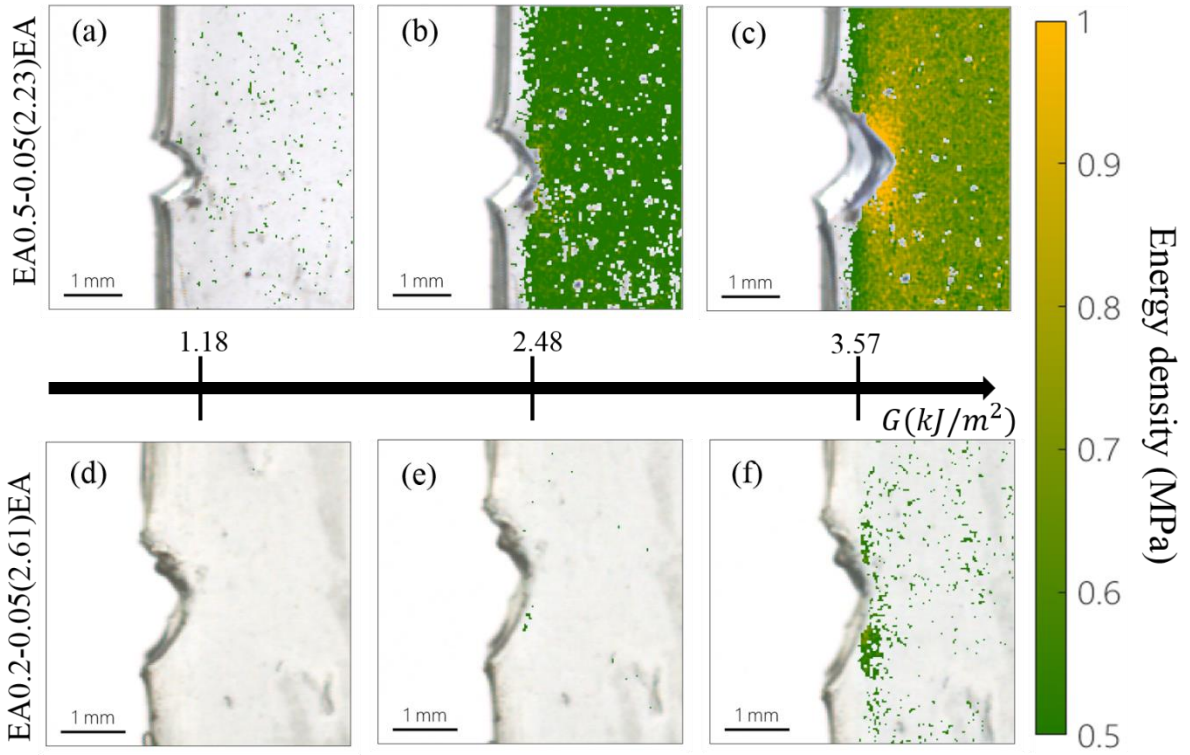

Figure 3.33 : The energy density distribution around the crack tip in the EA0.5-0.05(2.23)EA and EA0.2-0.05(2.61)EA samples at the same energy release rate

However, when comparing the maps of stress and energy density in EA0.2-0.05(2.61)EA prior to the propagation (a point where the stress is high enough to be detectable) *Figure 3.34* (b) shows a fairly similar pattern as that of the stiffer material in Figure 3.33 (c).

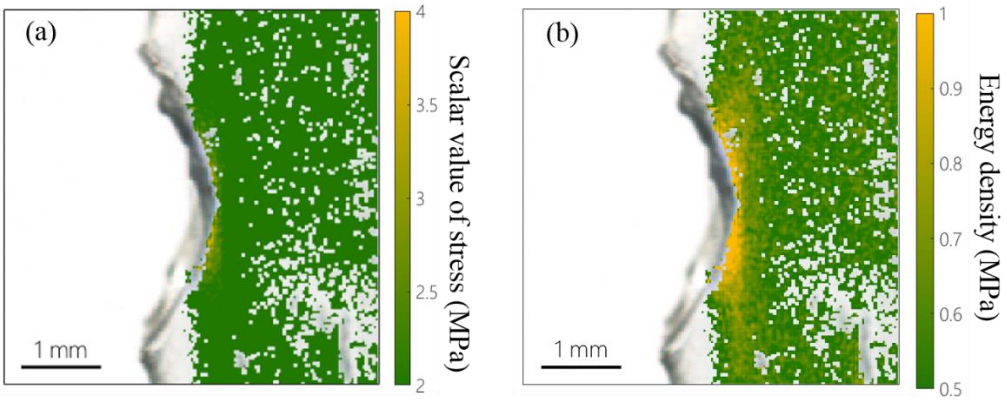

Figure 3.34: (a) The distribution of scalar value of nominal stress and (b) energy density around the crack tip in EA0.2-0.05(2.61)EA prior to the propagation

In conclusion it is interesting that both properties (stress and strain energy density) can be evaluated (with some precautions) based on the same calibration data, opening very interesting options in terms of modeling the behavior of the materials and comparing modeling and experiment.

7. Preliminary results of color change during unloading

7.1 Color change in cyclic loading

During the failure of samples in uniaxial extension, color changed from deep blue to purple immediately. Furthermore, in fracture tests, when the crack propagated, some purple regions were observed. According to previous reports[16,25,26], the purple color suggests that unloading occurs in the materials. To study the optical response during the unloading process, a cyclic loading was carried out. A specimen of EA0.5-0.05(2.23)EA was subjected to a four cyclic loading-unloading test with a $\lambda_{max} = 2.3$ as shown in Figure 3.35 (b). Figure 3.35 (a) shows the color change of the EA0.5-0.05(2.23)EA sample in the four cyclic loading. After the first cycle, the color change of the materials oscillated between blue and purple. For color analysis, the ΔRGB ratios are repeatable and reversible between cycles . A decay of ΔRGB ratios is not detected at least for four cycles as shown in Figure 3.35 (c), illustrating the relative stability of the MC crosslinker in cyclic loading.

In Figure 3.35 (d), the chromatic change calibration curve during the loading procedure of the first cycle is the same as that in uniaxial extension as expected. However, the chromatic change calibration curves exhibit a completely different behavior during the unloading process and the next cycles. The Blue channel remains at a high level with a detectable of systematic fluctuation; the red channel is also stable until the stress decreases to 2 MPa, which is the moment when the sample starts to convert to the purple color. The green channel, stable in uniaxial extension, however, shows an obvious variation. Combining the chromatic change behavior of all three channels, it should therefore be possible to map the stress for the materials having different loading histories.

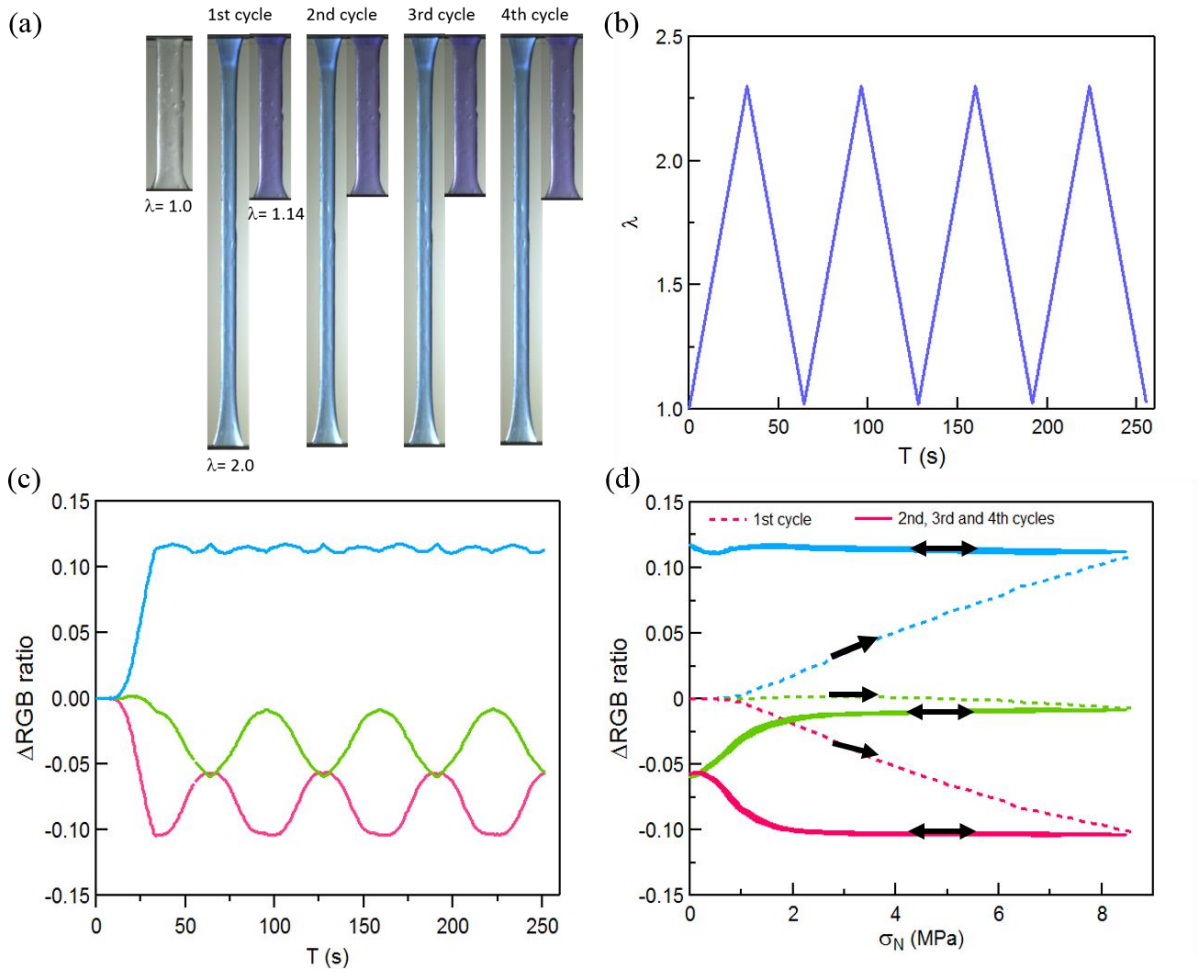

Figure 3.35: (a) The images of EA0.5-0.05(2.23)EA material in cycle loading and its respective ΔRGB ratio curves as a function of stress

7.2 Color change during the relaxation process

During the unloading process, the color of the samples change as the stress and strain reduce. Additionally, the comparison between EA0.5-0.05 and EA0.2-0.05 with different mechanical properties demonstrated that SP is more sensitive to stress.

It is therefore interesting to explore the color change in a proper relaxation test, where the strain is kept constant after the materials change color. As shown in Figure 3.36, EA0.5-0.05(2.23)EA sample exhibits a relatively stable chromatic change in relaxation. While the nominal stress decreases from 6.3 MPa to 5 MPa, red and blue channel do not occur great change, which is consistent with the result of the cyclic test that the alternation of blue and purple color takes only place below the nominal stress of 2 MPa. The small increasing/decreasing trend for the ΔBlue ratio (ΔRed ratios) is due to a slight slip of the sample from the clamps. Figure 3.35 (c) shows that in the beginning of the unloading process,

the ΔBlue ratio increases slightly. But the green channel decreases obviously at the beginning of the relaxation and the trend of reduction slows down with the decreased rate of relaxation.

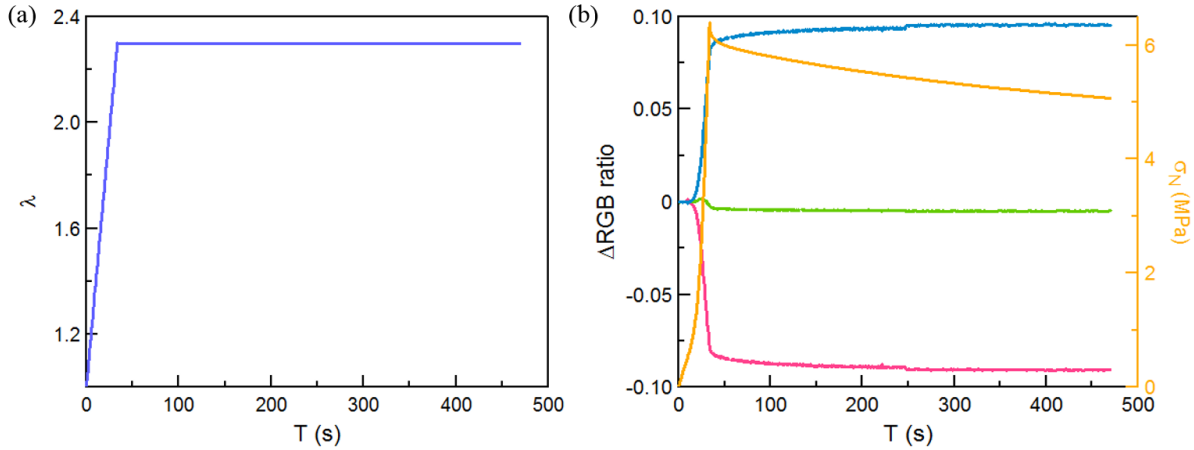

Figure 3.36: ΔRGB ratio and nominal stress as a function of time in relaxation

These preliminary results in cyclic loading and relaxation, suggest that it will be possible to probe the stress by the color change of SP also during the unloading process. If the detection is feasible, it should then be possible to map the stress, not only during the static loading phase of a crack before propagation but also during the dynamic crack propagation itself. This will be the topic that we will introduce in the next chapter.

Summary of Main Conclusions

The approach of mechanically reinforcing elastomers with interpenetrating multiple networks has been demonstrated for several families of materials based on different SN also called filler networks. . The mechanical properties of the SN itself was critical to control the mechanical properties of multiple networks and was not affected by the SP concentration. When the cross-link density of the filler network was decreased from 0.5 mol% to 0.2 mol%, the improvement of multiple network elastomers in terms of Young's modulus, stress at break and fracture toughness is still obvious. For SN with a very low crosslinking density, the synthesized multiple networks are clearly much softer but show a distinctive strain hardening and appear quite tough.

In the uniaxial extension at various stretch rates, multiple network elastomers showed a very low level of viscoelasticity, which means that the measurement of stress is insensitive to strain rate.

The correlation between the color change of multiple network elastomers and their nominal stress was established by quantifying the chromatic change with color analysis. Moreover, it was confirmed that SP was more sensitive to stress than to strain by varying the cross-linker density in the filler network and then tailoring the mechanical properties of multiple networks. Based on the calibration curve of chromatic change vs. nominal stress, the stress around the crack tip during the fracture tests was mapped. According to the initial onset of color change and to the hysteresis in step cyclic loading, the activation of SP occurred before the damage of the filler network. By detecting the stress at which damage occurs by the hysteresis of step cyclic loading, the damage areas around the crack could also be obtained and the dimensions of damage areas was confirmed to be consistent with the prediction by Brown[23] and Tanaka[24]. Furthermore, according to the data of cyclic loading and relaxation, the activation of SP show a great repeatability and a high sensitivity.

Reference:

1. Pierre, M.; *Université Pierre et Maire Curie: Paris* **2017**.
2. Ducrot, E.; *Université Pierre et Maire Curie: Paris* **2013**.
3. Pierre, M.; Ducrot, E.; Clough, J.; Wiseman, M.; Hugh, R. B.; Rint, P. S.; Creton, C.; *PNAS* **2018**, *in revision*.
4. Ducrot, E.; Creton, C.; *Advanced Functional Materials* **2016**, *26*, 2482.
5. Gong, J. P.; *Soft Matter* **2010**, *6*, 2583.
6. Gong, J. P.; Katsuyama, Y.; Kurokawa, T.; Osada, Y.; *Advanced materials* **2003**, *15*, 1155.
7. Appel, W. P. J.; Portale, G.; Wisse, E.; Dankers, P. Y. W.; Meijer, E. W.; *Macromolecules* **2011**, *44*, 6776.
8. Guo, M.; Pitet, L. M.; Wyss, H. M.; Vos, M.; Dankers, P. Y.; Meijer, E. W.; *Journal of the American Chemical Society* **2014**, *136*, 6969.
9. Kushner, A. M.; Vossler, J. D.; Williams, G. A.; Guan, Z. B.; *Journal of the American Chemical Society* **2009**, *131*, 8766.
10. Koevoets, R. A.; Versteegen, R. M.; Kooijman, H.; Spek, A. L.; Sijbesma, R. P.; Meijer, E. W.; *Journal of the American Chemical Society* **2005**, *127*, 2999.
11. Liu, J.; Tan, C. S.; Yu, Z.; Lan, Y.; Abell, C.; Scherman, O. A.; *Advanced materials* **2017**, *29*.
12. Widin, J. M.; Schmitt, A. K.; Schmitt, A. L.; Im, K.; Mahanthappa, M. K.; *Journal of the American Chemical Society* **2012**, *134*, 3834.
13. Jiang, S.; Zhang, L.; Xie, T.; Lin, Y.; Zhang, H.; Xu, Y.; Weng, W.; Dai, L.; *ACS Macro Letters* **2013**, *2*, 705.
14. Sun, J. Y.; Zhao, X.; Illeperuma, W. R.; Chaudhuri, O.; Oh, K. H.; Mooney, D. J.; Vlassak, J. J.; Suo, Z.; *Nature* **2012**, *489*, 133.
15. RIVLIN, R. S.; THOMAS, A. G.; *Journal of polymer science* **1953**, *10*, 291.
16. Gossweiler, G. R.; Kouznetsova, T. B.; Craig, S. L.; *Journal of the American Chemical Society* **2015**, *137*, 6148.
17. Miquelard-Garnier, G.; *Université Pierre et Maire Curie: Paris* **2007**.
18. Miquelard-Garnier, G.; Demoures, S.; Creton, C.; Hourdet, D.; *Macromolecules* **2006**, *39*, 8128.
19. Etienne, D.; Yulan, C.; Markus, B.; Rint, P. S.; Costantino, C.; *science* **2014**, *344*, 4.
20. Davis, D. A.; Hamilton, A.; Yang, J.; Cremar, L. D.; Van Gough, D.; Potisek, S. L.; Ong, M. T.; Braun, P. V.; Martinez, T. J.; White, S. R.; Moore, J. S.; Sottos, N. R.; *Nature* **2009**, *459*, 68.
21. Lake, G. J.; Thomas, A. G.; *Proceedings of the Royal Society of London Series a-Mathematical and Physical Sciences* **1967**, *300*, 108.
22. Mohammadi, N.; Klein, A.; Sperling, L. H.; *Macromolecules* **1993**, *26*, 1019.
23. Brown, H. R.; *Macromolecules* **2007**, *40*, 3815.
24. Tanaka, Y.; *Europhysics Letters (EPL)* **2007**, *78*, 56005.
25. Gossweiler, G. R.; Hewage, G. B.; Soriano, G.; Wang, Q.; Welshofer, G. W.; Zhao, X.; Craig, S. L.; *ACS Macro Letters* **2014**, *3*, 216.
26. Zhang, H.; Chen, Y.; Lin, Y.; Fang, X.; Xu, Y.; Ruan, Y.; Weng, W.; *Macromolecules* **2014**, *47*, 6783.

Chapter 4: Mapping the stress in unloading process

Introduction

The previous chapter focused on the exploration of the relationship between chromatic change and stress (strain). By varying the cross-linker densities and SP concentration in the first network, we demonstrated that when SP was incorporated as a crosslinker in the filler network it could be used as a stress sensor in multiple network elastomers and as a calibration curve between chromatic change and stress. Using this calibration curve, the correlated stress around the crack tip during loading was mapped in different materials. Moreover, in a cyclic loading test, the slightly different absorption spectrum of the two MC isomers in the loaded and unloaded state after activation suggested the possibility of mapping the stress in the relaxation regime. In this chapter, a strategy to map the correlated stress during the crack propagation will be introduced.

To study the stress distribution during crack propagation, a color map of stress as function of chromatic change upon loading and unloading will be introduced. This map will be used to detect the variation in the correlated loading distribution during crack propagation. The relaxed regions and the quantity of active SP around the crack tip will be explored.

1. Construction of a color map of the stress

During the fracture test, a chromatic change from blue to purple was observed in the areas where the crack propagated and the material was unloaded. To understand the variation in stress distribution during crack propagation, we discuss how the mapping of both loading and unloading can be examined.

1.1 Color change during the unloading process

1.1.1 Mechanism of color change during the unloading process

In the previous chapter, the color immediately changed from blue to purple when the samples failed in the extension tests. This color change can be controlled and observed by performing cyclic loading tests of EA0.5-0.05(2.23)EA as shown in *Figure 4.1*. Different from the uniaxial extension, the materials did not immediately change to purple in the unloading process. Only when the nominal stress decreased to a relatively low level, the material gradually turned purple, which suggests that this process is also sensitive to the stress. The nominal stress is around 2 MPa when the color change can be observed by naked eyes.

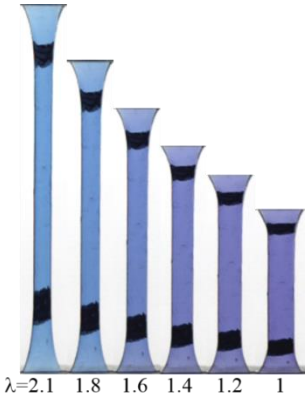

Figure 4.1 Color change in the cyclic loading test of EA0.5-0.05(2.23)EA sample

According to reports by Craig[1,2], Kuciauskas[3] and Jonathan[4], the color change during unloading is due to the isomerization of MC. MC during loading and unloading changes between different main configurations of isomers. Scheme 1 shows various conformers of MC isomers. These isomers are reversibly interconvertible besides the ground-state isomers[3]. TTC and TTT are the two predominant ground-state isomers as they have the lowest ground-state energies as shown in Scheme 1. CTC and CTT are excited-state isomers and can convert into ground-state in excited-state isomerization reactions. Furthermore, the most stable isomers vary with the substituent groups and the points connecting to polymer chains on the SP molecule. This suggests that the absorption spectrum of the MC is different during loading (blue) and its relaxed state (purple) due to the different proportion of the main MC isomers[1,3]. According to Kuciauskas's result, the absorption peaks of CTC, TTT and TTC are located at

630, 568 and 600 nm, respectively. When the excited-state isomers convert to the ground-state, the color changes are due to the blue shift of the absorption spectrum.

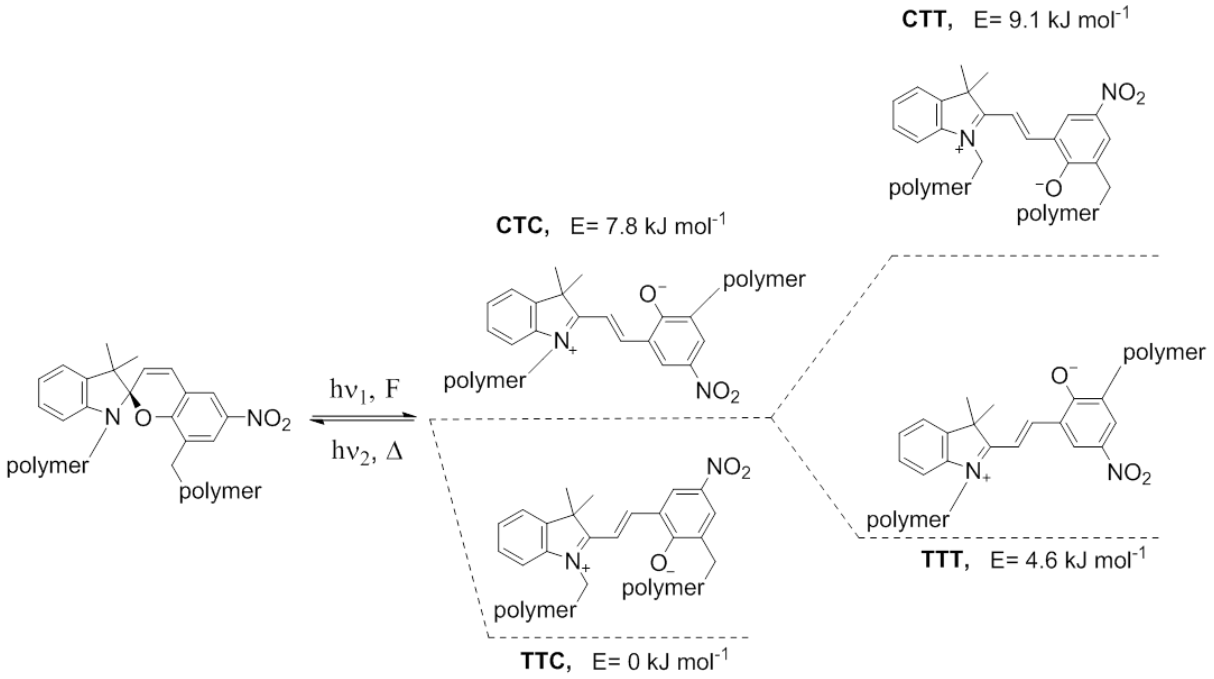

Scheme 1: The transformation of SP into MC and its isomers

Based on Craig's computational and experimental results[1,2], CTC is the main configuration observed in the loaded state for our SP mechanophore, but it converts into TTT upon unloading[3]. Since the distance between the two points where the polymer chains attach to is largest in TTT relative to all other isomers, TTT could be in principle more stable than TTC after activation of SP by force despite the lowest energy of TTC. But the activation of SP is under kinetic rather than thermodynamic control, which can lead to counterintuitive experimental results. The relative isomer energies are shown in Scheme 1 deduced from quantum chemical calculations and NMR line broadening data[4-6]. In addition, due to the differences in absorption bands between TTT (568 nm) and CTC (630 nm), materials appear blue and purple during the loading and unloading processes.

In our absorption spectrum during cyclic extension shown in Figure 4.*2*, only one peak appears in the spectrum taken in the unloaded state and its wavelength is identical with that of the material exposed by UV light. Moreover, when the nominal stress increases to 11.1 MPa two peaks emerge at the wavelengths of 580 and 625 nm. According to literatures[3,5], the main peak (625 nm) corresponds to the main isomers of CTC in loading and the other peak suggests the existence of TTT. TTT indicates that part of the material is unloaded and may be related to damage in the materials. This is qualitatively consistent with the previous results showing that materials start to damage when the uniaxial nominal stress is above 3 MPa, but it is not clear whether quantitatively the fraction of broken bonds is large enough to cause that shift.

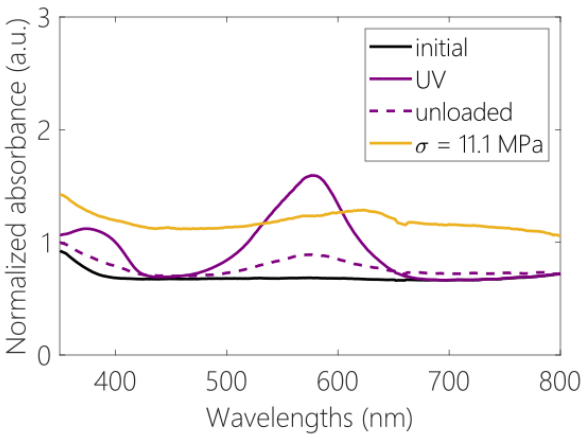

Figure 4.2 : The absorption Spectrum of EA0.5-0.05(2.23)EA in the extension and under the exposure of UV light

The stability of CTC depends on the force applied on the molecule. When the macroscopic stress decreases during unloading, more and more CTC switches to TTT. Based on the transformation of the two isomers and to their color change, the map of stress was constructed in the following section.

1.1.2 Color map of stress in standard multiple network elastomers

To map the stress during unloading or relaxation, it is necessary to construct an appropriate chromatic calibration curve. As discussed briefly above, a color change between blue and purple is observed during the unloading process. Combining both processes (from transparent to blue upon loading and from blue to purple upon unloading), a step cyclic loading test was performed to construct a stress-color calibration map.

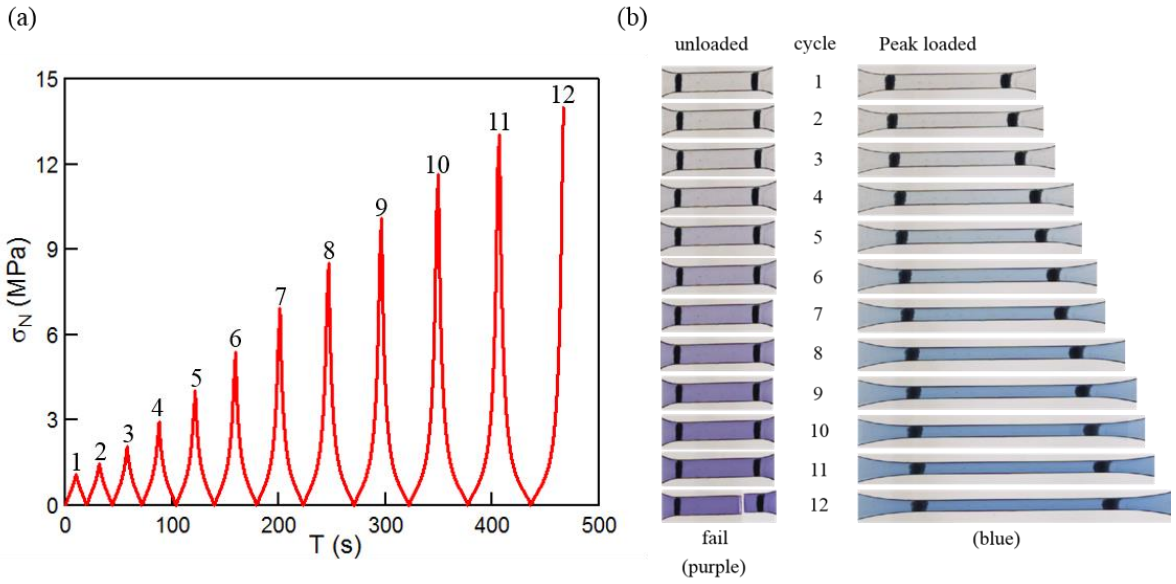

Figure 4.3 The step cyclic loading of EA0.5-0.05(2.23)EA: (a) Nominal stress as a function of time; (b) the frames of material show color change.

Figure 4.3 (a) shows the curve of the nominal stress as a function of time in the step cyclic loading test. According to the results presented in chapter 3, SP starts to transform into MC when the nominal stress exceeds ~1.5 MPa, which is achieved at the maximum stress in the second cycle. Therefore, in the beginning of the step cycle extension, negligible chromatic change is observed until a maximum deformation of 60% is reached as shown in Figure 4.3 (b). Note that the color change occurs before significant hysteresis is seen at 80% deformation. This result is consistent with uniaxial tests showing activation of SP before the inflection point, suggesting damage. With the increase in strain, the chromaticity of blue and purple increases with each step cycle, implying an increasing concentration of MC.

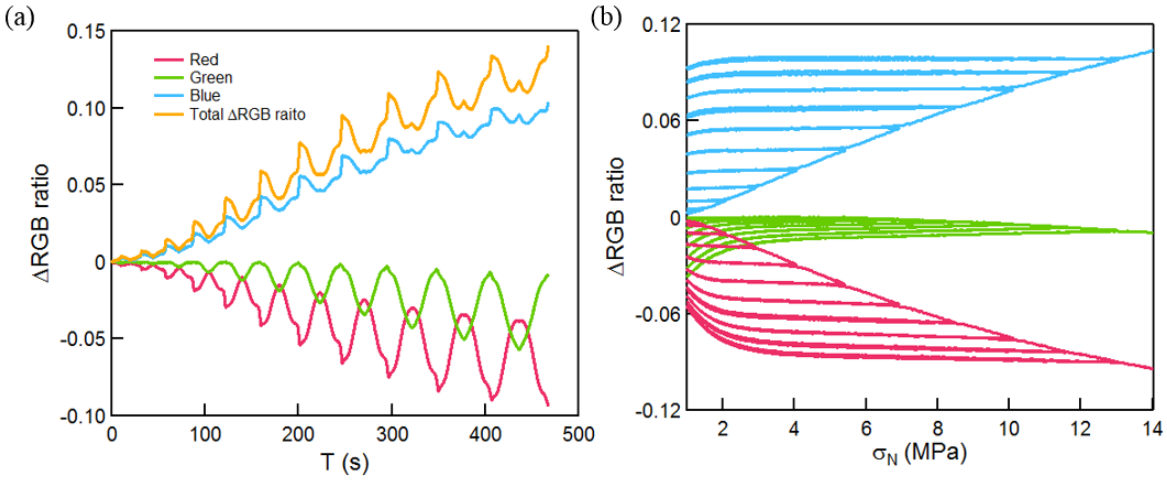

Figure 4.4: Chromatic change as a function of (a) time and (b) nominal stress in step cycle extension with EA0.5-0.05(2.23)EA materials

The calibration curve of chromatic change during the step cyclic loading is shown in Figure 4.4. The curve of ΔBlue ratio as a function of time gradually increases. Furthermore, the ΔBlue ratio presents two peaks per cycle between the maximum and minimum deformation as shown in Figure 4.4(a). The minimums and maximum of ΔRed and ΔGreen ratios for each cycle decrease step by step. Moreover, they show the opposite varying tendency. ΔGreen ratio has its minimum value at the lower limit of deformation or stress as shown in Figure 4.4(b), and almost recovers the same level when the stress reaches the top in every cycle. The ΔRed ratio varies in an opposite way upon unloading and the minimum value gradually decreases. Furthermore, the maximum of ΔRed ratio also decreases at each step cycle resulting in the small peak of ΔRed ratio in relaxation. The curve of chromatic change in the loading process is the same as that of the uniaxial tensile tests as shown in Figure 4.4 (b). In relaxation, however the curves can overlap with the loading curve of the next cycle, which demonstrates the great repeatability of the optical response. These curves in loading and unloading show that the blue channel and red channel can both be used for the detection of stress in the loading process in uniaxial extension, and that the green channel can be used to measure the

stress during the relaxation process. Therefore, it is feasible to build a 3D-map to detect the stress of a material under loading or unloading.

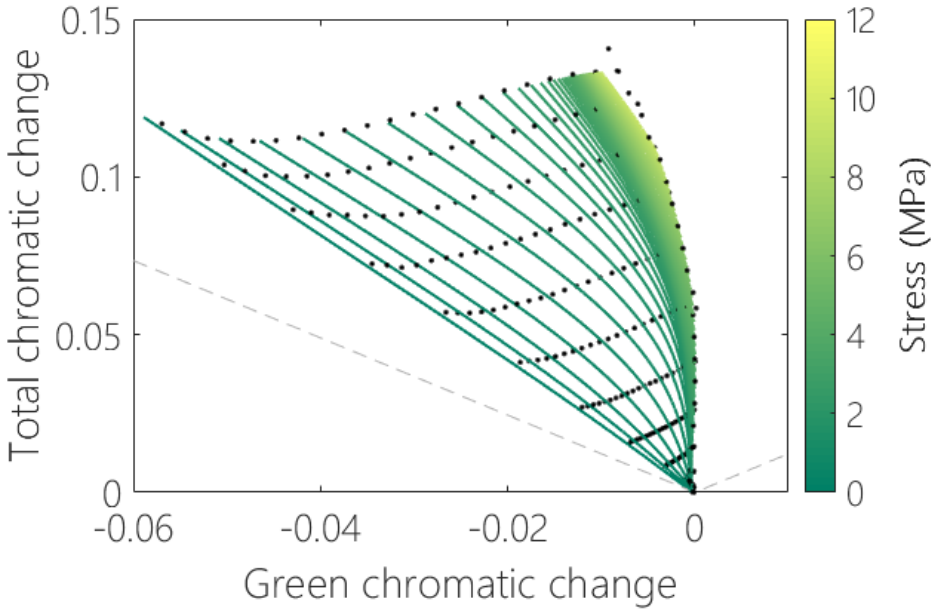

Figure 4.5 : The color-stress map of EA0.5-0.05(2.23)EA is plotted, where the nominal stress is represented as a function of Green and of total chromatic change and the color represents the magnitude of the nominal stress.

In Figure 4.4(a), we show also (in yellow) the curve of total chromatic change, which is calculated from Equation 1:

$$Total\ chromatic\ change = \sqrt{(\Delta Red^2 + \Delta Green^2 + \Delta Blue^2)} \qquad \text{Equation 1}$$

Total chromatic change combines information from the three channels. Thus, it is most sensitive to the stress compared to three channels individually. It is used as a reference for the measurement of stress during loading and the ΔGreen calibration curve is used to detect the stress during relaxation. A 3D map can then be plotted, where the green and total chromatic change are the x and y variables, respectively. Color coded curves of nominal stress as a function of green and total chromatic change are shown in Figure 4.5 where the stress is plotted in terms of the color gradient. Based on a interpolation procedure, the color map of stress as a function of green and total chromatic change can be constructed as shown in Figure 4.5. The right edge of the map is the stress curve during virgin loading where SP changes into MC The left part of the map is the process of relaxation and reloading, i.e. reflects the reversible change from MC-CTC to MC-TTT. The black dots are the experimental points and the green curves are the fitted curves for the relaxation. Thus when the two values of green and total chromatic change are obtained from each pixel of the image of materials, the position of this pixel in the color map can be located and the value of the nominal stress at this pixel can be determined.

1.1.3 Multiple network elastomers with different mechanical property

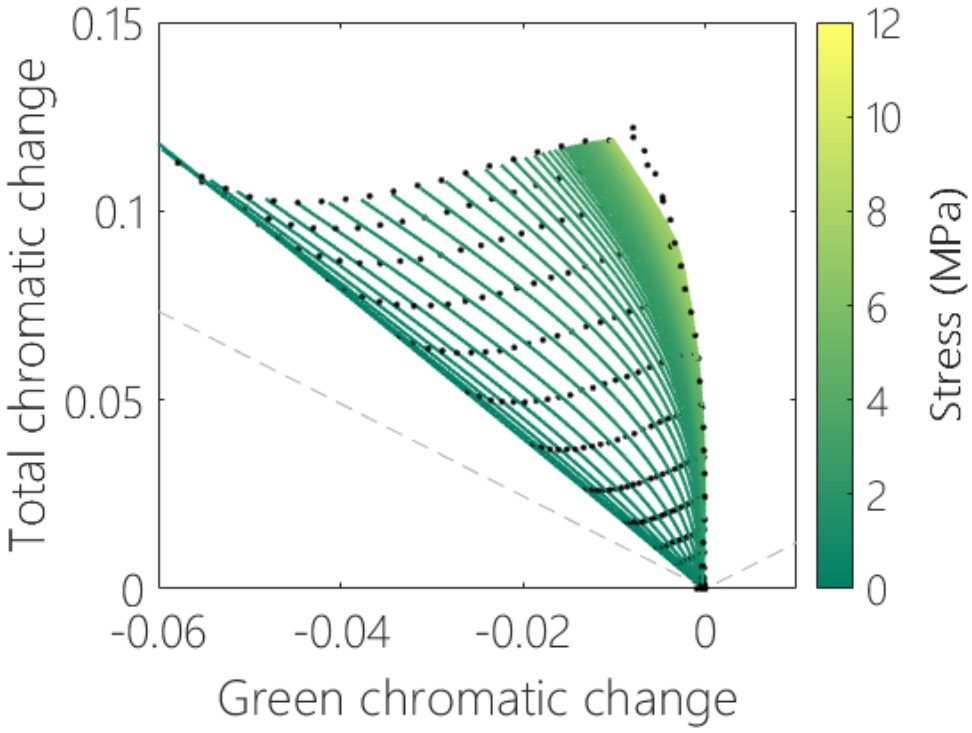

Figure 4.6: The color-stress map of EA0.2-0.05(2.61)EA sample was plotted in loading and unloading. The black dots are the experimental points detected in step cyclic loading tests.

In the last chapter, we showed that the EA0.5-0.05 and EA0.2-0.05 families had the same calibration curve of chromatic change as a function of stress in uniaxial tensile tests. In the color map of stress, the chromatic change during loading is plotted at the right edge. Comparing the two color map of stress in Figure 4.5 and Figure 4.6, the border line is consistent with each other and the color map of the EA0.2-0.05(2.61)EA sample seems very similar to that of EA0.5-0.05(2.23)EA with a difference in the stress values. At the top right corner of the map in Figure 4.6, the stress is lower than Figure 4.5. That is due to the mechanical properties of EA0.2-0.05(2.61)EA. The stress at break of EA0.2-0.05(2.61)EA is lower than that of EA0.5-0.05(2.23)EA due to the lower cross-linker density in the filler network. During unloading at the same value of stress, chromatic change of EA0.5-0.05(2.23)EA decreases more than EA0.2-0.05(2.61)EA. It confirms that EA0.5-0.05(2.23)EA is more sensitive to the stress than EA0.2-0.05(2.61)EA. Although the color map of stress can not be fixed on a master or standard color map of stress, these colormaps can still be generated for each family of materials.

1.1.4 Elastomers with various SP concentrations

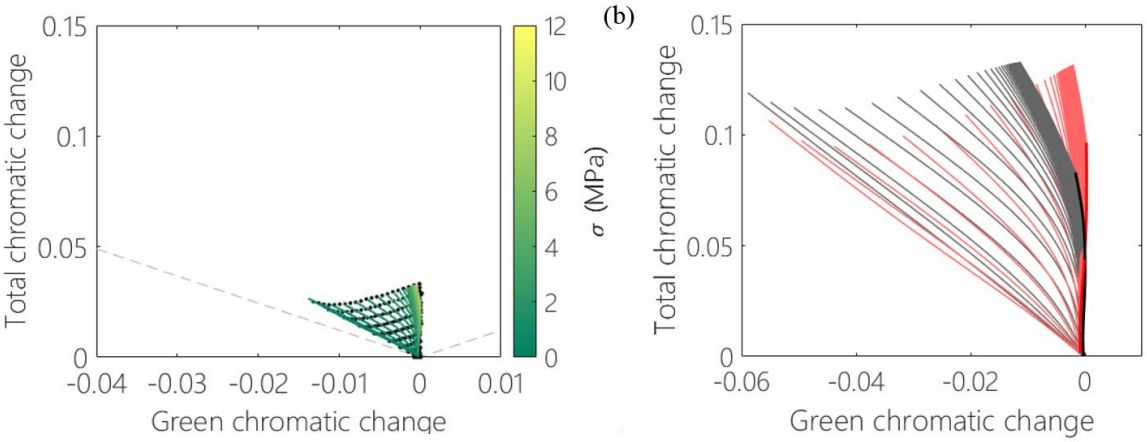

Figure 4.7: (a) The map of stress acts as functions of green and total chromatic change in EA0.5-0.025(2.35)EA sample. (b) The stress-color map of EA0.5-0.05(2.23)EA (black curves) and EA0.5-0.025(2.35)EA (red curves) after normalization and the bold curves (on the right edge) represent the loading chromatic pathway.

The chromaticity is also affected by the concentration of MC. When the SP concentration decreases to 50% of the original value, the chromatic change decreases to approximately half of the original value, which is observed in the previous chapter. The color map of stress in the step cyclic loading is also plotted in Figure 4.7 (a). The plotted scale of the map of EA0.5-0.05(2.23)EA is two times larger than EA0.5-0.025(2.35)EA sample. Although the EA0.5-0.025(2.35)EA sample only possesses half of the chromatic change in comparison to EA0.5-0.05(2.23)EA sample, the stress-color map is still able to measure the stress in the materials for the loading and unloading or the materials possessing stretched history despite a relatively low resolution. Moreover, after the normalization of the SP concentration, the stress-color map can be amplified and forms a same magnitude map as EA0.5-0.05(2.23)EA as shown inFigure 4.7 (b). Comparing the two maps, for the loading pathway the curves of chromatic change overlap. However, the unloading process exhibit an observable difference. This attributed to the higher concentration of SP in EA0.5-0.05(2.23)EA, which can introduce non-linear effects in the absorption spectrum.

2. Stress distribution around the crack tip during crack propagation

2.1 Color change during crack propagation

When prenotched samples are stretched and the deformation exceeds a critical strain, the crack catastrophically propagates. Due to the sudden propagation, the color camera (capturing at a rate of 25 frames per second) only captured two frames during the fast propagation process. As shown in Figure 4.8, the frame prior to failure is blurry, however, regions of deep

blue and purple are clearly visible. The color distribution on both sides of the crack tip are approximately symmetrical. Due to known isomeric forms of MC that exhibit slight differences in absorbance spectrums, the purple regions suggests a distribution shift between isomeric MC populations due to unloading[1,7]. To observe the crack propagation clearly, a notched sample was stretched to the critical stress and subsequently maintained at a constant displacement. To improve video quality, the frame rate was increased to 30 fps. Color analysis was performed on each frame in order to create a stress map of loaded and unloaded regions.

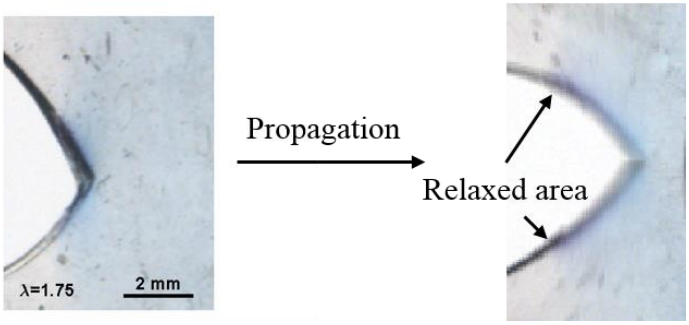

Figure 4.8: The frames of EA0.5-0.05(2.23)EA materials before (left) and after (right) crack propagation show the color change in the area far away from the crack tip.

2.2 Stress distribution in crack propagation

After creating a stress color map from uniaxial tension experiments, this information can be used to detect the correlated uniaxial stress in a sample where a crack propagates. However, as described in chapter three, the chromaticity only relates to the stress in the tensile direction; whereas, the stress is multiaxial near the crack tip. In other words, the activation of SP (as measured by color change) correspond to the stress derived from any direction. Thus, the scalar value of the correlated stress corresponds to the uniaxial force. It is more physically interpretable to represent the correlated stress distribution as an energy density as shown in the loading process. The transformation between stress and energy density is based on the stress-strain curves of uniaxial tension. But different from the loading process, the unloading process when material is stretched to different maximum stress or strain varies. To calculate the energy density during unloading, it is necessary to know the maximum stress in each pixel in their stretched history and interpolate the unloading stress-strain curve. This approach represents an ongoing effort to produce quantitative mapping around a crack tip. For presenting the primary results, the scalar value of stress distribution is shown.

To map the stress or energy density around a crack tip, crack propagation tests were carried out on 1 mm notched EA0.5-0.05(2.23)EA rectangular samples with dimensions of 5 mm by 20 mm. A color camera (30 fps, frame rate) was set to record the color change in the crack propagation. Because of the speed of the crack propagation, capturing clear frames during this process was difficult. Thus, the fracture test was modified. Based on previous results on

fracture testing, the critical stress for crack propagation was determined. The Instron was set to reach the critical stress and hold the clamps at constant displacement, allowing for the crack to grow at a slower rate for clearer video capture to occur. Selected frames prior to fast propagation are shown in Figure 4.*9*.

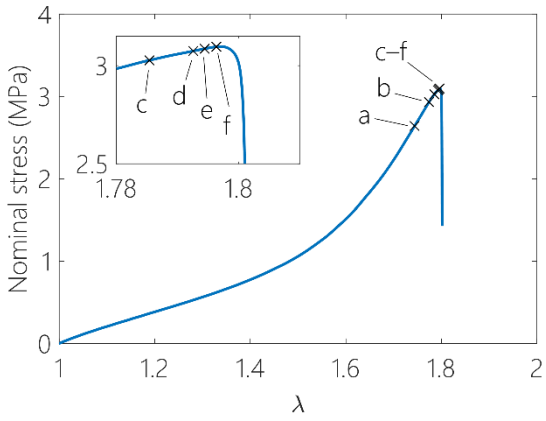

Figure 4.9: Stress as a function of time in the fracture test of EA0.5-0.05(2.23)EA sample with a notch. ‘a’ is the location prior to the propagation and ‘b’ to ‘f’ is the location during propagation.

The scalar correlated uniaxial stress can be computed for each pixel with the stress-color map. In Figure 4.*10* (a), the raw image shows two purple zone located at the edge of crack but far from the crack tip. Using the stress-color map to detect the unloading process, the correlated stress distribution is shown in Figure 4.*10* (b). There are two regions in the shape of wedges where the material is unloaded. The unloaded regions start from the area that exhibits the maximum stress before crack propagation right in front of the crack. The region of maximum stress moves from left to right following the crack tip. The areas near the edge of the crack start to unload after the crack passes through, which gradually extend to areas further away from the crack. In unloaded areas, the magnitude of relaxation of stress increase with the distance away from the crack tip as shown in Figure 4.*10* (b). The stress in pink areas almost relaxes to 0. According to *Figure 4.10*, most of the material is still under load prior to fast crack propagation and the unloaded zone correspond to the purple areas in the raw image.

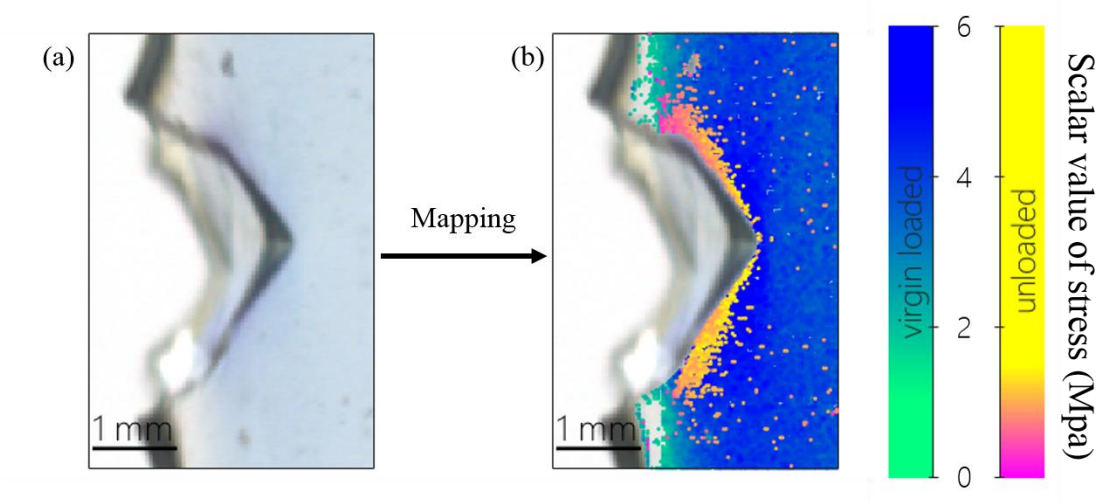

Figure 4.10: (a) The raw image of EA0.5-0.05(2.23)EA sample during the crack propagation (b) Spatial mapping of pixels in front of a propagating crack where the stress for each pixel is obtained from the chromatic change map of the stress in EA0.5-0.05(2.23)EA sample. The color between yellow and pink means the stress relaxes from various values.

Due to the damage that occurs prior to fast propagation, some areas close to the crack tip have been unloaded. To define and quantify the unloaded area, different frames extracted from various locations on the stress-strain curve before fast propagation as shown in Figure 4.*9* (the six frames corresponding to the six point in Figure 4.*9* are before the fast propagation). They are shown in Figure 4.*11*. Some purple areas can be observed on both sides of the crack.

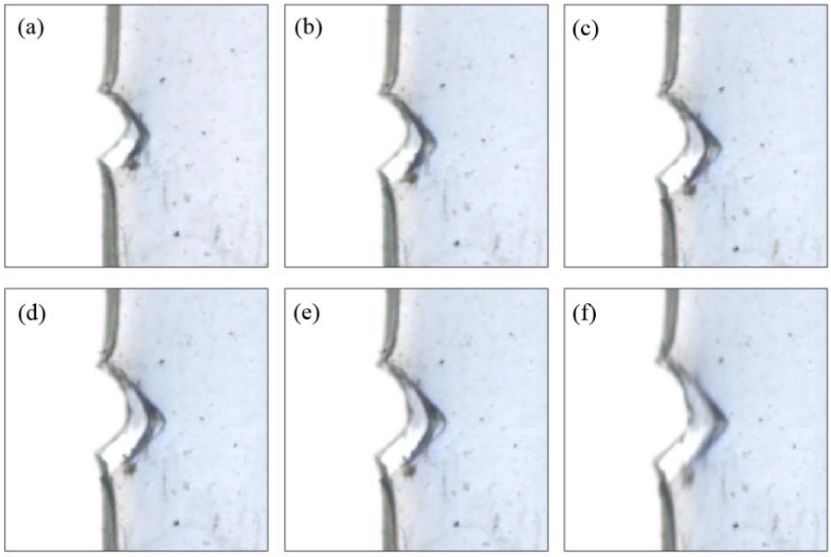

Figure 4.11 : Six frames at different moments prior to the crack propagation as shown in Figure 4.9

The six frames prior to fast propagation were mapped according to the stress-color map as shown in Figure 4.*12*. Most of the areas in front of crack tip show the virgin stress distribution. Furthermore, a distinct pink region appears at the edge of the crack, which subsequently extend as the stress increases.

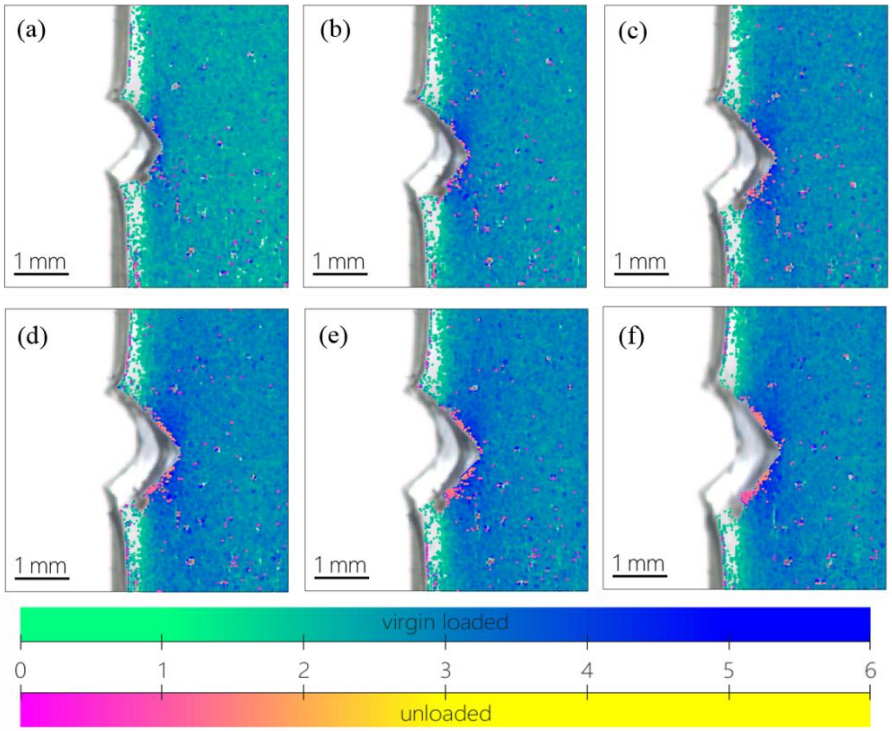

Figure 4.12 : Stress maps of the six frames are shown Figure 4.11. The color from green to blue represent the magnitude of the virgin load and color between pink and yellow is the unloaded areas mapping with pixel.

Since the stress was mapped for each individual pixels, a statistical analysis was made to categorize the pixel as loading or unloading. The schematic of stress-color map is shown in Figure 4.*13* (a). Pixels were systematically separated into unloading, loading, background and other objects (such as noise, dust, edges, etc.). In Figure 4.*13*(b), the color distribution of a transparent sample area extracted from the start of the experiment was used to statistically define the boundary between the loading and unloading regions on the stress-color map. Since the green chromaticity is primarily sensitive to unloading, the distribution of the green chromatic change in the sample area was used to determine a threshold value used to differentiate loading and unloading pixels. For results shown herein, pixels labeled as being unloaded have an associated 99% confidence level.

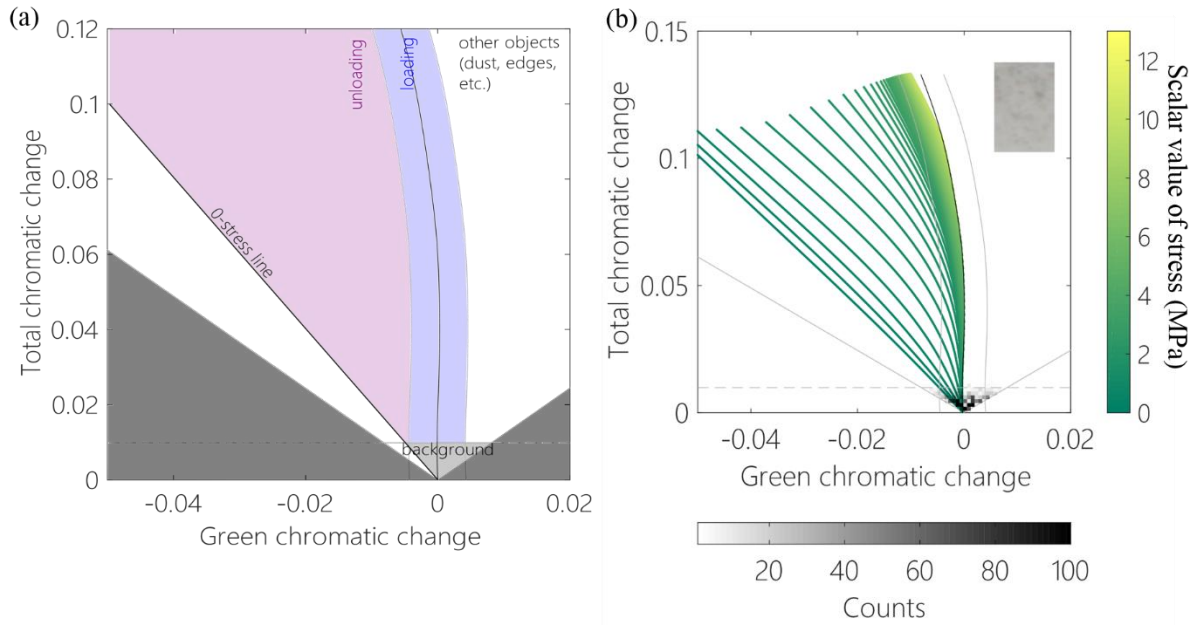

Figure 4.13 : (a) The schematic of stress-color map displays the loading (blue) and unloading (pink) regions. The white region and gray areas are other objects (including dust, edges, etc.) and the noise. The black region is a unpossible region that pixels can be located according to the principle of the color composition. (b) A hexagonal bivariate histogram prior to mechanical load.

The hexagonal bivariate histogram for the six frames from in Figure 4.*11* are shown in Figure 4.*14*. The color intensities represent the pixel counts in one hexagonal bin, while the three colors, pink, blue, and black, corresponds to pixels labelled as unloading, loading, and noise/background, respectively. From frames Figure 4.*11a* to *f*, the unloading and loading pixel counts increase.

The increase in unloading pixels implies that crack propagation occurred. This is evident in Figure 4.*12(b)* and *(c)*, where pixels around the crack have been labelled as unloaded. Interestingly, this corresponds to points (b) and (c) in Figure 4.*9*, in which both occur before the sample reach its failure stress. In other words, the onset of crack growth can be detected optically before the notched sample catastrophically fails. Thus, this analysis can be used to quantitatively define a time period in the stress-strain curve that is associated with the onset of crack growth.

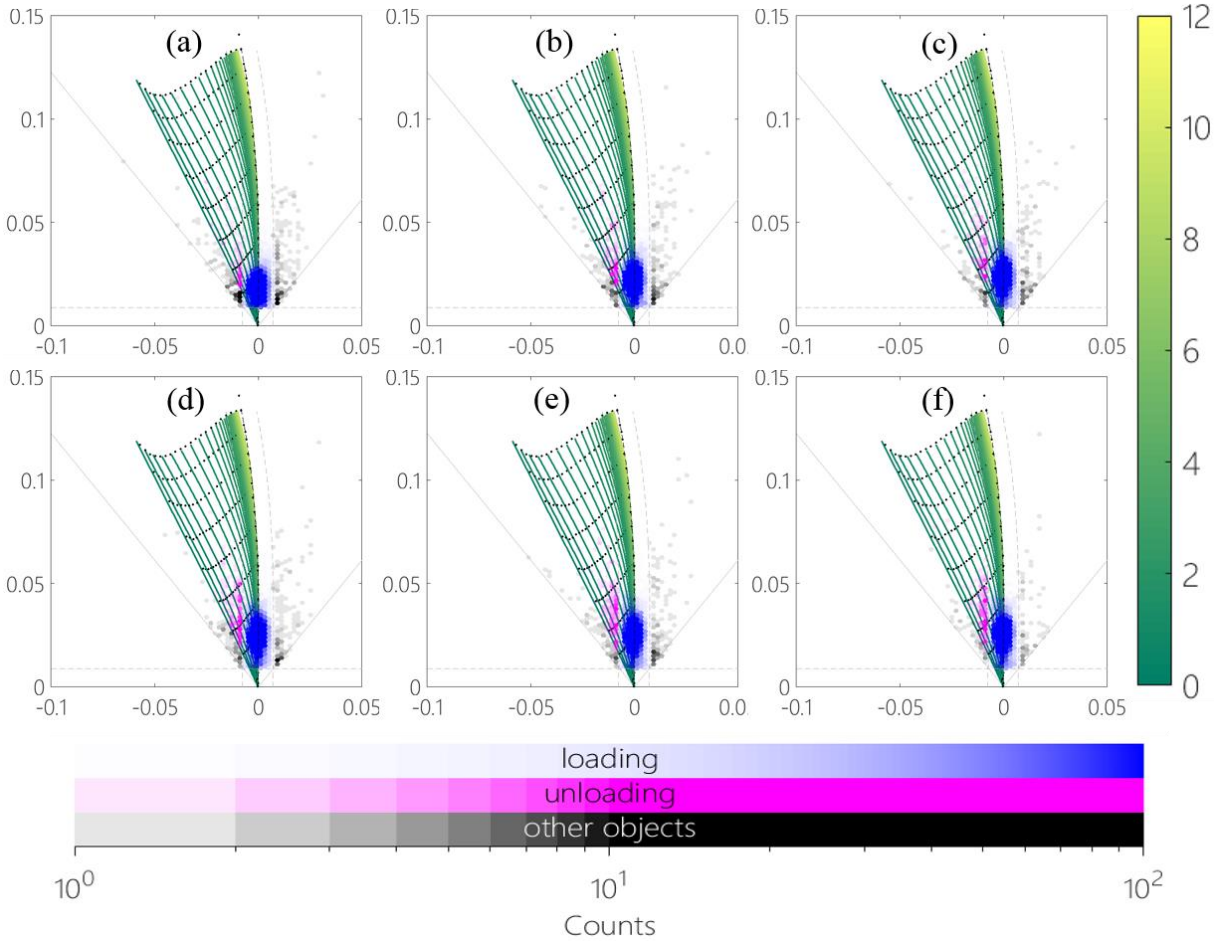

Figure 4.14 The statistic of loaded and unloaded pixels for the six frames in Figure 4.12: the intensity of the three colors represent the number of the pixel. Blue, pink and black points are the loaded, unloaded and noisy pixels, respectively.

3. Quantify the level of activation of SP near the crack tip

In the cyclic loading test, more and more SP are activated with the increase of the maximum strain. The assumption here is that we can quantify the fraction of SP by exposing the sample to UV light as described in chapter 1. In order to be quantitative we first exposed a transparent section of the same material to UV light for 5 mins, where all the SP in the materials are assumed to be activated. This chromatic change is define as the color change with 100% MC. Then the MC concentration in cyclic loading test was quantified according to the chromatic change relative to the total chromatic change by UV exposure. The result is shown in Figure 4.*15* (a). The dots are the experimental points at the maximum strains and they are fitted by polynomial. According to the fitted curve, SP is activated at the stress of 1.7 MPa and when the stress is 3 MPa (the initial stress that damage occurs in filler network) there are 0.4% SP converting into MC.

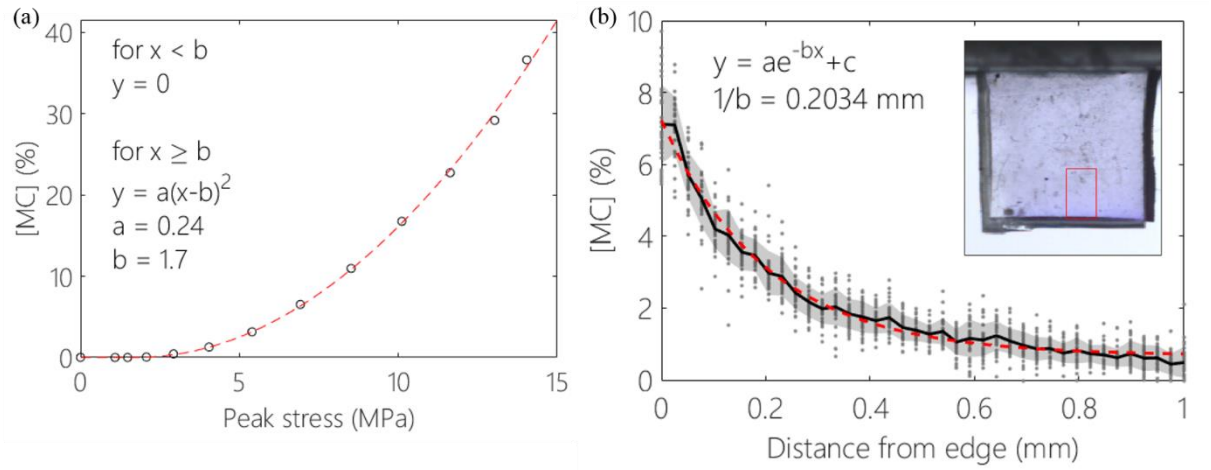

Figure 4.15: (a) The MC concentration is quantified in the step cyclic loading above and the red curve is fitted with polynomial according to the experimental data. (b)The MC concentration is quantified post-mortem in a EA0.5-0.05(2.23) sample. Transparent patches represent twice the estimated standard deviation (based on a statistical distribution of a reference image with no mechanophore activation) of the determined total chromatic change.

After crack propagation in fracture tests, the top half of the post-mortem sample were used to perform color analysis as shown in Figure 4.*15* (b). The chromatic change relative to the transparent sample was determined and associated with complete activation. The total chromatic change of the pixels located on the red line in Figure 4.*15* (b) is divided by the total chromatic change of 100% MC to quantify the percent of SP activated during crack propagation. From *Figure 4.15* (b), about 6% of SP is activated very close to the crack plane and about 1% is activated in the bulk of the sample. The percent of MC activated around the crack was plotted against to the distance away from the crack in Figure 4.*155* (b). A decaying exponential function can be fitted to the data as shown in Figure 4.*15*5 (b). From the fit, the width of the high stress zone is estimated to be 1 mm. However, the high stress zone is not equivalent to the damage zone since the force to activate SP is much lower than the force (3-4 nN) to break the C-C bonds in the polymer chains. Based on the results of the step cyclic loading in Figure 3.9 (d) (in chapter 3), damage occurs in the filler network, when the uniaxial stress reaches 3 MPa, which corresponds to a MC concentration of 0.4% according to the fit in Figure 4.*15* (a). Thus, according to the fit in Figure 4.*15* (b), the damage zone is about 600 μm wide around the crack involving in dissipating energy. This result is close to the prediction of double network models[8,9]. But the result has a significant difference from the damage zone (250 μm) prior to the propagation, which illustrates during the crack propagation there are more areas involving in dissipating energy.

Conclusion

The strategy, using the secondary color change of SP to map the stress in the unloading process, is confirmed in this chapter. The secondary color change between blue and purple deriving from the isomerization reaction of MC is sensitive to the stress. With the color change in the step cyclic loading, the color map of stress in loading and unloading has been constructed. Varying the cross-linker density in the filler network the color map of stress for different materials of multiple networks approximately overlap. Although a different color map of stress revealed by tailoring the concentration of SP in the filler network, the normalization the color map is consistent with the previous one. Based on the stress-color map, the correlated stress distribution around the crack tip has been mapped during crack propagation.

Referring to the chromatic change of 100% SP activated by the exposure of UV light, we have quantified the magnitude of active SP in the fracture test. In addition, according to the initial stress of damage, the damage zone around the crack was estimated and was consistent with the prediction by Brown[8] and Tanaka[9].

In summary, the fracture mechanism and stress distribution in the multiple network elastomers, so far, was known that the filler network undergoes the main stress and damages to dissipate energy. However, when the damage takes place in the filler network, especially after the yielding where large amount of scission occur, but they do not lead to eventual failure of the specimen. So ‘how does the stress transfer in the multiple during the damage?’ becomes an interesting topic. Moreover, when a notch exists in the materials, a large zone of high stress distributes in front of the crack tip. In the high stress zone, the damage zone is about 250 μm wide. It is also critical for the fracture mechanism to comprehend ‘what is the action of the second network in the damage zone’. The fifth chapter explores these topics.

Reference:

1. Gossweiler, G. R.; Hewage, G. B.; Soriano, G.; Wang, Q.; Welshofer, G. W.; Zhao, X.; Craig, S. L.; *ACS Macro Letters* **2014**, *3*, 216.
2. Gossweiler, G. R.; Kouznetsova, T. B.; Craig, S. L.; *Journal of the American Chemical Society* **2015**, *137*, 6148.
3. Wohl, C. J.; Kuciauskas, D.; *J. Phys. Chem. B* **2005**, *109*, 22186.
4. Hobley, J.; Malatesta, V.; *Phys. Chem. Chem. Phys.* **2000**, *2*, 57.
5. Cottone, G.; Noto, R.; La Manna, G.; *Molecules* **2008**, *13*, 1246.
6. Kovalenko, O.; Lopatkin, Y.; Kondratenko, P.; Belous, D.; *The European Physical Journal D* **2018**, *72*.
7. Zhang, H.; Chen, Y.; Lin, Y.; Fang, X.; Xu, Y.; Ruan, Y.; Weng, W.; *Macromolecules* **2014**, *47*, 6783.
8. Brown, H. R.; *Macromolecules* **2007**, *40*, 3815.
9. Tanaka, Y.; *Europhysics Letters (EPL)* **2007**, *78*, 56005.

Chapter 5: The fracture mechanism of multiple network elastomers

Abstract

In the previous chapter, we focused on the nonlinear elastic properties of multiple networks and on the fracture of the filler network due to its crucial role in controlling the mechanical properties of multiple network elastomers. However, the second network and other networks prevent the failure of materials when large amount of damage occurs in the filler network, especially during yielding. There is considerable bond scission in the first network in the necking areas. What is the role of the matrix networks which are unstretched and how do the stress transfers into the second or other networks in this process? These are still open questions and few people have so far addressed these topics.

In this chapter, we explore by mechanochemistry the deformation of the second network during the fracture process of multiple networks elastomers. SP, our mechanophore cross-linker, was incorporated into the second and the third networks of QNs, respectively. Performing extension tests with these QNs, where SP was incorporated only into the second network, a color change could be observed in the necked area where large proportions of the first network was damaged. The color change confirmed that significant stress was transferred to the second network resulting in a large deformation during yielding. However, due to the labile H on the alpha position of acrylate monomers, chain-transfer reaction occurred during the polymerization of the synthesis of the DN. This resulted in some level of crosslinking between the first and the second networks. To avoid the effect of these crosslinks due to transfer to the chain, ethyl acrylate monomers of the filler network were replaced by hexyl methacrylate (HMA) monomers. Then TNs and QNs were prepared from this filler network. Performing elongation tests, yielding was observed in the TNs and the QNs and the interesting thing was that they did not present the color change in the necking area during yielding until the elastomer displayed a second strain hardening. This verifies that the transmission of stress from the filler network to the second network was delayed when the level of intra network crosslinking was limited. Additionally, the second strain hardening is due to the limiting extensibility of the second network.

In a second stage, the contribution of the second network to the resistance to crack propagation was studied. Color change was not observed near the crack tip with a naked eye in fracture tests of QNs. It is probably due to the low concentration of the active SP around the crack tip. When using the fluorescent signal of MC to detect the stress with a fluorescence microscope, a small fluorescent region was observed in front of the crack tip in ethyl acrylate based TNs and QNs and in hexyl methacrylate based QNs with limited intranetwork crosslinks. It suggested that the second network was active in resisting crack propagation. These results offered insight in the fracture mechanism of multiple networks at the molecular level.

This chapter will be presented in an article format.

Introduction

Elastomers are widely used as industrial materials because of their high level of reversible deformation and high fracture toughness. A frequently used strategy to improve the fracture toughness while maintaining a high elasticity is to incorporate nanofillers[1-6], including carbon black[7,8], silica[9,10], graphene[11-13] and carbon nanotubes[14]. However, it is still a challenge to prepare tough unfilled elastomers. In order to reinforce unfilled elastomers lots of strategies have been proposed to incorporate sacrificial covalent[15-17] or non-covalent bonds[18-25] in the bulk of the materials, for instance, super-molecular interaction motifs[18,19,24-28]. When these moieties are loaded, the bond scission is able to dissipate energy and delays the nucleation of cracks. This allows for the extensibility and fracture toughness to increase simultaneously.

Recently, tough elastomers prepared by interpenetrating multiple networks were reported by our group[29,30], through an approach previously applied in hydrogels by Gong[15,31,32]. In the multiple networks, the filler network with dense cross-linkers acts as a continuous filler. Covalent bonds in the filler network are regarded as sacrificial bonds and rupture to dissipate energy during loading, which substantially improves the deformation and toughness. However, owing to the lack of molecular model for the fracture of multiple networks, it still a challenge to completely comprehend the fracture mechanism of multiple network at the molecular scale.

Mechanochemistry is an effective tool to detect the deformation and fracture in elastomers. It converts mechanical stimuli into other observable signals in polymer materials including luminescence, fluorescence, color change, etc. Mechanophores are force-sensitive molecules found in mechanochemistry. Spiropyran (SP), a classic mechanochromic mechanophore, has attracted lots of attention due to its distinct change in optical properties (from colorless to blue or purple) and fluorescent signal after activation by a mechanical force. Active SP becomes merocyanine (MC) and polyacrylates networks turn blue during loading and purple during unloading. SP has been used as molecular probe to sense the stress and show the damage inside the materials by many groups including Moore[33-36], Craig[37-40] and Weng[26,27,41,42].

In our previous work, mechanophores (dioxetane or SP) have been incorporated into the first network and the materials show fascinating optical responses (luminescence or color change) upon deformation in uniaxial extension. These mechanically triggered optical responses demonstrate that the filler network sustains the main stress in the multiple networks and is substantially damaged with increasing stress prior to the yielding of multiple network elastomers. In addition, the yielding (or necking) process initiated by large amount of breakage of the first network does not lead to the eventual failure of the materials, i.e. the propagation of a macroscopic crack. In this process the transmission of the stress from filler network to matrix networks plays a critical role for the toughening of these interpenetrated multiple networks. Therefore, how and when the stress is transferred from the filler network

to the other networks is an important topic for the understanding of the fracture mechanisms of tough interpenetrating multiple networks elastomers.

Yet, few groups have focused on the role of the second network in multiple networks elastomers, especially, when large fractions of the first network rupture leading to a macroscopic necking phenomenon. Furthermore, when a notch is made on the sample the bond breakage in the filler network dissipates energy and forms a damage zone. The shape of the stress field in the damage zone is still an open question.

In this work, SP was incorporated in the first, but also into the second and third networks as a molecular sensor to measure their mechanical behavior before and after yielding and detect the stress transmission between the first and the second/third networks. To avoid the influence of the cross-linker between the first and other networks due to the chain transfer reaction, poly(ethyl acrylate) of the filler network was replaced by poly(hexyl methacrylate). In addition, in fracture tests the roles of the second and the third networks are explored by using the fluorescent signal of MC when part of filler network is damaged to dissipate energy around the crack tip.

2. Results

2.1. Mechanical properties of multiple network elastomers

Table 5.1. Labelled and unlabelled families of multiple network elastomers

Family	**SN**	**DN**	**TN**	**QN**
1	EA0.5-0(1)	EA0.5-0(1.62)EA	EA0.5-0(2.4)EA	EA0.5-0(3.1)EA
2	EA0.5-0(1)	EA0.2-0.05(1.70)EA1	EA0.2-0.05(2.61)EA1	EA0.2-0.05(3.49)EA1
3	EA0.5-0(1)	EA 0.5-0(1.60)EA2	EA0.5-0(2.34)EA2	EA0.5-0(2.98)EA2
4	EA0.5-0(1)	EA0.5-0(1.56)EA	EA0.5-0(2.34)EA3	EA0.5-0(2.76)EA3
5	HMA0.5-0(1)	HMA0.5-0(1.71)EA2	HMA0.5-0(2.85)EA2	HMA0.5-0(3.84)EA2

Four families of multiple interpenetrated network elastomers have been synthesized according to the procedure published by Ducrot[30] as described in the experimental section. Their components are shown in Table 5.1, where samples are identified as Ax-y(z)Bn, with ‘A’ and ‘B’ as the monomer of the first and second/third/fourth networks, ‘x’ the cross-linker density in the first network, ‘y’ the SP concentration in the first network, ’z’ the pre-stretch (λ_0) in the filler network, ‘n’ the position of SP in the multiple networks, including the second and third networks. Ethyl acrylate (EA) and hexyl methacrylate (HMA) are used to prepare the first network and EA is the only monomer used in second/third/fourth network. SP is used as the cross-linker of either the second or third network.

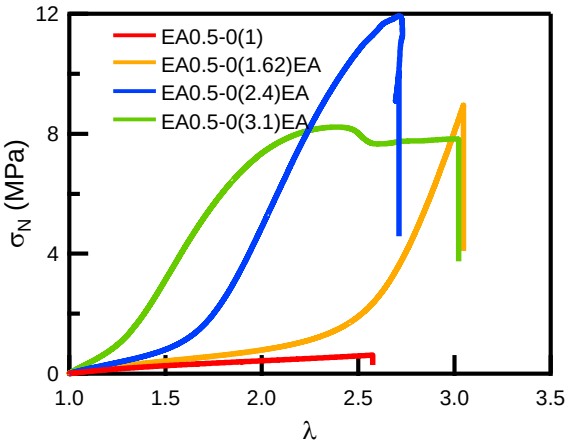

Figure 5.1: Stress-strain curves of the first family of multiple network elastomers

Within a family, varying the number of networks results in striking differences in mechanical properties, as described by Ducrot[29,30]. The single networks (SN) are brittle, however, as the number of polymer networks increases so do the Young's modulus, the stress at break and the toughness (integral under the stress strain curve) as shown in Table 5.2. Double networks (DN), triple networks (TN) and quadruple networks (QN) all present strain hardening. TN and QN show a softening part at high strain, but QN also experience yielding and necking at higher strains as shown in Figure 5.1.

Table 5.2 : The mechanical properties of the first family of materials without SP

Polymers	EA0.5-0(1)	EA0.5-0(1.62)EA	EA0.5-0(2.4)EA	EA0.5-0(3.1)EA
Young's modulus / MPa	0.68	1.03	1.5	3.5
Stress at break / MPa	0.62	8.93	11.5	7.82
λ at break	2.60	3.05	2.58	3.02

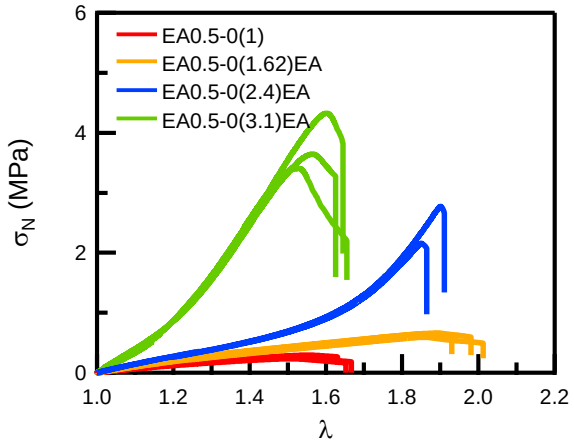

Figure 5.2: Stress-strain curves of the first family materials with a notch on one edge

The fracture energy Γ of multiple network elastomers is measured by performing fracture tests on the first family of materials. Figure 5.2 shows the distinct improvement in fracture toughness (Γ) as the number of networks increases. Fracture toughness is calculated by applying Equation 1:

$$\Gamma = 2C \times W(\lambda_C) \times a \quad \text{Equation 1}$$

$$C = \frac{3}{\sqrt{\lambda_C}} \quad \text{Equation 2}$$

Where $W(\lambda_C)$ is the strain energy density at the critical stretch $\lambda_C$of crack propagation in an un-notched sample. '*a*' is the length of the notch and '*C*' is a strain dependent empirical correction and can be calculated by Equation 2.

The results are shown in Table 5.33. It is obvious that the fracture toughness increases and the Young's modulus improves at the same time.

Table 5.3. Fracture energy (Γ) of multiple network elastomers

Polymer	EA0.5-0(1)	EA0.5-0(1.62)EA	EA0.5-0(2.4)EA	EA0.5-0(3.1)EA
Fracture energy (Γ) $kJ \cdot m^{-2}$	0.40 ±0.02	1.43 ±0.04	3.76 ±0.48	4.11 ±0.64
Young's modulus/MPa	0.69	1.08	1.52	3.38

The enhancement of the mechanical properties of the multiple networks as described above is attributed to the presence of a pre-stretched first network. The damage in the first network dissipates energy and delays crack propagation. In the QNs the stress transfer occurring from the filler network to the matrix networks needs to be addressed, especially in the necking region where there is a high fraction of scission of the first network.

2.2. Mechanical response in uniaxial extension

The strain hardening in unfilled elastomers typically occurs in response to the limiting extensibility of the chains composing the network[43]. Thus the softening behavior observed at high strain for high prestretch of the filler network probably corresponds to the beginning of the damage of the filler network after the strain hardening has occurred. This was confirmed directly with mechanoluminescence experiments by Millereau et al[44]. However the Dioxetane mechanophore does only report the bond scission and was incorporated only in the filler network. It would be very useful to have informations on the transfer of stress in between networks.

To do this, three families of materials in which SP is used as a cross-linker in the first, second or third network were synthesized and tested in uniaxial tension. For reproducibility, nearly the same single network was used to prepare all three families of materials and the same cross-linking density was used in the second, third and fourth networks. As a result for the second/third family the incorporation of SP did not generate significant differences in mechanical properties compared to the unlabeled family. According to the literature[45-47] the force to activate SP is lower than that to break carbon-carbon bonds in the main polymer

chains. That means the activation of SP occurs before the scission of the polymer chains. Therefore, a color change is the sign of a high stress in polymer chains.

According to the results of Millereau [48], when the pre-stretch increases to a high level ($\lambda_0 \sim 3$), at a high stress the materials undergoes a necking phenomenon after yielding due to a high proportion of damage in the filler network as shown in

Figure 5.3. The yielding takes place at the stretch ratio λ_1 and then some regions of the sample become thin in the direction of width and thickness and elongate in the tensile direction: this is called necking phenomenon and is often observed in the (irreversible) plasticity of polyolefins like polyethylene. Accompanying the necking phenomenon, the nominal stress of the material becomes roughly constant as shown in

Figure 5.3. At this stage the material does no longer deform homogeneously but separates into two regions. At that stage, the same tensile force (and hence nominal stress) applies on the Centre of the sample on the necked and un-necked areas. But comparing to the un-necked areas, necking areas have a higher deformation and that deformation is constant during the necking process, less thickness and areal chains density of the filler network due to the damage. It suggests the polymer chains in the necked area should undergo a larger true stress (force divided by the actual cross-sectional area). If the larger true stress was only sustained by the filler network it would lead to more damage and the sample would fail. But the sample did not, which means part of the stress was transferred into other networks.

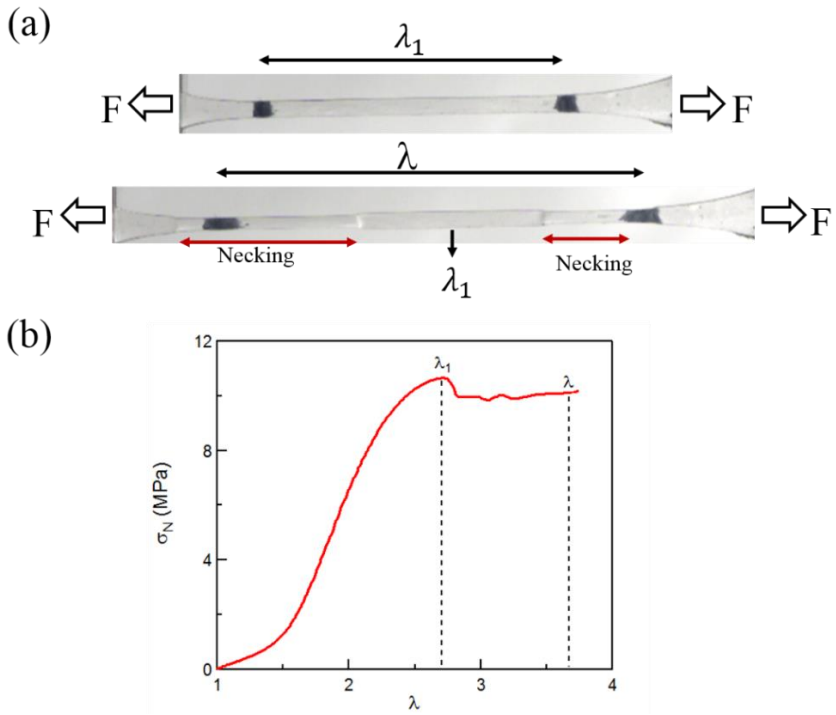

Figure 5.3 : (a) Images of EA0.5-0(2.76)EA3 sample are extracted from the uniaxial extension during the yielding and necking. (b) The stress-strain curve of EA0.5-0(2.76)EA3 sample in uniaxial tensile test.

When the SP is located in the filler network, SP can sense the variation of stress during necking. Additionally, according to the literature[38,41,45], MC, the active SP, should in principle show a secondary color change (blue to purple) if it is in its relaxed state due to the filler network damage. From Figure 5.4 (a) at the necking area a slight purple color is observed at $\lambda_{correct}$=10 and 10.6 and this signal is also detected from the result of color analysis as shown in Figure 5.4 (b). For the un-necking area chromatic change is constant due to the plateau of stress during necking. In the necking area red ratio (blue ratio) increases (decreases) during necking and it is consistent with the unloading process. But it can not eliminate the variation is attributed to the effect of thickness which dramatically change at the necking area. According to the result of chapter 3, the decrease of thickness of sample results in the decrease of the blue ratio and the increase of red and green ratios. However, the green ratio at the necking area decreases. Thus it confirms the color change at the necking area is due to damage of the filler network resulting in the relaxation of part of the filler network. But there is still a high fraction of blue composition at the necking area, which means the filler network does not completely relax. The optical response of SP at the necking area illustrates the filler network does not completely damage and still sustain lots of stress.

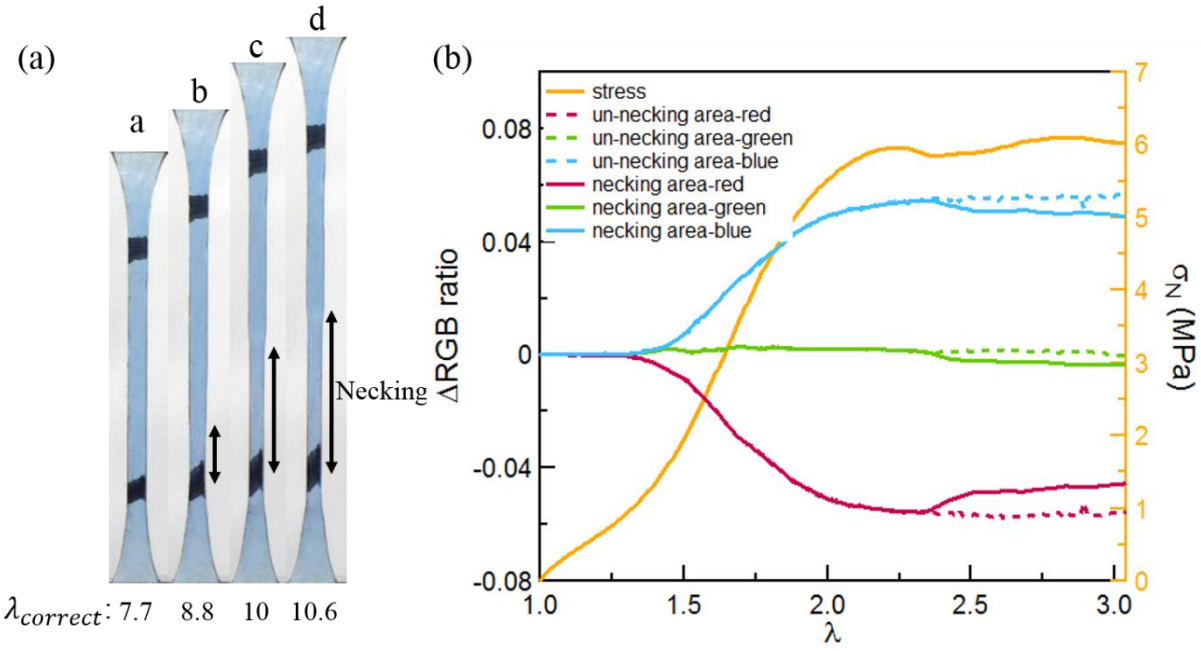

Figure 5.4 : (a) Image of EA0.2-0.05(3.49)EA sample at different $\lambda_{correct}$ is extracted from the video of uniaxial tensile test. (b) Chromatic change and stress as a function of the corrected strain is plotted. The dots line and solids line respectively represent the color analysis focusing on the un-necking and necking areas after necking.

The result of Figure 5.4 for the EA0.2-0.05(3.49)EA material shows that the filler network still sustains some stress in the necked areas, but part of the stress is also carried by the other networks. To quantify the transfer of stress in the multiple network materials, EA0.5-1(2.98)EA2 and EA0.5-1(2.76)EA3 materials, containg SP in the second and third network respectively were tested in uniaxial extension. Figure 5.5 shows that a color change takes

place only in the necked area after yielding for the EA0.5-0(2.98)EA2 materials. On the contrary, in the EA0.5-0(2.76)EA3 materials no color change is observed during the whole extension despite the occurrence of a necked area, as shown in Figure 5.5 (b). The phenomenon above illustrates that, once the filler network starts to fails the partially stretched second network becomes fully stretched and sustains at least an average force per strand of the order of 240 pN. Yet the load supported by the third network is still low (no color) and the broken bits of the filler network are still loaded in the necked area.

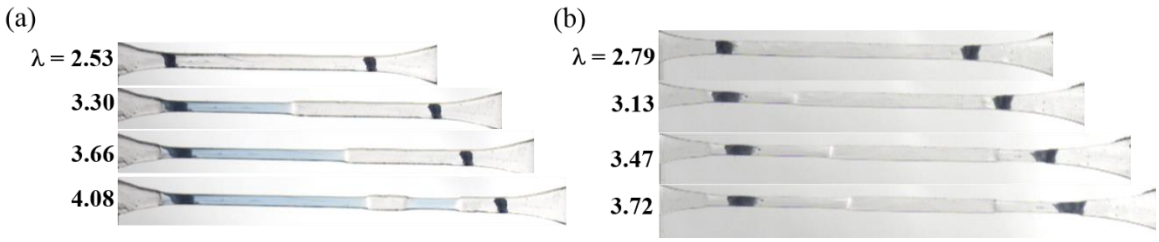

Figure 5.5: SP cross-linker incorporated into the second or third network. The images of (a) EA0.5-0(2.98)EA2 (b) EA0.5-0(2.76)EA3samples in uniaxial tensile tests.

3. Discussion

While a color change shows that a high stress is carried by the chains of the relevant network containing SP during necking, the interesting thing is to discuss in more detail how the stress is transferred to the second network and what is the role played by the second network to improve the resistance to crack propagation.

3.1 Influence of the SP position in multiple networks

Comparing the stress-strain curves of EA0.5-0(2.98)EA2 and EA0.5-0(2.76)EA3 in Figure 5.6 (a), they have qualitatively the same mechanical behavior but the yield stress is a little different. It is attributed to the slightly lower pre-stretch of the first network in EA0.5-0(2.76)EA3 compared to EA0.5-0(2.98)EA2 samples. But after the respective correction of stress and strain by the areal chain density and pre-stretch of the filler network, stress-strain curves of EA0.5-0(2.98)EA2 and EA0.5-0(2.76)EA3 almost overlap with each other as shown in Figure 5.6 (b). The yield stress of EA0.2-0.05(3.49)EA1 is lower due to the lower areal density of chains of the filler network compared to the other two samples. The lower crosslinker density leads to a longer polymer chains between crosslinkers and a lower areal chain density of the filler network in EA0.2-0.05(3.49)EA1. Finally, the lower areal chain density results in the lower yielding stress.

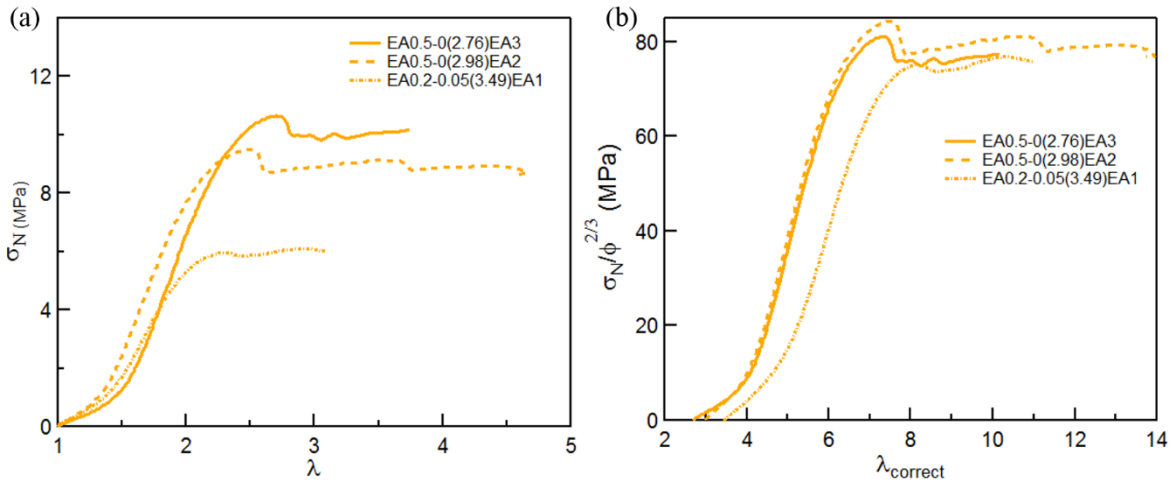

Figure 5.6 (a) Stress-strain curves of EA0.5-0(2.98)EA2, EA0.5-0(2.76)EA3 and EA0.5-0.05(3.49)EA1; (b) After the correction of areal chain density and pre-stretch of filler network, corrected tress as a function of the corrected strain in the filler network for the three samples

To quantify the color change in the necking area for the materials containing SP in the different networks, color analysis was used, as shown in Figure 5.7. From chapter 3, the magnitude of the chromatic change is proportional to the concentration of SP activated into MC. Note that the color analysis is able to detect color changes which are not visible to the naked eye. Figure 5.7 shows the optical response of three samples of EA0.2-0.05(3.49)EA1, EA0.5-0(2.98)EA2 and EA0.5-0(2.76)EA3. In Figure 5.7, SP1, SP2 and SP3 represent the materials of EA0.2-0.05(3.49)EA1, EA0.5-0(2.98)EA2 and EA0.5-0(2.76)EA3,where SP was incorporated only in the first, second or third network, respectively. The three categories of materials show a completely different optical response. EA0.2-0.05(3.49)EA1 changes color first as SP is located in the filler network and the filler network sustains the main stress in the multiple network before yielding. For EA0.5-0(2.98)EA2 the color rapidly changes at the onset of necking. Then in this necked area a plateau appears, where the MC concentration does not seem to change. For the sample EA0.5-0(2.76)EA3 which contains SP as a crosslinker in the third network, there is no detectable color change associated with necking. Comparing the three chromatic change curves, shows that the stress is mainly sustained by the first network in the beginning of the extension and then starts to transfer to the second network just before yielding. This results indicate that a sufficiently high stress exists in the second network to activate SP. Most of the stress is still sustained by the first network at the un-necked regions, however in the necked area, part of the stress has been transferred to the second network. Furthermore, although significant damage to the first network occurs in the necked area, the third network is not stretched to the point of activating the SP crosslinker.

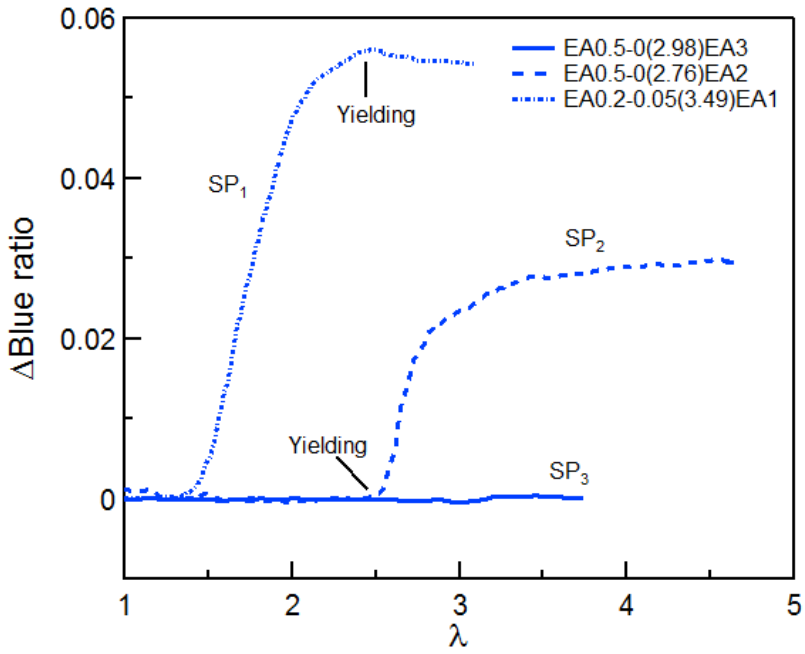

Figure 5.7 : Chromatic change (blue ratio) as a function of strain for quadruple networks with a different labelling: EA0.2-0.05(3.49)EA1, EA0.5-0(2.98)EA2 and EA0.5-0(2.76)EA3.

3.2. The effect of the connectivity between the first and the second network

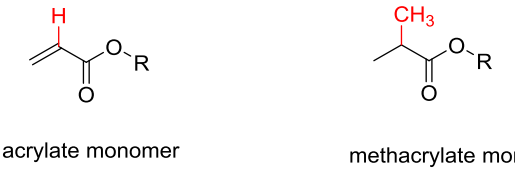

acrylate monomer methacrylate monomer

Figure 5.8: The molecular structure of acrylate an methacrylate monomers

In double network hydrogels, Gong demonstrated that the mechanical properties[49] were significantly affected by the existence of cross-links between the two networks. In multiple network elastomers, chain transfer reactions[50] occur easily during the polymerization of the second network, because of the labile hydrogen in the alpha position of the acrylate monomers, as shown in Figure 5.8. It gives rise to the crosslinking between the first and the second networks.

To avoid this type of side reaction, acrylate monomers of the first network can be replaced by methacrylate monomers. Figure 5.9 and Figure 5.10 show the color change and stress-strain curves of two HMA0.5-0(3.84)EA2 samples during elongation tests which both contain SP in the second poly(ethyl acrylate) network. Examining the mechanical properties and comparing with the QNs in other families of materials, HMA0.5-0(3.84)EA2 has a much lower Young's modulus and yield stress despite a higher pre-stretch. According to the literature[29,48], the lower initial modulus and yield stress is due to the lower crosslinker density and areal density of

chain. In order to obtain similar mechanical properties (Young's modulus) and areal density of the single networks made from varying monomers, the key is to control the equivalent molecular weight between the crosslinkers. Due to the higher molecular weight of HMA monomer comparable to EA, at the same molar concentration of cross-linkers the single network comprised of HMA possesses a lower Young's modulus and areal density of chains than EA monomer. In Figure 5.10, one of the samples of HMA0.5-0(3.84)EA2 displayed a second strain hardening at high strain, a very different behavior from that of EA0.5-0(2.98)EA samples. The interesting thing is that the first sample with a second strain hardening phenomenon shows a slight color change after the propagation of the necked area but the second one (where the second strain hardening is not observed) does not as shown in Figure 5.10. Comparing both samples before and after the tensile test, as shown in Figure 5.11, indeed, only the first sample exhibits an obvious color change.

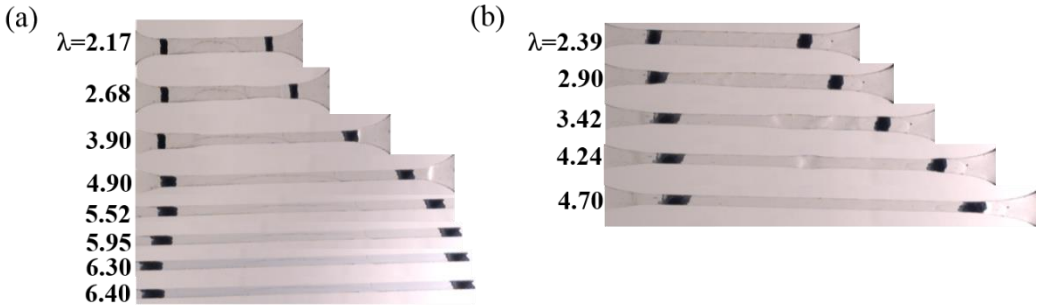

Figure 5.9: The images of two samples of HMA0.5-0(3.84)EA2 in elongation tests

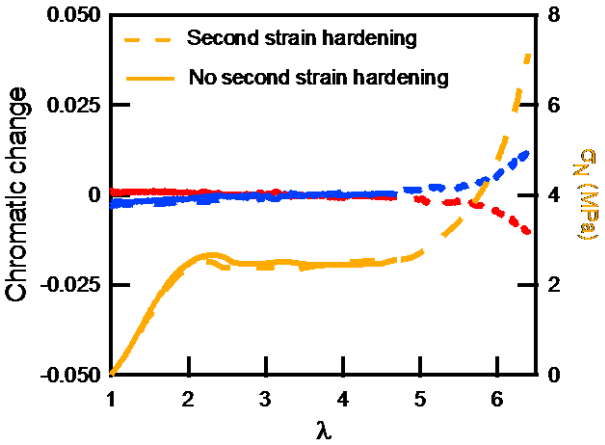

Figure 5.10: Chromatic change curves and stress-strain curves of two HMA0.5-0(3.84)EA2 samples: one sample presents a second strain hardening (dashed line) and another one fails before the second strain hardening.

To clarify the difference between the two samples of HMA0.5-0(3.84)EA2, color analysis is performed. Comparing the chromatic change curves and the stress-strain curves, the first

sample starts to change color at the onset of the second strain hardening, suggesting that the second strain hardening is in response to the maximum extensibility of the second network. Recalling the results of the EA0.5-0(2.98)EA2, the stress is transmitted from the first to the second network at the yielding. When the yielding occurs, the second network EA network is stretched leading to the activation of SP. However, in HMA0.5-0(3.84)EA2 the transfer reactions between the first and the second networks are eliminated making the chains of the second network less closely coupled to the first and hence more stretchable. As a result the activation of SP only occurs when the sample is fully necked and the nominal stress increases again. At this stage the deformation approaches the maximum extensibility of the second network, and a second strain hardening is generated and more SP are activated.

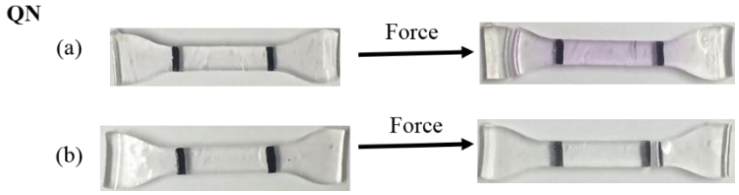

Figure 5.11. Images of two samples of HMA0.5-0(3.84)EA2 with different degrees of yielding before and after elongation tests

2.3. Stress transfer to the matrix network during the crack propagation process

When the SP is incorporated in the filler network, observations of the crack tip clearly reveal a zone of high stress over distances of the order of mm. This was discussed in chapter 4. Yet when we incorporate SP in the matrix networks (second or third), the change in color can only occur when the first network is severely damaged and sufficient stress is transferred to the matrix as discussed in the first part of this chapter. It is interesting to check whether this change in color can be detected at the tip of the crack since this can be a way to detect severe damage (equivalent to yielding). Note that mechanophores detecting chain scission cannot distinguish between chain scission before yielding or after yielding.

To explore the role played by the second network in the improvement of the fracture toughness of multiple networks, fracture tests were carried out on an EA0.5-0(2.98)EA2 sample. A color change was not observed in front of the crack tip prior to or after propagation as shown in Figure 5.12. According to the Lake-Thomas theory, when a crack propagates at least all the covalent bonds across the plane of the crack should be broken. This suggests that some color change should appear on both sides of the crack. Therefore the lack of color change is probably due to the low initial concentration and small fraction of active SP. However it suggests that the extent of full scale yielding taking place at the tip of the crack must be small for these samples.

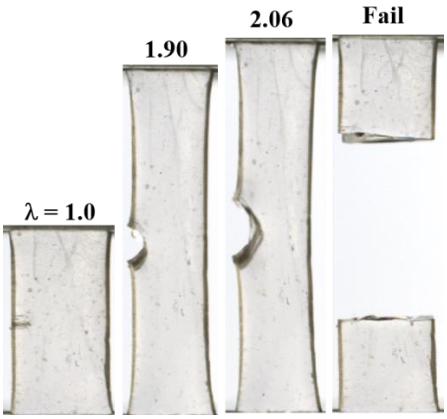

Figure 5.12: Images of an EA0.5-0(2.98)EA2 sample in a fracture test

3.3 Higher magnification detection of the stress in the matrix network

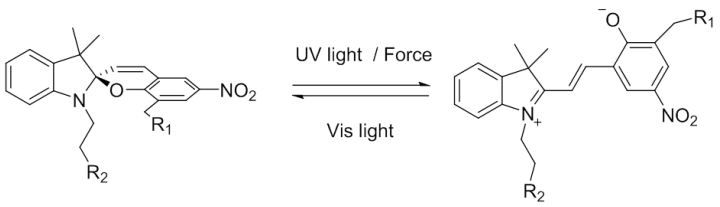

Scheme 5.1 : SP is activated by external stimuli.

Fortunately, when SP converts into MC, the conjugated region in SP molecule significantly increases as shown in Scheme 5.1. SP consists of the two parts of indole and salicylaldehyde. This two parts are in two vertical planes and do not have a conjugation relationship, but after the activation the two parts are twisted to the same plane and the conjugated range extends to the whole molecule because of the formation of the double bond of C=N. Due to the large range of conjugation, the absorption spectrum of SP has a red shift resulting in a fluorescent emission by absorbing visible light (568 or 630 nm). This ability makes it possible to detect a low level of MC in a small area at a higher magnification due to the high sensitivity of the fluorescent spectrum.

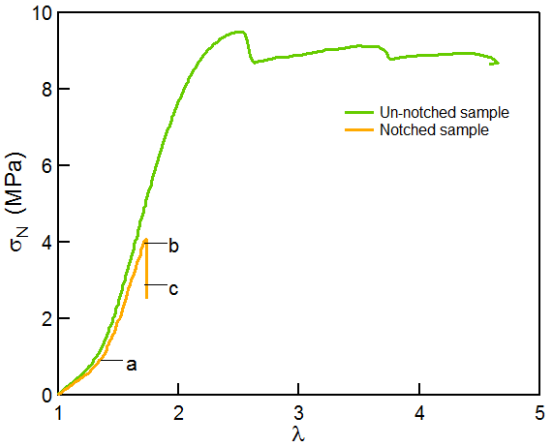

Figure 5.13 The stress-strain curves of EA0.5-0(2.98)EA2 with notched samples and un-notched sample: in the figure ‘a’, ‘b’ and ‘c’ represent the region of low strain, critical strain and propagation in Figure 5.14, respectively.

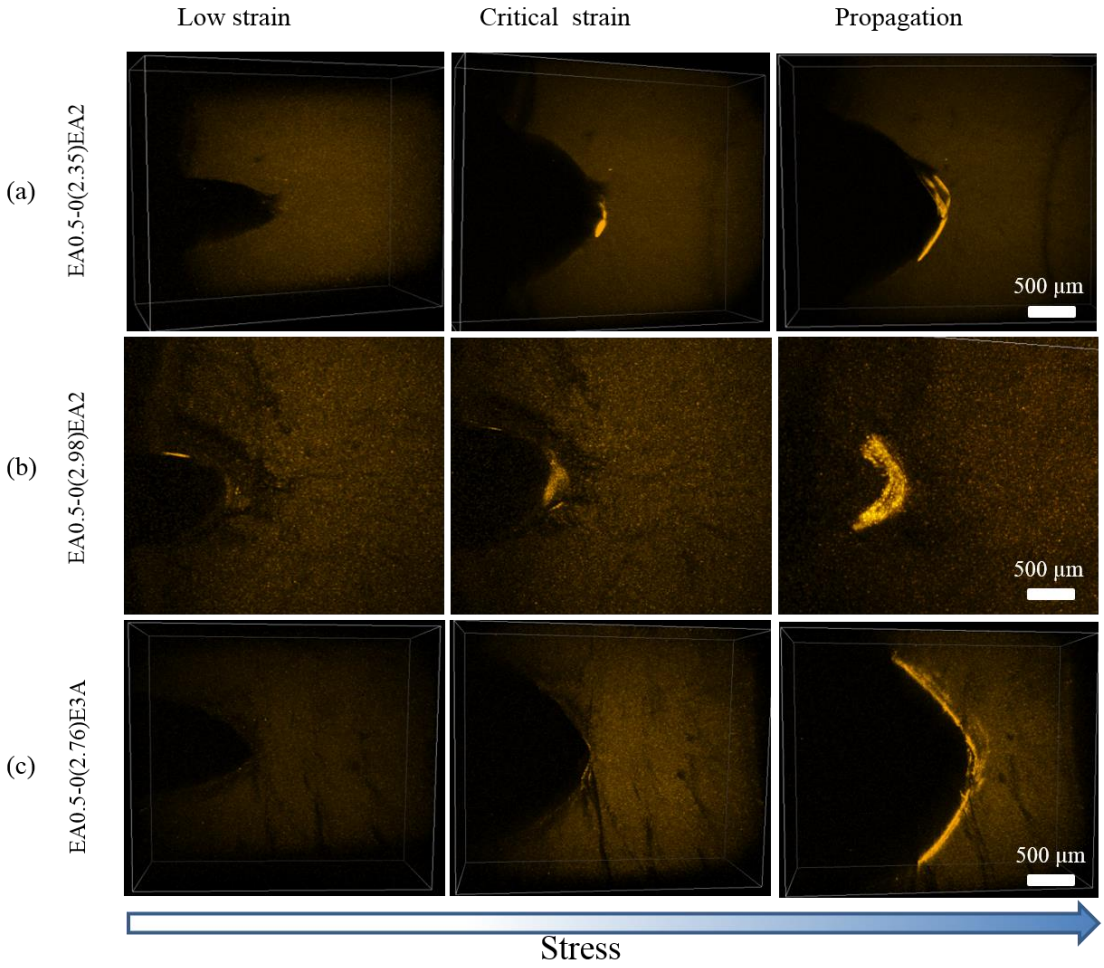

Figure 5.14: Fluorescent images of multiple networks with high prestretch show the fluorescent distribution around the crack tip at low strain, critical strain for propagation and during propagation. (a) EA0.5-0(2.34)EA2, (b) EA0.5-0(2.98)EA2 and(c) EA0.5-0(2.76)EA3

Using the fluorescent signal of MC, the high stress and elongation in the second network can still be detected by fluorescence microscopy. Comparing the fluorescent images extracted from different stretch levels in a fracture test as shown in Figure 5.13 and Figure 5.14, EA0.5-0(2.34)EA2 (Figure 5.144 (a)) and EA0.5-0(2.98)EA2 (Figure 5.144 (b)) both samples show the fluorescent signal in front of the crack tip before propagation. However a fluorescent signal is not observed prior to propagation for the EA0.5-0(2.76)EA3 sample (Figure 5.144 (c)) and MC is detected only when the crack propagates. These interesting results suggest that the failure of the second network triggers crack propagation, at least for this class of materials where some covalent bonds exist between the first and the second networks. It also shows that the third network only carried load just before failing, i.e. during propagation which is consistent with the uniaxial tensile results. Additionally, as seen from the distribution of the fluorescent signal, a larger region of the second network is loaded in the QN (Figure 5.144 (b)) than in the TN (Figure 5.144 (a)).

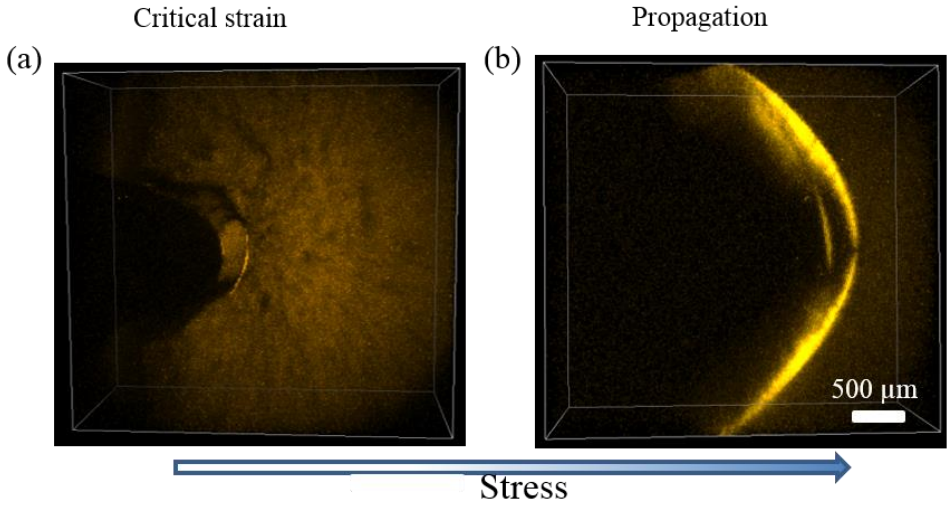

Figure 5.15: The 3D fluorescent images of HMA0.5-0(3.84)EA2 in fracture test

Replacing the filler network of poly(ethyl acrylate) with poly(hexyl methacrylate, the cross-linking between the first network and the second network is avoided. This approach reduces the transmission of stress from the filler network to the second network by the covalent cross-linkers between them. During the fracture test of HMA0.5-0(3.84)EA2, the confocal microscope was used to detect the fluorescent signal in front of the crack tip. An obvious fluorescent signal was observed in a small area very close to the crack tip before crack propagation as shown in Figure 5.155(a). When the crack propagated the area around the fracture emerged brightly fluorescent. This illustrates that, prior to the crack propagation, stress has transferred to the second network only in a small area very close to the crack tip, where there is a large amount of damage of the filler network. The existence of a large fluorescent region upon propagation suggests that the filler network breaks catastrophically in a large region in front of the crack and effectively instantly loads the second network over a significant area. This may contribute to the still relatively high value of the stress and strain at break of this material.

More generally, these results of fluorescence suggest that a small yielded region appears near the crack tip before propagation. While the breakup of the first network dissipates energy the extension of the second network until MC is activated must also dissipate energy[48]. The activation of the second network is actually equivalent to detecting the yielding of the first network.

Conclusion

Five groups of multiple network elastomers have been synthesized and SP was incorporated as a crosslinker into the first, second and third networks, respectively. Based on the temporal and spatial position of the color change in the five families materials, one can propose the following scenario. The stress in general is sustained by the first network in extension. The stress in the first network transfers partially to the second network around the yield point where the second network becomes extended. However, when the connection between the first and the second networks is removed, stress in the first network transfer much less to the second network and the second network is more extensible. In addition, the fluorescence of MC displays the contribution of the second network on the fracture toughness of multiple network elastomers. These results suggests the vital role played by the second network to resist crack propagation and the existence of yield area in fracture tests. To the best of our knowledge, the result is found at the first time in multiple network.

Experimental section

Materials: the monomer, ethyl acrylate (EA), hexyl methacrylate (HMA) and the cross-linker 1, 4-butanediol diacrylate (BDA) purchased from Sigma and were purified by a column of alumina to remove the inhibitor. Spiropyran modified with terminated group of acrylate was synthesized as previously described[26,41]. 2-hydroxy-e-mechylpropiophenone (HMP) was used as UV initiator without purification. Other reagents purchased from Sigma were used as received.

Preparation of the SNs: The rubbery stiff single network was synthesized by free-radical polymerization. The preparation of multiple network elastomers is similar to the previous reports by our group[29,30]. A pre-gel solution mixing monomer (EA or HMA), cross-linkers (BDA, 0.5% respective to monomer) and UV initiator (HMP) was poured in a glass mold. The glass mold is composed of two pieces of glass and a 1mm silicone spacer. The whole setup was fixed by two metal scaffolds with screws. Due to the variation of density during the polymerization, it was easy to form some random surface pattern on the surface of single network due to debonding of the sample from the mold surface. To ensure smooth surfaces of single networks, two thin hydrophobic PET films were placed on the internal surface of the glass mold. Because of the interaction of PET film and single network, PET film always had a good contact with single network in polymerized process. The polymerization was initiated

by UV light (Vilbert Lourmat VL-215.L lamp, 365 nm, 10 μW/cm^2 and conducted 2 hours. All the operation was carried out in a glove box. After polymerization, the single network was taken out of the glove box and was dried in vacuum for one day to remove the unreactive monomers. Then the sample was stored at room temperature in a black box for later use.

Preparation of DNs, TNs and QNs: DNs, TNs and QNs elastomers were prepared by multiple steps of radical polymerization using identical first networks. First, a piece of single network (m_{SN}) was swollen in a solution composed of EA monomer, cross-linker (SP or BDA, 0.01 mol%) and HMP initiator (0.01 mol%). After equilibrium swelling (2 hours), the swollen sample was taken out from the solution and the excess liquid was wiped from the surface. Then the swollen sample was placed in PET sheets and fixed in the mold for photo-polymerization via a two hours UV irradiation. The sample was dried in vacuum for a day and then weighed (m_{DN}).

To increase the pre-stretch in the first network, the same procedure of swelling, polymerization and drying were performed again starting from DNs to synthesize TNs. Finally, QNs were prepared by repeating this procedure for the third time starting from TNs. All the multiple network elastomers are noted as ABspBB, where A refers to the first network monomer and B to the second network monomer. In addition, the number of B stands for the number of polymer networks and 'sp' is the position of SP in the multiple networks. It should be noted that except for the stiff first network other polymer networks were loosely cross-linked and almost unstretched in the multiple network elastomers. Furthermore, due to the chains transfer reaction, loose connection between polymer networks were formed during the second and subsequent polymerization.

Calculation of pre-stretch:

To calculate the pre-stretch in the first network, the weight of multiple network elastomers before and after polymerization was used. The weight fraction of the first network was determined with Eq. (3) and then the pre-stretch can be calculated by the weight fraction of the first network as shown in Eq. (4).

$$\phi_{SN} = \frac{m_{SN}}{m} \qquad \text{Eq. (3)}$$

$$\lambda_0 = \sqrt[3]{\frac{V}{V_0}} = \sqrt[3]{\frac{m}{m_{SN}}} = (\frac{1}{\phi_{SN}})^{\frac{1}{3}} \qquad \text{Eq. (4)}$$

Uniaxial extension tests:

Mechanical tests were carried out on an Instron machine model 5565 with a pair of homemade pneumatic clamps and a 100 N load cell. Samples with a dumbbell shape were punched from the pieces of multiple network elastomers using a normalized cutter (central part: length 200 mm, width: 4 mm). To precisely detect the strain, two black marks were made on the central part of the samples and a camera was set to record the position of the marks in the whole tensile process. The strain was calculated by the displacement of the

marks using Matlab software. Uniaxial tensile tests were performed at a constant velocity of 1 mm s^{-1} and the initial strain rate in the central part of the dumbbell sample was about 0.05 s^{-1}.

Fracture tests:

Fracture tests were performed on the same Instron machine. Samples were cut into a rectangular shape (length: 20 mm, width: 5 mm) by a normal cutter and a notch with a length of around 1 mm was made on one side of the sample. In addition, the initial stretch rate was around 0.05 s-1 and the same camera as described above was set to record the mechanical response around the crack tip during the measurement.

Confocal microscope tests:

Confocal microscope (Nikon AZ100) with a 561 nm laser and a deben micro-tensile stage was used to detect the fluorescent signal around the crack tip in the fracture tests. The same samples in the fracture tests were used here and the tensile velocity was set to 1 mm/min which was limited by the setup of deben. During the fracture test, 3D images around the crack tip were scanned with an interval of 0.5 mm until the failure of samples. Theses 3D images were used to define the deformation of the second network with the fluorescence of MC (the activated state of SP).

Reference:

1. Haraguchi, K.; Song, L.; *Macromolecules* **2007**, *40*, 5526.
2. Liff, S. M.; Kumar, N.; McKinley, G. H.; *Nature materials* **2007**, *6*, 76.
3. Podsiadlo, P.; Kaushik, A. K.; Arruda, E. M.; Waas, A. M.; Shim, B. S.; Xu, J.; Nandivada, H.; Pumplin, B. G.; Lahann, J.; Ramamoorthy, A.; Kotov, N. A.; *science* **2007**, *318*, 80.
4. Amjadi, M.; Pichitpajongkit, A.; Lee, S.; Ryu, S.; Par, I.; *ASC NANO* **2014**, *8*, 5154.
5. Fukasawa, M.; Sakai, T.; Chung, U.-i.; Haraguchi, K.; *Macromolecules* **2010**, *43*, 4370.
6. Wang, X.; Liu, X.; Yuan, H.; Liu, H.; Liu, C.; Li, T.; Yan, C.; Yan, X.; Shen, C.; Guo, Z.; *Materials & Design* **2018**, *139*, 372.
7. KARASEK, L.; SUMITA, M.; *Journal of materials Science* **1996**, *31*, 281.
8. Payne, A. R.; Wheittaker, R. e.; *Rubber Chemistry and Technology* **1971**, *44*, 440.
9. Fröhlich, J.; Niedermeier, W.; Luginsland, H. D.; *Composites Part A: Applied Science and Manufacturing* **2005**, *36*, 449.
10. Yatsuyanagi, F.; Suzuki, N.; Ito, M.; Kaidou, H.; *Polymer* **2001**, *42*, 9523.
11. Ha, H.; Ha, K.; Ellison, C. J.; *Journal of Polymer Science Part B: Polymer Physics* **2017**, *55*, 1406.
12. Li, C.; Shi, G.; *Advanced materials* **2014**, *26*, 3992.
13. Wan, S.; Cheng, Q.; *Advanced Functional Materials* **2017**, *27*, 1703459.
14. Li, H.; Yang, L.; Weng, G.; Xing, W.; Wu, J.; Huang, G.; *Journal of Materials Chemistry A* **2015**, *3*, 22385.
15. Gong, J. P.; Katsuyama, Y.; Kurokawa, T.; Osada, Y.; *Advanced materials* **2003**, *15*, 1155.
16. Clough, J. M.; Creton, C.; Craig, S. L.; Sijbesma, R. P.; *Advanced Functional Materials* **2016**, *26*, 9063.
17. Gostl, R.; Sijbesma, R. P.; *Chemical science* **2016**, *7*, 370.
18. Buerkle, L. E.; Rowan, S. J.; *Chemical Society reviews* **2012**, *41*, 6089.
19. Burattini, S.; Greenland, B. W.; Hayes, W.; Mackay, M. E.; Rowan, S. J.; Colquhoun, H. M.; *Chemistry of Materials* **2011**, *23*, 6.
20. Burnworth, M.; Rowan, S. J.; Weder, C.; *Macromolecules* **2011**, *45*, 126.
21. Liu, J.; Tan, C. S.; Yu, Z.; Lan, Y.; Abell, C.; Scherman, O. A.; *Advanced materials* **2017**, *29*.
22. Liu, Y.; Yu, C.; Jin, H.; Jiang, B.; Zhu, X.; Zhou, Y.; Lu, Z.; Yan, D.; *Journal of the American Chemical Society* **2013**, *135*, 4765.
23. Way, A. E.; Korpusik, A. B.; Dorsey, T. B.; Buerkle, L. E.; von Recum, H. A.; Rowan, S. J.; *Macromolecules* **2014**, *47*, 1810.
24. Yu, G.; Jie, K.; Huang, F.; *Chemical reviews* **2015**, *115*, 7240.
25. Appel, W. P. J.; Portale, G.; Wisse, E.; Dankers, P. Y. W.; Meijer, E. W.; *Macromolecules* **2011**, *44*, 6776.
26. Chen, Y.; Zhang, H.; Fang, X.; Lin, Y.; Xu, Y.; Weng, W.; *ACS Macro Letters* **2014**, *3*, 141.
27. Fang, X.; Zhang, H.; Chen, Y.; Lin, Y.; Xu, Y.; Weng, W.; *Macromolecules* **2013**, *46*, 6566.
28. Kushner, A. M.; Vossler, J. D.; Williams, G. A.; Guan, Z. B.; *Journal of the American Chemical Society* **2009**, *131*, 8766.
29. Ducrot, E.; Creton, C.; *Advanced Functional Materials* **2016**, *26*, 2482.
30. Etienne, D.; Yulan, C.; Markus, B.; Rint, P. S.; Costantino, C.; *science* **2014**, *344*, 4.
31. Gong, J. P.; *Soft Matter* **2010**, *6*, 2583.
32. Gong, J. P.; *Science* **2014**, *344*, 161.

33. Beiermann, B. A.; Kramer, S. L. B.; May, P. A.; Moore, J. S.; White, S. R.; Sottos, N. R.; *Advanced Functional Materials* **2014**, *24*, 1529.
34. Celestine, A.-D. N.; Beiermann, B. A.; May, P. A.; Moore, J. S.; Sottos, N. R.; White, S. R.; *Polymer* **2014**, *55*, 4164.
35. Grady, M. E.; Beiermann, B. A.; Moore, J. S.; Sottos, N. R.; *ACS applied materials & interfaces* **2014**, *6*, 5350.
36. Lee, C. K.; Diesendruck, C. E.; Lu, E.; Pickett, A. N.; May, P. A.; Moore, J. S.; Braun, P. V.; *Macromolecules* **2014**, *47*, 2690.
37. Gossweiler, G. R.; Brown, C. L.; Hewage, G. B.; Sapiro-Gheiler, E.; Trautman, W. J.; Welshofer, G. W.; Craig, S. L.; *ACS applied materials & interfaces* **2015**, *7*, 22431.
38. Gossweiler, G. R.; Hewage, G. B.; Soriano, G.; Wang, Q.; Welshofer, G. W.; Zhao, X.; Craig, S. L.; *ACS Macro Letters* **2014**, *3*, 216.
39. Wang, Q.; Gossweiler, G. R.; Craig, S. L.; Zhao, X.; *Nature communications* **2014**, *5*, 4899.
40. Wang, Q.; Gossweiler, G. R.; Craig, S. L.; Zhao, X.; *J. Mech. Phys. Solids* **2015**, *82*, 320.
41. Zhang, H.; Chen, Y.; Lin, Y.; Fang, X.; Xu, Y.; Ruan, Y.; Weng, W.; *Macromolecules* **2014**, *47*, 6783.
42. Jiang, S.; Zhang, L.; Xie, T.; Lin, Y.; Zhang, H.; Xu, Y.; Weng, W.; Dai, L.; *ACS Macro Letters* **2013**, *2*, 705.
43. G., T. L. R.; *Rep. Prog. Phys.* **1973**, *36*, 755.
44. Pierre, M.; Ducrot, E.; Clough, J.; Wiseman, M.; Hugh, R. B.; Rint, P. S.; Creton, C.; *PNAS* **2018**, *in revision*.
45. Gossweiler, G. R.; Kouznetsova, T. B.; Craig, S. L.; *Journal of the American Chemical Society* **2015**, *137*, 6148.
46. Mohammadi, N.; Klein, A.; Sperling, L. H.; *Macromolecules* **1993**, *26*, 1019.
47. Davis, D. A.; Hamilton, A.; Yang, J.; Cremar, L. D.; Van Gough, D.; Potisek, S. L.; Ong, M. T.; Braun, P. V.; Martinez, T. J.; White, S. R.; Moore, J. S.; Sottos, N. R.; *Nature* **2009**, *459*, 68.
48. Pierre, M.; *Université Pierre et Maire Curie: Paris* **2017**.
49. Nakajima, T.; Furukawa, H.; Tanaka, Y.; Kurokawa, T.; Osada, Y.; Gong, J. P.; *Macromolecules* **2009**, *42*, 2184.
50. Mayo, F. R.; *Journal of the American Chemical Society* **1943**, *65*, 2324.

Chapter 6: Construction of the strain field around the crack tip

Introduction

One of the main goals of this thesis is to measure the stress and strain distribution inside multiple network elastomers near crack tips. In chapter 3 we demonstrated that the SP mechanophore can be used as a good stress sensor as the transition to merocyanine occurs when the stress attains a critical value. However, in order to determine the stress-strain relationship which depend on the deformation rate and on the history of loading, one needs to measure separately the strain field and it is interesting to use direct methods of strain mapping. Inspired by the particle tracking experimental method of Hui and Long[1] which is in principle well adapted for large displacements and deformations, we formulated multiple network elastomers containing dispersed fluorescent beads and detected the relative position of these fluorescent particles by confocal laser scanning microscopy during fracture tests. Then, in a collaboration with Professor Rong Long and Qi Yuan from Colorado University, we reconstructed the strain field by analyzing the relative displacement of fluorescent beads while the crack opens (before propagation).

In this chapter, we first present the synthesis of multiple network elastomers containing various concentrations of fluorescent beads. Next, these materials were used to perform tensile and fracture tests. The distribution of fluorescent beads in the samples is characterized by taking confocal microscope images at different crack opening displacements. These images were treated by Qi who calculated the bead displacements as a function of macorcopic displacement and reconstructed the strain distribution near the crack tip. The preliminary results are shown at the end of the chapter.

1. Synthesis of multiple network elastomers containing fluorescent beads

1.1 The choice of fluorescent beads

The choice of fluorescent beads is of primary importance for the precise measurement of the strain field. If the particles are too small (submicron sizes), then the measurement is limited by the optical resolution of the microscope. However, too large beads limit the resolution of the strain field detection. In addition, the stability of the fluorescent beads suspension in the monomer mixture will determine the homogeneity of its dispersion in multiple network elastomers. Finally, when working with fluorescent mechanophores, the excitation and emission of fluorescent beads should ideally be chosen to avoid the overlap with the excitation band of SP (490 nm) and the emission band of MC (around 620 nm). This will in principle make it possible to determine simultaneously the stress field by the intensity of MC fluorescence and the strain field with the displacement of the fluorescence beads in an analogous way to what biologists do with multiple fluorescent markers into one material.

Silica particles with a size of 3 μm and a green fluorescence emission were purchased from Micromod company (42-17-303). These silica particles possess a uniform size and spherical shape. The excitation and emission bands of fluorescent silica particles are centered at 480 and 510 nm, respectively. Moreover, the surface of the silica particles is modified with a tetramethyl silane group which makes their suspension stable in organic solvents. This helps to disperse the silica particle homogeneously in the pre-gel solution before polymerization. Thus, the parameters of these silica particles satisfy our requirements of the size, fluorescent band position and intensity, stability in organic solvents.

1.2 Synthesis of elastomers

The preparation method of multiple networks containing fluorescent beads was similar to that without beads described in Chapter 2. We adopted the same mold and applied similar synthesis condition, but only BDA cross-linker was used in the synthesis. In order to make a homogenous pre-gel solution, ultrasound was applied to promote the dispersion of fluorescent beads after mixing with the monomer solution. After 1 min of ultrasonic treatment, the solution was poured into the mold and submitted to photo-polymerization during 2 hours. The simple network samples were dried under vacuum for one day and next swollen to prepare double and triple networks (DNs and TNs). Because the quantity of fluorescent beads in the samples does not change during the swelling step, the concentration of the beads was gradually reduced from SNs to TNs. To prepare DNs and TNs with suitable concentration of fluorescent beads, we varied the mass of silica particles in the monomer mixture which was

used for synthesis of single networks. These single networks containing concentrated silica particles suspensions were used to prepare DNs and TNs. All the samples are listed in Table 1. The name of the samples has the form Ax-y(z)B, where A and B are the monomers composing the first and the second/third network; x, y and z are the cross-linking density, the weight percent of silica particles in the sample and the pre-stretch of the first network, respectively.

Table 1: Composition of multiple network elastomers containing various concentration of fluorescent beads

Sample name	First network	Fraction of SN/wt%	λ_0	Concentration of silica particle/wt%
EA0.5-0.26(1)	EA0.5-0.26(1)	100	1.0	0.26
EA0.5-0.26(1.60)EA	EA0.5-0.26(1)	24.3	1.60	0.26
EA0.5-0.26(2.23)EA	EA0.5-0.26(1)	8.99	2.23	0.26
EA0.5-0.11(1)	EA0.5-0.11(1)	100	1.0	0.11
EA0.5-0.11(1.61)EA	EA0.5-0.11(1)	24.1	1.61	0.11
EA0.5-0.11(2.39)EA	EA0.5-0.11(1)	7.35	2.39	0.11
EA0.5-0.07(1)	EA0.5-0.07(1)	100	1.0	0.07
EA0.5-0.07(1.61)EA	EA0.5-0.07(1)	23.9	1.61	.0.07
EA0.5-0.03(1)	EA0.5-0.03(1)	100	1.0	0.03
EA0.5-0.03(1.60)EA	EA0.5-0.03(1)	24.5	1.60	0.03
EA0.5-0.02(1)	EA0.5-0.02(1)	100	1.0	0.02
EA0.5-0 (1)	EA0.5-0(1)	100	1.0	0
EA0.5-0(1.62)EA	EA0.5-0(1)	23.5	1.62	0
EA0.5-0(2.4)EA	EA0.5-0(1)	7.23	2.4	0

Figure 5.1 shows a typical green fluorescence image of silica particles in a DN under the confocal microscope (Nikon AZ100) with excitation at 480 nm and emission band from 500 to 540 nm. The different size and intensity of the fluorescent spots in Figure 5.1 are due to the different location of the fluorescent beads with respect to the focal plane. It shows a homogeneous distribution of fluorescent beads in multiple networks.

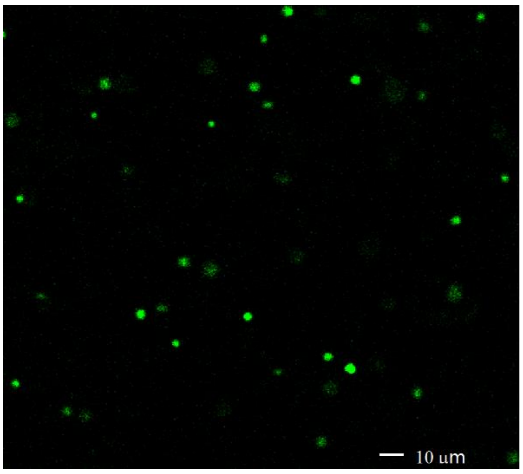

Figure 5.1: Image of silica particles with green fluorescence in a sample of EA0.5-1(0.02)

2. Characterization of elastomers

2.1 The effect of fluorescent beads on mechanical properties

In the first chapter, we mentioned that in nano-composites the presence of nano-fillers reinforces the rubber. Here, we disperse fluorescent silica beads in the multiple networks. Even though the concentration of silica particles is rather low, it could affect the mechanical properties of multiple network elastomers. To check if this effect is present, tensile tests were carried out for all elastomers containing silica beads. The stress-strain curves were compared with the blank samples without beads.

These curves presented in Figure 5.2 illustrate that the incorporation of silica beads does not affect the Young's modulus of multiple network elastomers comparing with the blank samples without fluorescent particles (synthesis in chapter 5). However, we observed a remarkable variation of transparency during the tensile tests of DNs and TNs containing fluorescent beads except for EA0.5-0.03(1.6)EA, which contained the lowest concentration of silica particles. Transparent samples became homogeneously opaque at high level of stress as shown in Figure 5.2 (d). According to the conclusion of Binhu[2] and Creton[3] for nanocomposites, the opaque appearance may be attributed to the formation of light scattering cavities inside the material at high deformation. In addition, we observed that for the materials with different concentrations of silica beads, the opacity appeared at different strain levels. The fact that the possible cavitation does not affect the mechanical properties is probably due to the low concentration of particles. Hence, the multiple network elastomers containing low concentration of silica beads can be used to map the strain field to research the mechanism of reinforcement. Moreover, due to the cavitation only occurring at high stress and strain, when a

notch was made on the sample the crack propagated at a relatively low stress. Thus the cavitation was not observed in the fracture test, which was performed on a Deben micro-tensile stage. Therefore, it also did not affect the subsequent the observation of fluorescent beads on confocal microscope.

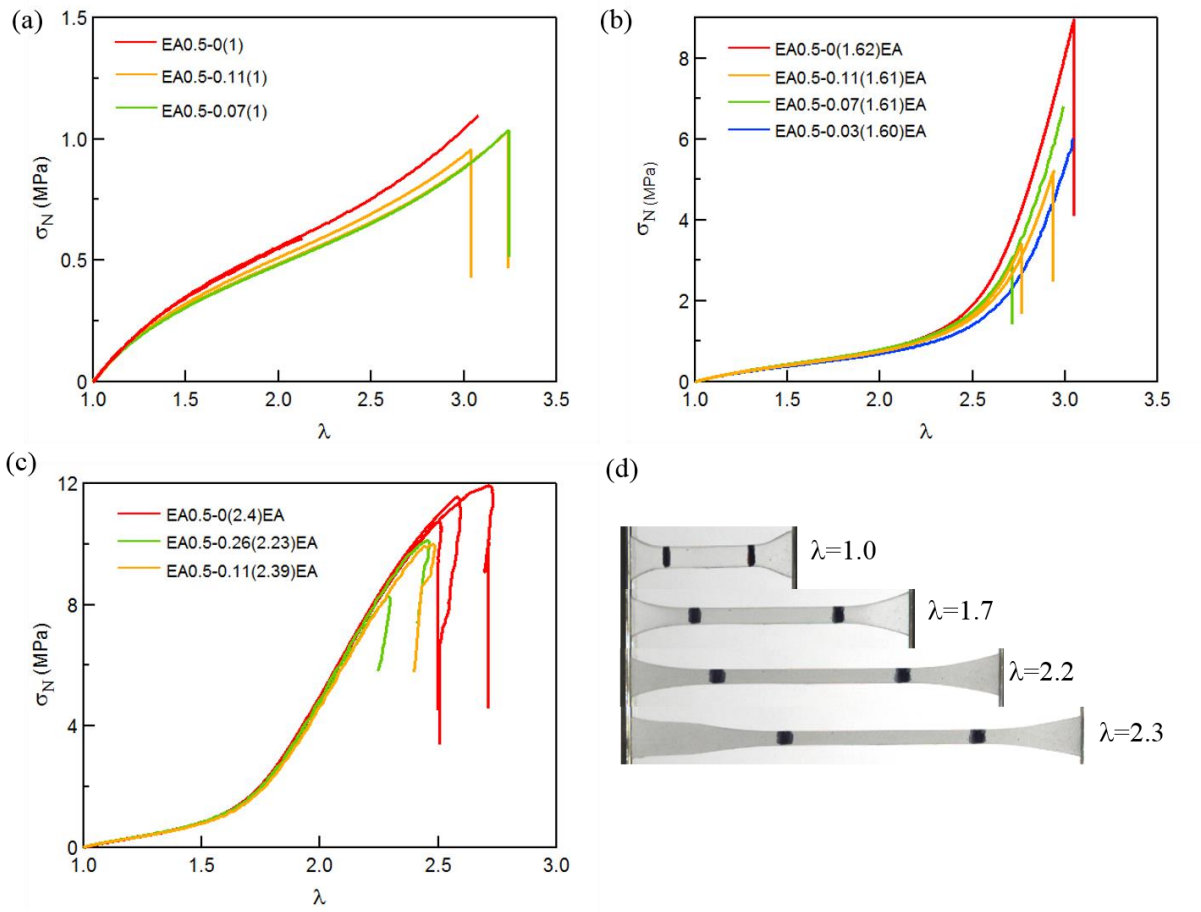

Figure 5.2: Stress-strain curves of (a) SNs, (b) DNs and (c) TNs with and without fluorescent silica beads; (d) The images of EA0.5-0.26(2.23)EA showing the change in transparency in a tensile test.

2.2 Confocal microscope observations

The distribution of fluorescent beads in multiple networks is detected by confocal microscope (Nikon AZ100) with an excitation laser wavelength of 488 nm and the fluorescence acquisition range between 500 nm and 550 nm. In order to construct a 3D strain field around the crack tip, a 3D fluorescent image was made for every frame by the superposition of 2D images in the thickness direction. Due to the reflection of fluorescence in confocal microscope[4], the images of spherical fluorescent beads are stretched in the thickness direction and have a shape of a rugby ball. Hence, even if the diameter of fluorescent beads is 3 μm, the

length of the fluorescent bead in the ‘z’ direction will be extended to about 30 μm. To save the scanning time and obtain clean fluorescent images of beads, the interval between two planes in the 3D images was set as 12 μm. In addition, to ensure most of the fluorescent beads in elastomers can be tracked from the first frame to the last one, the displacement between two frames of 3D images was set based on the subsequent calculation. The result displayed the optimal interval of displacement between two frames was 0.25 mm. With this interval of displacement, it ensures that most of fluorescent beads in two contiguous images can be tracked and decreases the sample frequency to save the time of measurement or experiment. The images of SNs, DNs and TNs are shown in Figure 5.3. The SNs with high concentration of fluorescent beads provide images containing dense fluorescent dots. When these SNs are used to prepare DNs, the concentration of fluorescent beads significantly reduces due to dilution. We found optimal concentration of the fluorescent beads, which from one side assures high resolution of measurement of strain field, at the same time allows to avoid the superposition or attachment of two fluorescent bead during fracture tests. This concentration was about 0.03, 0.07 and 0.11 wt% for SN, DN and TN, respectively.

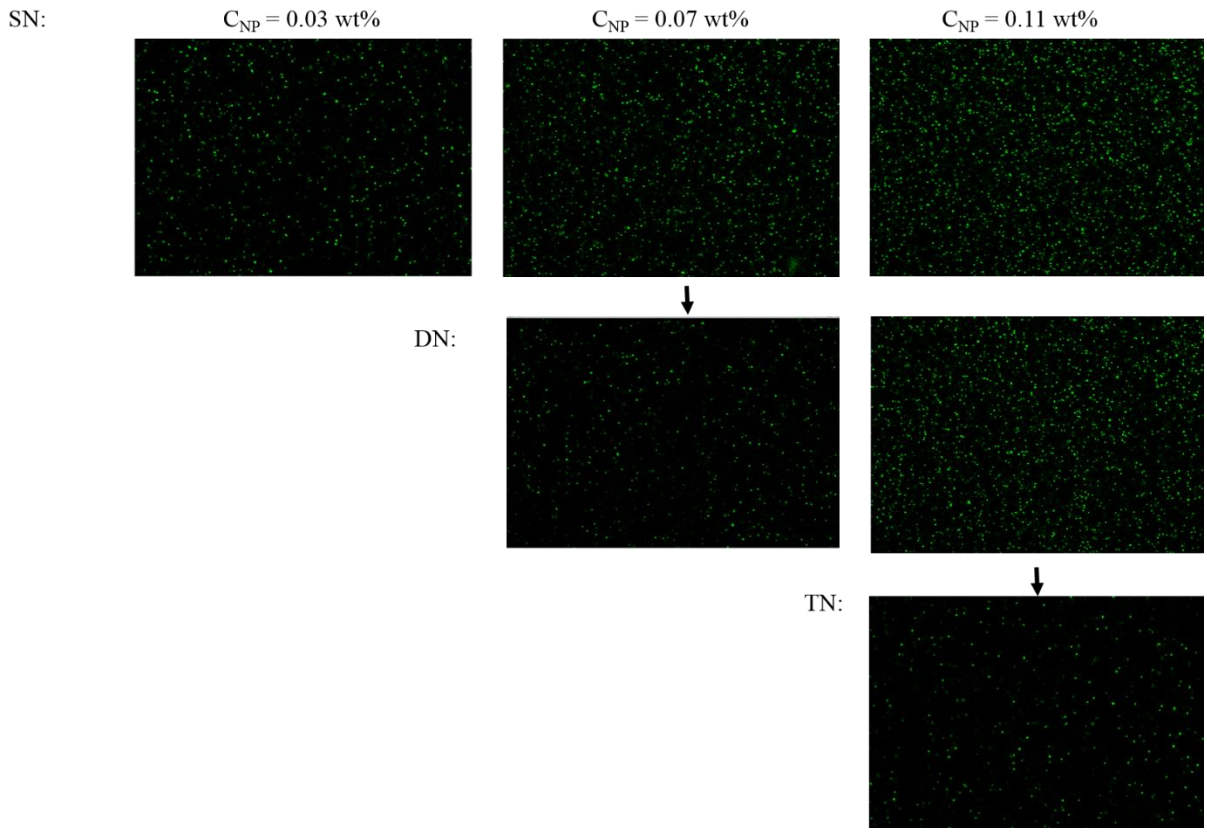

Figure 5.3: Fluorescent images of multiple network elastomers with different concentrations of fluorescent beads

These multiple network elastomers with optimal concentration of fluorescent beads were used to perform fracture tests. A Deben micro-tensile stage was used to carry out fracture tests

under a confocal microscope. The device provides a 200 N load cell and a maximum span of 10 mm between two small clamps. The tensile strain velocity was set at 1 mm/s and the interval between two frames of the 3D image was around 0.25 mm. Figure 5.4 shows the projection of the 3D images of EA0.5-0.07(1.61)EA in fracture tests on the horizontal plane. The image confirms a homogeneous dispersion of silica particles around the crack tip. The usable volume of the sample in the observed region reduces during the experiment due to the in-plane deformation and propagation of the fracture towards the tensile direction, which leads to a reduction in thickness. Therefore, the number of fluorescent beads in this area reduces gradually. We suppose that the beads can change their position only by following the deformation of the polymer and no significant slip may occur between particles and polymer, since the size of particles dispersed in the first network is much larger than the mesh size of the cross-linked polymer network.

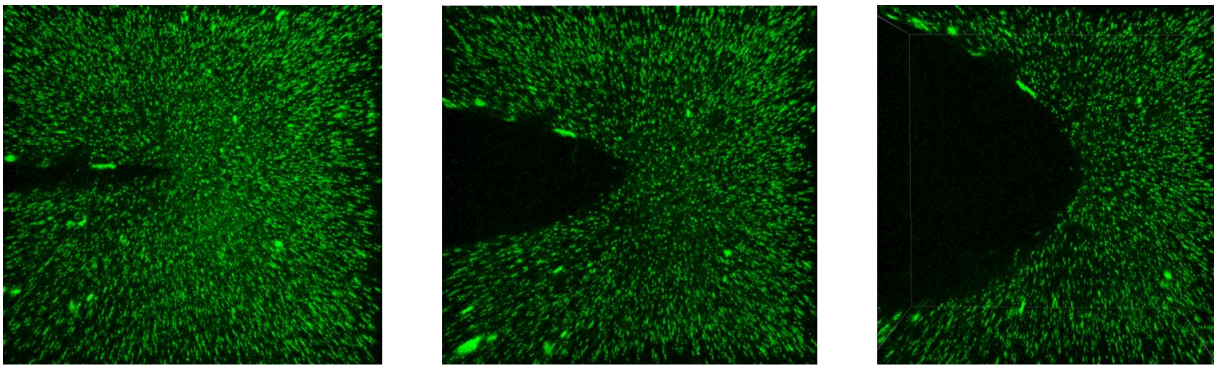

Figure 5.4: Fluorescent images of EA0.5-0.07(1.61)EA in a fracture test

2.3 Calculation

To calculate the displacement of the fluorescent beads, we cooperated with Yuan QI in Long's group at Colorado University. They used Imaris software to extract the position of each fluorescent bead and then constructed a spherical shell for every fluorescent bead. They marked the center of shell as the initial position of the fluorescent beads and matched the position of all the fluorescent beads for a sequence of 3D frames to calculate the displacement of the silica beads. Table 2 illustrates the quality of the matching procedure for five consequent frames. In the first frame we identified 7500 particles but only 4531 particles were matched in the second frame, which corresponds to 63.6%. 2588 particles could be tracked from the first frame to the fifth frame. Because of the high concentration of silica beads, the image of some of them can merge into other ones which decreases the efficiency of matching. The efficiency of matching can be evaluated by the pair ratio of two contiguous frames of 3D images and the linked pair number of beads. The pair ratio was calculated with Eq. 1.

$$\gamma = \frac{N_{m+1}}{N_m} \qquad (1 \leq m \leq n) \qquad \text{Eq. 1}$$

Where γ, m N and n are the pair ratio of the matching, the sequence number of the 3D frame, the number of beads in the 'm' frame and the total number of frames, respectively. In order to improve the pair ratio and the number of linked pairs of particles, we need to decrease the concentration of beads in the multiple network elastomers and improve the quality of the fluorescent images.

Table 2: Data of matching the fluorescent beads in five consequent fluorescent 3D frames

Frame NO.	Displacement u /mm	Increment Δu /mm	Identified beads number	Pair ratio	Pair number	Linked pair number
0	0	NA	7500	NA	NA	NA
1	0.251	0.251	7129	0.6356	4531	4531
2	0.504	0.253	6757	0.8467	5720	3759
3	0.753	0.249	6412	0.8562	5489	3432
4	1.007	0.254	5845	0.7512	4390	2588

3. Preliminary results

3.1 The vector displacement field of fluorescent beads

Based on the data above, we obtained images of displacement vectors of fluorescent beads between two consecutive frames as shown in Figure 5.5. A rectangular sample with a single notch was stretched in X direction. Figure 5.5 (a) shows the view of the x-y plane and a notch on the left of the sample. We observe the fluorescent beads on the top of notch move in the upper right direction. On the contrary, the beads toward the bottom of the notch move to the bottom right direction. The image is symmetric with respect to the notch axis. Figure 5.5 (b) gives a side view of the displacement of the beads in the x-z plane (h is defined as the thickness of the specimen). A clear trend of beads moving oppositely along the loading direction (x axis) can be observed, i.e. right beads going right and left beads going left; while beads in the middle have negligible x displacements due to symmetry. This symmetry can also be observed along the z axis where beads on the top were dragged downwards and beads in the bottom were lifted upwards, which was expected due to Poisson effect.

However, we find that many fluorescent beads around the crack tip are lost in the mapping process, which is probably caused by the large deformation. The large deformation near the crack significantly change the environment of the beads resulting in the failure of tracking or

identification by the software. During the compression of the samples in the y-direction the fluorescent beads aggregate together and the image of aggregated beads can't match with the previous frame and is regarded as noise and removed from the frame. Therefore, elastomers with dilute silica beads suspension are necessary to avoid the aggregation of particle in fracture test and to improve the percent of matching.

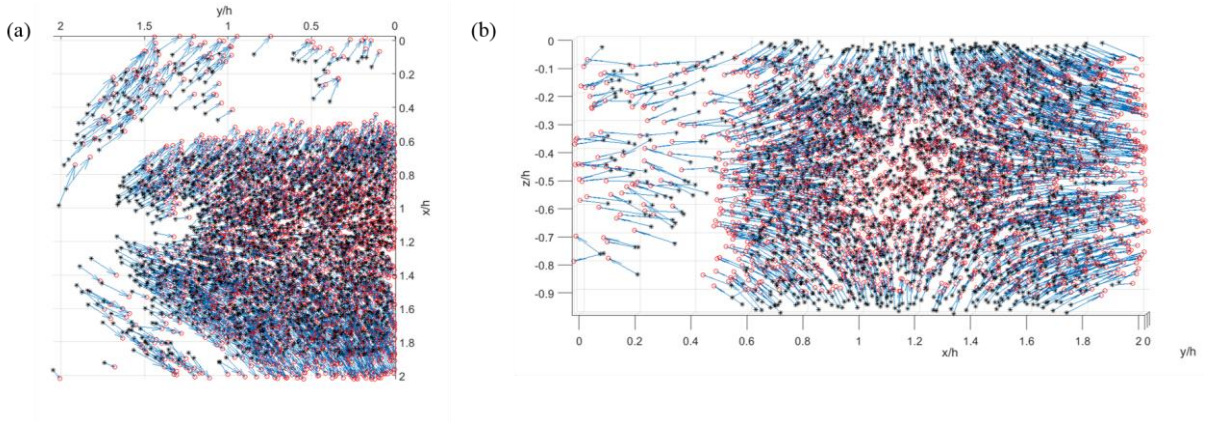

Figure 5.5: The displacement field around the crack tip (a) in x-y plane and (b) x-z plane. Red circles are bead positions in the deformed state, black stars are bead positions in the reference state and blue arrows are displacement vectors.

3.2 The strain field around the crack tip

Based on the displacement field, we also constructed the strain field shown in Figure 5.6. First, the displacement projections on the x and y axes (**ux** and **uy**, respectively) were obtained and plotted on Figure 5.6 (a). The images are rather symmetric with respect to the fracture plane. The deformation fields for ϵ_{xx} and ϵ_{yy} near the crack tip are shown in Figure 5.6 (b). The maximum deformation ϵ_{xx} corresponds to the strain λ_{xx} about 1.25, which means the deformation in the observed region are elastic. Since it is generally accepted that near the crack tip there exist a highly stretched dissipative zone, we suppose that its size is below the resolution of our imaging. The determination of the size of this zone near the crack is critical for the understanding of the reinforcement of multiple network elastomers. The determination of strain field near the tip was limited by the failure to tracking procedure of the fluorescent beads. We are currently trying to decrease the concentration of silica beads to avoid their aggregation and to improve the quality of fluorescent images obtained in the confocal microscope.

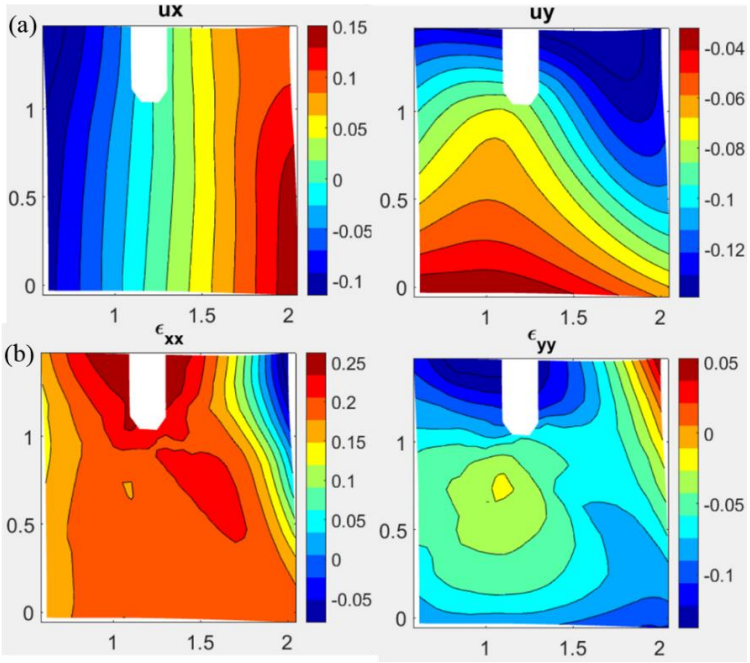

Figure 5.6: (a) The displacement field of x and y direction around the crack tip. (b) The deformation field in x and y direction. The plane is located on the center of the sample, i.e. at z = -0.5 h.

As future work, the strain field of the SNs, DNs and TNs around the crack tip will be compared to understand the reinforcement of multiple network elastomers. In the next step, the SP mechanophore, the stress sensor, will be incorporated into the elastomers together with the fluorescent beads to measure the stress and strain field at the same time. The stress field will be compared with that obtained from the SP color change analysis carried out in the third chapter. We hope that the data will be helpful to build a molecular model of the fracture and to explain the mechanism of the reinforcement of the multiple network elastomers.

Conclusion

We have synthesized series of multiple network elastomers that contain homogeneous fluorescent beads. In addition, we found a suitable concentration of fluorescent beads for different multiple network elastomers allowing particle tracking. Using a confocal microscope we characterized the spatial distribution of fluorescent beads around the crack tip in fracture tests.

In cooperation with Long's group, the primary results of displacement field and strain field around the crack tip have been obtained by particles tracking. Although we do not have the information about the size of the highly stretched dissipative zone near the crack tip, we found a way to map the strain field near the crack tip and will focus on improving the resolution of this method.

References

1. Hall, M. S.; Long, R.; Hui, C. Y.; Wu, M.; *Biophysical journal* **2012**, *102*, 2241.
2. Bindu, P.; Thomas, S.; *The journal of physical chemistry. B* **2013**, *117*, 12632.
3. Zhang, H.; Scholz, A. K.; de Crevoisier, J.; Vion-Loisel, F.; Besnard, G.; Hexemer, A.; Brown, H. R.; Kramer, E. J.; Creton, C.; *Macromolecules* **2012**, *45*, 1529.
4. Semwogerere, D.; Weeks, E. R.; *Encyclopedia of Biomaterials and Bimedical Engineering* **2005**.

Chapter 7. Perspective and discussion

Introduction

In this work, we examined the reinforcement and fracture mechanism of multiple network elastomers at the molecular scale by quantitatively mapping the stress distribution around the crack tip. The quantification of stress in multiple networks was performed by incorporating mechanochemistry. The chromatic response to mechanical force is used to map the stress distribution in multiple network elastomers. According to the stress map, for the tougher materials, almost all the area in front of the crack tip exhibit a high stress level prior to propagation. This high stress region spanning several hundred micrometers represent an area where damage occurs and dissipate energy. To properly understand (and model) how much energy is dissipated, it is important to have access to the unloading response of the material once the crack propagated.

To investigate the unloading process, we used secondary color changes (from blue to purple) of SP. Also, the stress transfer was studied, which showed that part of the stress was transferred from the filler network to the second network at the yielding point. We showed from the fluorescence experiments that the second network also contributed to the energy dissipation in front of the crack tip since the third network also activated over a certain volume. However, a molecular understanding or model to understand or predict the value of the fracture energy Γ is still lacking. Specifically, the fracture mechanism and the stress transfer at the necking areas, including the relationship between the damaged zone, yielding regions and relaxed areas around the crack tip, and the fracture approach in the filler network, and the fraction of the polymer chains in the second network actually involved in carrying load during the necking, etc. remains as topics of interest.

In this chapter, we will discuss these open questions and propose some possible approaches to construct a molecular model to explain the simultaneous improvement of modulus and fracture toughness of interpenetrating multiple networks.

1. Discussion around the quantification of polymer chains involved in the damage

The stress distribution was detected by the stress-color map in both loading and unloading. However, because of the non-scission nature of SP, the stress map displayed by the color change is the high stress distribution region and not the damage zone. The area of high stress is defined by the threshold of SP activation (240 pN), which is lower than the carbon-carbon bond (4 nN). According to the hysteresis in the step cyclic loading experiments, damage in the filler network for our standard EA0.5-0.05 family of materials starts at the critical stress of 3 MPa and significant damage occurs at about 5 MPa. The stress distribution above 3 MPa in front of the crack prior to and at the critical strain of propagation in EA0.5-0.05(2.23)EA are shown in Figure 7.*1*. The location of the two images on the stress-strain curve is shown in Figure 7.*1* (a). Comparing these two images, the location close to the critical strain has a corresponding damage zone of about 250 microns. However, as shown in Figure 7.*1* (b), the damage zone rapidly extends to 1 mm prior to fast propagation, which leads to the catastrophic failure of sample. The result illustrates many chemical bonds are broken around the crack tip between points (b) and (c) in Figure 7.*1*, dissipating energy. This part of the energy dissipation is the main contributor to the fracture toughness for this class of materials due to the high bond energy of covalent carbon-carbon bond and the relatively low level of viscoelasticity.

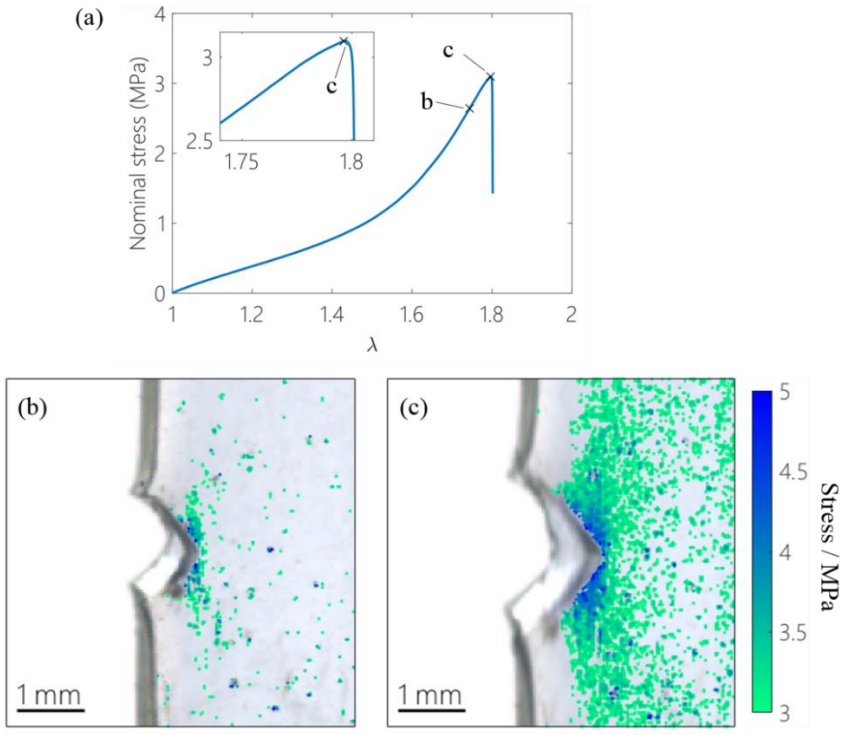

Figure 7.1 : (a) The location of (b) and (c) on the stress-strain curve of EA0.5-0.05(2.23)EA; The high stress (above 3 MPa) zone distributed around the crack tip (b) before and (c) during the propagation.

Comparing the loading and unloading stress distribution is useful to understand better the fracture mechanism. A stress distribution of the frame during the onset of propagation is shown in Figure 7.*2*. There are two small unloading areas (about 200 µm) behind the crack. Moreover, the dimension and the location of the relaxed regions are almost consistent with the damage zone of the image of *Figure 7.1* (b). The bond scission in the filler network in the damage zone relaxed first during propagation. According to the result of chapter five, a large amount of damage occurs in the filler network where there is a small necking (or yielded) region (around 100~200µm) ahead of the crack tip. Comparing the two areas of damage, the relaxed and necking zone (fluorescence images of chapter 5), it is deduce that about 250 µm damage zone appears ahead of the crack tip prior to propagation. A purple zone is observed in the wake of the crack tip (Figure 7.*2*), which may be enhanced by a large amount of damage occurring in the localized necking area. This promotes a fast relaxation of the stress due to the reduced areal chain density of the filler network after damage relative to the other regions.

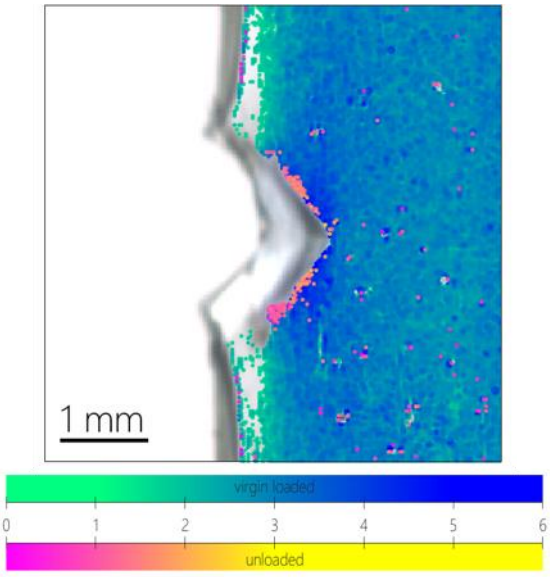

Figure 7.2 : The stress distribution around the crack tip prior to the fast propagation

2. Discussion about the fracture of the first network after yielding

Necking appears after the yielding of the materials, which has been observed in multiple network elastomers and double network hydrogels[1,2]. Gong's group attributed the necking phenomenon of double network hydrogels to the damage of the first network. They speculated that the necking area consists of a damaged first network made up of clusters that acted as physical crosslinkers, increasing the crosslinker density of the second network[1,2]. In chapter five, when SP was incorporated into the filler network, a secondary color change of SP (blue to purple) at the necking region is caused by the isomerization of MC undergoing unloading as shown in Figure 7.3 (a) at $\lambda_{correct}$=10 and 10.6. However, the necked areas only slightly changed to purple (the

color of MC at the loading state), which suggested that part of the MC was still loaded. Additionally, the result of the color analysis displays that chromatic change has a little variation which is not attributed to the change of thickness at the necking area. The result is consistent with the phenomenon we observe. But the necking area still maintains a high ratio of blue color. It suggests that the filler network is partially loaded. The experimental phenomenon and results confirm the filler network does not break into clusters.

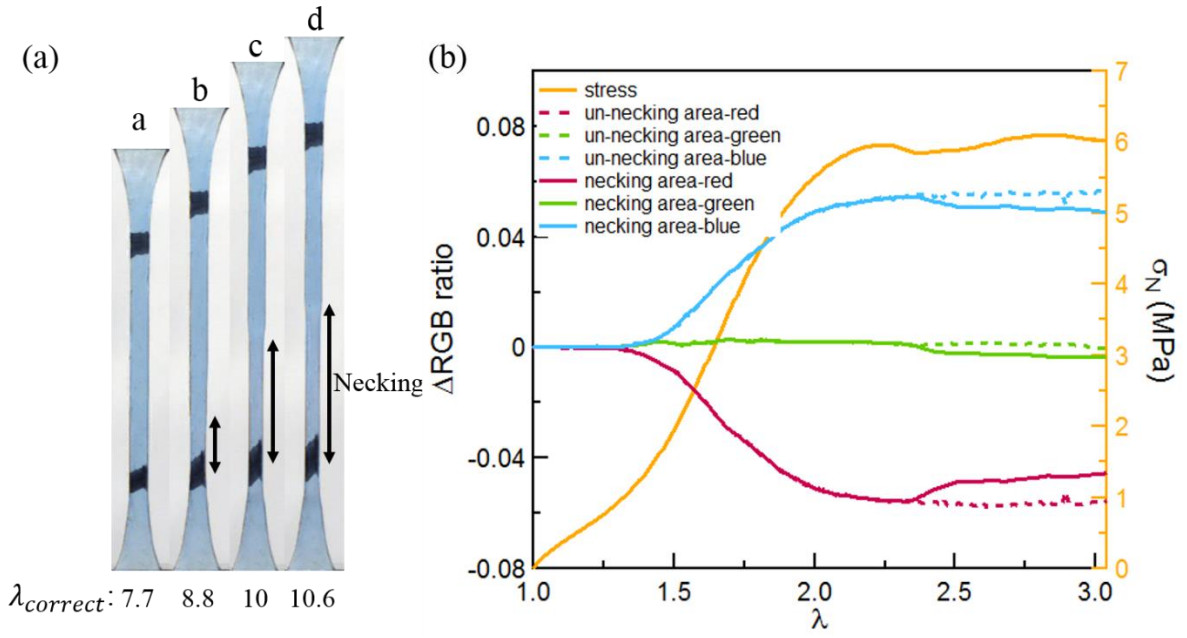

Figure 7.3 : (a) Images of EA0.2-0.05(3.49)EA are extracted from the uniaxial extension with various deformation. (b) Chromatic change and stress are plotted as a function of the total deformation in the filler network for EA0.2-0.05(3.49)EA sample. The dotted and solid lines are the chromatic change focusing on the un-necking and necking areas during necking, respectively.

An interesting phenomenon was observed after the uniaxial extension of EA0.2-0.05(3.49)EA. As shown in Figure 7.4, the EA0.2-0.05(3.49)EA sample exhibits two colors. At the two ends of the dog-bone sample a blue color can be clearly seen. While the middle of sample between the two black marks displays a distinctly purple color. Due to the high pre-stretch in the filler network, the SP in EA0.2-0.05(3.49)EA is activated during the swelling. After synthesizing the material, the MC molecules resisted converting back to SP. When the sample is stored for a long time, MC can slowly convert back to SP, but the sample remains slightly blue with no purple observed when it is loaded to a stress < 3 MPa. Based on the central part of the sample in Figure 7.4, the filler network is relaxed due to damage (the middle part of sample is the necked area as shown in Figure 7.3 (a)).

Figure 7.4 : Image of EA0.2-0.05(3.49)EA after the uniaxial tensile test

The color of the central part in figure 7.4 is clearly much more purple than the necked region under load of Figure 7.3. This shows that the first network is partially loaded during the necking and carries part of the stress. Therefore, it is unlikely that the filler network breaks into fragments. We deduce there are lots of damage in the filler network prior to the failure in extension, which is caused by many micro-cracks. However, the filler network still carry a large proportion of load. Thus, the filler network becomes blue during the necking process. After the failure of the sample, the filler network releases the pre-stress due to the damage, resulting in MC in the relaxed purple state.

3. The combination of the stress field and strain field around the crack tip

The stress and strain field in the multiple network elastomers was mapped by the chromatic change of SP and by the fluorescent particle tracking, respectively. The combination of stress and strain field is critical for comparing with a mechanical model. However, this is challenging since the fluorescent particle tracking needs a black or dark environment for detection by the confocal microscope. However, the color change of SP can only be observed or recorded by camera with light. In addition, the separated measurement of stress and strain field introduce another challenge to combine and analyze the stress and strain field due to the low reproducibility of the shape of the crack. The best way would be to detect the stress and strain field simultaneously. Due to the fluorescent feature of MC[3-5], the stress field can be mapped by the fluorescent intensity of MC on the confocal microscope.

In the previous chapter, we showed that the concentration of MC is proportional to the stress and the fluorescent intensity depends on the MC concentration. Therefore, the fluorescent intensity is also related to the stress. Their relationship can be used for the measurement of the stress field during virgin loading. As shown in Figure 7.5 (b) and (c), a notched sample of EA0.5-0.05(2.23)EA manually stretched by hand shows a fluorescent signal in front of the crack tip and the fluorescent intensity and region increase with the force. It confirms the feasibility of the approach that the stress can in principle be mapped by fluorescent intensity.

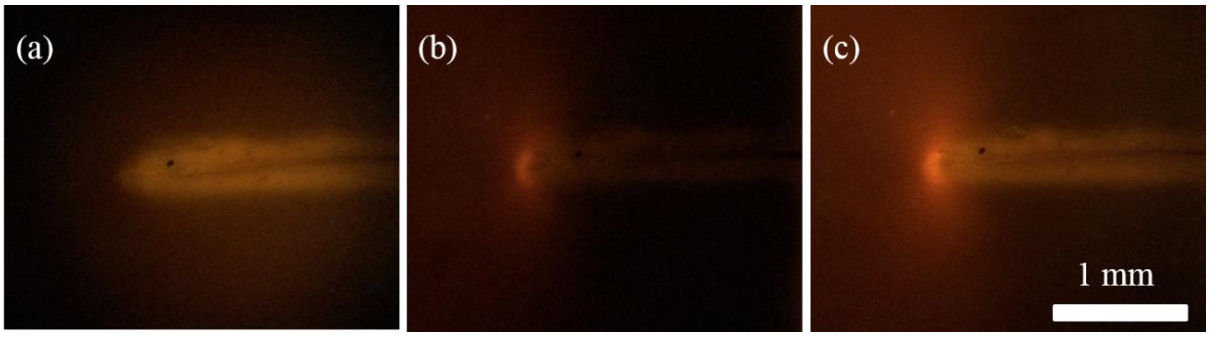

Figure 7.5: A notched sample of EA0.5-0.05(2.23)EA was stretched by hand. (a) The image of the notched sample was taken by microscope with a green laser after 5 mins exposure of white light. Other two images were taken after the notch sample was stretched with a (a) low and (b) high force by hand. The white regions are the crack and the luminous areas are fluorescent zone where some of SP are activated.

For further demonstration of the relationship between fluorescent intensity and stress, various multiple network elastomer were observed. As shown in Figure 7.*6*, various notched samples of the EA0.5-0.05 family of materials were stretched to a high stress and the fluorescent distribution was detected before and after extension. From Figure 7.*6*, it is obvious that the fluorescent regions increase from SN (EA0.5-0.05(1)) to TN (EA0.5-0.05(2.23)EA), which are consistent with the results of Ducrot et al[6]. It verifies the practical approach towards mapping a stress field by fluorescence.

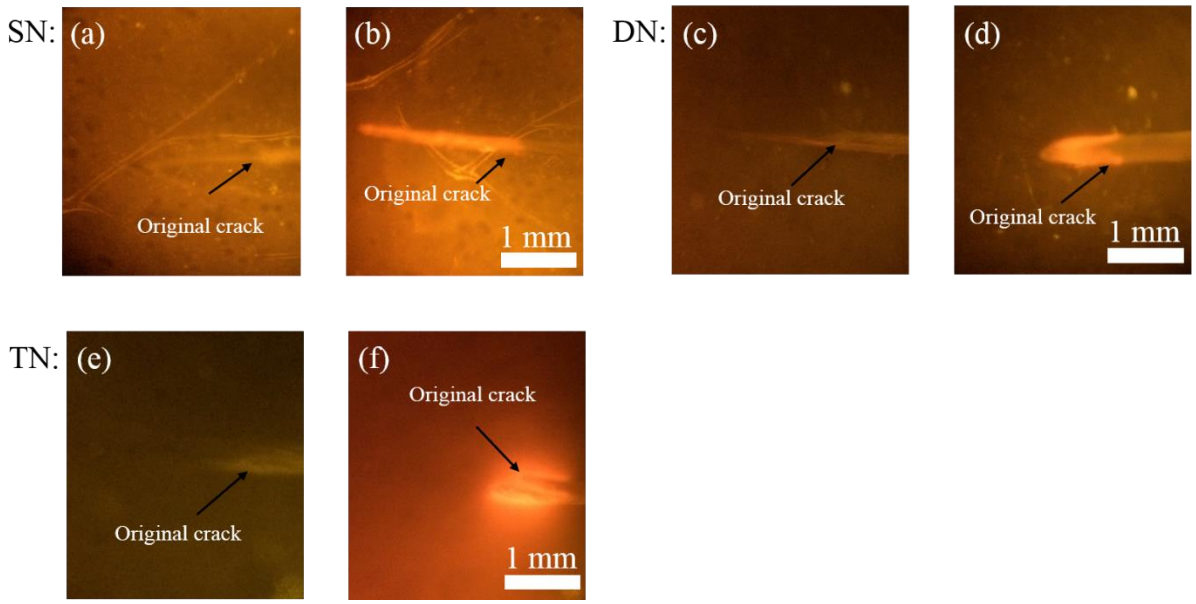

Figure 7.6 : The fluorescent images of various notch samples for SN (EA0.5-0.05(1)), DN (EA0.5-0.05(1.56)EA), TN (EA0.5-0.05(2.23)EA were detected by microscope with a green laser and camera before and after extension. The luminous areas are the fluorescent regions.

3.1 Calibration curve of fluorescence

SP transforms into MC by mechanical stimuli, which is accompanied with color change and red fluorescence[7-10]. The color change is used to detect the stress field in previous chapters. Due to the visible signal of color change, this approach to map the stress field is convenient. However, when the concentration of active SP is low, color change is not easy to detect. On the contrary, MC is able to generate strong fluorescence. Thus, the fluorescent signal of MC is sensitive to the stress. When a small part of SP is activated, the fluorescent signal around the crack tip can be detected by the microscope as described in chapter five.

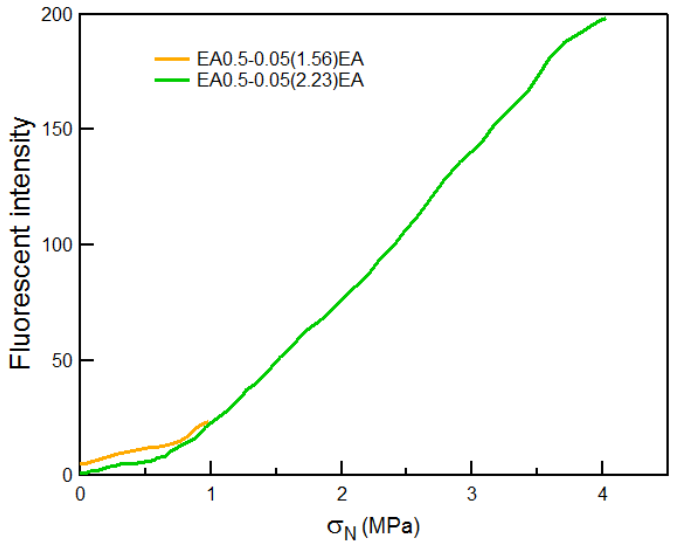

Figure 7.7: Fluorescent calibration curves of EA0.5-0.05(1.56)EA and EA0.5-0.05(2.23)EA

Similar to the strategy for detecting stress by color change, the stress field can also be mapped by constructing a calibration curve between stress and fluorescent intensity. Dog-bone samples are fixed on the Deben micro-tensile tester and the Deben setup is placed on the sample stage of confocal microscope. During the tensile tests on the Deben, the fluorescent intensity is measured by confocal microscopy. Thus, a calibration curve of fluorescent intensity in response to stress can also be constructed using the signal of the confocal microscope and the stress coming from the Deben as shown in Figure 7.7. However, when SP in the material is activated, the fluorescent intensity decreases with the increase of scanning depth due to the absorption and reflection of materials. For a precise measurement of the fluorescence, the fluorescent intensity should be calibrated and corrected depending on the thickness of samples. But it is difficult for the correction due to the complicated paths of the fluorescence during collection in the detector. Therefore, more experiments are necessary to accurately map the stress by fluorescent intensity.

Another challenge for the combining the detection of stress by fluorescence and strain field by fluorescent particle tracking is the fluorescent intensity of the background. As shown in Figure 7.8, when SP is incorporated into the first network, the images to track fluorescent particles exhibits a strong fluorescent background, which causes tracking of fluorescent particles difficult. Therefore, more experiments and investigations are necessary to combine the detection of stress and strain.

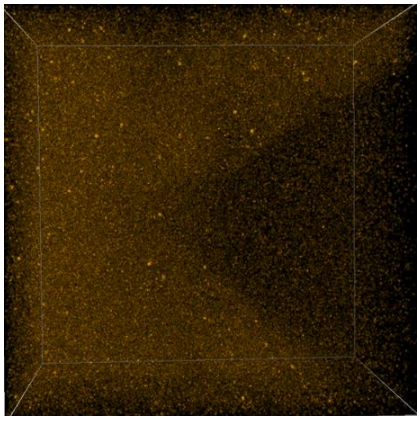

Figure 7.8: The image of DN with fluorescent particles and SP in fracture test

Conclusion:

We have discussed the close relationship between the damaged zone, necking regions and relaxed areas around the crack tip. The damage zone results in the necking regions due to large amount of the scission of carbon-carbon bonds. Necking leads to more damage in the filler network. Thus, the necked regions relaxes first during crack propagation. In addition, according to the behavior of MC in the necked areas, we propose a new and possible fracture mechanism in the necking areas. The filler network does not fracture into fragments but forms many micro-cracks. Within the cracks, the second network is stretched. Most importantly, results show that the filler network is still under load despite the presence of micro-cracks.

The combination of the detection of the stress and strain field by fluorescent intensity and fluorescent particle tracking is demonstrated. This approach is promising, but there are still a lot of challenges, including the correction and calibration of that fluorescent intensity on the confocal microscope and the elimination of the background noise when incorporating fluorescent particle tracking.

Reference:

1. Gong, J. P.; *Soft Matter* **2010**, *6*, 2583.
2. Matsuda, T.; Nakajima, T.; Fukuda, Y.; Hong, W.; Sakai, T.; Kurokawa, T.; Chung, U.; Gong, J. P.; *Macromolecules* **2016**, *49*, 1865.
3. Grady, M. E.; Beiermann, B. A.; Moore, J. S.; Sottos, N. R.; *ACS applied materials & interfaces* **2014**, *6*, 5350.
4. Kim, T. A.; Beiermann, B. A.; White, S. R.; Sottos, N. R.; *ACS Macro Letters* **2016**, *5*, 1312.
5. Chen, Y.; Zhang, H.; Fang, X.; Lin, Y.; Xu, Y.; Weng, W.; *ACS Macro Letters* **2014**, *3*, 141.
6. Etienne, D.; Yulan, C.; Markus, B.; Rint, P. S.; Costantino, C.; *science* **2014**, *344*, 4.
7. Beiermann, B. A.; Davis, D. A.; Kramer, S. L. B.; Moore, J. S.; Sottos, N. R.; White, S. R.; *Journal of Materials Chemistry* **2011**, *21*, 8443.
8. Beiermann, B. A.; Kramer, S. L. B.; May, P. A.; Moore, J. S.; White, S. R.; Sottos, N. R.; *Advanced Functional Materials* **2014**, *24*, 1529.
9. Beiermann, B. A.; Kramer, S. L. B.; Moore, J. S.; White, S. R.; Sottos, N. R.; *ACS Macro Letters* **2011**, *1*, 163.
10. Celestine, A.-D. N.; Beiermann, B. A.; May, P. A.; Moore, J. S.; Sottos, N. R.; White, S. R.; *Polymer* **2014**, *55*, 4164.

General conclusion

Inspired by the methodology of double network hydrogels, our group developed a category of tough and extensible unfilled elastomers based on interpenetrating multiple networks (Ducrot et al.). In contrast to the common unfilled elastomers, the fracture toughness and Young's modulus of the multiple network elastomers were improved at the same time. Ducrot confirmed the close relationship between Young's modulus and cross-linker density in the filler network and the dimension of damaged areas around the crack increased with the number of the networks. Millereau provided significant additional insight into the fracture mechanism of this multiple network elastomers. He showed that the increase of Young's modulus and fracture toughness derived directly from the level of prestretch and that the highly damaged filler network led to the yielding and necking phenomenon. However, while the general principle of the reinforcement by internal molecular damage due to sacrificial bond scission was established, the details of the fracture process at the molecular scale remained largely unknown and better molecular tools were needed to address these questions.

In this thesis, spiropyran mechanophore (SP), a molecular probe, was used to directly sense the stress in multiple network elastomers by its color change after activation. Based on the relationship between color change and the magnitude of stress, the stress distribution in the filler network was quantitatively mapped around the tip of a crack in various multiple network elastomers during loading and for the first time unloading. In addition, SP was incorporated into the second or third network to study the transmission of stress between the different networks.

First, a quantitative relationship between color change and stress was constructed by incorporating SP into the first network which acts as the filler network and sustains the main load in the multiple network elastomers. Comparing the color change in the family of multiple network elastomers, the following results were obtained:

1. SNs (with no presetretch) only changed its color near the edge of a crack during the failure in extension;
2. SP in the filler networks of DNs, TNs and QNs can be activated at the same onset of stress (1.5 MPa). Additionally, due to the higher stress at break in TNs there are more SP converting into MC after failure despite the lower SP concentration comparable to DNs.
3. QNs ($\lambda_0 \geq 2.81$) changed it color already after synthesis and showed two colors (blue and purple) after the failure in extension.

These phenomena illustrated that with the progressive increase of the pre-stretch in

the filler network, more and more polymer chains are involved to sustain the load resulting in more SP converting into merocyanine (MC). In other words, the pre-stretch makes the filler network more homogeneous and stiff in some degrees and is able to sustain larger and larger loads as the multiple networks stiffen. Since SP is sensitive to the stress and the color intensity depends on the concentration of MC. When more polymer chains are loaded with a force exceeding the activation threshold of SP into MC (240 pN) more SP converts into MC and more color change is observed. For highly prestretched filler networks activation can occur during the synthesis due to the osmotic pressure imposed by the swelling monomer. According to our estimate, the average force imposed by the osmotic swelling (264 pN) can exceed the threshold of SP and results in the activation of SP before any mechanical testing. After failure of these highly prestretched samples, the heterogeneous purple color suggests extensive damage of the filler network in extension. These results demonstrate that the stiffening of the multiple networks derives from the pre-stretching in the filler network and bond scission in the pre-stretched chains makes multiple network become tougher.

Then color analysis was used to quantify the color change. According to the results of color analysis, the onset of the color change in multiple networks was 1.5 MPa and these curves of chromatic change as a function of stress can form a master curve for the family of multiple network elastomers. When tailoring the crosslinker density in the filler networks and keeping a constant SP concentration, the mechanical properties of multiple networks were varied. But their master curves of color hue vs stress was very similar. Furthermore, varying the SP concentration in the filler network did not change the master curves after the normalization by the SP concentration. The stability of the master curve in various materials verified a robust relationship between color change and stress making us confident that the master curves can be used as a calibration curve to map the stress in multiple network elastomers.

Finally, the stress distribution around the crack tip was mapped with these calibration curves for samples with a relatively high level of prestretching. For EA0.5-0.05(2.23)EA or EA0.2-0.05(2.61)EA, the result showed that the magnitude of the stress and the volume of high stress (> 1.5 MPa) around the crack tip gradually increased with increasing loading. Prior to propagation there was a large volume of high stress distribution around the crack tip and the area almost covered all the zone in front of the crack tip. Since SP is a non-scission mechanophore, the activation of SP does not signal the breakage of polymer chains but simply a high stress in the

polymer chains. Thus the large area of high stress distribution did not represent the damage zone. The damage was investigated for the same material by step cyclic loading test. With the increase of strain, lots of hysteresis were observed on the stress-strain curve. The hysteresis confirmed that the damage occurred in the filler network at the critical stress of 3 MPa. According to the critical stress, prior to the crack propagation the damage zone length around the crack tip was estimated to about 250 µm at the Centre of crack tip, but during the crack propagation there were more area involving in dissipating energy and it was estimated about 600 µm near the crack, which was consistent with the prediction by Brown and Tanaka.

In step cyclic loading and fracture tests, a secondary color (blue to purple) was observed when the material was unloaded and this color change was demonstrated to be due to the stress-sensitive reversible isomerization of MC. A new stress-color map where stress was represented as a function of the total chromatic change and of the green chromatic change was constructed and calibrated with by step cyclic loading-unloading tests. That stress-color map was then used to map the spatial and temporal variation in stress during crack propagation. From the stress map, it was confirmed that the relaxation of stress near the crack tip started from the edge of crack, relatively far away from the crack tip. In addition, we proposed a statistical analysis differentiating the loaded and unloaded pixels during the propagation. The statistical data showed that more and more areas relaxed from high stress as the crack slowly propagates, while the areas under load keep also increasing in size and intensity in the beginning of propagation. Observing the relaxed area, its dimension was close to that of the damage zone. It was possible that the scission of polymer chains in the filler network has led to the detected relaxation.

After investigating the stress distribution around the crack tip, the stress transfer between networks was studied by incorporating SP as a crosslinker into the second or the third networks. In uniaxial tensile tests, only the EA0.5-0(2.98)EA2 sample with SP in the second network showed a color change in the necked area. It suggested that the second network sustains a high stress after the damage of the filler network caused the necking process. Our data shows that stress started to transfer into the second network but not to the third network. Due to the chains transfer reaction, there were some connections between the filler network and other networks polymerized afterward.

When that connection was reduced by replacing the acrylate monomers by methacrylate in the first network, the color change at the necked area was no longer

observed during the necking but only once the whole gauge length of the sample was necked and the stress continued to increase. Fluorescence results of these material containing SP in the second or third network showed that in fracture tests, the second network also contributes to dissipate energy very close to the crack tip. The same experiments demonstrated also that the necking process which activates the second network, existed in front of the crack tip. Therefore, the stress transmission in the multiple network can be summarized in the following way:

1. The filler network sustains most of the load in extension and controls the Young's modulus of the materials before the yield point.
2. After yielding, part of stress is transferred to the second network and the second hardening phenomenon derives from the maximum extensibility of the second network.
3. At the crack tip, we see evidence of the same process since the second network is only activated just before propagation and the third network only during propagation. Successive breakage of bonds at different distances from the crack must all contribute to the toughness.

Although the mapping of the stress is a highly innovative approach and has contributed important insight, it would certainly be desirable to couple it with a simultaneous detection of the strain field on order to validate material's models. Another approach was therefore used to map the strain field around the crack tip. It was tracking fluorescent beads which were incorporated into the multiple network. By cooperating with Long's group at Colorado University we have gotten some preliminary results and shown the strain field around the crack. But more experiments should be conducted to improve the resolution of the mapping in particular near the tip of the crack where gradients are very steep.

Finally a few words about prospective. This thesis has laid a solid foundation for the construction of better molecular models of fracture of multiple network elastomers. But of course there are still some promising directions that could be explored to lead to a better understanding of the reinforcement mechanism of multiple network elastomers. In particular as mentioned above it would be very interesting to be able to map stress and strain at the same crack tip. A direct assessment of bond scission with a different type of mechanophore would also be very complementary and of course the technique that we have developed may have much more general uses as a mapping tool in transparent materials as long as an SP bond can be incorporated and loaded

inside the material it can act as a molecular force probe. Finally dynamic experiments carried out with a fast camera may be a natural extension taking advantage of the specific response of the SP and MC in the absorption spectrum.

Résumé

Des élastomères à réseaux multiples résistants et présentant une réponse optique (changement de couleur) ont été conçus, synthétisés et examinés. Les propriétés de renforcement de ces réseaux multiples découlent du premier réseau, rigide et pré-étiré, qui se comporte comme un réseau de charge percolant. Du spiropyrane (SP) a été incorporé dans le premier réseau pour permettre la visualisation de la distribution de contraintes élevées par changement de couleur. En adaptant les densités de réticulants et la concentration de SP dans le réseau de charge, nous avons démontré que le SP se comportait comme un capteur de contrainte moléculaire. Une courbe d'étalonnage de la variation chromatique en fonction de la contrainte nominale a été construite par analyse de couleur, et a ensuite été utilisée pour cartographier la contrainte et la densité d'énergie autour d'une pointe de fissure. De plus, une carte de contrainte-couleur a été créée en effectuant des tests de chargements cycliques incrémentaux et des analyses de couleurs, ce qui a permis de cartographier la contrainte subie lors du chargement et du déchargement pendant la propagation de la fissure. En comparant la répartition des contraintes lors du chargement et du déchargement, les régions à forte contrainte et la zone endommagée dans le réseau de charge ont été déterminées, en cohérence avec les prédictions du modèle. Lorsque le SP a été incorporé dans le deuxième réseau, les résultats ont montré que la contrainte était transférée dans le deuxième réseau près de la limite élastique, ce qui implique que le second réseau contribue à la résistance à la croissance des fissures. En outre, les mécanismes d'endommagement qui conduisent à la striction lors des essais de traction uniaxiale ont été étudiés. Les résultats ont montré que dans la zone de striction une grande fraction du réseau de charge était endommagée. Cependant, cet endommagement n'amène ni à la formation de clusters de réseau de charge ni à sa complète relaxation. Enfin, nous avons développé une approche pour mesurer le champ de déformation dans les matériaux en utilisant le suivi des particules fluorescentes.

Mots Clés

Elastomères à réseaux multiples interpénétrés, mécanochimie, mécanphore, spiropyran, réseau de remplissage, carte de stress, perles fluorescentes

Abstract

Tough multiple network elastomers exhibiting optical response (color change) have been designed, synthesized, and examined. The reinforcing properties of multiple networks were derived from the pre-stretched, stiff first network, which behaved like a percolated filler network. Spiropyran (SP) was incorporated into the first network to provide visualization, via color change, of the high stress distribution. By tailoring the crosslinker densities and SP concentration in the filler network, we demonstrated that SP behaved as a molecular stress sensor. A calibration curve of the chromatic change as a function of nominal stress was constructed through color analysis, which was used to construct a stress and energy density mapping around a crack tip. Furthermore, a stress-color map was created by performing step cyclic loading tests and color analysis, which allowed mapping of the stress undergoing loading and unloading during crack propagation. Comparing the stress distribution in loading and unloading, the high stress regions and damage zone in the filler network were determined, which was consistent with model predictions. When SP was incorporated into the second network, results showed that stress was transferred into the second network near the yield point, implying that the second network contributed to the resistance of crack growth. Also, damage mechanisms that led to necking during uniaxial tensile testing were investigated. Results showed that in the necking area there were large amount of filler network damage. However, the damage did not result in the filler network fracturing into clusters and relaxing completely. Finally, we developed an approach to measure the strain field in materials by utilizing fluorescent particle tracking.

Keywords

Interpenetrated multiple network elastomers, mechanochemistry, mechanophore, spiropyran, filler network, stress map, fluorescent beads

Résumé

Des élastomères à réseaux multiples résistants et présentant une réponse optique (changement de couleur) ont été conçus, synthétisés et examinés. Les propriétés de renforcement de ces réseaux multiples découlent du premier réseau, rigide et pré-étiré, qui se comporte comme un réseau de charge percolant. Du spiropyrane (SP) a été incorporé dans le premier réseau pour permettre la visualisation de la distribution de contraintes élevées par changement de couleur. En adaptant les densités de réticulants et la concentration de SP dans le réseau de charge, nous avons démontré que le SP se comportait comme un capteur de contrainte moléculaire. Une courbe d'étalonnage de la variation chromatique en fonction de la contrainte nominale a été construite par analyse de couleur, et a ensuite été utilisée pour cartographier la contrainte et la densité d'énergie autour d'une pointe de fissure. De plus, une carte de contrainte-couleur a été créée en effectuant des tests de chargements cycliques incrémentaux et des analyses de couleurs, ce qui a permis de cartographier la contrainte subie lors du chargement et du déchargement pendant la propagation de la fissure. En comparant la répartition des contraintes lors du chargement et du déchargement, les régions à forte contrainte et la zone endommagée dans le réseau de charge ont été déterminées, en cohérence avec les prédictions du modèle. Lorsque le SP a été incorporé dans le deuxième réseau, les résultats ont montré que la contrainte était transférée dans le deuxième réseau près de la limite élastique, ce qui implique que le second réseau contribue à la résistance à la croissance des fissures. En outre, les mécanismes d'endommagement qui conduisent à la striction lors des essais de traction uniaxiale ont été étudiés. Les résultats ont montré que dans la zone de striction une grande fraction du réseau de charge était endommagée. Cependant, cet endommagement n'amène ni à la formation de clusters de réseau de charge ni à sa complète relaxation. Enfin, nous avons développé une approche pour mesurer le champ de déformation dans les matériaux en utilisant le suivi des particules fluorescentes.

Mots Clés

Elastomères à réseaux multiples interpénétrés, mécanochimie, mécanphore, spiropyran, réseau de remplissage, carte de stress, perles fluorescentes

Abstract

Tough multiple network elastomers exhibiting optical response (color change) have been designed, synthesized, and examined. The reinforcing properties of multiple networks were derived from the pre-stretched, stiff first network, which behaved like a percolated filler network. Spiropyran (SP) was incorporated into the first network to provide visualization, via color change, of the high stress distribution. By tailoring the crosslinker densities and SP concentration in the filler network, we demonstrated that SP behaved as a molecular stress sensor. A calibration curve of the chromatic change as a function of nominal stress was constructed through color analysis, which was used to construct a stress and energy density mapping around a crack tip. Furthermore, a stress-color map was created by performing step cyclic loading tests and color analysis, which allowed mapping of the stress undergoing loading and unloading during crack propagation. Comparing the stress distribution in loading and unloading, the high stress regions and damage zone in the filler network were determined, which was consistent with model predictions. When SP was incorporated into the second network, results showed that stress was transferred into the second network near the yield point, implying that the second network contributed to the resistance of crack growth. Also, damage mechanisms that led to necking during uniaxial tensile testing were investigated. Results showed that in the necking area there were large amount of filler network damage. However, the damage did not result in the filler network fracturing into clusters and relaxing completely. Finally, we developed an approach to measure the strain field in materials by utilizing fluorescent particle tracking.

Keywords

Interpenetrated multiple network elastomers, mechanochemistry, mechanophore, spiropyran, filler network, stress map, fluorescent beads